Synthetic Models for Iron Sulfur and Molybdenum Cofactor Enzymes

By Ziyi Zhao

B.S. Nankai University

A Dissertation Submitted in Partial Fulfillment of the Requirements for the Degree of Doctor of

Philosophy in the Department of Chemistry at Brown University

Providence, Rhode Island, 2024

This dissertation by Ziyi Zhao is accepted in its present form by the Department of Chemistry as satisfying the dissertation requirement for the degree of Doctor of Philosophy.

Date_____   _____

Eunsuk Kim, Ph.D. Advisor

Recommended to the Graduate Council

Date_____   _____

Jerome Robinson, Ph.D. Reader

Date_____   _____

Ou Chen, Ph.D. Reader

Approved by the Graduate Council

Date_____   _____

Andrew. G. Campbell, Ph.D.

Dean of Graduate School

Curriculum Vitae

Ziyi Zhao

Education

Brown University, Providence, RI   **09/2018-11/2023**

- Ph.D. in Chemistry

Nankai University, Tianjin, China   **09/2014-06/2018**

- B.Sc. in Chemistry

Research Experience

Department of Chemistry, Brown University, Providence, RI   **02/2019-11/2023**

Graduate Research Assistant

- Explored the design, synthesis, and characterization of innovative organic ligands to imitate the coordination environment of natural enzyme active site

- Developed and optimized a new type of biomimetic molybdenum compounds as oxygen/sulfur atom transfer catalysts, resulting in significant improvement in turnover numbers and yields

- Created inventive synthetic models for natural iron-sulfur clusters and conducted reactivity assessments with relevant signaling molecules to reveal the reaction mechanisms of natural proteins

Department of Chemistry, Nankai University, Tianjin, China   **04/2016-07/2017**

Undergraduate Research Assistant

- Constructed novel water-soluble oxocalix[3]arene derivatives with positively charged substituents at the upper rim and evaluated their ability in recognizing the negatively charged polysaccharides

- Awarded with the first prize scholarship

Publications

- **Zhao, Z.**, Kim, E. Construction of Fe-S Core by Persulfide: Nature Strategy for Fe-S Cluster Repairing. *Manuscript in progress*

- **Zhao, Z.**, Kim, E. Reactivity, mechanism, and active intermediate of binuclear μ-oxo Mo(V) catalyzed sulfur atom transfer reaction. *Manuscript in progress*

- Chen, S.L., **Zhao, Z.**, Kim, E. Catalytic Sulfur Atom Transfer by Bimetallic Mo(V) complex. *Manuscript in progress*

- Chen, S.L., L.T. Elrod, L.T., **Zhao, Z.**, Kim, E. Nitrate and Perchlorate Reduction by a Dinuclear Mo(V) Complex. *Manuscript in progress*

- Oakley, K. M., Lehane, R. L., **Zhao, Z.**, & Kim, E. (2022). Dioxygen reactivity of a biomimetic [4Fe-4S] compound exhibits [4Fe-4S] to [2Fe-2S] cluster conversion. *Journal of Inorganic Biochemistry*, 228, 111714.

- Oakley, K. M., **Zhao, Z.**, Lehane, R. L., Ma, J., & Kim, E. (2021). Generation of H2S from Thiol-Dependent NO Reactivity of Model [4Fe-4S] Cluster and Roussin's Black Anion. *Inorganic Chemistry*, 60(21), 15910-15917.

- Wang, Y. Y., Kong, Y., Zheng, Z., Geng, W. C., **Zhao, Z. Y.**, Sun, H., & Guo, D. S. (2019). Complexation of a guanidinium-modified calixarene with diverse dyes and investigation of the corresponding photophysical response. *Beilstein journal of organic chemistry*, *15*(1), 1394-1406.

Presentations

- Reactivity, mechanism, and active intermediate of binuclear μ-oxo Mo(V) catalyzed sulfur atom transfer reaction, ACS Spring 2023 Meeting, Indianapolis, IN. (March 2023) (Expected), *Oral Presentation*

- Construction of Fe-S Core by Persulfide: Chemistry of Natural Strategies to Repair Damaged Fe-S Clusters, Chemistry Department Poster Session, Brown University, Providence, RI. (Oct 2022), *Poster Presentation*

- Generation of H2S from Thiol-Dependent NO Reactivity of Model [4Fe-4S] Cluster and Roussin's Black Anion, 53rd Boston Regional Inorganic Colloquium, Dartmouth College, online. (May 2021), *Poster Presentation*

- Synthetic Analogs of the Active Sites of Iron-Sulfur Proteins and Their Physiological Reactivity, Chemistry Department Inorganic Chemistry Seminar, Brown University, Providence, RI. (Nov 2019), *Oral Presentation*

Acknowledgement

First and foremost, I must express my deepest gratitude to my advisor, Professor Kim. I am incredibly fortunate to have been a member of your research group, and I am profoundly thankful for your unwavering support in my research and career development. Your expertise and perceptive guidance have been the beacon throughout my PhD journey. Your open-door policy, always welcoming my queries and concerns, has provided me with an environment where I am able to seek guidance and find inspiration whenever I needed it most. Your mentorship has stretched well beyond the academic sphere, playing a crucial role in shaping who I am today.

I also extend my gratitude to the members of my thesis committee, Professor Robinson, and Professor Chen. Your expert feedback, encouragement, and rigorous standards have greatly contributed to the depth and quality of my research.

My appreciation extends to all my lab mates and colleagues, particularly Shui, Kady, John and Stephen for an environment filled with intellectual curiosity, collaboration, and innovation. Your friendship and shared passion for discovery have made my time in the lab truly enjoyable. I am also grateful for the undergraduate student Richard and Aaron who have collaborated with me during my PhD journey. Your excellent work has not gone unnoticed and has been a vital component of our success.

My endless gratitude goes to my family—my parents, whose unconditional love and belief in me never wavered; to my boyfriend, for your steadfast support and patience.

My gratitude extends to all who have walked this path with me. Thank you.

Table of Contents

List of Figures

List of Schemes

List of Tables

Chapte 1 Introduction to Fe-S Clusters

1.1 Iron–sulfur

1.1.1 Iron–sulfur clusters in proteins and their role in metabolism

Iron-sulfur (Fe-S) clusters are ubiquitous cofactors composed of iron and inorganic sulfur, and proteins that contain [Fe-S] clusters, referred to as [Fe-S] proteins, are critical components in the key life processes with varied functions that include electron transport, regulation of gene expression, substrate binding and activation, radical generation, and DNA repair.[1-3] They are found in all life forms.[3,4] Since the discovery of ferredoxins in the early 1960s, the number of identified [Fe-S] proteins have greatly proliferated. More than 120 distinct types of enzymes and proteins are known to contain [Fe-S] clusters, and the discovery of new types of [Fe-S] proteins and [Fe-S] clusters has resulted in an appreciation of their remarkable functional and structural diversity.[1,5,6]

It is now clear that several rare and seemingly dissimilar human diseases are attributable to defects in the basic process of Fe-S cluster biogenesis, including Friedreich's ataxia (FRDA), ISCU myopathy, and multiple mitochondrial dysfunctions syndrome.[2] Although those disease affect different tissues, all of them seem to be caused by mutations in proteins which causes defect in the main [Fe-S] cluster biogenesis pathway.[2-4]

1.1.2 Common types of clusters

Multiple types of nature [Fe-S] clusters were discovered, of which the most common type of biological [Fe-S] clusters in proteins are [4Fe-4S] clusters, followed by [2Fe-2S] clusters and [3Fe-4S] clusters (Figure 1.1).[2] Others in which a single iron atom was tetrahedrally coordinated by four

cysteines known as rubredoxin, and more complex structures were found in enzymes such as nitrogenase and hydrogenase.[1,5] In most of the case, the iron atoms ligated by protein-derived cysteine thiols and inorganic sulfide ions in tetrahedral geometry to form the clusters, nevertheless, histidine and arginine ligation has also been observed in some kinds of proteins, for example, mitoNEET.[1,12-31]
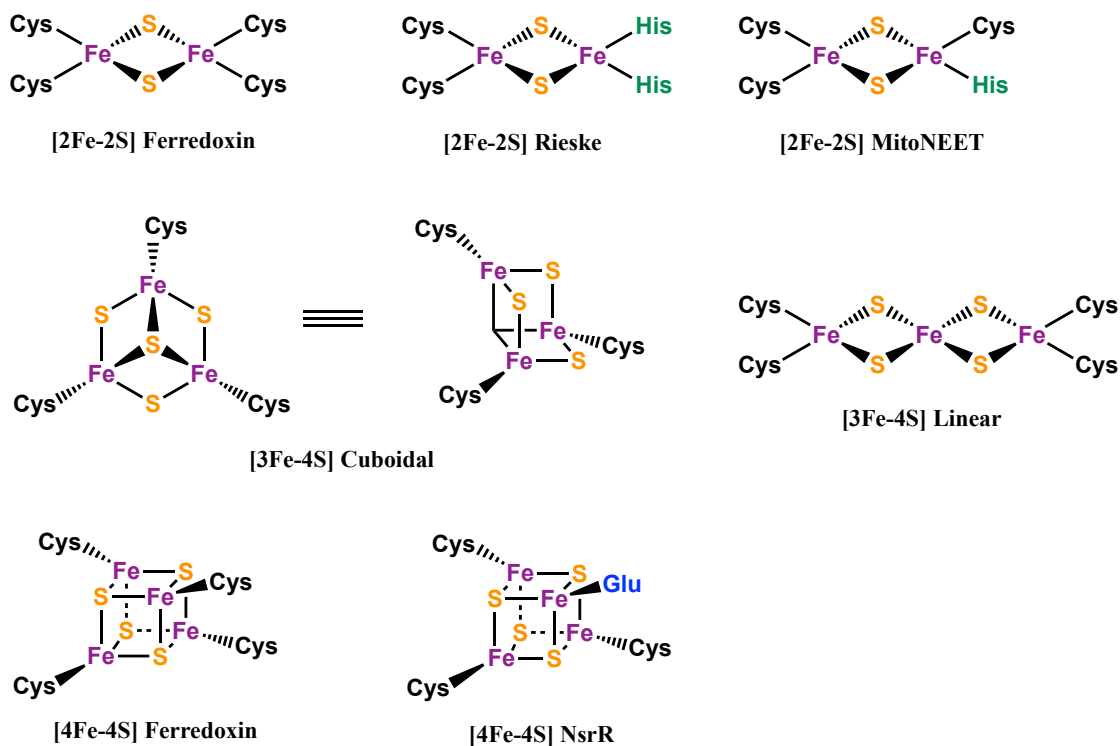
Figure 1.1 Common types of [Fe-S] clusters found in proteins.

Started from 1970s, many structural analogues of [Fe-S] clusters were able to synthesize and characterize, leading us go insight into how the active sites in metalloenzymes operate at the molecular level (Figure 1.2).[5]
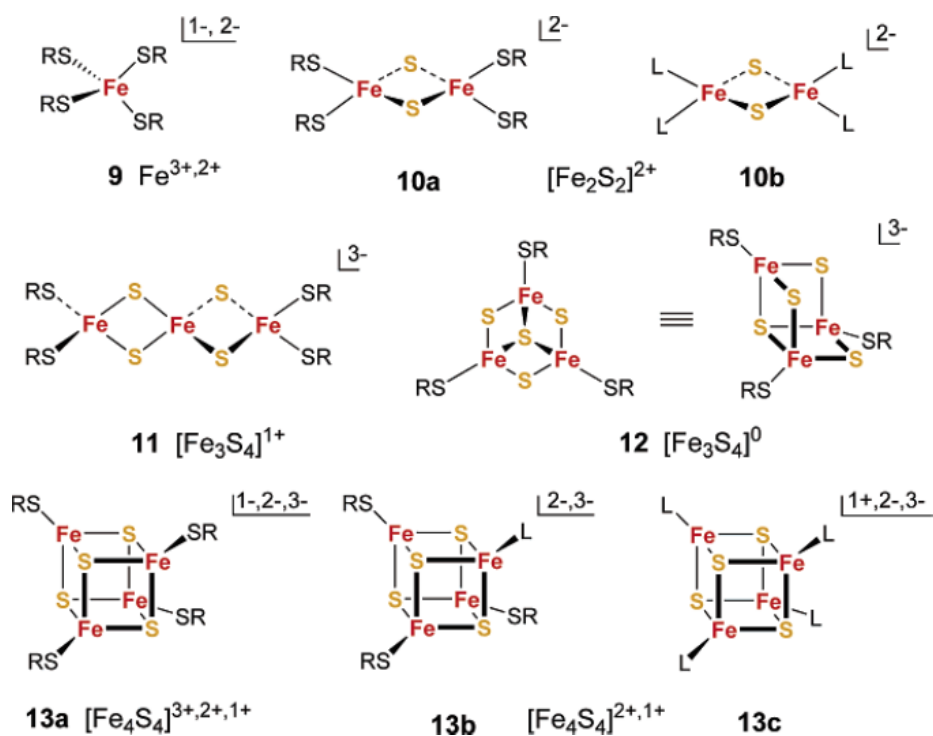
Figure 1.2 Synthetic analogues of protein sites containing one (9), two (10a), three (11, 12), and four (13ab) iron atoms. Adapted from *Rao VP, Holm RH, Chem Rev. 2004, 104, 527–559.*

1.1.3 Synthetic Analogues of [Fe-S] Cluster

The synthetic analogue approach to the metal sites in iron-sulfur proteins was initiated in the early 1970s, and after decades of development it is now a mature research area.[1,5-9] The preparation method and the stability of these clusters as a function of their nuclearity and of the nature, size, and reactivity of terminal ligands was investigated by the Holm group and by many others, with a variety of excellent reviews having appeared.[5,6] We are now reaching a stage where the laboratory synthesis of Fe-S-based clusters with different nuclearities, topologies, and composition are known and the common synthetic methodologies are established for these clusters. Here, we introduce four methodologies that are considered to possess significant pragmatic value.

A. Self-Assembly

The term self-Assembly here refers to the spontaneous reaction in which the assembly of the product clusters is from simple mononuclear precursors (metal salt, core ligand, and terminal ligand precursors).[7] In general, the most popular binuclear and tetranuclear type of [Fe-S] clusters are prepared from methanolic mixtures of $FeCl_3$, RS^-, and HS^-, and the clusters being isolated in high yields after the addition of $[NR_4]^+$ salts to the reaction mixture.[7-9] Reaction 1-4 are common methods for synthesizing simple [2Fe-2S] and [4Fe-4S] clusters.

$$2FeCl_3 + 4RS^- + 2HS^- + 2MeO^- \rightarrow [Fe_2S_2(SR)_4]^{2-} + 6Cl^- + 2MeOH \qquad (1)$$

$$4FeCl_3 + 6RS^- + 4HS^- + 4MeO^- \rightarrow [Fe_4S_4(SR)_4]^{2-} + RSSR + 12Cl^- + 4MeOH \quad (2)$$

$$4FeCl_2 + 10RS^- + 4S \rightarrow [Fe_4S_4(SR)_4]^{2-} + 3RSSR + 8Cl^- \qquad (3)$$

$$4FeCl_3 + 14RS^- + 4S \rightarrow [Fe_4S_4(SR)_4]^{2-} + 5RSSR + 12Cl^- \qquad (4)$$
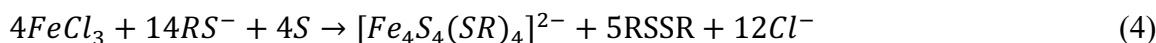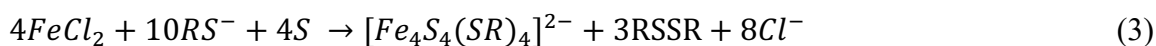
B. Fragment Condensation

In this method, a preexisting cluster is combined with itself or with another mononuclear or polynuclear species to form (usually) higher nuclearity clusters; ideally, product composition and structure are predictable from precursors.[5,7]

$$2[Fe_2S_2(SR)_4]^{2-} \rightarrow [Fe_4S_4(SR)_4]^{2-} + 2RS^- + 4RSH \qquad (5)$$

$$2[Fe(SR)_4]^{2-} + 2S \rightarrow [Fe_2S_2(SR)_4]^{2-} + RSSR + 2RS^- \qquad (6)$$

$$2[Fe(SR)_4]^- + 2S \rightarrow [Fe_2S_2(SR)_4]^{2-} + 2RSSR \qquad (7)$$
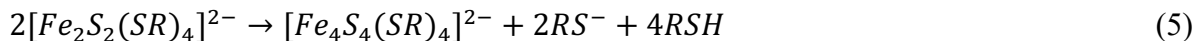
Since $[Fe_4S_4]^{2+}$ is evidently more stable structure than $[Fe_2S_2]^{2+}$, with monodentate thiolates, reaction 2 is always more preferred than reaction 1, leading to the formation of $[Fe_4S_4(SR)_4]^{2-}$, reactions 6 and 7 are more useful method to obtain $[Fe_2S_2(SR)_4]^{2-}$.[5,10]

C. Ligand Substitution

In general, ligand substitution involves the exchange of one kinds of terminal ligands for another, with no change at the cluster core center structure. Ligand substitution is usually an equilibrium reaction but it can be fully displaced to product by a sufficient excess of reactant thiol and/or removal of product thiol from the reaction mixture.[5]

$$[Fe_2S_2(SR)_4]^{2-} + 4R'SH \rightleftharpoons [Fe_2S_2(SR')_4]^{2-} + 4RSH \tag{8}$$

$$[Fe_2S_2X_4]^{2-} + 4RS^- \rightleftharpoons [Fe_2S_2(SR)_4]^{2-} + 4X^- \tag{9}$$

$$[Fe_4S_4(SR)_4]^{2-} + 4R'SH \rightleftharpoons [Fe_4S_4(SR')_4]^{2-} + 4RSH \tag{10}$$

$$[Fe_4S_4X_4]^{2-} + nRS^- \rightleftharpoons [Fe_4S_4X_{4-n}(SR)_n]^{2-} + nX^- \tag{11}$$
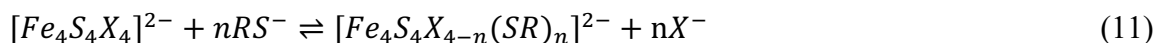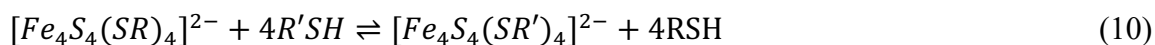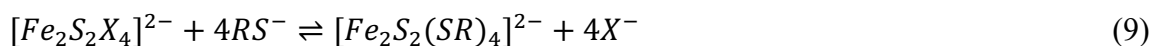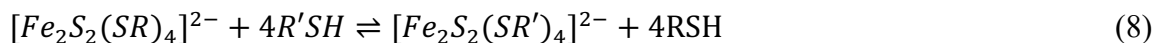
Reaction 8-11 has proven extremely useful in expanding the scope of synthetic [2Fe-2S] and [4Fe-4S] analogues.

D. Core Rearrangement and Fragmentation

Core rearrangement method allows the transformation of a preexisting cluster to a different core geometry while retaining the original nuclearity using thermal treatment, oxidation−reduction, or ligand substitution or addition (Figure 1.3).[5,7]
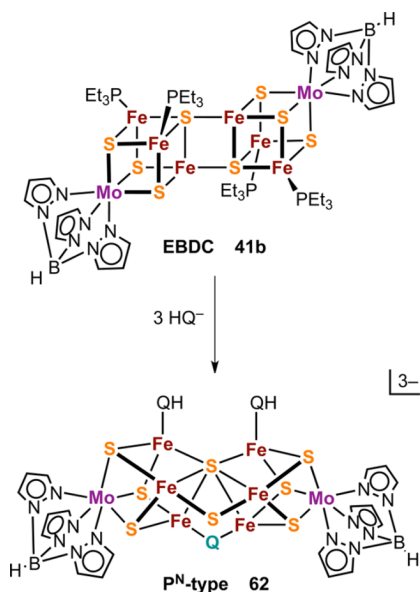
Figure 1.3 Core rearrangement of EBDC 41b to the PN-type cluster 62 by reaction with the external nucleophiles HQ− (Q = S, Se). Adapted from *Sonny C. Lee et al. Chem. Rev. 2014, 114, 3579−3600.*

Fragmentation, as the name suggests, means the transformation of a preexisting cluster to a lower nuclearity product. This reaction type is the reverse of fragment condensation. However, since high nuclearity cluster is usually the desired objective in cluster synthesis, fragmentation is not commonly used compared with the methods mentioned before.[5,8,9]

1.1.4 Cluster Conversions

One important property of iron-sulfur cluster species is their unusual ability to interconvert between structures, which means in a single or multistep process, an iron−sulfur cluster core can convert to another core without retention of composition and nuclearity.[1,5-9] The first observed example of cluster conversion was the spontaneous binuclear to tetranuclear conversion

$[Fe_2S_2(SPh)_4]^{2-} \rightarrow [Fe_4S_4(SPh)_4]^{2-}$ during the study of removal of cores from holoproteins in the form of their benzenethiolate analogues, and with the further study, many different types of synthetic cluster conversion processes have been identified and explained.[6,11] Synthetic cluster conversion reactions are schematically summarized in Figure 1.4.

Figure 1.4 Cluster conversion scheme for [Fe-S] cluster. Adapted from *Rao VP, Holm RH, Chem Rev. 2004, 104, 527–559.*

Clusters containing the cubane-type Fe4S4 core play a central role in conversion chemistry. Among all the reactions listed, conversions $[Fe_2S_2]^{2+} \leftrightarrow [Fe_4S_4]^{2+}$, the first established iron−sulfur core conversions of any type, are also the most common and important of core conversions in biological functions.[5,6] Interconversion between tetranuclear and binuclear conversion is widespread and has been well documented for a number of proteins, including nitrogenase protein, the FNR transcription factor etc.[11]

1.2 Reactivity of Fe-S Cluster with Signaling Molecule

The inherent chemical properties of Fe-S clusters uniquely position them as sensors for stress induced by reactive oxygen species and reactive nitrogen species (Figure 1.5). These Fe-S clusters, integral to a multitude of enzymatic processes, exhibit a profound sensitivity to changes in the cellular redox environment.[1,5,12-17] Their interactions with O_2 and NO not only underscore the dynamic nature of cellular metabolic pathways but also highlight the delicate balance organisms maintain in response to oxidative and nitrosative stresses.[13,17]
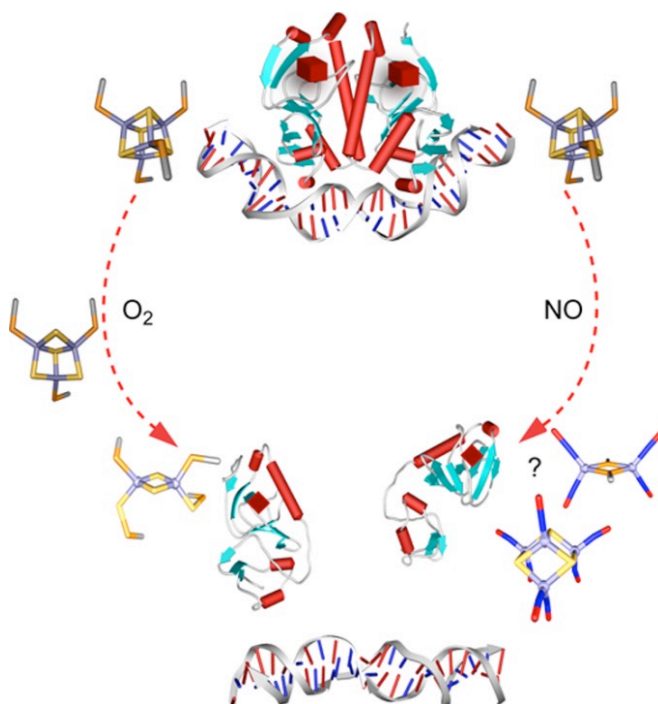
Figure 1.5 E. coli FNR and its reaction with O2 and NO. Obtained from *Jason C. Crack et al. Acc. Chem. Res. 2014, 47, 3196−3205*

1.2.1 Conversion of [4Fe-4S] to [2Fe-2S] by O_2 in FNR

Iron−sulfur clusters are susceptible to damage from redox reactions with reactive oxygen species, like molecular oxygen (O_2), which can lead to cluster interconversion or partial or complete loss of iron.[1,5,13,17] This property is utilized by several regulatory proteins that function as sensors of reactive oxygen species, enabling cells to respond to changing external conditions. J.C Crack *et al.* used a combined strategy of in vivo and in vitro studies to explore O_2 reaction mechanism of iron−sulfur cluster in an O_2-sensing DNA-binding protein called FNR.[13] Experiments show that when expose to O_2, the [4Fe-4S] cluster within the DNA-binding dimeric FNR quickly converts to a persulfide-coordinated [2Fe-2S] form, leading to protein

monomerization and the loss of DNA binding ability. Spectroscopic evidence suggests that the cluster conversion involves two-step process via a transient formation of $[3Fe\text{-}4S]^+$ intermediate as shown in Figure 1.6.[13,18]

Step 1
$[4Fe\text{-}4S]^{2+} + O_2 \rightarrow [3Fe\text{-}4S]^{1+} + Fe^{2+} + O_2^-$
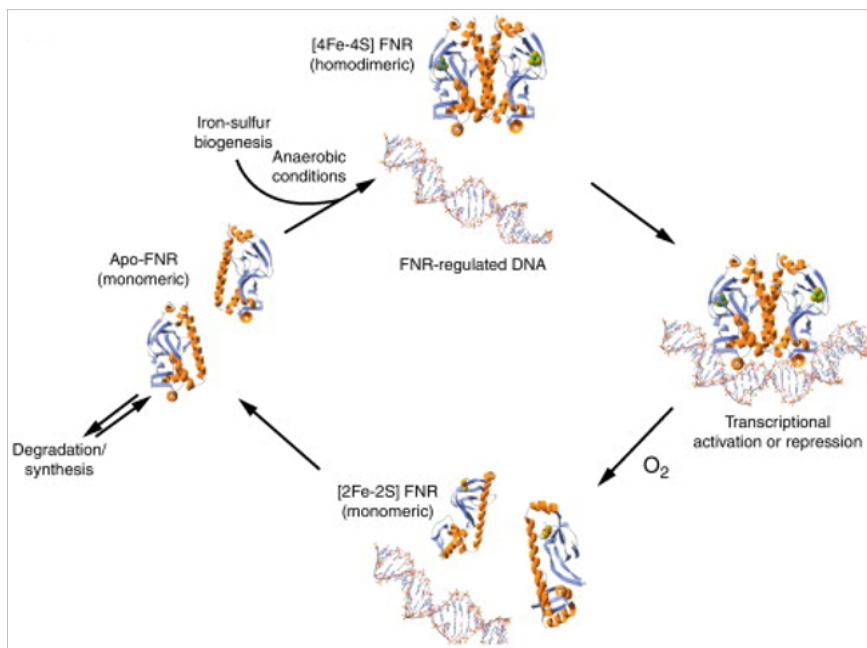
Step 2
$[3Fe\text{-}4S]^{1+} \rightarrow [2Fe\text{-}2S]^{2+} + Fe^{3+} + 2S^{2-}$

Step 2 - one persulfide ligand reaction
$[3Fe\text{-}4S](CysS)_3 + CysS^- + O_2 + 2H^+ \rightarrow [2Fe\text{-}2S](CysS)_3(CysSS) + Fe^{3+} + S^{2-} + H_2O_2$

Step 2 - two persulfide ligand reaction
$[3Fe\text{-}4S](CysS)_3 + CysS^- + O_2 + 4H^+ \rightarrow [2Fe\text{-}2S](CysS)_2(CysSS)_2 + Fe^{3+} + 2H_2O$

Overall reaction
$[4Fe\text{-}4S](CysS)_4 + nO_2 \rightarrow [2Fe\text{-}2S](CysS)_2(CysSS)_2 + Fe^{2+} + Fe^{3+} + \text{reduced } O_2 \text{ species}$
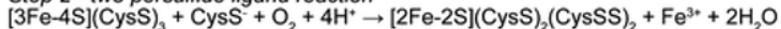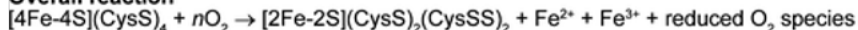
Figure 1.6 O_2 sensing by FNR. Obtained from *Jason C. Crack et al. Current opinion in chemical biology, 2012, 16(1-2), 35-44.*

Synthetic modeling of FNR's cluster conversion by O_2 is a difficult task because most [Fe-S] clusters decompose in aerobic conditions. The first example came from Holm and coworkers using

an outer sphere oxidant, ferricenium, to convert model cluster $[Fe_4S_4Cl_4]^{2-}$ to $[Fe_2S_2Cl_2]^{2-}$ (Scheme 1.1A).[19] More recently, a report by Tatsumi showed that the conversion between $[4Fe-4S]^0$ and $[2Fe-2S]^0$ is possible with clusters bearing amide ligands: $2 [Fe_2S_2\{N(SiMe_3)_2\}_2(py)_2] \leftrightarrow [Fe_4S_4\{N(SiMe_3)_2\}_4] + 4$ py, where py = pyridine. In this reaction, both species remain all-ferric and the cluster interconversion is facilitated by reversible binding of pyridine (Scheme 1.1B).[20]
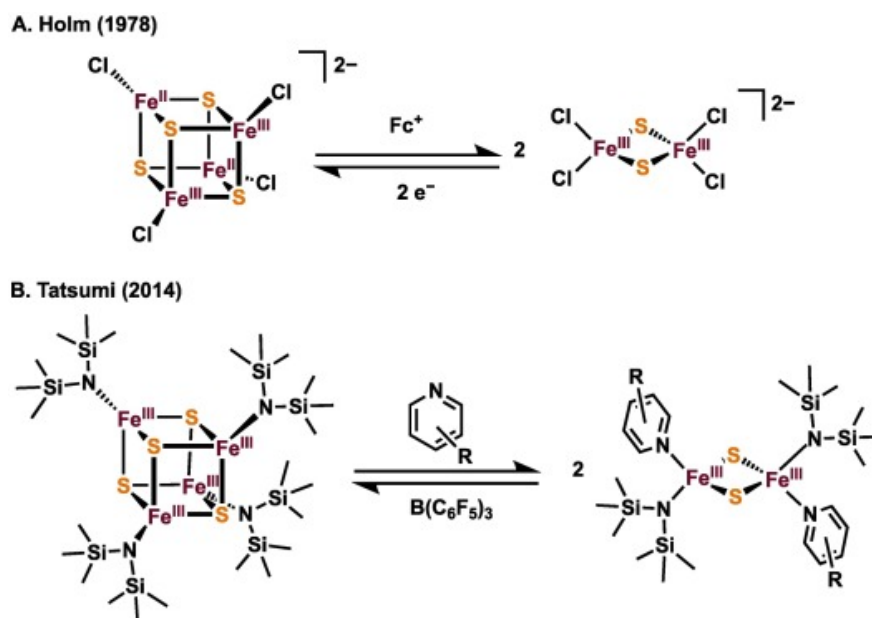
Scheme 1.1 Synthetic cluster conversions

1.2.2 NO Sensing by [Fe-S] proteins

Nitric oxide (NO), a reactive, membrane permeable radical, plays important roles in many biological processes.[13-15] As signaling molecule in living organisms, the major targets for NO are metal cofactors, and iron−sulfur proteins are especially susceptible to NO-induced damage. A number of iron−sulfur regulators have evolved to function as NO sensors.[12-20] Normally, the

reaction of [Fe-S] cluster and NO will lead to the cluster degradation, converting to various iron nitrosyl species.

1.2.2.1 Nitrosylation of Protein-Bound Fe-S Clusters

SoxR is a transcriptional regulator protein that contains a [2Fe-2S] cluster. Upon reaction with nitric oxide (NO), SoxR undergoes a transformative activation process.[21] This process is characterized by a direct modification of the [2Fe-2S] centers within SoxR, leading to the formation of protein-bound dinitrosyl-iron adducts, $[Fe(NO)_2(RS)_2]^-$ (DNIC), where RS^- are cysteine residues (Table 1.1).[21,22] This chemical modification plays a pivotal role in the functional activation of SoxR, propelling it to express a robust assembly of over 40 defense genes that encode proteins with antioxidant, metabolic, and repair functions.[22-25]

Protein	Cluster type	Function	Identified Fe nitrosyl species
SoxR	[2Fe-2S]	Redox/O$_2$ stress sensor	DNIC
FNR	[4Fe-4S]	Global regulator O$_2$ sensor in a wide range of bacteria. Secondary function in NO sensing.	DNIC (minor species); RRE; Persulfide RRE; Dimerized RRE; RRE-like (major species)
WBl	[4Fe-4S]	Key roles in cell developmental processes in actinomycetes	
Ferredoxin	[4Fe-4S]	Electron donor to the hydrogenase	RBS-like (major species); RBS
NsrR	[4Fe-4S]	Global regulator of NO stress response	RBE
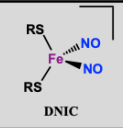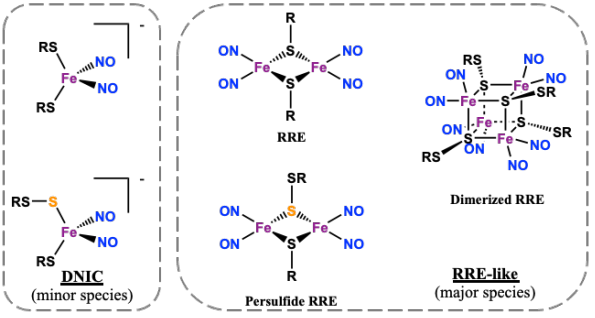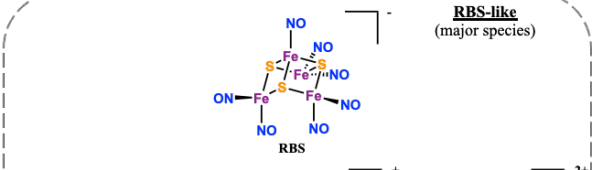
Table 1.1 Regulatory [Fe-S] proteins and the identified Fe species after nitrosylation.

Dinitrosyl iron complex [Fe(NO)$_2$(RS)$_2$]$^-$ (DNIC), have been widely reported in previous literatures as the product of [Fe-S] cluster nitrosylation.[21,25,26] This mainly because the intrinsic paramagnetic characteristics of DNICs, which exhibit a magnetic moment (S=1/2) that results in a distinct and readily detectable electron paramagnetic resonance (EPR) signal at g=2.03.[26] However, in the case of [4Fe-4S] protein, quantification of the EPR after the nitrosylation indicates DNIC is only a minor product and there other EPR silent iron nitrosyl species exist.[13,18] EPR and spectroscopic studies on the [4Fe−4S] cluster-containing Wbl proteins, WhiD from *S. coelicolor* and WhiB1 from *M. tuberculosis*, shows that the stepwise nitrosylation reaction on additions up

to 8 equivalent NO, yielding an EPR-silent product, $[Fe_2(NO)_4(SR)_2]$, known as Roussin's red ester (RRE) as final product (Table 1.1).[27] The reaction of NO with *E. Coli* FNR [4Fe-4S] cluster gives similar spectra.[30] In the case of WhiD, it was proposed that if two RRE species are formed in close proximity, two RRE could dimerize affording a tetranuclear species composed of 4 irons bridged by cysteine residues and each iron bound by 2 NO.[27] The formation of RRE can also be observed during the reaction of NO with [2Fe-2S] ferredoxin from spinach in the presence of trace amounts of O_2.[23,24] In this scenario, oxygen plays a pivotal role by effectively trapping the thiolates that are liberated during the dimerization of two DNICs, leading to the formation of a RRE.[23,30,42]

Another EPR silent iron nitrosyl species, Roussin's Black Salt (RBS $[Fe_4(NO)_7(S)_3]^-$), has been identified as the principal product from the nitrosylation of *P. furiosus* [4Fe-4S] ferredoxin, as confirmed by Nuclear Resonance Vibrational (NRV) spectroscopic studies (Table 1.1).[31] Recent investigations employing a combination of Mössbauer spectroscopy, NRVS, and Density Functional Theory (DFT) on WhiD and NsrR (both sourced from *S. coelicolor*) have confirmed the formation of multiple products that bear structural resemblances to RRE and RBS upon nitrosylation.[27] However, in these instances, the absence of $^{32}S/^{34}S$ shifts in the Fe-S regions of the NRVS spectra negated the formation of authentic RBS. Instead, a novel Roussin's Black Ester (RBE) species was proposed, characterized by the substitution of one or more bridging sulfides of RBS with Cys thiolates (Table 1.1). This intricate interplay of structural modifications sheds light on the diverse array of products resulting from the nitrosylation of iron-sulfur clusters.

1.2.2.2 Nitrosylation of Synthetic model Fe-S Clusters

NO reactivity with both synthetic small molecule thiolate bound [2Fe-2S] and [4Fe-4S] models have been reported.[14,32] With synthetic [2Fe-2S] systems, the reaction with reaction of excess NO in the present of at least 2 equivalent of thiolate is sufficient to allow full conversion to the corresponding DNIC (Scheme 1.2 Top).[14] In the case of [4Fe-4S] cluster, although $[Fe_4S_4(NO)_4]^-$ species was observed as an intermediate with the site differentiated models, the reaction between NO and [4Fe-4S] complexes formed RBS in all cases without adding thiolate (Scheme 1.2 Bottom). With additional thiolate are present, the corresponding DNIC is observed as the sole nitrosylated product.[14] During these reported nitrosylation, the bridging sulfide could get oxidized form S^{2-} to S^0, giving elemental sulfur (S_x) side products or just released as sulfide (S^{2-}). Recently, our group reported H_2S is also a likely reaction product generated from nitrosylation of synthetic [2Fe-2S] clusters in the precent of H· (e-/H+) donor (Scheme 1.2 Top). These results were interpreted as evidence for the possibility that crosstalk exists between the biological signaling of NO and H_2S, the latter being a gaseous signaling molecule that is coming to be implicated in a growing number of biological processes.[15]
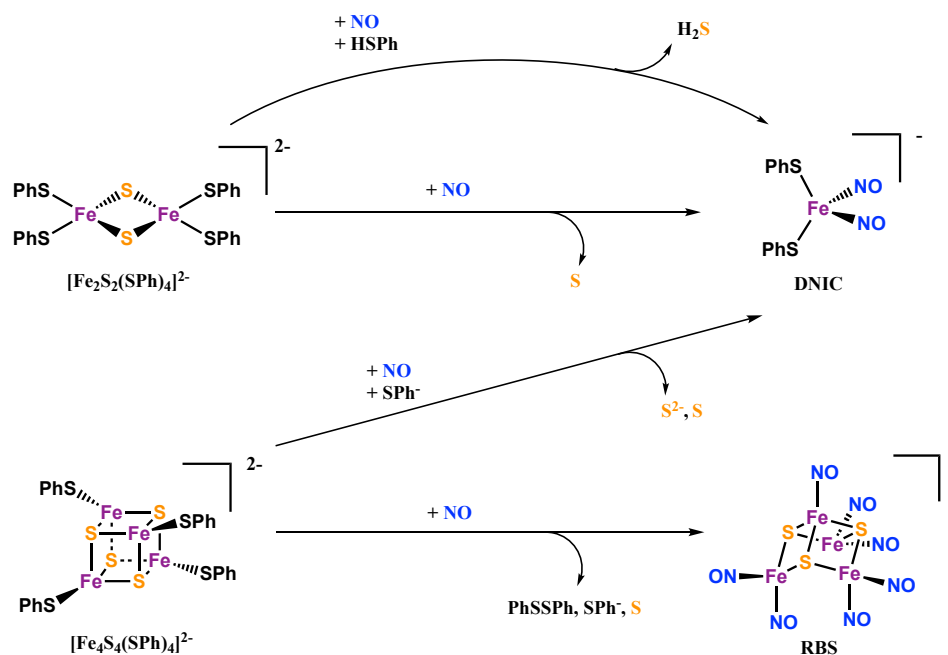
Scheme 1.2 Synthetic Fe-S clusters with NO reaction

1.3 Repair of Fe-S Cluster

As described above, high level of O_2 can convert the [4Fe-4S] cluster in FNR to a [2Fe-2S] cluster, triggering a protein conformational change.[13,33-36] The [2Fe-2S]-FNR slowly degrades further to form apo-protein which can import a newly biosynthesized [4Fe-4S] cluster. However, a direct repair from [2Fe-2S]-FNR to [4Fe-4S] is also possible (Scheme 1.3 Top). It's observed that after O_2 exposure, bridging sulfides from the [4Fe-4S] cluster, remain intact within the persulfide-coordinated [2Fe-2S]-FNR. This arrangement is conducive to a direct repair back to the [4Fe-4S] cluster, facilitated by addition of Fe2+ and dithiothreitol (DTT).[13,37]
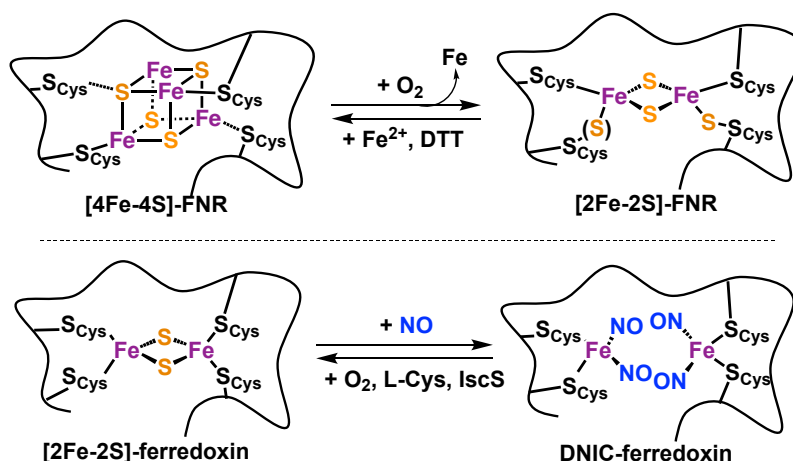
Scheme 1.3 Examples of Fe-S protein repair

Much less is known about the repair of nitrosylated [Fe-S] clusters. The nitrosylated SoxR, DNIC-SoxR, exhibits pronounced stability under in vitro conditions.[21] However, it reverts efficiently to its original SoxR form, maintaining the [2Fe-2S] cluster in vivo upon NO removal (Scheme 1.3 Botttom).[21] But the exact mechanisms of SoxR repair, be it through a *de novo* synthesis of the [2Fe-2S] cluster or via a direct repair like FNR, remain elusive. Dedicated biochemical studies on another [2Fe-2S] protein, ferredoxin (Fdx), indicate that DNIC-Fdx can be restored to its pristine [2Fe-2S]-Fdx form using L-cysteine, O2, and cysteine desulfurase (IscS) in vitro, without the need for supplemental Fe.[24,38,39] These results suggest that a direct repair pathway for DNIC-SoxR, along with other nitrosylated [Fe-S] proteins, might indeed be feasible.

1.4 Research Objectives

While a considerable effort has been made to identify iron nitrosyl products derived from the reaction of Fe-S proteins with NO, the fate of the bridging sulfides during the reaction has been rarely investigated. Furthermore, the precise nature of the iron-nitrosyl products generated from

18

NO-sensing [4Fe-4S] regulatory proteins still remain a mystery. The work presented in this thesis focus on synthetic modeling systems designed to proffer molecular insights into pivotal biochemical transformations involving Fe-S clusters. Chapter 3 describes the construction of Fe-S core by persulfide using Salen-supported model system. Chapter 4 pivots towards the ability of persulfide in repairing NO-damanged Fe-S cluster. Proceeding to chapter 5, an exploration of the NO chemistry of [4Fe-4S] clusters is undertaken. Finally, chapter 6 unravels the intricacies of the conversion of [4Fe-4S] clusters to [2Fe-2S] under the influence of oxidation.

1.5 References

(1) Beinert, H.; Holm, R. H.; Münck, E. Münck E: Iron-Sulfur Clusters: Nature's Modular, Multipurpose Structures. *Science* **1997**, *277* (5326), 653–659.

(2) Rouault, T. A. Biogenesis of Iron-Sulfur Clusters in Mammalian Cells: New Insights and Relevance to Human Disease. *Dis. Model. Mech.* **2012**, *5* (2), 155–164. https://doi.org/10.1242/dmm.009019.

(3) Cardenas-Rodriguez, M.; Chatzi, A.; Tokatlidis, K. Iron-Sulfur Clusters: From Metals through Mitochondria Biogenesis to Disease. *J. Biol. Inorg. Chem.* **2018**, *23* (4), 509–520. https://doi.org/10.1007/s00775-018-1548-6.

(4) Lill, R. Function and Biogenesis of Iron–Sulphur Proteins. *Nature* **2009**, *460* (7257), 831–838. https://doi.org/10.1038/nature08301.

(5) Venkateswara, R. P.; Holm, R. H. Synthetic Analogues of the Active Sites of Iron− Sulfur Proteins. *Chem. Rev* **2004**, *104*, 527–559.

(6) Holm, R. H.; Lo, W. Structural Conversions of Synthetic and Protein-Bound Iron−Sulfur Clusters. *Chem. Rev* **2016**, *116*, 13685–13713.

(7) Lee, S. C.; Lo, W.; Holm, R. H. Developments in the Biomimetic Chemistry of Cubane-Type and Higher Nuclearity Iron-Sulfur Clusters. *Chem. Rev.* **2014**, *114* (7), 3579–3600. https://doi.org/10.1021/cr4004067.

(8) Mayerle, J. J.; Frankel, R. B.; Holm, R. H.; Ibers, J. A.; Phillips, W. D.; Weiher, J. F. Synthetic Analogs of the Active Sites of Iron-Sulfur Proteins. Structure and Properties of Bis [o-Xylyldithiolato-M2-Sulfidoferrate (III)], an Analog of the 2Fe-2S Proteins. *Proc. Natl. Acad. Sci. U.S.A* **1973**.

(9) Mayerle, J. J.; Denmark, S. E.; Depamphilis, B. V.; Ibers, J. A.; Holm, R. H. Synthetic Analogs of the Active Sites of Iron-Sulfur Proteins. XI. Synthesis and Properties of Complexes Containing the Iron Sulfide (Fe2S2) Core and the Structures of Bis [o-Xylyl-. Alpha.,. Alpha.'-Dithiolato-. Mu.-Sulfido-Ferrate (III)] and Bis [p-Tolylthiolato-. Mu.-Sulfido-Ferrate (III)] Dianions. *J. Am. Chem. Soc* **1975**.

(10) Han, S.; Czernuszewicz, R. S.; Spiro, T. G. Convenient Synthetic Route to [Fe2S2 (SR) 4] 2-via Reaction of [Fe (SR) 4]-with Sulfur. *Inorg. Chem* **1986**.

(11) Cambray, J.; Lane, R. W.; Wedd, A. G.; Johnson, R. W.; Holm, R. H. Chemical and Electrochemical Interrelationships of the 1-Fe, 2-Fe, and 4-Fe Analogs of the Active Sites of Iron-Sulfur Proteins. *Inorg. Chem.* **1977**, *16* (10), 2565–2571. https://doi.org/10.1021/ic50176a030.

(12) Henderson, R. Proton Transfer to Synthetic Fe–S-Based Clusters. *Coord. Chem. Rev.* **2005**, *249* (17–18), 1841–1856. https://doi.org/10.1016/j.ccr.2004.12.021.

(13) Crack, J. C.; Green, J.; Thomson, A. J.; Le Brun, N. E. Iron-Sulfur Clusters as Biological Sensors: The Chemistry of Reactions with Molecular Oxygen and Nitric Oxide. *Acc. Chem. Res.* **2014**, *47* (10), 3196–3205. https://doi.org/10.1021/ar5002507.

(14) Harrop, T. C.; Tonzetich, Z. J.; Reisner, E.; Lippard, S. J. Reactions of Synthetic [2Fe-2S] and [4Fe-4S] Clusters with Nitric Oxide and Nitrosothiols. *J. Am. Chem. Soc.* **2008**, *130* (46), 15602–15610. https://doi.org/10.1021/ja8054996.

(15) Tran, C. T.; Williard, P. G.; Kim, E. Nitric Oxide Reactivity of [2Fe-2S] Clusters Leading to H2S Generation. *J. Am. Chem. Soc.* **2014**, *136* (34), 11874–11877. https://doi.org/10.1021/ja505415c.

(16) Fitzpatrick, J.; Kim, E. Synthetic Modeling Chemistry of Iron−Sulfur Clusters in Nitric Oxide Signaling, Acc. *Acc. Chem. Res* **2015**, *48*, 2453–2461.

(17) Singh, A.; Guidry, L.; Narasimhulu, K. V.; Mai, D.; Trombley, J.; Redding, K. E.; Giles, G. I.; Lancaster, J. R., Jr; Steyn, A. J. C. Mycobacterium Tuberculosis WhiB3 Responds to O2 and Nitric Oxide via Its [4Fe-4S] Cluster and Is Essential for Nutrient Starvation Survival. *Proc. Natl. Acad. Sci. U. S. A.* **2007**, *104* (28), 11562–11567. https://doi.org/10.1073/pnas.0700490104.

(18) Crack, J. C.; Green, J.; Thomson, A. J.; Le Brun, N. E. Iron-Sulfur Cluster Sensor-Regulators. *Curr. Opin. Chem. Biol.* **2012**, *16* (1–2), 35–44. https://doi.org/10.1016/j.cbpa.2012.02.009.

(19) Wong, G. B.; Bobrik, M. A.; Holm, R. H. Inorganic Derivatives of Iron Sulfide Thiolate Dimers and Tetramers: Synthesis and Properties of the Halide Series 2− and 2− (X = Cl, Br, I). *Inorg. Chem* **1978**, *17*, 578–584.

(20) Tanifuji, K.; Yamada, N.; Tajima, T.; Sasamori, T.; Tokitoh, N.; Matsuo, T.; Tamao, K.; Ohki, Y.; Tatsumi, K. A Convenient Route to Synthetic Analogues of the Oxidized Form of High-

Potential Iron-Sulfur Proteins. *Inorg. Chem.* **2014**, *53* (8), 4000–4009. https://doi.org/10.1021/ic402890k.

(21) Ding, H.; Demple, B. Direct Nitric Oxide Signal Transduction via Nitrosylation of Iron-Sulfur Centers in the SoxR Transcription Activator. *Proc. Natl. Acad. Sci. U. S. A.* **2000**, *97* (10), 5146–5150. https://doi.org/10.1073/pnas.97.10.5146.

(22) Imlay, J. A. Transcription Factors That Defend Bacteria against Reactive Oxygen Species. *Annu. Rev. Microbiol.* **2015**, *69* (1), 93–108. https://doi.org/10.1146/annurev-micro-091014-104322.

(23) Grabarczyk, D. B.; Ash, P. A.; Vincent, K. A. Infrared Spectroscopy Provides Insight into the Role of Dioxygen in the Nitrosylation Pathway of a [2Fe2S] Cluster Iron-Sulfur Protein. *J. Am. Chem. Soc.* **2014**, *136* (32), 11236–11239. https://doi.org/10.1021/ja505291j.

(24) Rogers, P. A.; Ding, H. L-Cysteine-Mediated Destabilization of Dinitrosyl Iron Complexes in Proteins. *J. Biol. Chem.* **2001**, *276* (33), 30980–30986. https://doi.org/10.1074/jbc.M101037200.

(25) Tinberg, C. E.; Tonzetich, Z. J.; Wang, H.; Do, L. H.; Yoda, Y.; Cramer, S. P.; Lippard, S. J. Characterization of Iron Dinitrosyl Species Formed in the Reaction of Nitric Oxide with a Biological Rieske Center. *J. Am. Chem. Soc.* **2010**, *132* (51), 18168–18176. https://doi.org/10.1021/ja106290p.

(26) Reddy, D.; Lancaster, J. R., Jr; Cornforth, D. P. Nitrite Inhibition of Clostridium Botulinum: Electron Spin Resonance Detection of Iron-Nitric Oxide Complexes. *Science* **1983**, *221* (4612), 769–770. https://doi.org/10.1126/science.6308761.

(27) Serrano, P. N.; Wang, H.; Crack, J. C.; Prior, C.; Hutchings, M. I.; Thomson, A. J.; Kamali, S.; Yoda, Y.; Zhao, J.; Hu, M. Y.; Alp, E. E.; Oganesyan, V. S.; Le Brun, N. E.; Cramer, S. P. Nitrosylation of Nitric-oxide-sensing Regulatory Proteins Containing [4Fe-4S] Clusters Gives Rise to Multiple Iron–Nitrosyl Complexes. *Angew. Chem. Int. Ed Engl.* **2016**, *55* (47), 14575–14579. https://doi.org/10.1002/anie.201607033.

(28) Crack, J. C.; Svistunenko, D. A.; Munnoch, J.; Thomson, A. J.; Hutchings, M. I.; Le Brun, N. E. Differentiated, Promoter-Specific Response of [4Fe-4S] NsrR DNA Binding to Reaction with Nitric Oxide. *J. Biol. Chem.* **2016**, *291* (16), 8663–8672. https://doi.org/10.1074/jbc.M115.693192.

(29) Volbeda, A.; Dodd, E. L.; Darnault, C.; Crack, J. C.; Renoux, O.; Hutchings, M. I.; Le Brun, N. E.; Fontecilla-Camps, J. C. Crystal Structures of the NO Sensor NsrR Reveal How Its Iron-Sulfur Cluster Modulates DNA Binding. *Nat. Commun.* **2017**, *8* (1), 15052. https://doi.org/10.1038/ncomms15052.

(30) Crack, J. C.; Stapleton, M. R.; Green, J.; Thomson, A. J.; Le Brun, N. E. Mechanism of [4Fe-4S](Cys)4 Cluster Nitrosylation Is Conserved among NO-Responsive Regulators. *J. Biol. Chem.* **2013**, *288* (16), 11492–11502. https://doi.org/10.1074/jbc.M112.439901.

(31) Tonzetich, Z. J.; Wang, H.; Mitra, D.; Tinberg, C. E.; Do, L. H.; Jenney, F. E., Jr; Adams, M. W. W.; Cramer, S. P.; Lippard, S. J. Identification of Protein-Bound Dinitrosyl Iron Complexes

by Nuclear Resonance Vibrational Spectroscopy. *J. Am. Chem. Soc.* **2010**, *132* (20), 6914–6916. https://doi.org/10.1021/ja101002f.

(32) Holm, R. H.; Lo, W. Structural Conversions of Synthetic and Protein-Bound Iron–Sulfur Clusters. *Chem. Rev.* **2016**, *116* (22), 13685–13713. https://doi.org/10.1021/acs.chemrev.6b00276.

(33) Hyduke, D. R.; Jarboe, L. R.; Tran, L. M.; Chou, K. J. Y.; Liao, J. C. Integrated Network Analysis Identifies Nitric Oxide Response Networks and Dihydroxyacid Dehydratase as a Crucial Target in Escherichia Coli. *Proc. Natl. Acad. Sci. U. S. A.* **2007**, *104* (20), 8484–8489. https://doi.org/10.1073/pnas.0610888104.

(34) Engel, P.; Trageser, M.; Unden, G. Reversible Interconversion of the Functional State of the Gene Regulator FNR from Escherichia Coli in Vivo by O2 and Iron Availability. *Arch. Microbiol.* **1991**, *156* (6), 463–470. https://doi.org/10.1007/bf00245393.

(35) Mettert, E. L.; Kiley, P. J. ClpXP-Dependent Proteolysis of FNR upon Loss of Its O2-Sensing [4Fe–4S] Cluster. *J. Mol. Biol.* **2005**, *354* (2), 220–232. https://doi.org/10.1016/j.jmb.2005.09.066.

(36) Dibden, D. P.; Green, J. In Vivo Cycling of the Escherichia Coli Transcription Factor FNR between Active and Inactive States. *Microbiology* **2005**, *151* (12), 4063–4070. https://doi.org/10.1099/mic.0.28253-0.

(37) Zhang, B.; Crack, J. C.; Subramanian, S.; Green, J.; Thomson, A. J.; Le Brun, N. E.; Johnson, M. K. Reversible Cycling between Cysteine Persulfide-Ligated [2Fe-2S] and Cysteine-

Ligated [4Fe-4S] Clusters in the FNR Regulatory Protein. *Proc. Natl. Acad. Sci. U. S. A.* **2012**, *109* (39), 15734–15739. https://doi.org/10.1073/pnas.1208787109.

(38) Yang, W.; Rogers, P. A.; Ding, H. Repair of Nitric Oxide-Modified Ferredoxin [2Fe-2S] Cluster by Cysteine Desulfurase (IscS). *J. Biol. Chem.* **2002**, *277* (15), 12868–12873. https://doi.org/10.1074/jbc.M109485200.

(39) Yang, J.; Duan, X.; Landry, A. P.; Ding, H. Oxygen Is Required for the L-Cysteine-Mediated Decomposition of Protein-Bound Dinitrosyl-Iron Complexes. *Free Radic. Biol. Med.* **2010**, *49* (2), 268–274. https://doi.org/10.1016/j.freeradbiomed.2010.04.012.

(40) Feigl, F. *Spot Tests in Inorganic Analysis; 5th*; Amsterdam: New York, 1958; Vol. 5.

(41) Olabe, J. A. The Coordination Chemistry of Nitrosyl in Cyanoferrates. An Exhibit of Bioinorganic Relevant Reactions. *Dalton Trans.* **2008**, No. 28, 3633–3648. https://doi.org/10.1039/b803153c.

(42) Fitzpatrick, J.; Kalyvas, H.; Shearer, J.; Kim, E. Dioxygen Mediated Conversion of Fe(NO)29 Dinitrosyl Iron Complexes to Roussin's Red Esters. *Chem. Commun. (Camb.)* **2013**, *49* (49), 5550. https://doi.org/10.1039/c3cc40352a.

(43) Lewandowska, H.; Kalinowska, M.; Brzóska, K.; Wójciuk, K.; Wójciuk, G.; Kruszewski, M. Nitrosyl Iron Complexes-Synthesis, Structure and Biology. *Dalton Transactions* **2011**, *40* (33), 8273–8289.

(44) Vanin, A. F. Dinitrosyl Iron Complexes with Thiolate Ligands: Physico-Chemistry, Biochemistry and Physiology. *Nitric Oxide* **2009**, *21* (1), 1–13. https://doi.org/10.1016/j.niox.2009.03.005.

(45) Vithayathil, A. J.; Ternberg, J. L.; Commoner, B. Changes in Electron Spin Resonance Signals of Rat Liver during Chemical Carcinogenesis. *Nature* **1965**, *207* (5003), 1246–1249. https://doi.org/10.1038/2071246a0.

(46) Enemark, J. H.; Feltham, R. D. Principles of Structure, Bonding, and Reactivity for Metal Nitrosyl Complexes. *Coord. Chem. Rev.* **1974**, *13* (4), 339–406. https://doi.org/10.1016/s0010-8545(00)80259-3.

(47) Lu, T.-T.; Chen, C.-H.; Liaw, W.-F. Formation of the Distinct Redox-Interrelated Forms of Nitric Oxide from Reaction of Dinitrosyl Iron Complexes (DNICs) and Substitution Ligands. *Chemistry* **2010**, *16* (27), 8088–8095. https://doi.org/10.1002/chem.201000524.

(48) Nicolet, Y.; Rohac, R.; Martin, L.; Fontecilla-Camps, J. C. X-Ray Snapshots of Possible Intermediates in the Time Course of Synthesis and Degradation of Protein-Bound Fe4S4 Clusters. *Proc. Natl. Acad. Sci. U. S. A.* **2013**, *110* (18), 7188–7192. https://doi.org/10.1073/pnas.1302388110.

(49) Tran, C. T.; Kim, E. Acid-Dependent Degradation of a [2Fe–2S] Cluster by Nitric Oxide. *Inorg. Chem.* **2012**, *51* (19), 10086–10088. https://doi.org/10.1021/ic301676f.

(50) Fitzpatrick, J.; Kim, E. Synthetic Modeling Chemistry of Iron–Sulfur Clusters in Nitric Oxide Signaling. *Acc. Chem. Res.* **2015**, *48* (8), 2453–2461. https://doi.org/10.1021/acs.accounts.5b00246.

(51) Tsai, M.-L.; Chen, C.-C.; Hsu, I.-J.; Ke, S.-C.; Hsieh, C.-H.; Chiang, K.-A.; Lee, G.-H.; Wang, Y.; Chen, J.-M.; Lee, J.-F.; Liaw, W.-F. Photochemistry of the Dinitrosyl Iron Complex $[S_5Fe(NO)_2]^-$ Leading to Reversible Formation of $[S_5Fe(\mu\text{-}S)_2FeS_5]^{2-}$: Spectroscopic Characterization of Species Relevant to the Nitric Oxide Modification and Repair of [2Fe−2S] Ferredoxins. *Inorg. Chem.* **2004**, *43* (16), 5159–5167. https://doi.org/10.1021/ic0494915.

(52) Tsai, F.-T.; Chiou, S.-J.; Tsai, M.-C.; Tsai, M.-L.; Huang, H.-W.; Chiang, M.-H.; Liaw, W.-F. Dinitrosyl Iron Complexes (DNICs) $[L_2Fe(NO)_2]^-$ (L = Thiolate): Interconversion among $Fe(NO)_2^9$ DNICs, $Fe(NO)_2^{10}$ DNICs, and [2Fe-2S] Clusters, and the Critical Role of the Thiolate Ligands in Regulating NO Release of DNICs. *Inorg. Chem.* **2005**, *44* (16), 5872–5881. https://doi.org/10.1021/ic0505044.

(53) Lu, T.-T.; Huang, H.-W.; Liaw, W.-F. Anionic Mixed Thiolate−Sulfide-Bridged Roussin's Red Esters $[(NO)_2Fe(\mu\text{-}SR)(\mu\text{-}S)Fe(NO)_2]^-$ (R = ET, Me, Ph): A Key Intermediate for Transformation of Dinitrosyl Iron Complexes (DNICs) to [2Fe-2S] Clusters. *Inorg. Chem.* **2009**, *48* (18), 9027–9035. https://doi.org/10.1021/ic9012679.

(54) Victor, E.; Lippard, S. J. A Tetranitrosyl [4Fe–4S] Cluster Forms En Route to Roussin's Black Anion: Nitric Oxide Reactivity of $[Fe_4S_4(LS_3)L']^{2-}$. *Inorg. Chem.* **2014**, *53* (10), 5311–5320. https://doi.org/10.1021/ic500586g.

(55) Tonzetich, Z. J.; Do, L. H.; Lippard, S. J. Dinitrosyl Iron Complexes Relevant to Rieske Cluster Nitrosylation. *J. Am. Chem. Soc.* **2009**, *131* (23), 7964–7965. https://doi.org/10.1021/ja9030159.

(56) Lehnert, N.; Kim, E.; Dong, H. T.; Harland, J. B.; Hunt, A. P.; Manickas, E. C.; Oakley, K. M.; Pham, J.; Reed, G. C.; Alfaro, V. S. The Biologically Relevant Coordination Chemistry of Iron and Nitric Oxide: Electronic Structure and Reactivity. *Chem. Rev.* **2021**, *121* (24), 14682–14905. https://doi.org/10.1021/acs.chemrev.1c00253.

(57) Ye, S.; Neese, F. The Unusual Electronic Structure of Dinitrosyl Iron Complexes. *J. Am. Chem. Soc.* **2010**, *132* (11), 3646–3647. https://doi.org/10.1021/ja9091616.

(58) Gall, R. S.; Chu, C. T. W.; Dahl, L. F. Preparation, Structure, and Bonding of Two Cubane-like Iron-Nitrosyl Complexes, Fe4(NO)4(.Mu.3-S)4 and Fe4(NO)4(.Mu.3-S2)(.Mu.3-NC(CH3)3)2. Stereochemical Consequences of Bridging Ligand Substitution on a Completely Bonding Tetrametal Cluster Unit and of Different Terminal Ligands on Cubane-like FeS4 Core. *J. Am. Chem. Soc.* **1974**, *96* (12), 4019–4023. https://doi.org/10.1021/ja00819a053.

(59) Fitzpatrick, J.; Kalyvas, H.; Filipovic, M. R.; Ivanović-Burmazović, I.; MacDonald, J. C.; Shearer, J.; Kim, E. Transformation of a Mononitrosyl Iron Complex to a [2Fe-2S] Cluster by a Cysteine Analogue. *J. Am. Chem. Soc.* **2014**, *136* (20), 7229–7232. https://doi.org/10.1021/ja5024207.

(60) Park, K.; Bell, C. B., III; Liu, L. V.; Wang, D.; Xue, G.; Kwak, Y.; Wong, S. D.; Light, K. M.; Zhao, J.; Alp, E. E.; Yoda, Y.; Saito, M.; Kobayashi, Y.; Ohta, T.; Seto, M.; Que, L., Jr; Solomon, E. I. Nuclear Resonance Vibrational Spectroscopic and Computational Study of High-

Valent Diiron Complexes Relevant to Enzyme Intermediates. *Proc. Natl. Acad. Sci. U. S. A.* **2013**, *110* (16), 6275–6280. https://doi.org/10.1073/pnas.1304238110.

(61) Lauterbach, L.; Gee, L. B.; Pelmenschikov, V.; Jenney, F. E.; Kamali, S.; Yoda, Y.; Adams, M. W. W.; Cramer, S. P. Characterization of the [3Fe–4S]$^{0/1+}$Cluster from the D14C Variant of Pyrococcus Furiosus Ferredoxin via Combined NRVS and DFT Analyses. *Dalton Trans.* **2016**, *45* (17), 7215–7219. https://doi.org/10.1039/c5dt04760a.

(62) Gee, L. B.; Pelmenschikov, V.; Wang, H.; Mishra, N.; Liu, Y.-C.; Yoda, Y.; Tamasaku, K.; Chiang, M.-H.; Cramer, S. P. Vibrational Characterization of a Diiron Bridging Hydride Complex – a Model for Hydrogen Catalysis. *Chem. Sci.* **2020**, *11* (21), 5487–5493. https://doi.org/10.1039/d0sc01290d.

(63) Gee, L. B.; Pelmenschikov, V.; Mons, C.; Mishra, N.; Wang, H.; Yoda, Y.; Tamasaku, K.; Golinelli-Cohen, M.-P.; Cramer, S. P. NRVS and DFT of MitoNEET: Understanding the Special Vibrational Structure of a [2Fe-2S] Cluster with (Cys)$_3$(His)$_1$ Ligation. *Biochemistry* **2021**, *60* (31), 2419–2424. https://doi.org/10.1021/acs.biochem.1c00252.

(64) Pelmenschikov, V.; Birrell, J. A.; Gee, L. B.; Richers, C. P.; Reijerse, E. J.; Wang, H.; Arragain, S.; Mishra, N.; Yoda, Y.; Matsuura, H.; Li, L.; Tamasaku, K.; Rauchfuss, T. B.; Lubitz, W.; Cramer, S. P. Vibrational Perturbation of the [FeFe] Hydrogenase H-Cluster Revealed by $^{13}C^2H$-ADT Labeling. *J. Am. Chem. Soc.* **2021**, *143* (22), 8237–8243. https://doi.org/10.1021/jacs.1c02323.

(65) Praneeth, V. K. K.; Näther, C.; Peters, G.; Lehnert, N. Spectroscopic Properties and Electronic Structure of Five- and Six-Coordinate Iron(II) Porphyrin NO Complexes: Effect of the Axial N-Donor Ligand. *Inorg. Chem.* **2006**, *45* (7), 2795–2811. https://doi.org/10.1021/ic050865j.

(66) Paulat, F.; Berto, T. C.; DeBeer George, S.; Goodrich, L.; Praneeth, V. K. K.; Sulok, C. D.; Lehnert, N. Vibrational Assignments of Six-Coordinate Ferrous Heme Nitrosyls: New Insight from Nuclear Resonance Vibrational Spectroscopy. *Inorg. Chem.* **2008**, *47* (24), 11449–11451. https://doi.org/10.1021/ic801626w.

(67) Lehnert, N. Quantum-chemistry-centered Normal Coordinate Analysis (QCC - NCA): Application of NCA for the Simulation of the Vibrational Spectra of Large Molecules. *Encyclopedia of Inorganic Chemistry*. Wiley September 7, 2005. https://doi.org/10.1002/0470862106.ia605.

(68) Lehnert, N.; George, S. D.; Solomon, E. I. Recent Advances in Bioinorganic Spectroscopy. *Curr. Opin. Chem. Biol.* **2001**, *5* (2), 176–187. https://doi.org/10.1016/s1367-5931(00)00188-5.

(69) Speelman, A. L.; Zhang, B.; Krebs, C.; Lehnert, N. Structural and Spectroscopic Characterization of a High-Spin (FeNO]® Complex with an Iron(IV)-NO• Electronic Structure. *Angew. Chem. Int. Ed* **2016**, *55*, 6685–6688.

(70) Filipovic, M. R.; Zivanovic, J.; Alvarez, B.; Banerjee, R. Chemical Biology of H2S Signaling through Persulfidation. *Chem. Rev.* **2018**, *118* (3), 1253–1337. https://doi.org/10.1021/acs.chemrev.7b00205.

(71) Harrop, T. C.; Song, D.; Lippard, S. J. Interaction of Nitric Oxide with Tetrathiolato Iron(I) Complexes: Relevance to the Reaction Pathways of Iron Nitrosyls in Sulfur-Rich Biological Coordination Environments. *J. Am. Chem. Soc* **2006**, *128*, 3528–3529.

(72) Speelman, A. L.; Zhang, B.; Silakov, A.; Skodje, K. M.; Alp, E. E.; Zhao, J.; Hu, M. Y.; Kim, E.; Krebs, C.; Lehnert, N. *Unusual Synthetic Pathway for an (Fe(NO))° Dinitrosyl Iron Complex (DNIC) and Insight Inte*.

(73) Van Stappen, C.; Lehnert, N. Mechanism of N-N Bond Formation by Transition Metal-Nitrosyl Complexes: Modeling Flavodiiron Nitric Oxide Reductases. *Inorg. Chem* **2018**, *57*, 4252–4269.

(74) Chmura, A.; Szaciłowski, K.; Waksmundzka-Góra, A.; Stasicka, Z. Photochemistry of the [Fe4(Mu3-S)3(NO)7]- Complex in the Presence of S-Nucleophiles: A Spectroscopic Study. *Nitric Oxide* **2006**, *14* (3), 247–260. https://doi.org/10.1016/j.niox.2005.10.005.

(75) Elrod, L. T.; Kim, E. Lewis Acid Assisted Nitrate Reduction with Biomimetic Molybdenum Oxotransferase Complex. *Inorg. Chem.* **2018**, *57* (5), 2594–2602. https://doi.org/10.1021/acs.inorgchem.7b02956.

(76) White, C. J.; Speelman, A. L.; Kupper, C.; Demeshko, S.; Meyer, F.; Shanahan, J. P.; Alp, E. E.; Hu, M.; Zhao, J.; Lehnert, N. The Semireduced Mechanism for Nitric Oxide Reduction by Non-Heme Diron Complexes: Modeling Flavodiiron Nitric Oxide Reductases. *J. Am. Chem. Soc* **2018**, *140*, 2562–2574.

(77) Skodje, K. M.; Kwon, M.-Y.; Chung, S. W.; Kim, E. Coordination-Triggered NO Release from a Dinitrosyl Iron Complex Leads to Anti-Inflammatory Activity. *Chem. Sci.* **2014**, *5* (6), 2374–2378. https://doi.org/10.1039/c3sc53319k.

(78) Bailey, T. S.; Pluth, M. D. Reactions of Isolated Persulfides Provide Insights into the Interplay between H›S and Persulfide Reactivity. Free Radic. *Biol. Med* **2015**, *89*, 662–667.

(79) Bailey, T. S.; Zakharov, L. N.; Pluth, M. D. Understanding Hydrogen Sulfide Storage: Probing Conditions for Sulfide Release from Hydrodisulfides. *J. Am. Chem. Soc.* **2014**, *136* (30), 10573–10576. https://doi.org/10.1021/ja505371z.

(80) Bergner, M.; Dechert, S.; Demeshko, S.; Kupper, C.; Mayer, J. M.; Meyer, F. Model of the MitoNEET [2Fe-2S] Cluster Shows Proton Coupled Electron Transfer. *J. Am. Chem. Soc.* **2017**, *139* (2), 701–707. https://doi.org/10.1021/jacs.6b09180.

(81) Pandelia, M.-E.; Lanz, N. D.; Booker, S. J.; Krebs, C. Mössbauer Spectroscopy of Fe/S Proteins. *Biochim. Biophys. Acta* **2015**, *1853* (6), 1395–1405. https://doi.org/10.1016/j.bbamcr.2014.12.005.

(82) Fee, J. A.; Findling, K. L.; Yoshida, T.; Hille, R.; Tarr, G. E.; Hearshen, D. O.; Dunham, W. R.; Day, E. P.; Kent, T. A.; Münck, E. Purification and Characterization of the Rieske Iron-Sulfur Protein from Thermus Thermophilus. Evidence for a [2Fe-2S] Cluster Having Non-Cysteine Ligands. *J. Biol. Chem.* **1984**, *259* (1), 124–133. https://doi.org/10.1016/s0021-9258(17)43630-1.

(83) Stack, T. D. P.; Holm, R. H. Subsite-Specific Functionalization of the [4Fe-4S]2* Analog of Iron Sulfur Protein Clusters. *J. Am. Chem. Soc* **1987**, *109*, 2546–2547.

(84) Stack, T. D. P.; Holm, R. H. Subsite-Differentiated Analogs of Biological [4Fe-4S]2* Clusters - Synthesis, Solution and Solid-State Structures, and Subsite-Specific Reactions. *J. Am. Chem. Soc* **1988**, *110*, 2484–2494.

(85) Mayerle, J. J.; Denmark, S. E.; Depamphilis, B. V.; Ibers, J. A.; Holm, R. H. Synthetic Analogs of Active- Sites of Iron-Sulfur Proteins. XI. Synthesis and Properties of Complexes Containing FezS2 Core and Structures of Bis[Ortho-Xylyl-Alpha,Alpha'-Dithiolato-Mu-Sulfido-Ferrate(Ill)]andBis[Para-Tolylthiolato- Mu-Sulfido-Ferrate(Ill)] Dianions. *J. Am. Chem. Soc* **1975**, *97*, 1032–1045.

Chapte 2 Introduction to synthetic models for Mo

enzyme

2.1 Mononuclear molybdenum enzymes

People interested in molybdenum chemistry because of its large number of accessible oxidation states as well as its ability to form stable complexes with oxygen, nitrogen and sulfur containing ligands with diverse coordination numbers and stereo chemistries.[1-6] Perhaps this versatility is what qualifies it for use by nature in various essential life processes as constituent part of several metalloenzymes.[1-11] In fact, Mo is the only essential trace element of second-row transition metal it is required by nearly all organisms (Archaea, Bacteria and Eukaryota).[1-6] More than 50 molybdenum-containing enzymes have been purified and biochemically characterized until now.[6,7] Three large families of molybdenum and tungsten enzymes have been identified and classified by Hille according to their unique active site structures (Scheme 2.1), namely sulfite oxidase/dehydrogenase (SO/SDH), xanthine oxidase (XO) and DMSO reductase (DMSOR).[6,11,12] The structures of the three canonical molybdenum centers in their oxidized Mo(VI) states are shown in Figure 1. The active site of molybdenum enzymes typically features a square-pyramidal or trigonal prismatic geometry, coordinate with sulfurs from protein bidentate enedithiolate ligand.[6,12] Remaining coordination sites at molybdenum(VI) are filled by one an apical Mo=O ligand and an oxido, sulfido or hydroxido ligands as well as Cystine residues. [6,11,12]
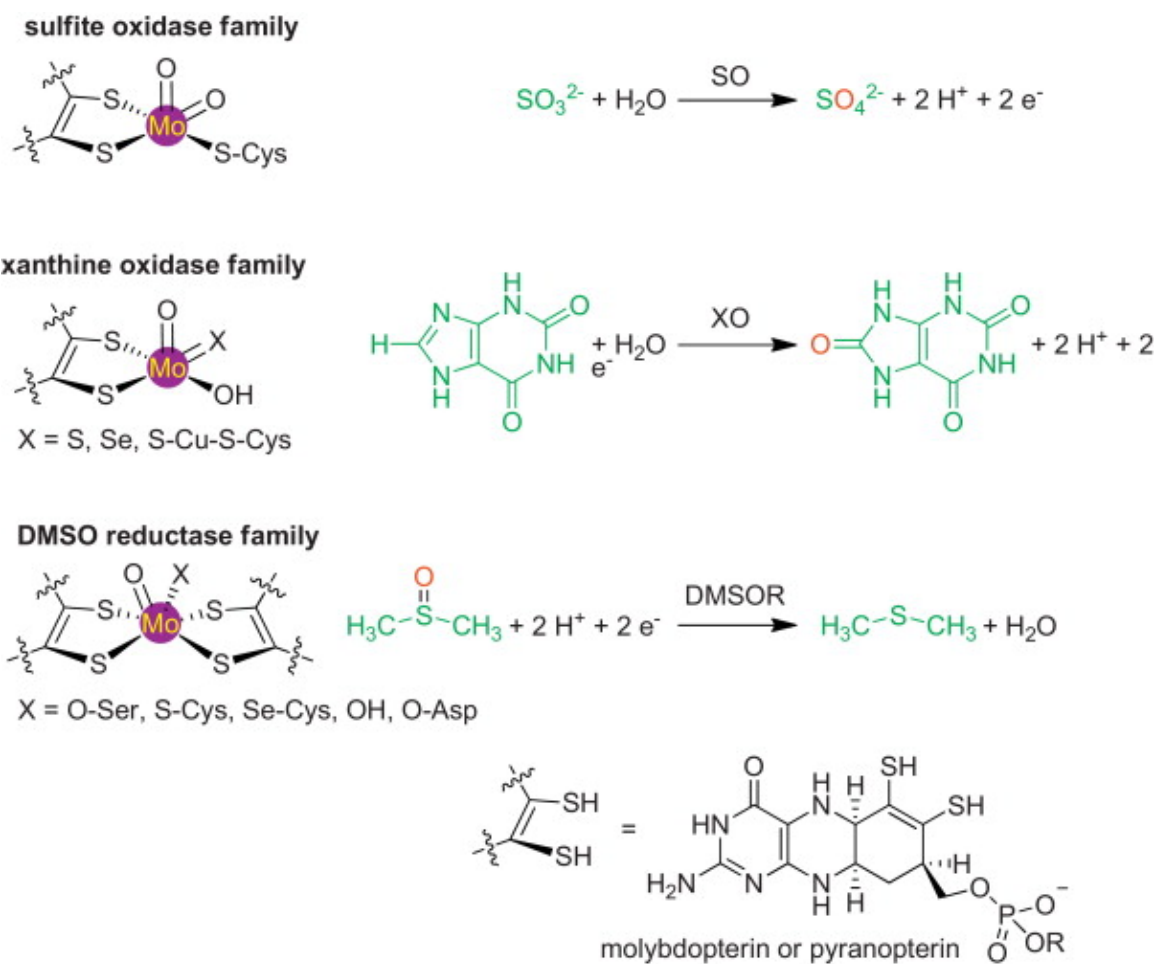
Figure 2.1 Structures of the oxidized active sites of the three families of mononuclear molybdenum enzymes and associated catalyzed reactions. *Adapted from Heinze, K. et al. Coord. Chem. Rev. 2015, 300, 121–141.*

Mo-containing enzymes play essential roles in the biological carbon, nitrogen and sulfur cycles.[6,7] Sulfite oxidase and xanthine oxidase family specialize in facilitating oxygen atom transfer (OAT) reactions efficiently, interacting with substrates such as xanthine, formate, and sulfite using water as an oxygen atom donor.[6,13-15] DMSO reductases, which carry out analogous reverse reactions, employing DMSO as an oxygen donor, producing DMS and oxygenated product,

water.[6-11] Following OAT, the regeneration of the molybdenum active site necessitates electron transfer (ET) and proton transfer (PT), processes supported by configurations involving iron-sulfur clusters, hemes, and other redox-active units that facilitate the electron flow.[6,12] It's proposed that the coupling of ET and PT could lower activation barriers, enhancing the enzyme's efficiency in various biological cycles.[16,17]

2.2 Synthetic Mo systems and their OAT Reactivity

2.2.1 Bioinspired dioxido Mo(VI) complexes

Molybdenum complexes featuring oxidation states from IV to VI, particularly those with a chalcogen-rich coordination sphere, are of interest since they resemble features of the active sites of the molybdenum containing enzyme. Dioxido molybdenum(VI) complexes with thiocarbamato chelating ligands are notable for mimicking the dual molybdopterin ligands in the DMSO reductase enzyme family. Mo^{VI} complex $Mo^{VI}(dtc)_2O_2$ with dialkyldithiocarbamato (dtc) ligand was first synthesized and it is able to transfer one of its terminal oxygen atoms to phosphanes (Scheme 2.1).[16,19] The resulting monooxido $Mo^{IV}(dtc)_2O$ can be reoxidized to $Mo^{VI}(dtc)_2O_2$ by various oxidant. These systems are complicated to an extent by the reversible formation of a oxo-bridged Mo^V complex u-O-$[MoO(dtc)_2]_2$ (Scheme 2.1).[16,21,22] This dinucleation is frequently observed in oxido molybdenum chemistry. Normally, this μ-oxo-Mo^V binuclear species are classified as abiological species and inactive for oxygen atom transfer.[16,22]
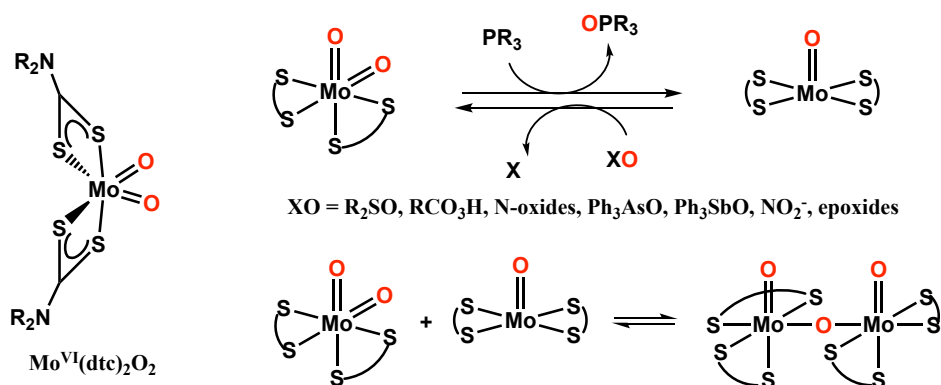
Scheme 2.1 OAT reactivity of $Mo^{VI}(dtc)_2O_2$

Forward and backward OAT reactions have been effectively replicated in various instances using simple coordination dioxido Mo^{VI} model compounds and PR_3 substrate as oxygen accepter.[7,23] Although phosphoryl intermediates have long been hypothesized in these reactions, their detection and isolation remained elusive until Smith *et al.* reported the detection of $Tp^*MoOX(OPPh_3)$ ($X=Cl^-, Br^-, OPh^-, SPh^-$) in gas-phase OAT reactions and the isolation of $Tp^{iPr}MoO(OPh)(OPEt_3)$ resulting from "incomplete" OAT between $Tp^{iPr}MoO_2(OPh)$ and PEt_3 (Scheme 2.2A).[24] These findings, alongside further research by Basu and Young, have enriched our understanding of the OAT reactions involving dioxido-Mo^{VI} complexes.[25-29] They have led to the hypothesis that the oxygen atom transfer from Tp^XMoO_2X to phosphanes occurs via a two-step mechanism, with the initial step yielding isolable phosphoryl complexes, $Tp^XMoOX(OPR_3)$, which exhibit a range of stabilities (Scheme 2.2B).[30-32] The second step in the OAT reactions involves the solvolysis of $Tp^*MoOX(OPR_3)$ to form $Tp^*MoOX(solvent)$ and OPR_3.
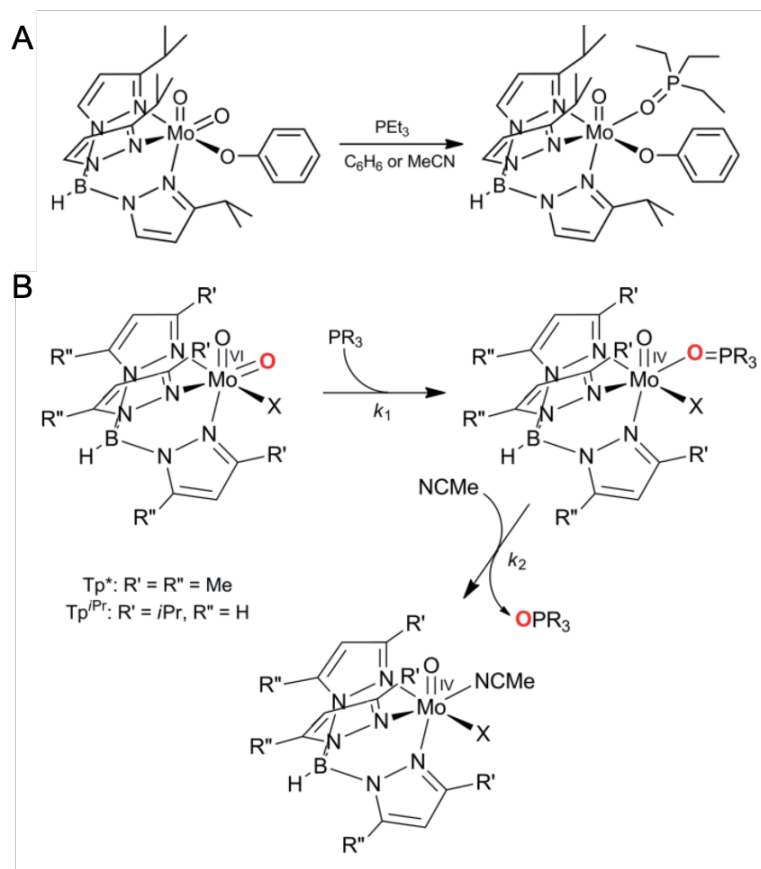
Scheme 2.2 A. Synthesis of Tp^{iPr}MoO(OPh)(OPEt$_3$). B. The two steps involved in OAT from Tp*MoOX(OPR$_3$) to PR$_3$. Adapted from *Young, C. G. et al. Eur. J. Inorg. Chem. 2016, 2016 (15–16), 2357–2376.*

2.2.2 Reactivity of μ-oxo-Mo^V dinuclear species

To suppress the dinucleartion, Holm et al. developed Mo model system using a sterically demanding pyridine-dithiolato ligand (L-NS$_2$)$^{2-}$, where (L-NS$_2$)$^{2-}$ = 2,6-bis(2,2-diphenyl-2-mercaptoethyl)pyridine(2–).[33-37] OAT from Mo^{VI}O$_2$(L-NS$_2$)$_2$ to oxygen-acceptors is successful and the mononuclear oxido molybdenum(IV) complex Mo^{IV}O(L-NS$_2$)$_2$ could be isolated (Scheme 2.3 Top). This Mo^{IV}(L-NS$_2$)$_2$O species proved to be a more robust oxo acceptor than the monooxo

Mo dtc species and could even achieve the reduction of nitrate to nitrite, a reaction unachievable by the dtc system. Despite the use of bulky phenylgroups, the oxo-bridged dimer μ-O-[MoO(L-NS$_2$)]$_2$. was still detected and contrary to expectations that the active catalyst would be monomeric, Young and coworkers demonstrated that the active catalyst was actually this μ-oxo dimer μ-O-[MoO(L-NS$_2$)]$_2$.[37,38] Remarkably, this μ-oxo-Mo^V dinuclear species, previously thought to be inactive, showed saturation kinetics in OAT reactions, with a proposed mechanism involving substrate pre-equilibrium binding to the dimer, followed by concerted oxygen transfer and O-X and (μ-O)-Mo bond cleavage.[38] This idea also supported by Holm's another report of nitrate reduction using a different dinuclear molybdenum(V) complex, μ-O-[MoO(ssp)]$_2$, (ssp = 2-(salicylideneamino)benzenethiolato(2-)) (Scheme 2.3 Bottom).[39]
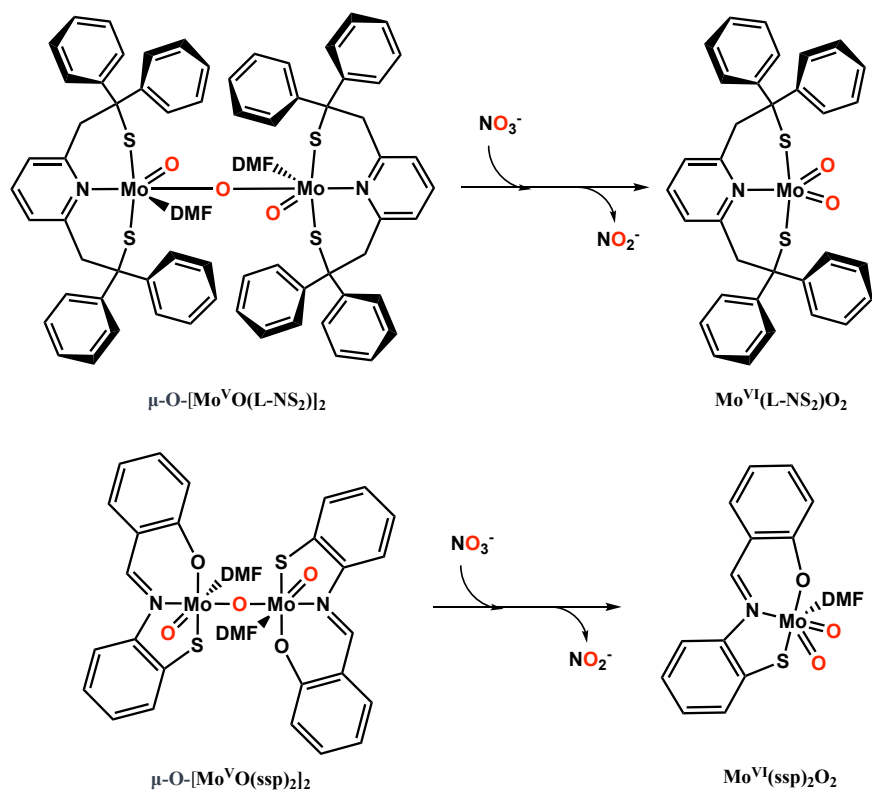
Scheme 2.3 OAT reactivity of μ-oxo-Mo^V dinuclear species μ-O-[MoO(L-NS$_2$)]$_2$ and μ-O-[MoO(ssp)]$_2$

2.2.3 OAT reaction with Mo^{IV}O/Mo^{IV} systems
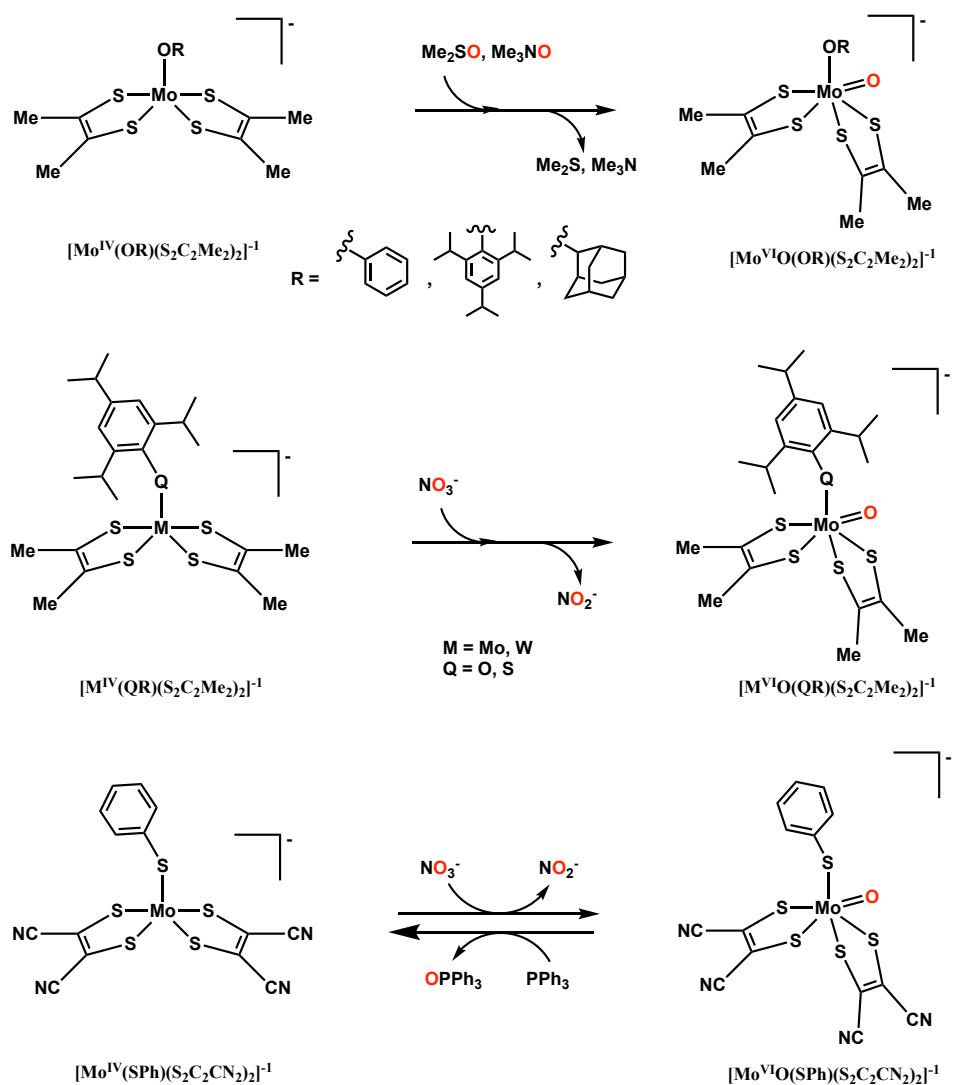
Scheme 2.4 OAT with dithiolene ligand supported Mo complexes

Another important structure analogous of DMSO reductase is prepared use two dithiolene ligand in conjunction with sterically hindered axial ligands to stabilize mononuclear square pyramidal structures.[8,40] As depicted in Scheme 2.4 the [Mo^{IV}(OR)(S$_2$C$_2$Me$_2$)$_2$]$^-$ type, efficiently abstract one oxygen atom from (CH$_3$)$_2$SO and Me$_3$NO converting to the corresponding

$[Mo^{VI}O(OR)(S_2C_2Me_2)_2]^-$.[8,9] Holm et al. have also described molybdenum- and tungsten-catalyzed nitrate reduction systems employing $[M^{IV}(QR)(S_2C_2Me_2)_2]^-$.[41] The proposed pathway for nitrate reduction, illustrated in Scheme 2.5, initiates with the coordination of the substrate cis to the axial QR ligand. Sarkar and coworkers achieved catalytic nitrate reduction by employing phosphine to reduce the Mo^{VI} back its original Mo^{IV} state.[42]
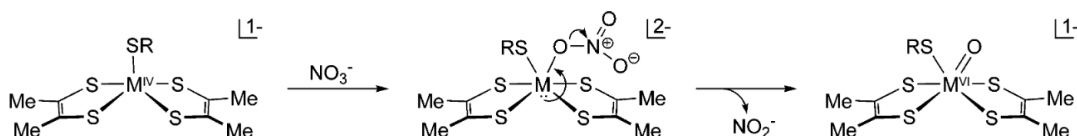
Scheme 2.5 Proposed reaction pathway for nitrate reduction using $[M^{IV}(SR)(S_2C_2Me_2)_2]^-$. Adapted from *Holm, R. H. et al. Inorg. Chem. 2005, 44 (4), 1068–1072.*

2.3 Sulfur Atom Transfer Reaction

2.3.1 Significance and impact

Sulfur compounds, prevalent as impurities in crude oil extracts, are a significant environmental concern due to their conversion into sulfur dioxide (SO_2) and sulfate particulate matter (SPM) upon combustion.[43] The release of sulfur oxides into the atmosphere can lead to the formation of sulfates and acid rain, with SO_2 emissions additionally linked to adverse health effects, including respiratory illnesses.[43,44] The persistence of such impurities, particularly from ongoing, large-scale activities like petroleum extraction, poses considerable risks to public health and the environment. As a remedial measure, sulfur atom transfer (SAT) systems designed for desulfurization could mitigate these issues by transferring sulfur atoms from pollutants to form benign byproducts, thereby reducing SO_2 and SPM emissions.[45] Further, research into SAT

systems holds promise not only for environmental applications but also for enhancing the synthetic efficiency of sulfur-containing pharmaceuticals, demonstrating the dual utility of this field in both ecological and medicinal chemistry.

Another possible application of SAT is the activation of elemental sulfur. Catalytic systems and synthetic methods frequently seek to utilize elemental sulfur, due to its non-toxicity, abundance, and cost-effectiveness. But the chemical inertness of elemental sulfur makes it hard to make any use. A catalytic system that effectively employs elemental sulfur as a source would facilitate in situ sulfur activation. With the global production of elemental sulfur currently exceeding 70 million metric tons annually—far outstripping demand—there is a pressing need to develop methods that utilize this excess.[46] Moreover, the incorporation of elemental sulfur could reduce the costs associated with catalyst usage and capitalize on a readily available and non-toxic source of sulfur.

2.3.2 Oxosulfido-Mo(VI) species

Mononuclear oxosulfido-Mo(VI) complexes $[Mo^{VI}(O)(S)]^{2+}$ are desirable synthetic models for xanthine oxidase enzyme family, due to their similarity to the enzyme's active site. However, the synthesis of these $[Mo^{VI}(O)(S)]^{2+}$ models is challenging due to instability of the Mo=S moiety, which readily undergoes redox reactions, often resulting in the formation of bi- or polynuclear μ-sulfido-Mo(V) species.[11,47-49]

Despite these challenges, successful synthesis strategies for the desired oxosulfido-Mo(VI) species with Tpx ligands have been reported by *Young et al.*, using sulfur atom transfer (SAT).[50-52] The reactions of Tp*MoO(S₂PR₂) (R = Pr^i, Ph) with the sulfur atom donor propylene sulfide

produce red Tp*MoOS(S$_2$PR$_2$) (Figure 2.2 Top). The terminal sulfido ligand introduced is stabilized by a weak S···S interaction between the Mo=S and an uncoordinated sulfur atom from the monodentate dithiophosphinate ligand (Figure 2.2 Bottom). Such complexes not only mimic the active site of xanthine oxidase but are also capable of engaging in sulfur atom transfer reactions. These reactions can facilitate the transfer of a sulfur atom to cyanide, forming thiocyanate and yielding compounds such as Tp*MoO(S$_2$PR$_2$) under anaerobic conditions or Tp*MoO$_2$(S$_2$PR$_2$) in the presence of oxygen.[52]
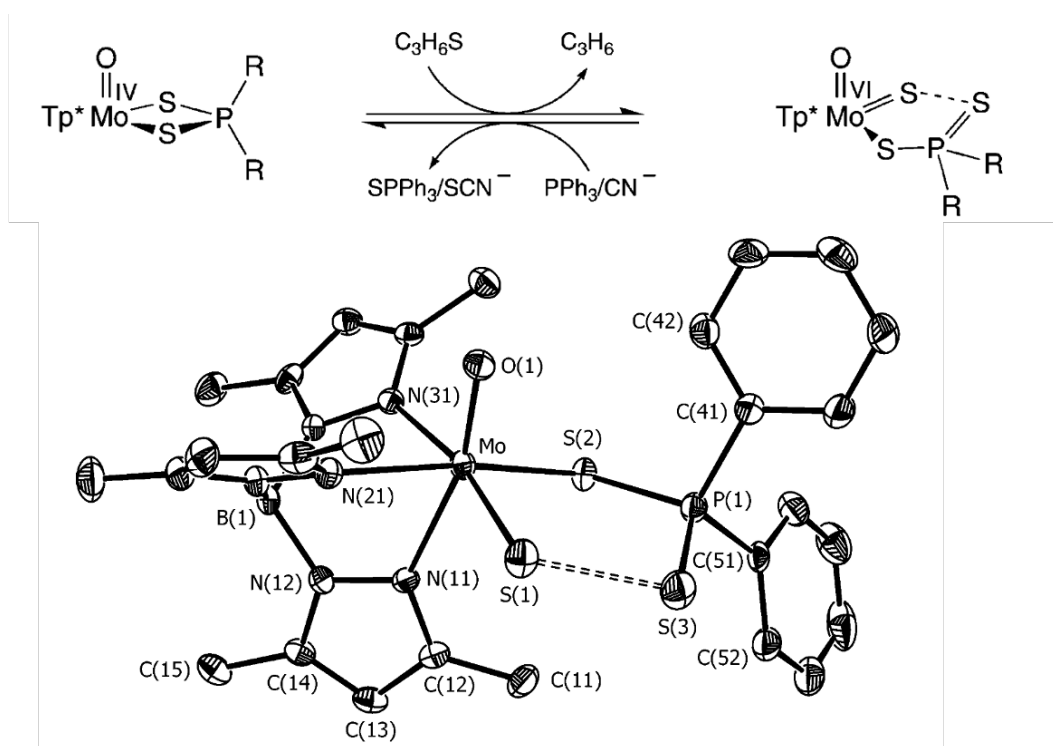
Figure 2.2 top: SAT between Tp*MoO(S$_2$PR$_2$) and Tp*MoOS(S$_2$PR$_2$). Bottom: Molecular structure of Tp*MoOS(S$_2$PR$_2$). Adopted from *Young, C. G. et al. Inorganic chemistry, 2007, 46 (3), 939–948.*

Oxosulfido-Mo(VI) complexes with non-interacting sulfido groups were synthesized using the sterically bulky Tp^{iPr} ligand.[50,53-55] Analytical techniques, including physical, spectroscopic, and electrochemical analyses, corroborated the structure of these compounds, confirmed the monomeric, oxosulfido-Mo(VI) configuration for the complex Tp^{iPr}MoOS(OPh). However, these complexes were found to exist in a monomer-dimer equilibrium, with both forms being isolable in solid states (Scheme 2.6).[50] In a separate advancement, Holm reported oxidosulfido-Mo(VI) complexes that evade dimerization by employing bulky auxiliary ligands (Figure 2.3).[56] The complexes [MoOS(OSiPh$_3$)$_2$(L-L)], with L-L being a phenanthroline or bipyridyl ligand, were synthesized through the silylation of [MoO$_3$S]$^{2-}$ in the presence of L-L. Furthermore, the complex [MoOS(OSiPh$_3$)$_2$(Me$_4$phen)] reacts with PPh$_3$ in dichloromethane to produce [Mo^{V}OCl(OSiPh$_3$)$_2$(Me$_4$phen)], with the pathway for sulfur versus oxygen abstraction being influenced by the relative bond energies of Mo=O and Mo=S, a factor that is likely to be a general determinant in such reactions.[56]
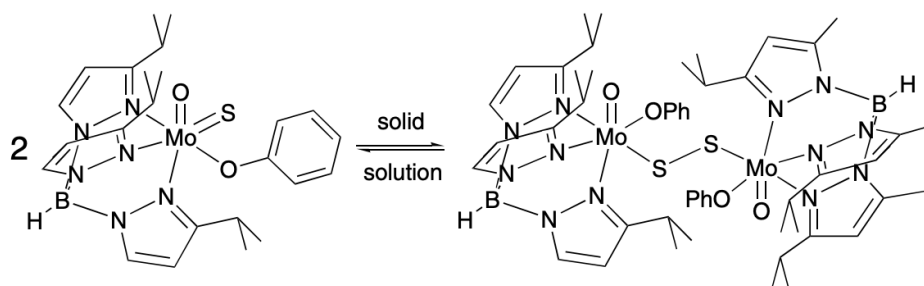
Scheme 2.6 Monomer-dimer equilibrium of Tp^{iPr}MoOS(OPh). Adapted from *Young, C. G. et al. J. Inorg. Biochem. 2007, 101 (11–12), 1562–1585.*
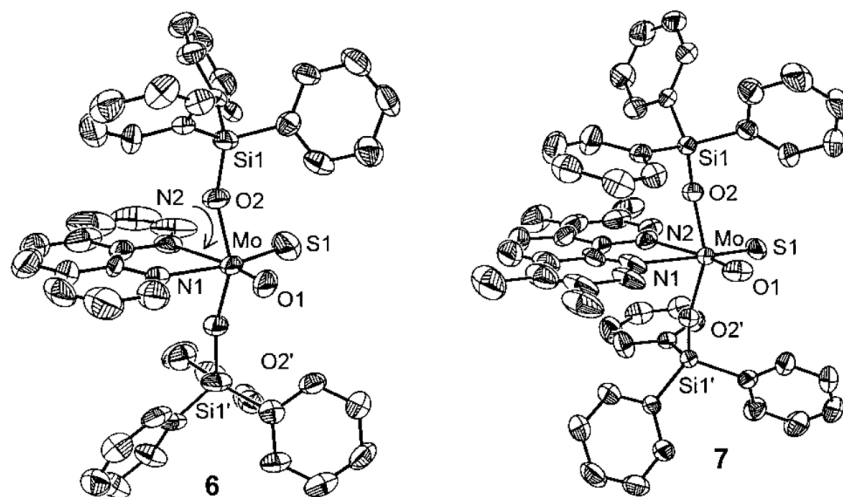
Figure 2.3 Structures of [MoOS(OSiPh$_3$)$_2$(phen)] (left) and [MoOS(OSiPh$_3$)$_2$(Me$_4$phen)] (right). Adapted from *Holm, R. H. et al. Inorg. Chem. 1999, 38 (18), 4104–4114.*

More recently, Itoh *et al.* successfully generated the Mo^{VI}O(S) with dithiolene ligand framework that identical to the enzyme active site coordination site environment.[57] The Mo^{VI}O(S)L (L = 1,2-dicarbomethoxyethylene-1,2-dithiolate) complex was synthesized through the reaction of (Et$_4$N)[Mo^{VI}O(OSiBuPh$_2$)L$_2$] with SH$^-$ at temperatures below -20°C (Scheme 2.7). This complex requires careful handling at low temperatures, and warming to room temperature triggers an intramolecular redox reaction that results in the loss of the terminal sulfido ligand, producing (Et$_4$N)$_2$[Mo^{IV}OL$_2$]. The terminal sulfide group displays high reactivity towards PPh$_3$ at −40 °C, leading to the formation of SPPh$_3$ and corresponding Mo(IV)(O) species.
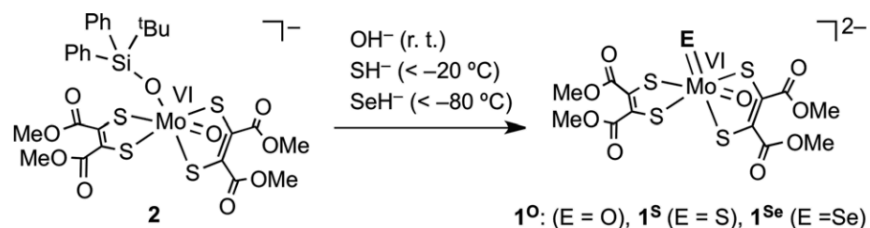
Scheme 2.7 Synthesis of Mo^{VI}O(S)L from (Et$_4$N)[Mo^{VI}O(OSiBuPh$_2$)L$_2$]. Adapted from *Itoh, S. et al. Chem. Commun. 2013, 49 (39), 4358–4360.*

2.3.3 Mo catalyzed SAT reaction

Exploring the realm of molybdenum-catalyzed sulfur atom transfer (SAT) reactions, Adam found that the Mo^{IV}O(dtc)$_2$ complex could effectively catalyze the transfer of sulfur atoms to various olefinic substrates in refluxing acetone, using elemental sulfur as the donor to regenerate the active catalyst.[58] They were able to isolate a disulfur complex Mo^{VI}O(dtc)$_2$(η^2-S$_2$) under stoichiometric conditions as sulfur-transferring agent (Scheme 2.8).[58,59] It is hypothesized that the next step involves sulfur atom abstraction from the disulfur bridge, forming an oxosulfido-Mo(VI) intermediate, Mo^{VI}O(dtc)$_2$(η^2-S$_2$), that subsequently transfers sulfur to the substrate. While propylene sulfide was also tested as a sulfur source, it did not seem to observe a disulfur intermediate in the oxidative half of the catalytic cycle.[58,59] Adam's investigations further led to the synthesis of isothiocyanates, demonstrating sulfur atom transfer to isonitriles.[59] For this reaction, when elemental sulfur was used as the sulfur source, reflux in acetone was necessary, whereas propylene sulfide allowed the reaction to proceed at room temperature.[59]
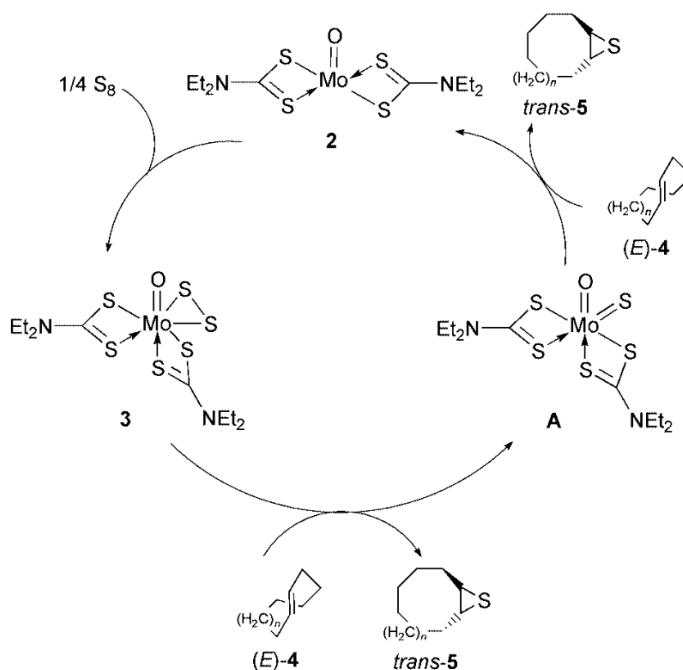
Scheme 2.8 Proposed catalytic cycle for $Mo^{IV}O(dtc)_2$ atalyzed SAT. Adapted from *Adam, W. et al. Chemical Communications 2000, No. 19, 1910–1911.*

Building on this foundation, a metal catalyst screening was performed to find a more effective catalyst, highlighting the molybdenum oxo complex $Mo^{IV}O(S_2P(OEt)_2)_2$ as a more reactive system for the episulfidation of alkenes, particularly when paired with styrene sulfide as the sulfur donor.[60] They also proposed a oxosulfido-Mo(VI) complexes as the active form of catalyst, though isolation of the active intermediate has not been successful so far.

More recently, Sita et al. reported a series of mono-cyclopentadienyl, mono-amidinate (CPAM) Mo(II) bis(isonitrile) complexes, $Cp*Mo[N(^iPr)C(Ph)N(^iPr)](CNR)_2$ (where $Cp* = \eta^5$-C_5Me_5; R=Me, ^tBu, 2,6-$(CH_3)_2C_6H_3$), to facilitate the catalytic sulfur atom transfer for the production of isothiocyanates.[61] Unlike previous systems that alternate between Mo states IV and

VI, these complexes function through a Mo(II)/Mo(IV) redox couple, demonstrating that SAT can be successfully executed using elemental sulfur under mild conditions, with an increased reaction rate upon heating (Scheme 2.9).
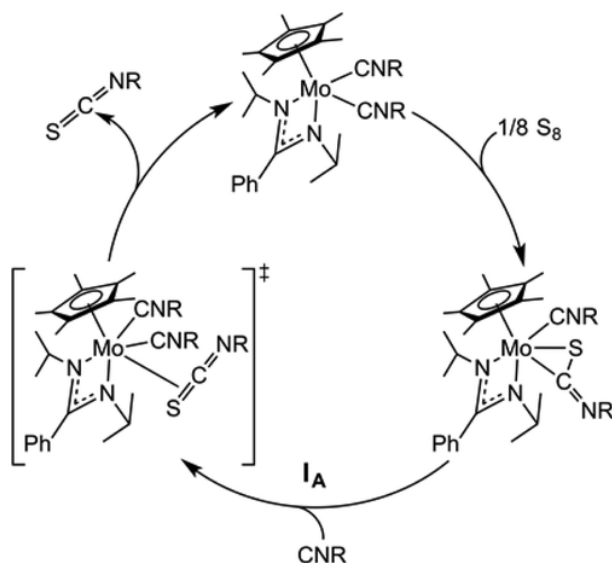
Scheme 2.9 Catalytic cycle for Cp*Mo[N(^{i}Pr)C(Ph)N(^{i}Pr)] (CNR)$_2$ catalyzed SAT. Adapted from *Sita, L. R. et al. Organometallics 2016, 35 (14), 2361–2366.*

2.3.4 SAT reaction catalyzed by other transition metal

Catalytic SAT has also been reported for transitional metal system other than Mo. Espenson *et al.* have reported on rhenium-catalyzed desulfurization of thiiranes, where MeReO$_3$ is first activated by Ph$_3$P through oxygen atom abstraction reaction, generating a highly reactive Re^V species capable of efficiently extracting sulfur from olefin sulfides (Scheme 2.10).[62] The Ph$_3$P then abstracts sulfur from the resultant Re^{VII} product to form phosphine sulfide and regenerate the active Re^V species.
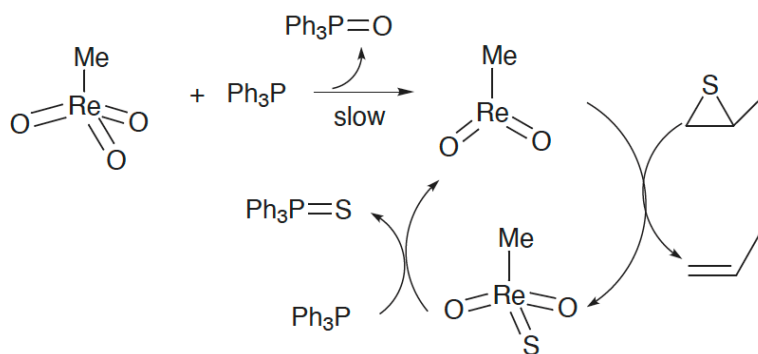
Scheme 2.10 Catalytic cycle for rhenium-catalyzed SAT. Adopted from *Espenson et al. Chem. Commun. 1999, No. 11, 1003–1004.*

Moreover, Young *et al.* have explored the catalytic SAT reactions between Ph$_3$P and propylene sulfide using tungsten complex Tp*WS$_2$Cl. With a catalyst loading of 10 mol %, this tungsten complex can achieve a 95% conversion to Ph$_3$PS and propylene over three days (Scheme 2.11).[63] The active catalyst in this system is remain unclear as the products of the reactions of Tp*WS$_2$Cl with phosphines are unstable even in the presence of coordinating solvents. Nevertheless, it was observed that the S$_2$PPh^{2-} auxiliary ligand stabilizes the products of the reactions of Tp*WS$_2$(S$_2$PPh$_2$) with phosphines, giving Tp*WS(S$_2$PPh$_2$). Those data suggesting the active, reduced form of the catalyst may be a similar W(IV) monosulfido complex.
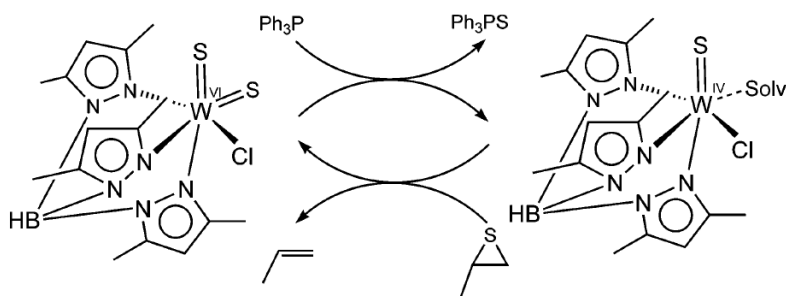
Scheme 2.11 SAT between propylene sulfide and PPh$_3$ catalyzed by Tp*WS$_2$Cl. Adapted from *Donahue, J. P. Chem. Rev. 2006, 106 (11), 4747–4783.*

Recently, Young and team have furthered their work in this area by developing a novel dinuclear tungsten(V) system for SAT reactions.[64] Complexes W$_2$(μ-S)(μ-S$_2$)(dtc)$_2$(dped)$_2$ proved capable of catalyzing SAT from propylene sulfide to triphenylphosphine with up to 17 turnovers per hour using 5 mol % catalyst loading. However, the catalyst is prone to rapid deactivation upon exposure to air, attributed to the formation of a terminal tungsten-oxo bond.
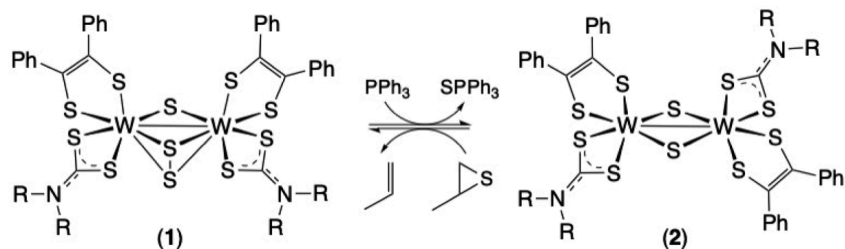
Scheme 2.12 SAT between propylene sulfide and PPh$_3$ catalyzed by W$_2$(μ-S)(μ-S$_2$)(dtc)$_2$(dped)$_2$. Adapted from *Young, C. G. Inorg. Chem. 2020, 59 (23), 16824–16828.*

2.4 Research Objectives

Despite various practical application of sulfur atom transfer, this reactivity remains rare in comparison to the numerous examples of OAT. In addition, catalytic reactivity is even more uncommon and has only been reported with a handful of cases. Among those cases, many of them require required heated conditions to proceed reactivity. Moreover, this reaction condition was incompatible for substrates containing hydroxy, ester and acetal functional groups. In this work, dinuclear Mo(V) thiosemicarbazone catalyst was prepared for challenging oxygen and sulfur atom transfer reactivates under mild condition. The active reaction intermediate and catalytic mechanism was carefully reviewed in chapter 7.

2.5 References

(1) De Renzo, E. C.; Heytler, P. G.; Kaleita, E. Further Evidence That Molybdenum Is a Co-Factor of Xanthine Oxidase. *Arch Biochem. Biophys* **1954**, *49, 242–244.*

(2) Mahler, H. R.; Mackler, B.; Green, D. E.; Bock, R. M. STUDIES ON METALLOFLAVOPROTEINS: III. ALDEHYDE OXIDASE: A MOLYBDOFLAVOPROTEIN. *Journal of Biological Chemistry* **1954**, *210, 465–480.*

(3) Nicholas, D. J. D.; Nason, A.; Mcelroy, W. D. Molybdenum and Nitrate Reductase: I. Effect of Molybdenum Deficiency on The Neurospora Enzyme. *Journal of Biological Chemistry* **1954**, *207 (1), 341–351.*

(4) Cohen, H. J.; Fridovich, I.; Rajagopalan, K. V. Hepatic Sulfite Oxidase: A Functional Role for Molybdenum. *Journal of Biological Chemistry* **1971**, *246 (2), 374–382.*

(5) Richert, D. A.; Westerfeld, W. W. Isolation and Identification of the Xanthine Oxidase Factor as Molybdenum. *J. Biol. Chem.* **1953**, *203 (2), 915–923.* https://doi.org/10.1016/s0021-9258(19)52361-4.

(6) Hille, R.; Hall, J.; Basu, P. The Mononuclear Molybdenum Enzymes. *Chem. Rev.* **2014**, *114 (7), 3963–4038.* https://doi.org/10.1021/cr400443z.

(7) Holm, R. H. Metal-Centered Oxygen Atom Transfer Reactions. *Chem. Rev.* **1987**, *87 (6), 1401–1449.* https://doi.org/10.1021/cr00082a005.

(8) Enemark, J. H.; Cooney, J. J. A.; Wang, J.-J.; Holm, R. H. Synthetic Analogues and Reaction Systems Relevant to the Molybdenum and Tungsten Oxotransferases. *Chem. Rev.* ***2004***, *104 (2), 1175–1200.* https://doi.org/10.1021/cr020609d.

(9) Sugimoto, H.; Tsukube, H. Chemical Analogues Relevant to Molybdenum and Tungsten Enzyme Reaction Centres toward Structural Dynamics and Reaction Diversity. *Chem. Soc. Rev.* ***2008***, *37 (12), 2609–2619.* https://doi.org/10.1039/b610235m.

(10) Elrod, L. T.; Kim, E. Lewis Acid Assisted Nitrate Reduction with Biomimetic Molybdenum Oxotransferase Complex. *Inorg. Chem.* ***2018***, *57 (5), 2594–2602.* https://doi.org/10.1021/acs.inorgchem.7b02956.

(11) Young, C. G. Scorpionate Complexes as Models for Molybdenum Enzymes: Scorpionate Complexes as Models for Molybdenum Enzymes. *Eur. J. Inorg. Chem.* ***2016***, *2016 (15–16), 2357–2376.* https://doi.org/10.1002/ejic.201501387.

(12) Hille, R. The Mononuclear Molybdenum Enzymes. *Chem. Rev.* ***1996***, *96 (7), 2757–2816.* https://doi.org/10.1021/cr950061t.

(13) Feng, C.; Tollin, G.; Enemark, J. H. Sulfite Oxidizing Enzymes. Biochim. *Biophys. Acta* ***2007***, *1774 (5), 527–539.* https://doi.org/10.1016/j.bbapap.2007.03.006.

(14) Johnson-Winters, K.; Tollin, G.; Enemark, J. H. Elucidating the Catalytic Mechanism of Sulfite Oxidizing Enzymes Using Structural, Spectroscopic, and Kinetic Analyses. *Biochemistry* ***2010***, *49 (34), 7242–7254.* https://doi.org/10.1021/bi1008485.

(15) Metz, S.; Thiel, W. Theoretical Studies on the Reactivity of Molybdenum Enzymes. *Coord. Chem. Rev.* **2011**, *255 (9–10), 1085–1103.* https://doi.org/10.1016/j.ccr.2011.01.027.

(16) Heinze, K. Bioinspired Functional Analogs of the Active Site of Molybdenum Enzymes: Intermediates and Mechanisms. *Coord. Chem. Rev.* **2015**, *300, 121–141.* https://doi.org/10.1016/j.ccr.2015.04.010.

(17) Huynh, M. H. V.; Meyer, T. J. Proton-Coupled Electron Transfer. *Chem. Rev.* **2007**, *107 (11), 5004–5064.* https://doi.org/10.1021/cr0500030.

(18) Lebrun, E.; Brugna, M.; Baymann, F.; Muller, D.; Lièvremont, D.; Lett, M.-C.; Nitschke, W. Arsenite Oxidase, an Ancient Bioenergetic Enzyme. *Mol. Biol. Evol.* **2003**, *20 (5), 686–693.* https://doi.org/10.1093/molbev/msg071.

(19) Barral, R.; Bocard, C.; de Roch, I. S.; Sajus, L. Activation de l'oxygene Moleculaire En Phase Liquide Homogene Par Des Complexes Oxo Du Molybdene Oxydation Catalytique Selective Des Phosphines Tertiaires. *Tetrahedron Lett.* **1972**, *13 (17), 1693–1696.* https://doi.org/10.1016/s0040-4039(01)84723-7.

(20) Reynolds, M. S.; Berg, J. M.; Holm, R. H. Kinetics of Oxygen Atom Transfer Reactions Involving Oxomolybdenum Complexes. General Treatment for Reactions with Intermediate Oxo-Bridged Molybdenum(V) Dimer Formation. *Inorg. Chem.* **1984**, *23 (20), 3057–3062.* https://doi.org/10.1021/ic00188a007.

(21) Young, C. G. Oxomolybdenum Chemistry: An Experiment. *J. Chem. Educ.* **1995**, *72 (8), 751.* https://doi.org/10.1021/ed072p751.

(22) Reynolds, M. S.; Berg, J. M.; Holm, R. H. Kinetics of Oxygen Atom Transfer Reactions Involving Oxomolybdenum Complexes. General Treatment for Reactions with Intermediate Oxo-Bridged Molybdenum (V) Dimer Formation. *Inorganic Chemistry* **1984**, *23 (20), 3057–3062.*

(23) Schultz, B. E.; Hille, R.; Holm, R. H. Direct Oxygen Atom Transfer in the Mechanism of Action of Rhodobacter Sphaeroides Dimethyl Sulfoxide Reductase. *J. Am. Chem. Soc.* **1995,** *117 (2), 827–828.* https://doi.org/10.1021/ja00107a031.

(24) Smith, P. D.; Millar, A. J.; Young, C. G.; Ghosh, A.; Basu, P. Detection, Isolation, and Characterization of Intermediates in Oxygen Atom Transfer Reactions in Molybdoenzyme Model Systems. *J. Am. Chem. Soc.* **2000,** *122 (38), 9298–9299.* https://doi.org/10.1021/ja0008362.

(25) Doonan, C. J.; Millar, A. J.; Nielsen, D. J.; Young, C. G. Cis-Dioxomolybdenum (VI) and Oxo (Phosphine Oxide) Molybdenum (Iv) Complexes: Steric and Electronic Fine-Tuning of Cis-[MoOS] 2+ Precursors. *Inorganic chemistry* **2005,** *44 (13), 4506–4514.*

(26) Malarek, M. S.; Evans, D. J.; Smith, P. D.; Bleeker, A. R.; White, J. M.; Young, C. G. Π-Acid/π-Base Carbonyloxomolybdenum(IV) Complexes and Their Oxomolybdenum(VI/IV) Precursors. *Inorg. Chem.* **2006,** *45 (5), 2209–2216.* https://doi.org/10.1021/ic0510314.

(27) Hill, L. M.; Taylor, M. K.; Ng, V. W. L.; Young, C. G. Toward Multifunctional Mo (VI− IV) Complexes: Cis-Dioxomolybdenum (VI) Complexes Containing Hydrogen-Bond Acceptors or Donors. *Inorganic chemistry* **2008,** *47 (3), 1044–1052.*

(28) Ng, V. W.; Taylor, M. K.; White, J. M.; Young, C. G. Cis-Dioxo-and Cis-(Hydroxo) Oxo-Mo (V) Complexes Stabilized by Intramolecular Hydrogen-Bonding. *Inorganic chemistry* **2010**, *49 (20), 9460–9469.*

(29) Basu, P.; Kail, B. W.; Adams, A. K.; Nemykin, V. N. Quantitation of the Ligand Effect in Oxo-Transfer Reactions of Dioxo-Mo (VI) Trispyrazolyl Borate Complexes. *Dalton Transactions 2013, 42 (9), 3071–3081.*

(30) Basu, P.; Nemykin, V. N.; Sengar, R. S. Substituent Effect on Oxygen Atom Transfer Reactivity from Oxomolybdenum Centers: Synthesis, Structure, Electrochemistry, and Mechanism. *Inorg. Chem.* **2009**, *48 (13), 6303–6313.* https://doi.org/10.1021/ic900579s.

(31) Kail, B. W.; Pérez, L. M.; Zarić, S. D.; Millar, A. J.; Young, C. G.; Hall, M. B.; Basu, P. Mechanistic Investigation of the Oxygen-Atom-Transfer Reactivity of Dioxo-Molybdenum (VI) Complexes. *Chemistry-A European Journal 2006, 12 (28), 7501–7509.*

(32) Basu, P.; Kail, B. W.; Young, C. G. Influence of the Oxygen Atom Acceptor on the Reaction Coordinate and Mechanism of Oxygen Atom Transfer From the Dioxo-Mo (VI) Complex, Tp i PrMoO2 (OPh), to Tertiary Phosphines. *Inorganic chemistry 2010, 49 (11), 4895–4900.*

(33) Berg, J. M.; Holm, R. H. Synthetic Approach to the Mononuclear Active Sites of Molybdoenzymes: Catalytic Oxygen Atom Transfer Reactions by Oxomolybdenum (IV, VI) Complexes with Saturation Kinetics and without Molybdenum (V) Dimer Formation. *Journal of the American Chemical Society* **1984**, *106 (10), 3035–3036.*

(34) Berg, J. M.; Holm, R. H. Model for the Active Site of Oxo-Transfer Molybdoenzymes: Synthesis, Structure, and Properties. *J. Am. Chem. Soc.* **1985**, *107 (4), 917–925.* https://doi.org/10.1021/ja00290a029.

(35) Berg, J. M.; Holm, R. H. Model for the Active Sites of Oxo-Transfer Molybdoenzymes: Reactivity, Kinetics, and Catalysis. *J. Am. Chem. Soc.* **1985**, *107 (4), 925– 932.* https://doi.org/10.1021/ja00290a030.

(36) Caradonna, J. P.; Reddy, P. R.; Holm, R. H. Kinetics, Mechanisms, and Catalysis of Oxygen Atom Transfer Reactions of S-Oxide and Pyridine N-Oxide Substrates with Molybdenum (IV, VI) Complexes: Relevance to Molybdoenzymes. *Journal of the American Chemical Society* **1988**, *110 (7), 2139–2144.*

(37) Craig, J. A.; Holm, R. H. Reduction of Nitrate to Nitrite by Molybdenum-Mediated Atom Transfer: A Nitrate Reductase Analog Reaction System. *J. Am. Chem. Soc.* **1989**, *111 (6), 2111–2115.* https://doi.org/10.1021/ja00188a026.

(38) Doonan, C. J.; Slizys, D. A.; Young, C. G. New Insights into the Berg−Holm Oxomolybdoenzyme Model. *J. Am. Chem. Soc.* **1999**, *121 (27), 6430–6436.* https://doi.org/10.1021/ja9900959.

(39) Craig, J. A.; Harlan, E. W.; Snyder, B. S.; Whitener, M. A.; Holm, R. H. Oxomolybdenum (IV, V, VI) Complexes: Structures, Reactivities, and Criteria of Detection of Binuclear (. Mu.-Oxo) Molybdenum (V) Products in Oxygen Atom Transfer Systems. *Inorganic Chemistry* **1989**, *28 (11), 2082–2091.*

(40) McMaster, J.; Tunney, J. M.; Garner, C. D. Chemical Analogues of the Catalytic Centers of Molybdenum and Tungsten Dithiolene-Containing Enzymes. *In Progress in Inorganic Chemistry; John Wiley & Sons, Inc.: Hoboken, NJ, USA*, **2004**; pp 539–583.

(41) Jiang, J.; Holm, R. H. Reaction Systems Related to Dissimilatory Nitrate Reductase: Nitrate Reduction Mediated by Bis(Dithiolene)Tungsten Complexes. *Inorg. Chem.* **2005**, *44 (4), 1068–1072.* https://doi.org/10.1021/ic040109y.

(42) Majumdar, A.; Pal, K.; Sarkar, S. Chemistry of [Et4N][MoIV(SPh)(PPh3)(Mnt)2] as an Analogue of Dissimilatory Nitrate Reductase with Its Inactivation on Substitution of Thiolate by Chloride. *J. Am. Chem. Soc.* **2006**, *128 (13), 4196–4197.* https://doi.org/10.1021/ja0586135.

(43) Chandra Srivastava, V. An Evaluation of Desulfurization Technologies for Sulfur Removal from Liquid Fuels. *RSC Adv.* **2012**, *2 (3), 759–783.* https://doi.org/10.1039/c1ra00309g.

(44) Adam, W.; Bargon, R. M. Synthesis of Thiiranes by Direct Sulfur Transfer: The Challenge of Developing Effective Sulfur Donors and Metal Catalysts. *Chem. Rev.* **2004**, *104 (1), 251–261.* https://doi.org/10.1021/cr030005p.

(45) Donahue, J. P. Thermodynamic Scales for Sulfur Atom Transfer and Oxo-for-Sulfido Exchange Reactions. *Chem. Rev.* **2006**, *106 (11), 4747–4783.* https://doi.org/10.1021/cr050044w.

(46) Nguyen, T. B. Recent Advances in Organic Reactions Involving Elemental Sulfur. *Adv. Synth. Catal.* **2017**, *359 (7), 1066–1130.* https://doi.org/10.1002/adsc.201601329.

(47) Inscore, F. E.; McNaughton, R.; Westcott, B. L.; Helton, M. E.; Jones, R.; Dhawan, I. K.; Enemark, J. H.; Kirk, M. L. Spectroscopic Evidence for a Unique Bonding Interaction in Oxo-Molybdenum Dithiolate Complexes: Implications for σ Electron Transfer Pathways in the Pyranopterin Dithiolate Centers of Enzymes. *Inorg. Chem.* **1999**, *38 (7), 1401–1410.* https://doi.org/10.1021/ic981126o.

(48) McNaughton, R. L.; Helton, M. E.; Rubie, N. D.; Kirk, M. L. The Oxo-Gate Hypothesis and DMSO Reductase: Implications for a Psuedo-σ Bonding Interaction Involved in Enzymatic Electron Transfer. *Inorg. Chem.* **2000**, *39 (20), 4386–4387.* https://doi.org/10.1021/ic000474z.

(49) Roberts, S. A.; Young, C. G.; Kipke, C. A.; Cleland, W. E., Jr; Yamanouchi, K.; Carducci, M. D.; Enemark, J. H. Dioxomolybdenum(VI) Complexes of the Hydrotris(3,5-Dimethyl-1-Pyrazolyl)Borate Ligand. Synthesis and Oxygen Atom Transfer Reactions. *Inorg. Chem.* **1990**, *29 (19), 3650–3656.* https://doi.org/10.1021/ic00344a007.

(50) Young, C. G. Facets of Early Transition Metal–Sulfur Chemistry: Metal–Sulfur Ligand Redox, Induced Internal Electron Transfer, and the Reactions of Metal–Sulfur Complexes with Alkynes. *J. Inorg. Biochem.* **2007**, *101 (11–12), 1562–1585.* https://doi.org/10.1016/j.jinorgbio.2007.06.040.

(51) Eagle, A. A.; Laughlin, L. J.; Young, C. G.; Tiekink, E. R. An Oxothio-Molybdenum (VI) Complex Stabilized by an Intramolecular Sulfur-Sulfur Interaction: Implications for the Active Site of Oxidized Xanthine Oxidase and Related Enzymes. *Journal of the American Chemical Society* **1992**, *114 (23), 9195–9197.*

(52) Laughlin, L. J.; Eagle, A. A.; George, G. N.; Tiekink, E. R.; Young, C. G. Synthesis, Characterization, and Biomimetic Chemistry of Cis-Oxosulfidomolybdenum (VI) Complexes Stabilized by an Intramolecular Mo (O) S⊙⊙⊙ S Interaction. *Inorganic chemistry* **2007**, *46 (3), 939–948.*

(53) Ng, V. W. L.; Taylor, M. K.; Young, C. G. Reactivity Studies of Oxo-Mo (IV) Complexes Containing Potential Hydrogen-Bond Acceptor/Donor Phenolate Ligands. *Inorganic Chemistry* **2012**, *51 (5), 3202–3211.*

(54) Smith, P. D.; Slizys, D. A.; George, G. N.; Young, C. G. Toward a Total Model for the Molybdenum Hydroxylases: Synthesis, Redox, and Biomimetic Chemistry of Oxo-Thio-Mo (vi) and-Mo (v) Complexes. *Journal of the American Chemical Society* **2000**, *122 (12), 2946–2947.*

(55) Doonan, C. J.; Nielsen, D. J.; Smith, P. D.; White, J. M.; George, G. N.; Young, C. G. Models for the Molybdenum Hydroxylases: Synthesis, Characterization and Reactivity of Cis-Oxosulfido-Mo (VI) Complexes. *Journal of the American Chemical Society* **2006**, *128 (1), 305–316.*

(56) Thapper, A.; Donahue, J. P.; Musgrave, K. B.; Willer, M. W.; Nordlander, E.; Hedman, B.; Hodgson, K. O.; Holm, R. H. The Unperturbed Oxo−Sulfido Functional Group Cis-MoVIOS Related to That in the Xanthine Oxidase Family of Molybdoenzymes: Synthesis, Structural Characterization, and Reactivity Aspects. *Inorg. Chem.* **1999**, *38 (18), 4104–4114.* https://doi.org/10.1021/ic990440v.

(57) Sugimoto, H.; Tatemoto, S.; Toyota, K.; Ashikari, K.; Kubo, M.; Ogura, T.; Itoh, S. Oxo-Sulfido- and Oxo-Selenido-Molybdenum(vi) Complexes Possessing a Dithioleneligand

Related to the Active Sites of Hydroxylases of Molybdoenzymes: Low Temperature Preparation and Characterisation. *Chem. Commun. (Camb.)* **2013**, *49 (39), 4358–4360.* https://doi.org/10.1039/c2cc35345h.

(58) Adam, W.; Bargon, R. M. Molybdenum-Catalyzed Episulfidation of (E)-Cycloalkenes with Elemental sulfurThis Work Was Presented at the XIXth International Symposium on the "Organic Chemistry of Sulfur." *Chemical Communications* **2000**, *No. 19, 1910–1911.*

(59) Adam, W.; Bargon, R. M.; Bosio, S. G.; Schenk, W. A.; Stalke, D. Direct Synthesis of Isothiocyanates from Isonitriles by Molybdenum-Catalyzed Sulfur Transfer with Elemental Sulfur. *J. Org. Chem.* **2002**, *67 (20), 7037–7041.* https://doi.org/10.1021/jo026042i.

(60) Adam, W.; Bargon, R. M.; Schenk, W. A. Direct Episulfidation of Alkenes and Allenes with Elemental Sulfur and Thiiranes as Sulfur Sources, Catalyzed by Molybdenum Oxo Complexes. *J. Am. Chem. Soc.* **2003**, *125 (13), 3871–3876.* https://doi.org/10.1021/ja029292p.

(61) Farrell, W. S.; Zavalij, P. Y.; Sita, L. R. Catalytic Production of Isothiocyanates via a Mo(II)/Mo(IV) Cycle for the "Soft" Sulfur Oxidation of Isonitriles. *Organometallics* **2016**, *35 (14), 2361–2366.* https://doi.org/10.1021/acs.organomet.6b00302.

(62) Jacob, J.; Espenson, J. H. Stereospecific Rhenium Catalyzed Desulfurization of Thiiranes. *Chem. Commun. (Camb.)* **1999**, *No. 11, 1003–1004.* https://doi.org/10.1039/a901708i.

(63) Eagle, A. A.; Gable, R. W.; Thomas, S.; Sproules, S. A.; Young, C. G. Sulfur Atom Transfer Reactions of Tungsten(VI) and Tungsten(IV) Chalcogenide Complexes. *Polyhedron* **2004**, *23 (2–3), 385–394.* https://doi.org/10.1016/j.poly.2003.11.026.

(64) Ward, J. P.; Lim, P. J.; Evans, D. J.; White, J. M.; Young, C. G. Tungsten Ligand-Based Sulfur-Atom-Transfer Catalysts: Synthesis, Characterization, Sustained Anaerobic Catalysis, and Mode of Aerial Deactivation. *Inorg. Chem.* **2020***, 59 (23), 16824–16828.* https://doi.org/10.1021/acs.inorgchem.0c02915.

Chapte 3 Construction of Fe-S Core by Persulfide

3.1 Abstract

The repair chemistry of oxidatively-damaged [Fe-S] clusters is involved in numerous biological processes. Biophysical and biochemical studies showed the presence of cysteine persulfide during the cluster repair in FNR and Fdx. However, the mechanism of the persulfide-mediated repair remains unknown. In order to gain chemical insights into the biological roles of persulfide in [Fe-S] cluster repairing, we have studied the reactivity of in situ generated organic persulfides with a series of ferric and ferrous iron complexes supported by *N,N'*-Ethylenebis(salicylimine) (salen) and its analogs. The mononuclear [Fe^{II}(salen)] and [Fe^{III}(salen)Cl] complex are converted to a μ-sulfidyl dimer species, [Fe^{III}(Salen)]$_2$S. This conversion was not able to achieve by other reactive sulfur species (RSS) or other commonly used organic sulfur donors. This present system implies that cellular persulfides might be able to repair damaged [Fe-S] clusters in cells serving as a source of bridging sulfide.

3.2 Introduction

Iron-sulfur (Fe-S) clusters are ancient and ubiquitous cofactors found in a wide range of proteins that perform essential functions in many cellular processes, including electron transfer, enzymatic catalysis, gene regulation.[1-3,9,45] The inherent redox chemistry of [Fe-S] cluster makes them particularly vulnerable to the damage by small molecule oxidants (like O_2, NO, O_2^-, H_2O_2 etc.), which enables regulatory proteins using [Fe-S] clusters to access the surrounding environment of cells.[4-6] Recent studies suggest that hydrogen sulfide (H_2S) and related reactive sulfur species like persulfide (RSSH/RSS[-]) are protective against oxidative and nitrosative stress in cells during infection.[25,42-45] In *Escherichia coli*, [Fe-S] protein Fumarate and nitrate reductase (FNR) is used to control gene expression in response to environmental O_2 level.[7-13] Exposure to air converts the [4Fe-4S] cluster in FNR to a [2Fe-2S] cluster, leading to a protein conformational change from DNA-binding dimer to monomer which can no longer bind to DNA (Scheme 3.1A).[13,14] Resonance Raman and structural studies indicate that in this cluster degradation, the bridging sulfides of the [4Fe-4S] cluster are stored in the form of [2Fe-2S] cluster-bound cysteine persulfides.[16,17] Thus, persulfide-ligated [2Fe-2S] clusters can be recycled back to [4Fe-4S] clusters with iron source and reductant in the absence of exogenous sulfide. Biochemical studies on another [2Fe-2S] protein, ferredoxin (Fdx), showed that NO damaged Fdx, DNIC-Fdx could be repaired to its original [2Fe-2S]-Fdx by incubation with cysteine, cysteine desulfurase, and O_2 (Scheme 3.1B).[17,18,20] Cysteine desulfurase can convert cysteine to protein bound persulfide, which serves as the sulfur source for the [2Fe-2S] cluster bridging sulfide.[19,20,26]
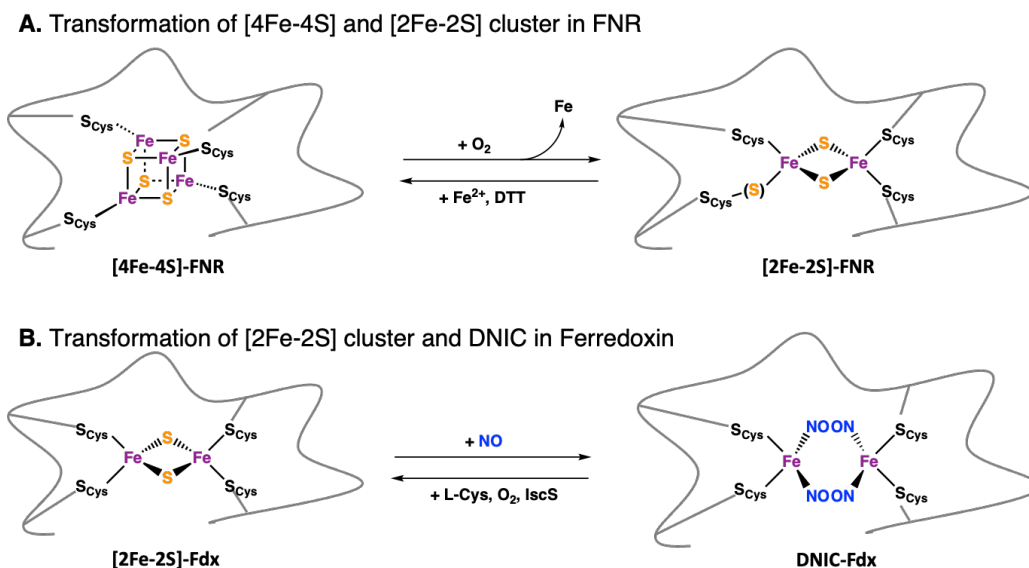
Scheme 3.1 In Vitro [Fe-S] cluster repair in FNR and ferredoxin
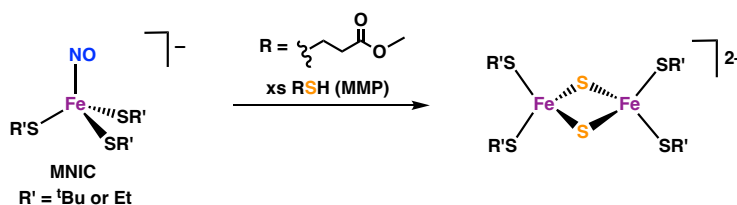
Scheme 3.2 Synthetic [2Fe-2S] cluster repair by MMP

We previously reported the repair chemistry of small molecule thiolate ligated mononitrosyl iron complexes (MNICs) to [2Fe-2S] clusters by the addition of nothing other than a cysteine analog methyl 3-mercaptopropionate (MMP) (Scheme 3.2).[21,22] The sulfur atom that forms the bridging sulfide in the [2Fe-2S] cluster was shown to be derived from MMP. Since cysteine persulfide is a better nucleophile than cysteine for metal binding,[23] and the S-S bond is easier to

break than the C-S bond providing the source for the bridging sulfide, we hypothesize that RSS⁻ would be a more efficient agent in the [Fe-S] repair than cysteine.

Despite the biological relevance, there have been no synthetic model systems for species with Fe-S core that can evaluate the role(s) of persulfides in the biosynthesis and the formation of Fe-S bridge. Due to the intricate and nuanced nature of the Fe-S core coupled with the cross-reactivity of the bounded thiolate ligand, interaction of persulfides and [Fe-S] cluster are difficult to detect directly.[2,3] Another challenge in conducting detailed studies on persulfides is their inherent instability.[24,27,28,36] Recently, Ming et al. reported a group of disulfide species with 9-Fluorenylmethyl (Fm) protecting group, which could degrade in response to base and lead to a reliable in situ release of persulfide (RSS⁻) (Scheme 3.3).[29] Herein, reported the first synthetic example for the Fe-S core construction by in situ generated small molecule persulfide using known N,N'-Ethylenebis(salicylimine) (salen) supported mononuclear iron complexes as model system. The redox-innocent salen ligand simplifies the reaction and the well-studied [Fe^{III}(salen)]$_2$S binuclear species makes it easier to monitor the Fe-S core assembly progress.[30, 31]

3.3 Results and Discussion

3.3.1 [Fe-S] cluster construction by persulfide

The base-sensitive persulfide donor FmSSPh^F was synthesized through a slightly modified literature procedure.[29] When treated with 1 equiv of DBU, the Fm protecting group of FmSSPh^F will be removed within 20 min, leading to the formation of 4-fluorophenyl persulfide (Ph^{F}SS⁻) as reactive species (Scheme 3.3). Without any trapping reagent, RSS⁻ are unstable species in solution. ¹H NMR study of the reaction solution showed the exist of protecting group fragment (9-

Vinylfluorene) and the formation of disulfide (Ph^F SSPh^F) which is the typical decomposition product of persulfides.[36]
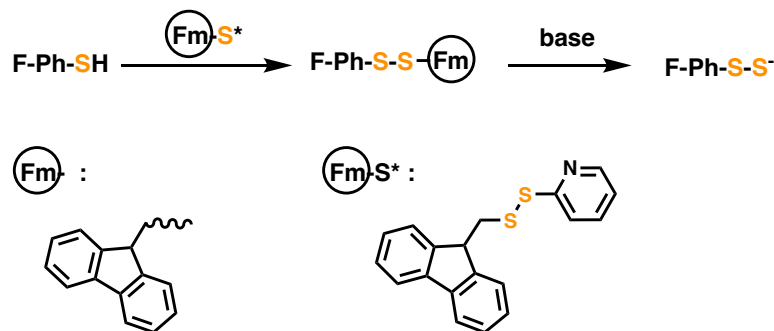
Scheme 3.3 *In situ* generation of persulfide from base sensitive precursor.

Introduction of equal molar amount of FmSSPh^F and base (DBU) in the solution of $(NEt_4)_2[Fe(SPh-F)_4]$ at $0\,^{\circ}C$ led to a rapid color change from yellow to purple, indicating the formation of $(NEt_4)_2 [Fe_2S_2(SPh^F)_4]$, which was further confirmed by UV-Vis and ^1H NMR. After the purification of the reaction mixture, the organic products are identified as corresponding thiolate (Ph^F S^-) and disulfide (Ph^F SSPh^F) by ^1H NMR (Eq (1)).

$$[Fe(SPh^F)_4]^{2-} + Ph^FSS^- \rightarrow 1/2 \ [Fe_2S_2(SPh^F)_4]^{2-} + 1/2 \ Ph^FSSPh^F + 2 \ Ph^FS^- \qquad (1)$$

$$[Fe(SPh^F)_4]^{2-} + S \rightarrow 1/2 \ [Fe_2S_2(SPh^F)_4]^{2-} + 1/2 \ Ph^FSSPh^F + Ph^FS^- \qquad (2)$$
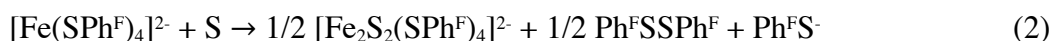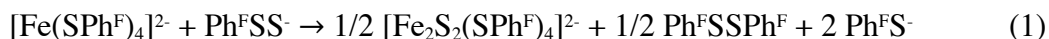
In general, synthetic assemble of binuclear [2Fe-2S] clusters always utilize sulfur as a source of bridging sulfide, the clusters being isolated in high yields from the reaction mixture of $[Fe(RS)_4]^{2-}$ and element sulfur (S_8) as shown in Eq. (2). While elemental sulfur is a typical decomposition product of persulfide, we questioned that whether persulfide is the one responsible

for the construction of [2Fe-2S]. Thus, analogous reaction with $(NEt_4)_2[Fe(SPh^F)_4]$ using element sulfur as sulfur source was also studied under same reaction condition, and this parallel experiment exhibited a significantly lower reaction rate than reaction starting from persulfide. Therefore, the hypothesis that the role of persulfide in [2Fe-2S] assembly is originated from its decay product element sulfur was ruled out. Addition of other possible decomposition product of persulfide, such as thiol or disulfide to $(NEt_4)_2[Fe(SPh^F)_4]^{2-}$ did not lead to the formation of [2Fe–2S] clusters. Under the reaction condition above, the *in situ* generated persulfide group served as an immediate sulfur donor for the following synthesis of [2Fe-2S] diamond core.

Persulfide is also involved in equilibrium ligand substitution reaction (Figure 3.1). Incubation of $(NEt_4)_2[Fe_2S_2(SPh)_4]$ with persulfide (Ph^FSS^-) generating from base-sensitive precursor and DBU will result in [2Fe-2S] cluster bearing F containing ligands confirmed by ^{19}F NMR spectrum. The ^1H NMR spectrum of the reaction solution features resonances in the 8.97 and 4.75 ppm, attributable to $(NEt_4)_2[Fe_2S_2(SPh^F)_4]$. Control experiment of $(NEt_4)_2[Fe_2S_2(SPh)_4]$ with same amount of thiolate (Ph^FS^-) gave similar result but with a much slower ligand substitution rate. This result matches with the fact that the persulfide is more acidic than corresponding thiol.
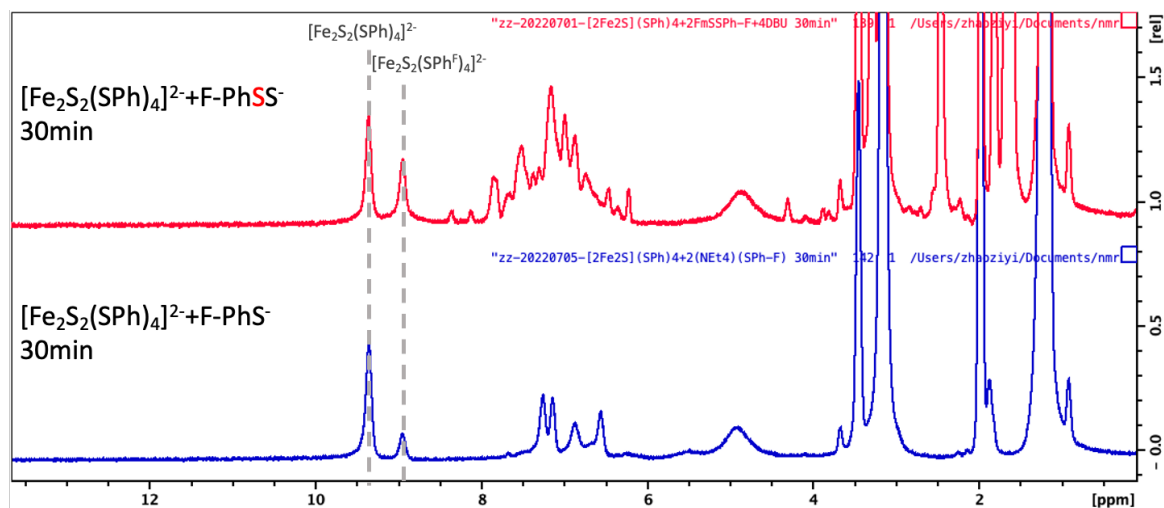
Figure 3.1 1H NMR of (NEt$_4$)$_2$[Fe$_2$S$_2$(SPh)$_4$] with persulfide and thiolate reaction.

Overall, persulfide possess different personality than other reactive sulfur species (RSS) found in biological systems (thiol/thiolate, disulfide and elemental sulfur), which makes it promising in some harder reaction which cannot be achieve by other RRS.

3.3.2 Persulfide Reactivity with Salen Supported Iron

While the construction of biorelevant [2Fe-2S] cluster is interesting, the thiol ligands of the mononuclear Fe source and the resulting cluster confuse the further study due to its redox non innocent. Moreover, considering the instability of persulfide, the fact that its decomposition products also involve in the reaction makes things more complicated.

In order to gain chemical insights into how persulfide can form a [Fe-S] cluster, we studied the reactivity of organic persulfides with ferrous iron complex supported by a more simplified ligand system, N,N′-Ethylenebis(salicylimine) (Salen). [Fe^{II}(Salen)] was prepared by mixing equal mol amount of Fe(OAc) and Salen ligand in MeCN solution as reported previously. Addition of 1

equiv *in situ* generated persulfide, $Ph^F\text{-}SS^-$ to $[Fe^{II}(Salen)]$ led to slightly color change to dark red. UV-vis monitor suggested the formation of a new species within 1h at room temperature. The reaction is very clean and even crude reaction mixture exhibit well-resolved paramagnetic NMR signals, which matches with pervious reported μ-sulfidyl dimer species, $[Fe^{III}(Salen)]_2S$ (Figure 3.2).[30] KBr IR of the product showed a μ-sulfidyl structure, which further confirmed the formation of $[Fe^{III}(Salen)]_2S$. Quantitative (96%) $[Fe^{III}(Salen)]_2S$ formation could be achieved using excess amount of persulfide (1eq. with respected to $[Fe^{II}(Salen)]$). When stoichiometric amount of persulfide (0.5 eq with respected to $[Fe^{II}(Salen)]$) is using, the reaction could also been performed, with a lower yield.
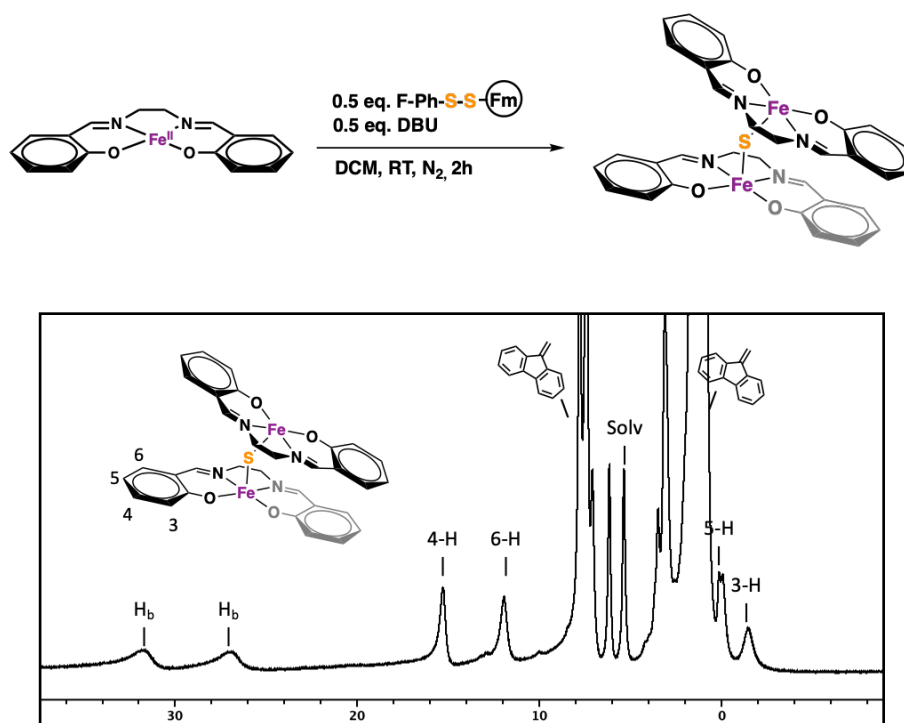
Figure 3.2 In situ MNR spectrum of $[Fe^{II}(salen)]$ with persulfide reaction.

Addition of thiol Ph^FSH or thiolate [NEt$_4$](SPh^F) to [Fe^{II}(salen)] did not lead to the formation of [Fe^{III}(Salen)]$_2$S. Instead, a new set of paramagnetic NMR signals were generated from the reaction mixture, which were assigned as [Fe^{II}(salen)(SPh^F)]$^-$. This observation also aligns with previous studies showing that [Fe^{II}(Salen)] can accept monoanionic ligands (L$^-$ = F$^-$, Cl$^-$, OH$^-$, NCS$^-$, CN$^-$, SH$^-$) at axial position to generate purplish five-coordinate [Fe^{II}(salen)L]$^-$ complexes.[40] While the ability of [Fe^{II}(salen)] binding axial ligands L$^-$ was recognized, a feasible reaction pathway of Fe-S core construction was proposed with deprotonated persulfide binding to ferrous center as the first step (Scheme 3.4).
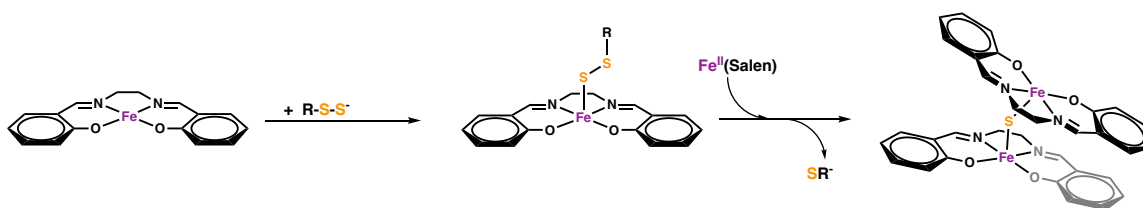
Scheme 3.4 Proposed reaction pathway for persulfide construction of [Fe^{III}(Salen)]$_2$S

Low-temperature UV-vis was used to capture the possibly formed intermediate. As shown in Figure 2, [Fe^{II}(Salen)] was pre mixed with base-sensitive persulfide donor, and the addition of DBU at -40°C result in an rapid color change from light red to purple. The [Fe^{II}(Salen)] feature at 479 nm disappear immediately after the generation of persulfide, confirming the formation of intermediate species. At -40°C, the intermediate species is stable for 10 min. As the system warm to room temperature, a new feature at 504 nm start growing, which matches the absorption brand of authentic [Fe^{III}(Salen)]$_2$S that independently synthesized form the oxo for sulfido exchange with [Fe^{III}(Salen)]$_2$O. (Figure 3.3)
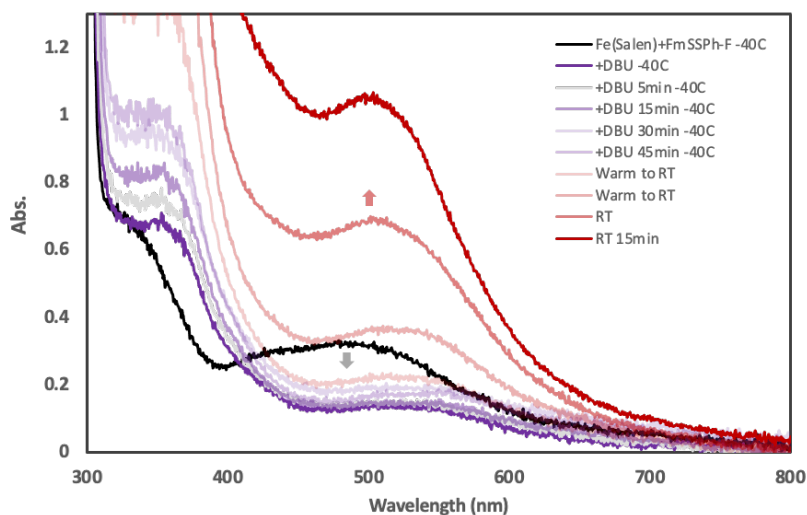
Figure 3.3 UV monitoring of [Fe(Salen)] with persulfide reaction at -40 °C The [Fe^{II}(salen)] feature at 479 nm disappear immediately after the generation of persulfide, indicating the formation of a new intermediate species.

One advantage of using ferrous salen as Fe source is its inertness toward other commonly used sulfur donors (Scheme 3.5). Treatment of elemental sulfur or $(Me_3Si)_2S$ to [Fe^{II}(Salen)] under similar reaction condition will not lead to any reaction. This helps to eliminate the influence of persulfide decay product on the Fe-S core generation, and thus the *in situ* generated persulfide itself is fully responsible for the [Fe^{II}(Salen)] to [Fe^{III}(Salen)]$_2$S conversion.
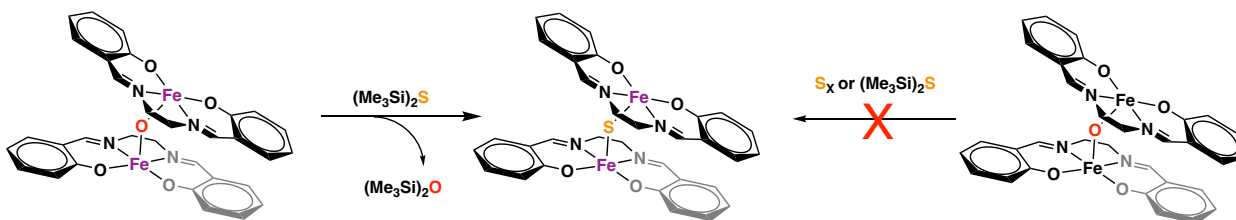
Scheme 3.5 Synthesis of authentic [Fe^{III}(Salen)]$_2$S

In situ generated persulfide were also able to convert [Fe^{III}(Salen)Cl] to [Fe^{III}(Salen)]$_2$S, 98%

conversion could be achieved within 2h when using excess amount of persulfide confirmed by 1H

NMR. (Scheme 3.6) Different from reaction started from [Fe^{II}(Salen)], at least 1 eq. of persulfide

per [Fe^{III}(Salen)Cl] is required to perform this reactivity. Insufficient persulfide (less than 1 eq. per

Fe center) lead to the generation of new unknow species on 1H NMR spectra. Analyzing the

pentane wash of equal molar amount [Fe^{III}(Salen)Cl] with persulfide reaction suggests disulfide

(Ph^F-SS-Ph^F) as the organic product of this reaction. Again, this reactivity shows its distinctiveness

towards persulfide, and the conversion could not be achieved by other reactive sulfur species, like

thiol, thiolate, or elemental sulfur. Sulfur donor like (Me$_3$Si)$_2$S is also ineffective.
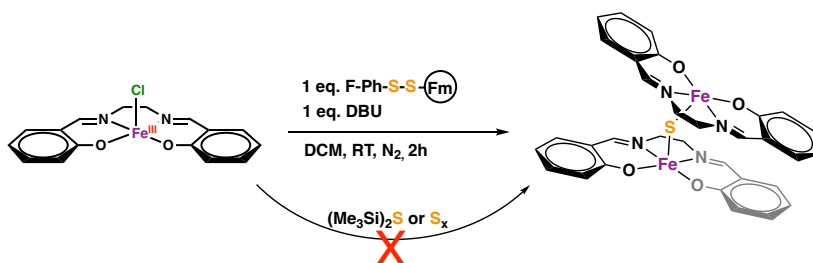
Scheme 3.6 Conversion of [Fe^{III}(Salen)Cl] to [Fe^{III}(Salen)]$_2$S upon addition of persulfide

Overall, the reaction of *in situ* generated persulfide with Salen supported Fe^{II} and Fe^{III}

complexes could be summarized as Eq. (3) and Eq. (4). In the case of [Fe^{II}(Salen)], the *in situ*

generated persulfide donates its sulfane sulfur (S^0) as source of bridging sulfide (S^{2-}) to generate

the Fe-S-Fe core structure. The Fe^{II} center was then oxidized by one electron and giving

[Fe^{III}(Salen)]$_2$S as the final product. (Eq. (3)). On the other hand, for the reaction start with

[Fe^{III}(Salen)Cl], the oxidation states remain unchanged for the Fe site, so excess amount of

persulfide is needed as a source of electron, and the reaction proceed following Eq. (4) where the

redox reaction takes place with the persulfide to yield the $[Fe^{III}(Salen)]_2S$ bridging sulfide (S^{2-}), along with elemental sulfur (S^0) and disulfide (S^{-1}).

$$2\ [Fe^{II}(Salen)] + R\text{-}SS^- \rightarrow [Fe^{III}(Salen)]_2S + RS^- \qquad (3)$$

$$2\ [Fe^{III}(Salen)Cl] + 2\ R\text{-}SS^- \rightarrow [Fe^{III}(Salen)]_2S + R\text{-}SS\text{-}R + S + 2\ Cl^- \qquad (4)$$

3.3.3 Conclusion

Persulfide are universally important species in the biosynthesis and repairing of damaged [Fe-S] clusters. *In situ* generated small molecule persulfide from the base-sensitive precursor FmSSPh^F were able to serve as a sulfur source for the assemble of $[Fe_2S_2(SPh^F)]^{2-}$ with $Fe(SPh^F)_4^{2-}$ as the source of iron. Treatment of persulfide to $[Fe^{II}(salen)]$ and $[Fe^{III}(salen)Cl]$ generates a μ-sulfidyl dimer species, $[Fe^{III}(salen)]_2S$, analogous to the formation of bridging sulfide by cysteine persulfide in FNR and Fdx. Furthermore, it was shown that it is specifically the persulfide achieves this conversion and not a thiol, providing evidence for the first time that persulfide RSS$^-$ is an effective reagent for the formation of [Fe-S] cores in discrete complexes.

3.4 Experimental Section

General Considerations. All synthesized products were assumed to be air- and moisture-sensitive. They were manipulated under argon on a standard Schlenk line or in an atmosphere of purified nitrogen in an MBraun Labmaster SP glovebox ($O_2 < 1$ ppm; $H_2O < 1$ ppm). Solvents were purified by passing through a series of two activated alumina columns (MBraun solvent purification system) under an Ar atmosphere and stored over 4 Å molecular sieves. Reagents 4-fluorothiophenol, bis-4-fluorodisulfide, 1,8-diazabicyclo[5.4.0]undec-7-ene (DBU), 9-

Fluorenylmethylthiol (FmSH), 4,4'- dithiodipyridine (PySSPy) were purchased from Sigma at the highest available purity and used as received. UV-Vis spectra were recorded on a Varian Cary 50 Bio spectrometer. NMR spectra were recorded at 400 MHz on a Bruker UltraShield spectrometer and residual solvent signals were used as an internal reference.

Synthesis and Reactivity Studies. Authentic $(NEt_4)_2[Fe(SPh^F)_4]$,[32,33] $(Et_4N)_2[Fe_2S_2(SPh^F)_4]$,[33] $(Et_4N)_2[Fe_2S_2(SPh)_4]$,[33] $[Fe^{II}(salen)]$,[30] $[Fe^{III}(salen)Cl]$,[34] $[Fe^{III}(Salen)]_2S$,[30] and $FmSSPy$[29] were prepared as described in literature with slight modifications.

Synthesis of FmSSPh^F. FmSSPy (91 mg, 0.284 mmol) was added into a stirred solution of 4-fluorothiophenol (Ph^{F}SH, 40 mg, 0.312 mmol) in 3.5 mL DCM at room temperature. The color of the reaction immediately became yellow and the reaction was allowed to stirred for 1h at room temperature. The mixture was diluted with DCM and washed with water and brine. A flash column chromatography using a mixture of EtOAc and hexanes on silica gel gave the corresponding products. ^{1}H NMR (400 MHz, CDCl$_3$) δ 7.79 (d, 2H), 7.65 (d, 2H), 7.53 (m, 2H), 7.43 (t, 2H), 7.34 (t, 2H), 7.06 (t, 2H), 4.33 (t, H), 3.30 (m, 2H)
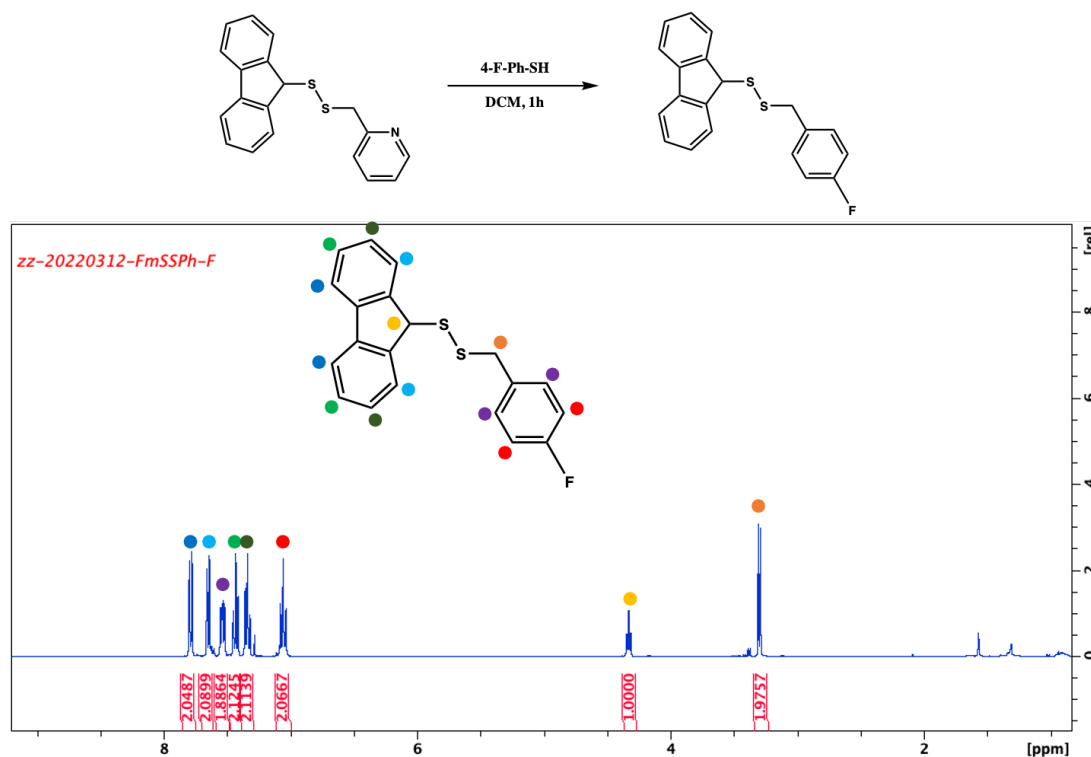
Figure 3.4 1H NMR of FmSSPh^F.

Reaction of (NEt₄)₂[Fe(SPh^F)₄] with FmSSPh^F and DBU. A solution of $(NEt_4)_2[Fe(SPh^F)_4]$ (24.4 mg, 0.03 mmol) in 2.0 mL of MeCN was transferred to a 10 mL Schlenk flask, to which 1 mL stock solution of FmSSPh^F (0.03 M in DCM) was added. The mixture was cooled in ice bath and DBU (1 mL of 0.03 M stock solution in DCM) was injected at 0°C. The reaction mixture was turned to a purplish color immediately. The reaction was allowed to be stirred for 1h and the solvent was then removed under vacuum. The solid was washed with pentane for 3 times to afford $(Et_4N)_2[Fe_2S_2(SPh^F)_4]$ which was confirmed by ^1H NMR and UV-vis spectroscopy. Further analyzation of the pentane wash by ^1H NMR showed the formation of corresponding thiolate (Ph^F S^-) and disulfide (Ph^F SSPh^F).
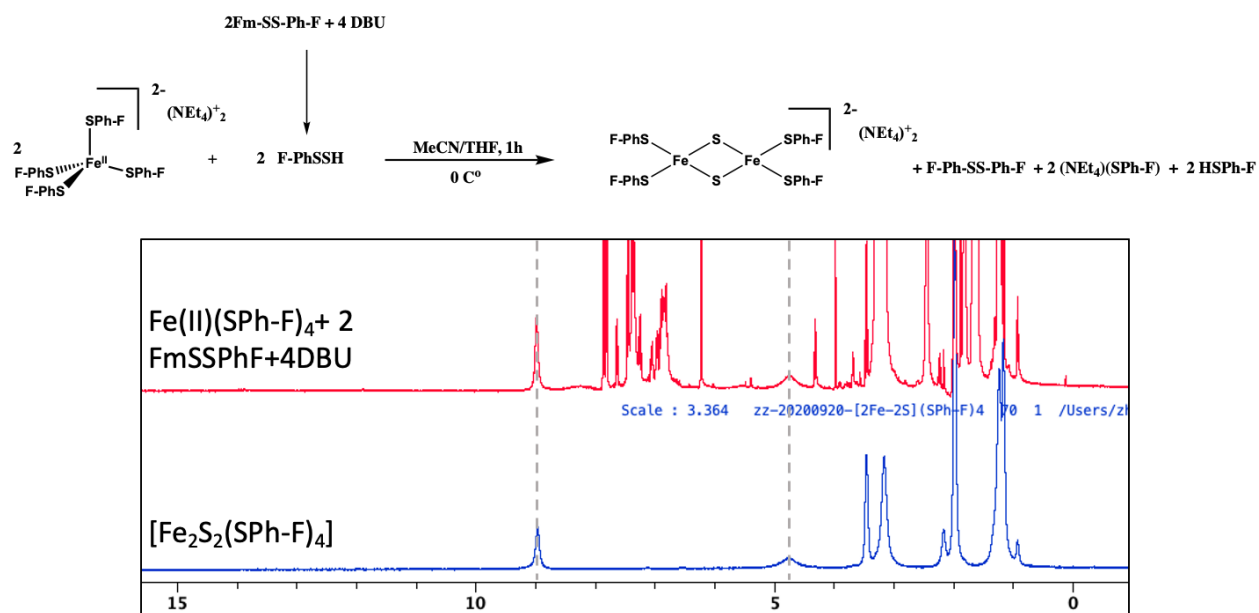
Figure 3.5 1H NMR of $(NEt_4)_2[Fe(SPh^F)_4]$ with FmSSPh^F and DBU reaction.

Reaction of $(Et_4N)_2[Fe_2S_2(SPh)_4]$ with FmSSPh^F and DBU. A solution of *$(Et_4N)_2[Fe_2S_2(SPh)_4]$*
(6.44 mg, 0.0075 mmol) in 2.0 mL of MeCN was transferred to a 10 mL Schlenk flask, to which
1 mL stock solution of FmSSPh^F (0.03 M in DCM) was added followed by the addition of DBU
(1 mL, 0.03 M in DCM). The reaction was allowed to be stirred for 30 min and the solvent was
then removed under vacuum. ^{1}H NMR indicated the formation of $(Et_4N)_2[Fe_2S_2(SPh^F)_4]$
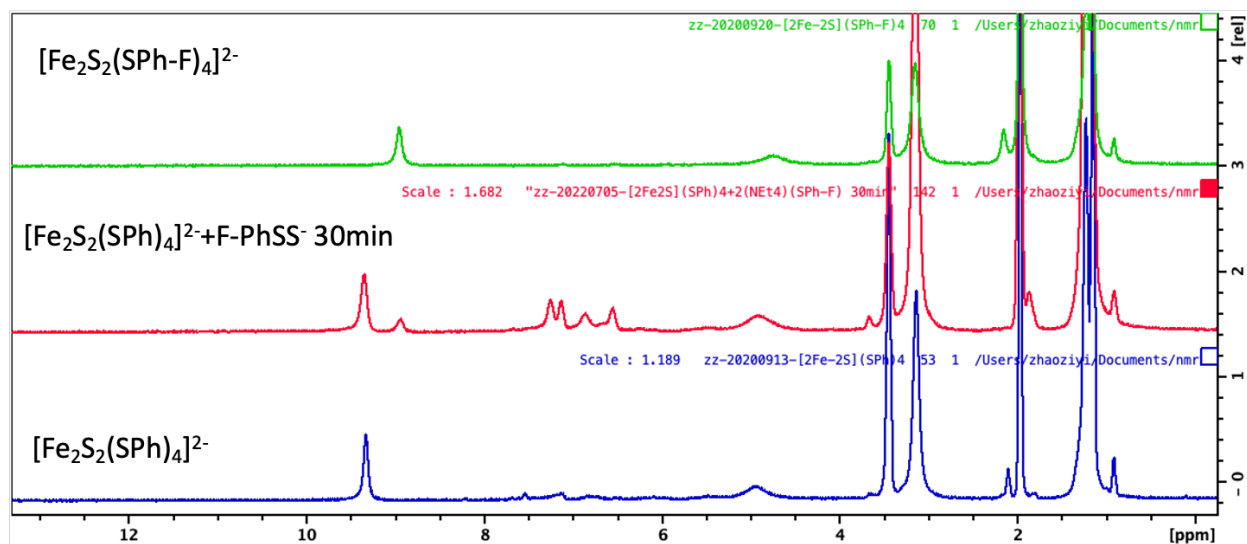
Figure 3.6 1H NMR of (Et₄N)₂[Fe₂S₂(SPh)₄] with FmSSPhᶠ and DBU reaction

Reaction of Fe(salen) with FmSSPhᶠ and DBU. To a stirred solution of [Feᴵᴵ(salen)] (19.0 mg, 0.06 mmol) in 2.0 mol of DCM was added 1 mL stock solution of FmSSPhᶠ (0.03 M in DCM), followed by DBU (1 mL of 0.03 M stock solution in DCM). The reaction was allowed to procced for 1h at room temperature, over which time the color of the reaction mixture was changed to dark red. The solvent was removed under vacuum and a crude NMR was collected in CD_2Cl_2. ¹H NMR and other physical characterization (UV-vis and IR spectroscopy) was in agreement with that previously reported for [Feᴵᴵᴵ(Salen)]₂S.[30,31]

Control reaction of [Feᴵᴵ(salen)] with other RSS.

a. *Reaction with (NEt₄)(SPhᶠ)*. To a stirred solution of [Feᴵᴵ(salen)] (19.0 mg, 0.06 mmol) in 2.0 mol of DCM was added 1 mL stock solution of (NEt₄)(SPhᶠ) (0.03 M in DCM). The color of the solution was turned into dark purple within 10s. The reaction was allowed to procced for 1h at room temperature. The solvent was removed under vacuum and a crude NMR was

collected in CDCl$_2$. ^{1}H NMR indicated the formation of a new paramagnetic species which was assigned as (NEt$_4$)[Fe(salen) (SPh^F)].

b. *Reaction with S$_8$ or (Me$_3$Si)$_2$S.* To a stirred solution of [Fe^{II}(salen)] (80 mg, 0.24 mmol) in 5.0 mol of DCM was added *(Me$_3$Si)$_2$S* (51μL, 0.12 mmol) or elemental S (7.68 mg, 0.24 mmol). The reaction was allowed to procced for 1h at room temperature. No reaction was observed by ^{1}H NMR.

Reaction of [Fe^{III}(salen)Cl], with excess FmSSPh^F and DBU. To a stirred solution of [Fe^{III}(salen)Cl] (10.6 mg, 0.06 mmol) in 1.0 mol of DCM was added 2 mL stock solution of FmSSPh^F (0.03 M in DCM), followed by DBU (2 mL of 0.03 M stock solution in DCM). The reaction was allowed to procced for 1h at room temperature, over which time the color of the reaction mixture was changed to dark red. The solvent was removed under vacuum. ^{1}H NMR and other physical characterization (UV-vis and IR spectroscopy) of the product matches with that previously reported for [Fe^{III}(Salen)]$_2$S.[30,31]

3.5 References

(1) Beinert, H.; Holm, R. H.; Münck, E. Iron-Sulfur Clusters: Nature's Modular, Multipurpose Structures. Science 1997, 277 (5326), 653–659. https://doi.org/10.1126/science.277.5326.653.

(2) Bian, S.; Cowan, J. A. Protein-Bound Iron–Sulfur Centers. Form, Function, and Assembly. Coord. Chem. Rev. 1999, 190–192, 1049–1066. https://doi.org/10.1016/s0010-8545(99)00157-5.

(3) Venkateswara Rao, P.; Holm, R. H. Synthetic Analogues of the Active Sites of Iron-Sulfur Proteins. Chem. Rev. 2004, 104 (2), 527–559. https://doi.org/10.1021/cr020615+.

(4) Mettert, E. L.; Kiley, P. J. Fe-S Proteins That Regulate Gene Expression. Biochim. Biophys. Acta 2015, 1853 (6), 1284–1293. https://doi.org/10.1016/j.bbamcr.2014.11.018.

(5) Crack, J. C.; Le Brun, N. E. Redox-Sensing Iron-Sulfur Cluster Regulators, Antioxid. Antioxid. Redox Signal 2018, 29, 1809–1829.

(6) Kiley, P. J.; Beinert, H. The Role of Fe-S Proteins in Sensing and Regulation in Bacteria. Curr. Opin. Microbiol. 2003, 6 (2), 181–185. https://doi.org/10.1016/s1369-5274(03)00039-0.

(7) Crack, J. C.; Green, J.; Thomson, A. J.; Le Brun, N. E. Iron-Sulfur Clusters as Biological Sensors: The Chemistry of Reactions with Molecular Oxygen and Nitric Oxide. Acc. Chem. Res. 2014, 47 (10), 3196–3205. https://doi.org/10.1021/ar5002507.

(8) Fleischhacker, A. S.; Kiley, P. J. Iron-Containing Transcription Factors and Their Roles as Sensors. Curr. Opin. Chem. Biol. 2011, 15 (2), 335–341. https://doi.org/10.1016/j.cbpa.2011.01.006.

(9) Crack, J. C.; Green, J.; Thomson, A. J.; Le Brun, N. E. Iron-Sulfur Cluster Sensor-Regulators. Curr. Opin. Chem. Biol. 2012, 16 (1–2), 35–44. https://doi.org/10.1016/j.cbpa.2012.02.009.

(10) Popescu, C. V.; Bates, D. M.; Beinert, H.; Munck, E.; Kiley, P. J. Mossbauer Spectroscopy as a Tool for the Study of Activation/Inactivation of the Transcription Regulator FNR in Whole Cells of Escherichia Coli. Proc Natl Acad Sci 1998, 95, 13431–13435.

(11) Sutton, V. R.; Mettert, E. L.; Beinert, H.; Kiley, P. Kinetic Analysis of the Oxidative Conversion of the 2+ Cluster of FNR to a 2+ Cluster. J Bacteriol 2004, 186, 8018–8025.

(12) Sutton, V. R.; Stubna, A.; Patschkowski, T.; Münck, E.; Beinert, H.; Kiley, P. J. Superoxide Destroys the [2Fe-2S]2+ Cluster of FNR from Escherichia Coli. Biochemistry 2004, 43 (3), 791–798. https://doi.org/10.1021/bi0357053.

(13) Khoroshilova, N.; Popescu, C.; Münck, E.; Beinert, H.; Kiley, P. J. Iron-Sulfur Cluster Disassembly in the FNR Protein of Escherichia Coli by O2: [4Fe-4S] to [2Fe-2S] Conversion with Loss of Biological Activity. Proc. Natl. Acad. Sci. U. S. A. 1997, 94 (12), 6087–6092. https://doi.org/10.1073/pnas.94.12.6087.

(14) Crack, J. C.; Gaskell, A. A.; Green, J.; Cheesman, M. R.; Le Brun, N. E.; Thomson, A. J.]2+ Cluster Switch in the Transcriptional Regulator FNR. J Am Chem Soc 2008, 130, 1749–1758.

(15) Zhang, B.; Crack, J. C.; Subramanian, S.; Green, J.; Thomson, A. J.; Le Brun, N. E.; Johnson, M. K. Reversible Cycling between Cysteine Persulfide-Ligated [2Fe-2S] and Cysteine-Ligated [4Fe-4S] Clusters in the FNR Regulatory Protein. Proc. Natl. Acad. Sci. U. S. A. 2012, 109 (39), 15734–15739. https://doi.org/10.1073/pnas.1208787109.

(16) Nicolet, Y.; Rohac, R.; Martin, L. Fontecilla-Camps, J. C. X-Ray Snapshots of Possible Intermediates in the Time Course of Synthesis and Degradation of Protein-Bound Fe4S4 Clusters. Proc Natl Acad Sci 2013, 110, 7188–7192.

(17) Grabarczyk, D. B.; Ash, P. A.; Vincent, K. A. Infrared Spectroscopy Provides Insight into the Role of Dioxygen in the Nitrosylation Pathway of a [2Fe2S] Cluster Iron-Sulfur Protein. J. Am. Chem. Soc. 2014, 136 (32), 11236–11239. https://doi.org/10.1021/ja505291j.

(18) Rogers, P. A.; Ding, H. L-Cysteine-Mediated Destabilization of Dinitrosyl Iron Complexes in Proteins. J. Biol. Chem. 2001, 276 (33), 30980–30986. https://doi.org/10.1074/jbc.M101037200.

(19) Yang, W.; Rogers, P. A.; Ding, H. Repair of Nitric Oxide-Modified Ferredoxin [2Fe-2S] Cluster by Cysteine Desulfurase (IscS). J. Biol. Chem. 2002, 277 (15), 12868–12873. https://doi.org/10.1074/jbc.M109485200.

(20) Yang, J.; Duan, X.; Landry, A. P.; Ding, H. Oxygen Is Required for the L-Cysteine-Mediated Decomposition of Protein-Bound Dinitrosyl-Iron Complexes. Free Radic. Biol. Med. 2010, 49 (2), 268–274. https://doi.org/10.1016/j.freeradbiomed.2010.04.012.

(21) Fitzpatrick, J.; Kalyvas, H.; Filipovic, M. R.; Ivanović-Burmazović, I.; MacDonald, J. C.; Shearer, J.; Kim, E. Transformation of a Mononitrosyl Iron Complex to a [2Fe-2S] Cluster by a Cysteine Analogue. J. Am. Chem. Soc. 2014, 136 (20), 7229–7232. https://doi.org/10.1021/ja5024207.

(22) Fitzpatrick, J.; Kim, E. New Synthetic Routes to Iron-Sulfur Clusters: Deciphering the Repair Chemistry of [2Fe-2S] Clusters from Mononitrosyl Iron Complexes. Inorg. Chem. 2015, 54 (22), 10559–10567. https://doi.org/10.1021/acs.inorgchem.5b00961.

(23) Álvarez, L.; Bianco, C. L.; Toscano, J. P.; Lin, J.; Akaike, T.; Fukuto, J. M. Chemical Biology of Hydropersulfides and Related Species: Possible Roles in Cellular Protection and Redox Signaling. Antioxid. Redox Signal. 2017, 27 (10), 622–633. https://doi.org/10.1089/ars.2017.7081.

(24) Dillon, K. M.; Matson, J. B. A Review of Chemical Tools for Studying Small Molecule Persulfides: Detection and Delivery. ACS Chem. Biol. 2021, 16 (7), 1128–1141. https://doi.org/10.1021/acschembio.1c00255.

(25) Ida, T.; Sawa, T.; Ihara, H.; Tsuchiya, Y.; Watanabe, Y.; Kumagai, Y.; Suematsu, M.; Motohashi, H.; Fujii, S.; Matsunaga, T.; Yamamoto, M.; Ono, K.; Devarie-Baez, N. O.; Xian, M.; Fukuto, J. M.; Akaike, T. Reactive Cysteine Persulfides and S-Polythiolation Regulate Oxidative Stress and Redox Signaling. Proc. Natl. Acad. Sci. U. S. A. 2014, 111 (21), 7606–7611. https://doi.org/10.1073/pnas.1321232111.

(26) Pandey, A.; Golla, R.; Yoon, H.; Dancis, A.; Pain, D. Persulfide Formation on Mitochondrial Cysteine Desulfurase: Enzyme Activation by a Eukaryote-Specific Interacting Protein and Fe-S Cluster Synthesis. Biochem. J. 2012, 448 (2), 171–187. https://doi.org/10.1042/BJ20120951.

(27) Cuevasanta, E.; Möller, M. N.; Alvarez, B. Biological Chemistry of Hydrogen Sulfide and Persulfides. Arch. Biochem. Biophys. 2017, 617, 9–25. https://doi.org/10.1016/j.abb.2016.09.018.

(28) Cuevasanta, E.; Benchoam, D.; Semelak, J. A.; Möller, M. N.; Zeida, A.; Trujillo, M.; Alvarez, B.; Estrin, D. A. Possible Molecular Basis of the Biochemical Effects of Cysteine-Derived Persulfides. Front. Mol. Biosci. 2022, 9, 975988. https://doi.org/10.3389/fmolb.2022.975988.

(29) Park, C.-M.; Johnson, B. A.; Duan, J.; Park, J.-J.; Day, J. J.; Gang, D.; Qian, W.-J.; Xian, M. 9-Fluorenylmethyl (Fm) Disulfides: Biomimetic Precursors for Persulfides. Org. Lett. 2016, 18 (5), 904–907. https://doi.org/10.1021/acs.orglett.5b03557.

(30) Dorfman, J. R.; Girerd, J. J.; Simhon, E. D.; Stack, T. D. P.; Holm, R. H. Synthesis, Structure, and Electronic Features of (.Mu.-Sulfido)Bis[(N,N'-Ethylenebis(Salicylaldiminato))Iron(III)], [Fe(Salen)]2S, Containing the Only Authenticated Example of the Iron(III)-Sulfur-Iron(III) Single Bridge. Inorg. Chem. 1984, 23 (26), 4407–4412. https://doi.org/10.1021/ic00194a002.

(31) Mukherjee, R. N.; Stack, T. D. P.; Holm, R. H. Angle Dependence of the Properties of the [Fe2X] 4+ Bridge Unit (X= O, S): Structures, Antiferromagnetic Coupling, and Properties in Solution. Journal of the American Chemical Society 1988, 110 (6), 1850–1861.

(32) Hagen, K. S.; Watson, A. D.; Holm, R. H. Synthetic Routes to Iron Sulfide (Fe2S2, Fe3S4, Fe4S4, and Fe6S9), Clusters from the Common Precursor Tetrakis (Ethanethiolate) Ferrate (2-) Ion ([Fe (SC2H5) 4] 2-): Structures and Properties of [Fe3S4 (SR) 4] 3-and Bis (Ethanethiolate) Nonathioxohexaferrate (4-) Ion ([Fe6S9 (SC2H5) 2] 4-), Examples of the Newest Types of Fe-S-SR Clusters. Journal of the American Chemical Society 1983, No. 12, 3905–3913.

(33) Han, S.; Czernuszewicz, R. S.; Spiro, T. G. Convenient Synthetic Route to [Fe2S2 (SR) 4] 2-via Reaction of [Fe (SR) 4]-with Sulfur. Inorganic Chemistry 1986, 25 (13), 2276–2277.

(34) Sharghi, H.; Aboonajmi, J.; Aberi, M. One-Pot Multicomponent Reaction of Catechols, Ammonium Acetate, and Aldehydes for the Synthesis of Benzoxazole Derivatives Using the Fe (III)-Salen Complex. The Journal of Organic Chemistry 2020, 85 (10), 6567–6577.

(35) Gervason, S.; Larkem, D.; Mansour, A. B.; Botzanowski, T.; Müller, C. S.; Pecqueur, L.; Le Pavec, G.; Delaunay-Moisan, A.; Brun, O.; Agramunt, J.; Grandas, A.; Fontecave, M.; Schünemann, V.; Cianférani, S.; Sizun, C.; Tolédano, M. B.; D'Autréaux, B. Physiologically Relevant Reconstitution of Iron-Sulfur Cluster Biosynthesis Uncovers Persulfide-Processing Functions of Ferredoxin-2 and Frataxin. Nat. Commun. 2019, 10 (1), 3566. https://doi.org/10.1038/s41467-019-11470-9.

(36) Lau, N.; Pluth, M. D. Reactive Sulfur Species (RSS): Persulfides, Polysulfides, Potential, and Problems. Curr. Opin. Chem. Biol. 2019, 49, 1–8. https://doi.org/10.1016/j.cbpa.2018.08.012.

(37) Fitzpatrick, J.; Kim, E. Synthetic Modeling Chemistry of Iron-Sulfur Clusters in Nitric Oxide Signaling. Acc. Chem. Res. 2015, 48 (8), 2453–2461. https://doi.org/10.1021/acs.accounts.5b00246.

(38) Sivasubramanian, V. K.; Ganesan, M.; Rajagopal, S.; Ramaraj, R. Iron (III)− Salen Complexes as Enzyme Models: Mechanistic Study of Oxo (Salen) Iron Complexes Oxygenation of Organic Sulfides. The Journal of organic chemistry 2002, 67 (5), 1506–1514.

(39) Smith, A. D.; Agar, J. N.; Johnson, K. A.; Frazzon, J.; Amster, I. J.; Dean, D. R.; Johnson, M. K. Sulfur Transfer from IscS to IscU: The First Step in Iron− Sulfur Cluster Biosynthesis. Journal of the american chemical society 2001, 123 (44), 11103–11104.

(40) Mukherjee, R. N.; Abrahamson, A. J.; Patterson, G. S.; Stack, T. D. P.; Holm, R. H. A New Class of (N,N'-Bis(Salicylideneamino)Ethanato)Iron(II) Complexes: Five-Coordinate [FeII(Salen)L]-. Preparation, Properties, and Mechanism of Electron-Transfer Reactions. Inorg. Chem. 1988, 27 (12), 2137–2144. https://doi.org/10.1021/ic00285a026.

(41) Gerloch, M.; Mabbs, F. E. The Crystal and Molecular Structure of NN′-Bis (Salicylideneiminato)-Iron (III) Chloride as a Five-Co-Ordinate Monomer. Journal of the Chemical Society A: Inorganic, Physical, Theoretical 1967, 1598–1608.

(42) Shatalin, K.; Shatalina, E.; Mironov, A.; Nudler, E. H2S: A Universal Defense against Antibiotics in Bacteria. Science 2011, 334 (6058), 986–990. https://doi.org/10.1126/science.1209855.

(43) Toliver-Kinsky, T.; Cui, W.; Törö, G.; Lee, S.-J.; Shatalin, K.; Nudler, E.; Szabo, C. H2S, a Bacterial Defense Mechanism against the Host Immune Response. Infect. Immun. 2019, 87 (1). https://doi.org/10.1128/IAI.00272-18.

(44) Mironov, A.; Seregina, T.; Nagornykh, M.; Luhachack, L. G.; Korolkova, N.; Lopes, L. E.; Kotova, V.; Zavilgelsky, G.; Shakulov, R.; Shatalin, K.; Nudler, E. Mechanism of H2S-Mediated Protection against Oxidative Stress in Escherichia Coli. Proc. Natl. Acad. Sci. U. S. A. 2017, 114 (23), 6022–6027. https://doi.org/10.1073/pnas.1703576114.

(45) Johnson, D. C.; Dean, D. R.; Smith, A. D.; Johnson, M. K. Structure, Function, and Formation of Biological Iron-Sulfur Clusters. Annu. Rev. Biochem. 2005, 74 (1), 247–281. https://doi.org/10.1146/annurev.biochem.74.082803.133518.

Chapte 4 Persulfide reactivity in the repair of NO-damaged Fe center

4.1 Abstract

Over the years, the restoration of NO-damanged [2Fe-2S] clusters from protein-bound dinitrosyl iron complexes (DNICs) have been reported in both in vivo and in vitro studies. However, the underlying mechanism remains elusive. Recent studies have suggested persulfide as a potential candidate for modifying and repairing nitrosylated iron species. Building on chapter 3's exploration of persulfide's ability to construct the Fe-S-Fe core from mononuclear Fe species, this chapter investigates persulfide's efficacy in repairing nitrosylated iron centers using the $\{Fe(NO)\}_7$ model complex, [Fe(Salen)](NO). Here, persulfide demonstrated capability in extracting NO from the iron center, as indicated by the disappearance of the characteristic NO feature in the IR spectrum, suggesting the formation of $[Fe(Salen)]_2S$. The research further examined the reactivity of persulfide with iron-nitrosylated products from the Fe-S cluster's reaction with NO, particularly focusing on the dinitrosyl iron complex (DNIC) and the mononitrosyl iron complex (MNIC) species. Persulfide showed effective in modifying the NO coordination in these complexes, indicating its potential role in addressing NO-related iron center damages. The findings highlight persulfide's significance in regulating nitrosylated iron species.

4.2 Introduction

Nitric oxide (NO) plays a pivotal role in numerous physiological and pathological processes, often interacting with iron-containing proteins and enzymes, leading to the formation of iron-nitrosyl complexes.[1,2] These interactions can modify the functionality of these metalloproteins, potentially causing cellular impairments.[3-5] Therefore, understanding the regulation and repair of nitrosylated iron centers is of paramount importance.

As described in chapter 3.2, NO damaged ferredoxin (Fd), DNIC-Fd, could be repaired to its original [2Fe-2S]-Fd by L-cysteine, O_2, and cysteine desulfurase (IscS) *in vitro* without having to add exogenous Fe (Scheme 3.1B).[7-9] Biochemical analyses of another [2Fe-2S] protein, SoxR, revealed that while nitrosylated SoxR (DNIC-SoxR) remains stable in vitro, it reverts to its intact [2Fe-2S] cluster form in vivo upon NO removal.[10] The exact mechanism—whether SoxR repair necessitates the de novo synthesis/insertion of the [2Fe-2S] cluster or if a direct repair route exists—is yet to be determined. Nevertheless, the observed repair process for DNIC-Fd implies that a direct restoration of DNIC-SoxR and other nitrosylated [Fe-S] proteins could be feasible. The precise chemical mechanisms underlying the DNIC-Fd repair remain elusive, highlighting the need for a deeper molecular understanding.[8,9]
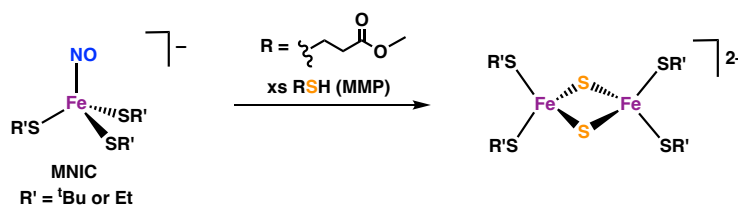
Scheme 4.1 Synthetic [2Fe-2S] cluster repair by MMP

We previously reported the repair chemistry of small molecule thiolate ligated mononitrosyl iron complexes (MNICs) to [2Fe-2S] clusters by the addition of nothing other than a cysteine analog methyl 3-mercaptopropionate (MMP) (Scheme 4.1).[11,12] The sulfur atom that forms the bridging sulfide in the [2Fe-2S] cluster was shown to be derived from MMP. Since cysteine persulfide is a better nucleophile than cysteine for metal binding,[13] and the S-S bond is easier to break than the C-S bond providing the source for the bridging sulfide, we hypothesize that RSS⁻ would be a more efficient agent in the [Fe-S] repair than cysteine.

In Chapter 3.3, we successfully demonstrated that persulfide alone can assemble the Fe-S core using a Salen-supported mononuclear iron complex. While the Salen-supported Fe species provides a reliable model for investigating persulfide reactivity, we synthesized the analogous $\{Fe(NO)\}_7$ complex, [Fe(Salen)](NO), to initiate our study on persulfide reactivity towards NO-damaged Fe centers.[14,15] This research was subsequently extended to DNIC and MNIC species.

4.3 Results and Discussion

4.3.1 Persulfide Reactivity with Salen-Supported Iron Nitrosyl Complexes

The $\{Fe(NO)\}_7$ model complex [Fe(Salen)](NO) was synthesized by reacting NO with [Fe^{II}(Salen)], using a modified literature procedure. When 1 equivalent of Ph$_3$CSNO, serving as the NO donor, was added to a methanol suspension of [Fe^{II}(Salen)], a color change to dark red-brown could be observed over 3 hours at room temperature. NMR analysis of the reaction mixture suggested the formation of a new paramagnetic species (Figure 4.1B bottom). After the nitrosylation, a distinct IR band around 1700 cm^{-1} appeared (Figure 4.1A black), differing from the starting reactant [Fe^{II}(Salen)]. This band is assigned to the N≡O stretching frequency and

aligns with previous literature, confirming the generation of [Fe(Salen)](NO).[14-16] However, as shown in Figure 4.1A, the relatively weak IR signal from the NO band suggests potential incomplete reactions, implying the presence of unreacted residual [Fe(Salen)] in the crude product. [Fe(Salen)](NO) is highly sensitive to oxygen; exposure to air rapidly transforms it into [Fe(Salen)]$_2$O, consistent with the literature.[14]
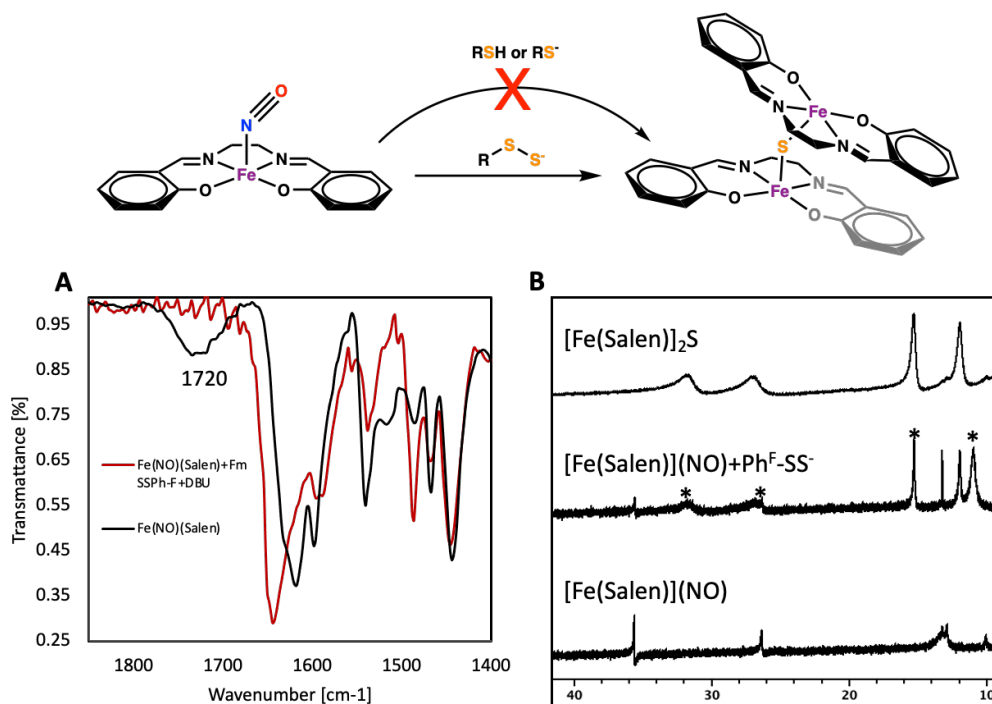
Figure 4.1 Reaction of [Fe(Salen)](NO) with persulfide. **A.** IR spectra (KBr pellet) of the v_{NO} (cm^{-1}) region comparing of [Fe(Salen)](NO) + 1 equiv. ^{F}Ph-SS$^-$ (red) to [Fe(Salen)](NO) (black). **B.** ^{1}H NMR (DCM-d$_2$) spectra comparing of [Fe(Salen)](NO) + 1 equiv. ^{F}Ph-SS$^-$ to authentic [Fe(Salen)](NO) and [Fe(Salen)$_2$]S. Key: * = authentic [Fe(Salen)$_2$]S

The efficacy of persulfide in repairing NO damage was evaluated using crude [Fe(Salen)](NO). When *in situ* generated persulfide (^{F}Ph-SS$^-$) was introduced to a DCM solution

containing [Fe(Salen)](NO), the characteristic NO feature in the IR spectrum vanished within 2 hours, as depicted in Figure 4.1A. This suggests that persulfide can effectively extract NO from the Fe center. The subsequent NMR spectrum, presented in Figure 4.1B, reveals the formation of [Fe(Salen)]$_2$S, indicating a Fe-S-Fe core construction. Given the faint NO signal in the starting [Fe(Salen)](NO), the actual amount of active [Fe(Salen)](NO) might be limited, making the added persulfide significantly in excess. Using enough persulfide is essential to effectively repair Fe damaged by NO and convert it into an Fe-S-Fe structure. Importantly, it's specifically persulfide driving this change, not thiol or thiolate, as control reactions under analogous conditions remained unchanged in the IR spectrum (Figure 4.8).

Various experimental conditions were explored to enhance the NO coordination rate and improve the purity of the synthesized [Fe(Salen)](NO). However, NO coordination to Fe with a Salen ligand proved challenging. To enhance the NO-binding capability of Fe(II) center, the H$_2$(Salen^{OMe}) ligand, bearing an electron-donating -OMe group, was developed. With new ligand, the metal center becomes more electron-rich and hopefully the Fe(II) center can more readily donate electron density to the antibonding orbitals of NO, facilitating the bonding between the metal and NO. Analogous complexes like [Fe(Salen^{OMe})], [Fe(Salen^{OMe})]$_2$O, and [Fe(Salen^{OMe})]$_2$S were synthesized similarly to their Salen counterparts.[17]

As expected, the reaction between [Fe(Salen^{OMe})] and Ph$_3$CSNO yielded a prominent band at 1735 cm^{-1} (Figure 4.2), suggesting a superior NO coordination yield. The formation of [Fe(Salen^{OMe})](NO) was also confirmed by 1H NMR (Figure 4.9). Upon treating synthesized [Fe(Salen^{OMe})](NO) with 2 equivalents of in-situ-generated persulfide, the IR spectra after 2 hours showed a significant decrease in intensity of the 1735 cm^{-1} band, as illustrated in Figure 4.3 left.

A new band at 1689 cm^{-1} appeared, also attributed to NO related species. This implies that the added persulfide modified the coordinated NO. For the reaction product, partial conversion to [Fe(Salen-OMe)]$_2$S could be confirmed by NMR (Figure 4.3).
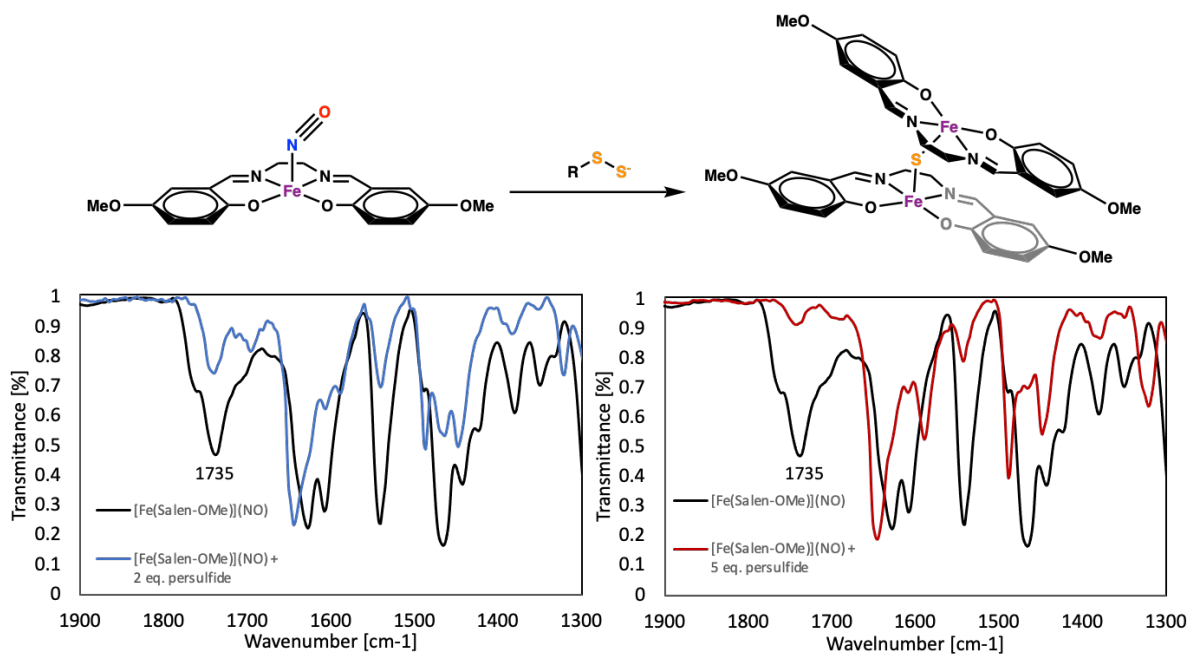
Figure 4.2 Reaction of [Fe(Salen^{OMe})](NO) with persulfide. **Left.** IR spectra (KBr pellet) of the v_{NO} (cm^{-1}) region comparing of [Fe(Salen^{OMe})](NO) + 2 equiv. ^{F}Ph-SS$^-$ (blue) to [Fe(Salen)](NO) (black). **Right.** IR spectra (KBr pellet) of the v_{NO} (cm^{-1}) region comparing of [Fe(Salen^{OMe})](NO) + 5 equiv. ^{F}Ph-SS$^-$ (red) to [Fe(Salen)](NO) (black).
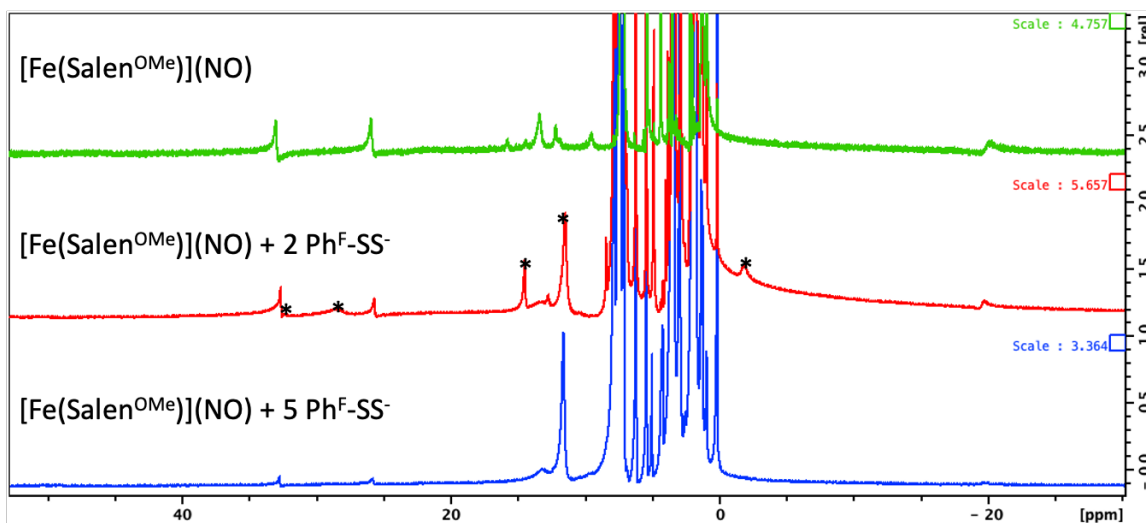
Figure 4.3 ^{1}H NMR (DCM-d_2) spectra of [Fe(Salen^{OMe})](NO) (green), [Fe(Salen^{OMe})](NO) + 2 equiv. ^{F}Ph-SS$^-$ (red) and [Fe(Salen^{OMe})](NO) + 5 equiv. ^{F}Ph-SS$^-$ (blue). Key: * = authentic [Fe(Salen^{OMe})$_2$]S

To achieve complete conversion, an additional excess of persulfide was introduced to drive the reaction. Combining [Fe(Salen^{OMe})](NO) with 5 equivalents of in situ generated persulfide resulted in the near-complete disappearance of the NO feature at the 1700 cm^{-1} region in IR spectra within 2 hours at room temperature (Figure 4.2 Right). NMR analysis of the reaction mixture revealed a decrease in the [Fe(Salen^{OMe})](NO) signal (Figure 4.3). However, instead of forming the anticipated [Fe(Salen^{OMe})]$_2$S, a distinct NMR signal emerged, suggesting the creation of a new entity, species A (Figure 4.3 Bottom). To understand the connection between species A and the expected product [Fe(Salen^{OMe})]$_2$S, a control reaction involving [Fe(Salen^{OMe})]$_2$S and persulfide was conducted. The IR spectra distinctly indicated that, after a 2-hour reaction with 2 equivalents of persulfide, the spectra of [Fe(Salen^{OMe})]$_2$S transformed to closely match that of species A (Figure 4.4 Right). Consequently, the hypothesized reaction pathway, depicted in Figure 4.4 left,

suggests that persulfide can extract NO from [Fe(Salen^{OMe})](NO) and introduce a bridging sulfide to produce [Fe(Salen^{OMe})]$_2$S. This compound, upon further interaction with an excess of persulfide, evolves into species A. The structure of species A will be further investigated.
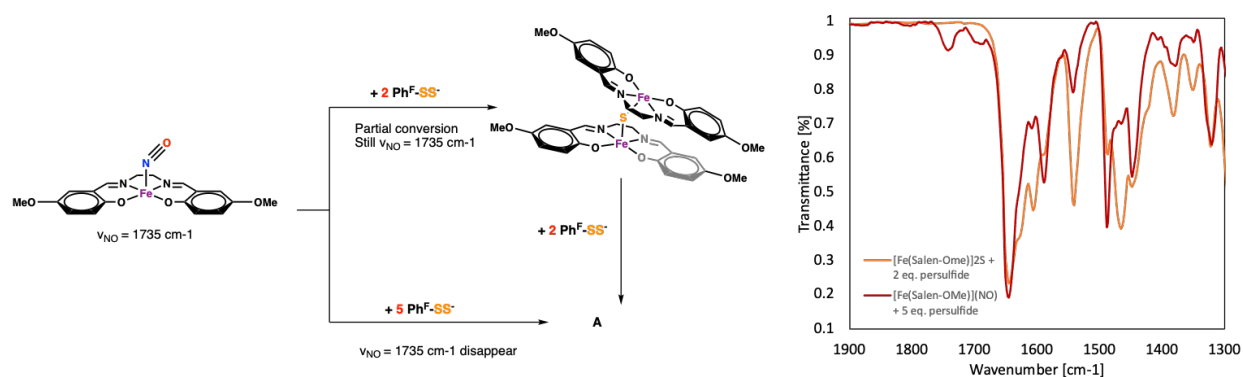
Figure 4.4 Hypothesized reaction pathway of [Fe(Salen^{OMe})](NO) with excess amount of persulfide

4.3.2 Persulfide reactivity with iron-nitrosylated products from Fe-S cluster with NO reaction

4.3.2.1 Persulfide reactivity with DNIC

While the capacity of persulfide to repair Salen-supported {Fe(NO)}^{7} model species has been established, we also delved into the reactivity of persulfide with iron-nitrosylated products resulting from the Fe-S cluster's interaction with NO.[3-5] As hinted at in Chapter 1, NO is believed to play a role in the disassembly of Fe-S clusters, leading to the formation of the dinitrosyl iron complex (DNIC).[10,18] As a final product of the reaction between [2Fe-2S] and [4Fe-4S] clusters with NO in the presence of thiolate, the DNIC species Fe(SPh)$_2$(NO)$_2^-$ was the primary subject of our persulfide tests. The reaction of thiolate DNIC, (NEt$_4$)[Fe(SPh)$_2$(NO)$_2$], with persulfide

precursor and DBU lead to significantly change in NO region of the IR spectra, indicating of modified NO binding (Figure 4.5). 1H MNR spectra also confirmed the formation of an unidentified species with a broad signal centered around 10.1 ppm (Figure 4.10).
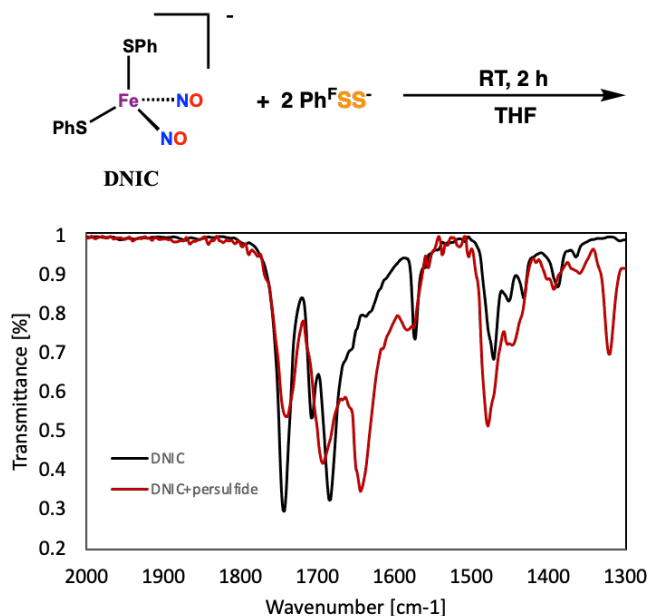
Figure 4.5 IR spectra (KBr pellet) of the υ_{NO} (cm^{-1}) region comparing of (NEt$_4$)[Fe(SPh)$_2$(NO)$_2$] + 2 equiv. ^{F}Ph-SS$^-$ (red) to (NEt$_4$)[Fe(SPh)$_2$(NO)$_2$] (black).

4.3.2.2 Persulfide reactivity with MNIC

The spectral shifts, when combined with the redox-active nature of the thiolate ligand, introduce complexity. To simplify the reaction and focus more on the Fe-NO interaction change, the MNIC species, (PPN)[FeCl$_3$(NO)] (PPN = Bis(triphenylphosphoranylidene)ammonium), was synthesized.[20] This species features Cl ligands, facilitating clearer NMR and IR spectral analyses, and incorporates only a single NO molecule. The compound (PPN)[FeCl$_3$(NO)] was derived from the reaction of tetrachloride (PPN)$_2$[FeCl$_4$] with the NO donor, Ph$_3$CSNO. The IR spectra of the

resultant green solid displayed a distinct signal at 1793 cm⁻¹, consistent with the NO stretch previously reported for (PPN)[FeCl₃(NO)].[20]
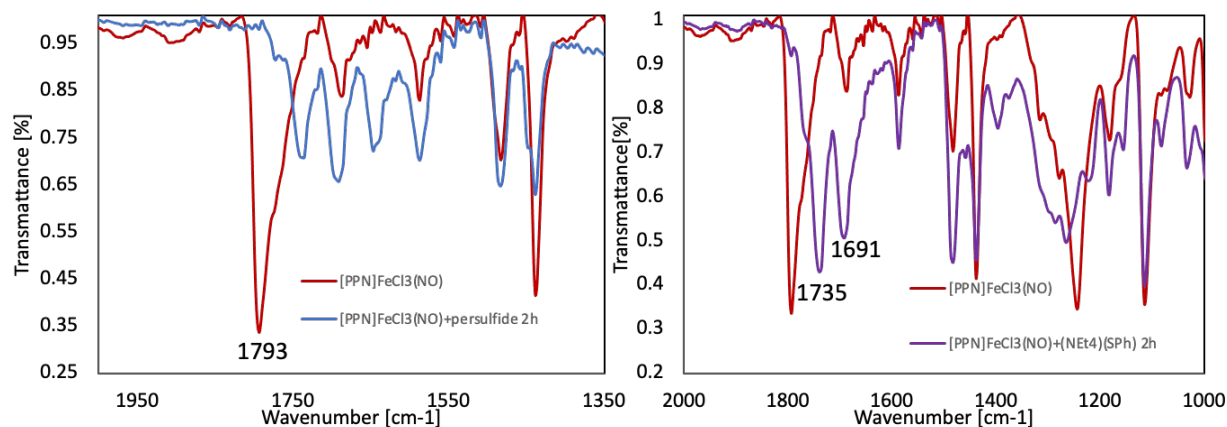
Figure 4.6 IR spectra (KBr pellet) of the v_{NO} (cm⁻¹) region of (PPN)[FeCl₃(NO)] + 2 equiv. Ph^F-SS⁻ reaction (blue) and (PPN)[FeCl₃(NO)] + SPh⁻ (purple) reaction to (PPN)[FeCl₃(NO)] (red).

Introducing 2 equivalents of in-situ generated persulfide Ph^FSS⁻ to (PPN)[FeCl₃(NO)] triggered a color shift from green to brown within two hours. Subsequent IR spectra of the mixture revealed the disappearance of the characteristic peak at 1793 cm⁻¹ and the formation of fainter peaks around the 1600-1700 cm cm⁻¹ range, specifically at 1739, 1691, and 1645 cm⁻¹ (Figure 4.6 left). The UV-vis spectral data gathered for this mix bears resemblance to that of [FeCl₄]²⁻ (Figure 4.11). A control experiment, mixing (PPN)[FeCl₃(NO)] with equal amount of thiolate (NEt₄)(SPh), leading to the formation of the corresponding thiolate DNIC, (PPN)[Fe(SPh)₂(NO)₂] (Figure 4.6 right).[21] The DNIC NO band in 1739 and 1691 cm⁻¹ aligned with the weak IR bands observed in the MNIC-persulfide reaction. Given these findings, we hypothesis that in reactions with limited persulfide, a portion of the MNIC might be transformed into the tetrachloride species [FeCl₄]²⁻, while the remainder converted to DNIC.

$$[FeCl_3(NO)]^- + RSS^- \rightarrow RSSNO + [FeCl_4]^{2-} + [Fe(RS)_2(NO)_2]^-$$

4.3.3 Proposed synthesis of persulfide-bound dinitrosyl iron complexes

A recent mass spectrometry analysis of the NO-sensing protein, NsrR, identified various iron nitrosyl products, one of which is a proposed persulfide-bridged RRE-type cluster $[Fe_2(NO)_4(\mu\text{-S-Cys})(\mu\text{-SS-Cys})]$.[22] Inspired by these findings, we aim to synthesize a persulfide-bound RRE cluster and investigate the repair mechanisms of these entities. The synthesis strategy for the persulfide-bridged compound involves reacting $[Fe_2(NO)_4(\mu\text{-I})_2]$ with persulfide at low temperature, which is a known synthetic method for analogous RREs.[23] The compound $[Fe_2(NO)_4(\mu\text{-I})_2]$ was obtained from the reaction of Ph_3CSNO, FeI_2 and Fe, with two characteristic NO stretch in the IR spectra at 1747 and 1735 cm^{-1} (Figure 4.7 left).[24]
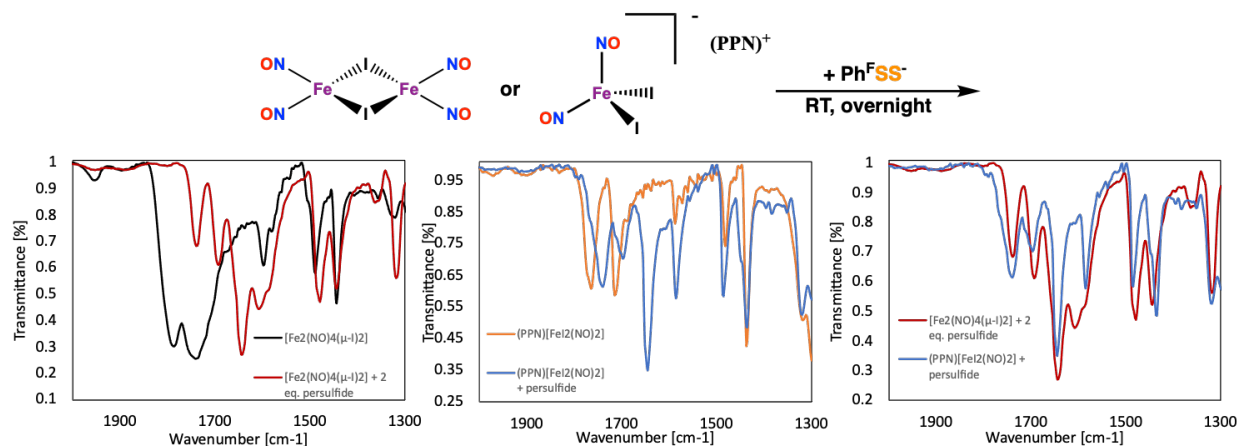
Figure 4.7 IR spectra (KBr pellet) v_{NO} (cm^{-1}) region change of $[Fe_2(NO)_4(\mu\text{-I})_2]$ + 2 equiv. Ph^F-SS$^-$ reaction (left), (PPN) $[FeI_2(NO)_2]$ + 1 equiv. Ph^F-SS$^-$ reaction (middle) and the comparison of the reaction products (right).

As shown in Figure 4.7 left, the preliminary experiment of $[Fe_2(NO)_4(\mu\text{-}I)_2]$ react with two equivalents of in situ generated persulfide at room temperature led to a shift in the IR signal, with the NO band moving to 1737 and 1685 cm^{-1}. Notably, significant peaks at 1643 and 1606 were attributed to the persulfide precursor $FmSSPh^F$ in conjunction with DBU. Intriguingly, a control reaction, using the related DNIC species (PPN) $[FeI_2(NO)_2]$ and persulfide, yielded an identical IR spectrum after stirring overnight at room temperature (Figure 4.7). This suggests the potential formation of the same product. NMR analysis of the reaction mixture of (PPN) $[FeI_2(NO)_2]$ with persulfide revealed a new species at 9.72 ppm (Figure 4.12).

Further experiment will involve reacting persulfide with $[Fe_2(NO)_4(\mu\text{-}I)_2]$ at -40 °C, targeting the synthesis of $[Fe_2(NO)_4(\mu\text{-}SSPh^F)_2]$ (Scheme 4.2). The resultant compound will be subjected to comprehensive characterization using NMR and IR spectroscopy, mass spectrometry, and X-ray crystallography to validate our hypothesis. Moreover, the repair chemistry of $[Fe_2(NO)_4(\mu\text{-}SSPh^F)_2]$ will be studied in conjunction with iron porphyrin complexes, specifically $[Fe^{III}(TPP)Cl]$ and $[Fe^{II}(TPP)]$, where TPP = tetraphenylporphyrinate(2–). Literature precedence shows NO transfer by DNICs (in the form of NO or NO^-) to these porphyrin complexes.[26,27] As shown in Scheme 4.2, when $[Fe_2(NO)_4(\mu\text{-}SSPh^F)_2]$ is warmed to room temperature conditions in the presence of an excess of thiolate and iron porphyrins, the formation of $[Fe(TPP)(NO)]$ can be tracked using UV-Vis, IR, and EPR spectroscopy, and the generation of [Fe-S] clusters can be detected using ^{19}F-NMR spectroscopy. We anticipate that [Fe-S] clusters will form without requiring an external sulfur source, as the sulfur atom from the persulfide undergoes transformation into a bridging sulfide.
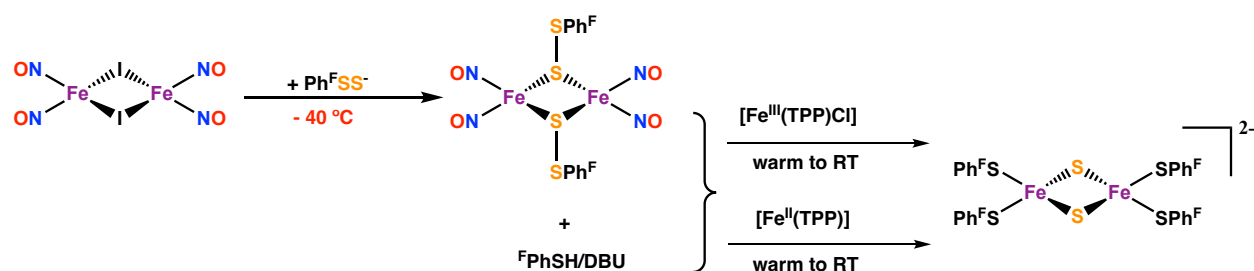
Scheme 4.2 Proposed synthesis and reactivity study of $[Fe_2(NO)_4(\mu\text{-}SSPh^F)_2]$.

4.4 Experimental Section

General Considerations. All synthesized products were assumed to be air- and moisture-sensitive. They were manipulated under argon on a standard Schlenk line or in an atmosphere of purified nitrogen in an MBraun Labmaster SP glovebox (O_2 < 1 ppm; H_2O < 1 ppm). Solvents were purified by passing through a series of two activated alumina columns (MBraun solvent purification system) under an Ar atmosphere and stored over 4 Å molecular sieves. Reagents 4-fluorothiophenol, bis-4-fluorodisulfide, 1,8-diazabicyclo[5.4.0]undec-7-ene (DBU), 9-Fluorenylmethylthiol (FmSH), 4,4'- dithiodipyridine (PySSPy) were purchased from Sigma at the highest available purity and used as received. UV-Vis spectra were recorded on a Varian Cary 50 Bio spectrometer. NMR spectra were recorded at 400 MHz on a Bruker UltraShield spectrometer and residual solvent signals were used as an internal reference.

Synthesis and Reactivity Studies. Authentic [Fe^{II}(salen)],[17] [Fe^{III}(Salen)]$_2$S,[17] Ph$_3$CSNO,[19] (NEt$_4$)[Fe(SPh)$_2$(NO)$_2$],[19] (PPN)[FeCl$_3$(NO)], [Fe$_2$(NO)$_4$(μ-I)$_2$],[24] (PPN)[FeI$_2$(NO)$_2$] and FmSSPy[25] were prepared as described in literature with slight modifications. As described in

Chapter 3, persulfide Ph^{F}SS$^-$ was generated in situ from the reaction of equal amount of base-sensitive precursor FmSSPh^F and DBU. All reactions were performed under an inert atmosphere.

Synthesis of [Fe(salen)](NO). [Fe(salen)](NO) was prepared by a modification of the method of Earnshaw, King and Larkworthy.[14] In the glovebox, 50 mg of [Fe(salen)] (0.15 mmol) and 45.12 mg (0.15 mmol) of Ph$_3$CSNO was mixed in 5 mL of MeOH, and the reaction was allowed to stir in dark for 1 day at room temperature. The solvent was removed under vacuum, and the residue was washed three times with Et$_2$O to give a red solid (33mg, ~62% yield) as crude product. IR (KBr, cm^{-1}): 1720 (ν_{NO}), was in agreement with that previously reported for [Fe(salen)](NO).

Reaction of [Fe(salen)](NO) with persulfide. To a stirred solution of [Fe(salen)](NO) (10.4 mg, 0.03 mmol) in 3 ml of DCM was added 10mg of FmSSPh^F (0.03 mmol), followed by DBU (1 mL of 0.03 M stock solution in DCM). The reaction was allowed to procced for 2h at room temperature, over which time the color of the reaction mixture was changed to reddish brown. The solvent was removed under vacuum. KBr IR and ^{1}H NMR in CD$_2$Cl$_2$ was then collected as shown in Figure 4.1. ^{1}H NMR indicated the formation of [Fe(salen)]$_2$S.

Control reaction of [Fe(salen)](NO) with thiol or thiolate. To a stirred solution of [Fe(salen)](NO) (10.4 mg, 0.03 mmol) in 2.0 mL of DCM was added 1 mL stock solution of (NEt$_4$)(SPh^F) or HSPh^F (0.03 M in DCM). The reaction was allowed to procced for 2h at room temperature. The solvent was removed under vacuum and a KBr IR was collected. IR spectra showed no change in the ν_{NO} region.
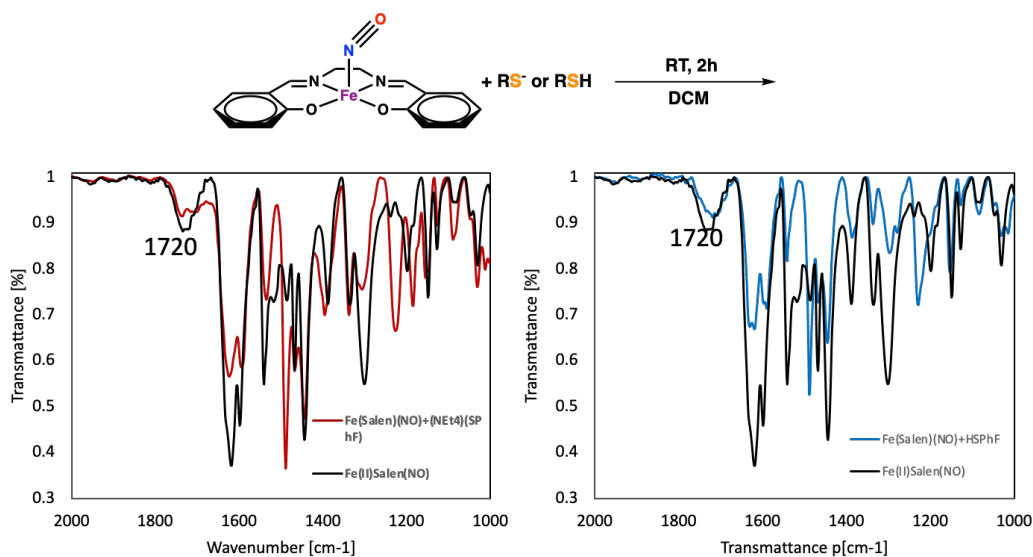
Figure 4.8 IR spectra (KBr pellet) of the υ_{NO} (cm^{-1}) region for [Fe(Salen)](NO) with thiol or thiolate control reaction.

Preparation of [Fe(Salen^{OMe})], [Fe(Salen^{OMe})]$_2$O and [Fe(Salen^{OMe})]$_2$S. [Fe(Salen^{OMe})], [Fe(Salen^{OMe})]$_2$O and [Fe(Salen^{OMe})]$_2$S were prepared similarly to the Salen-related species as described in the literature.

[Fe(Salen^{OMe})]$_2$O: ^{1}H NMR (400 MHz, DCM-d$_2$) δ 25.9 (4H), 20.8 (4H), 12.2 (2H), 9.5 (2H), 4.3 (6H), 0.9 (2H)

[Fe(Salen^{OMe})]$_2$S: ^{1}H NMR (400 MHz, DCM-d$_2$) δ 32.4 (4H), 28.6 (4H), 14.5 (2H), 11.5 (2H), 4.8 (6H), -1.9 (2H)
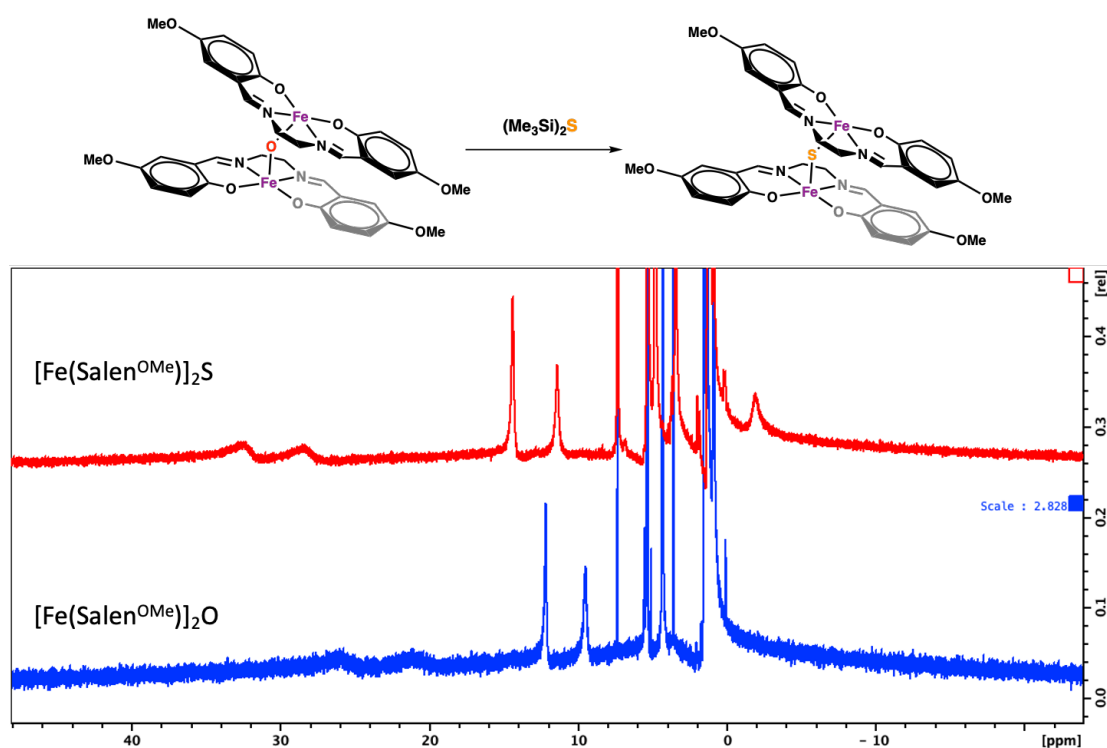
Figure 4.9 ^{1}H NMR (DCM-d$_2$) spectrum of [Fe(Salen^{OMe})]$_2$O and [Fe(Salen^{OMe})]$_2$S

Synthesis of [Fe(salen^{OMe})](NO). [Fe(salen^{OMe})](NO) was prepared in an analogous way as [Fe(salen)](NO). In a MeOH solution of [Fe(salen^{OMe})] (50 mg, 0.13 mmol), 40 mg of Ph$_3$CSNO (0.1 mmol) was added. After the reaction was stirred for 1 day under dark at room temperature, the solvent was evaporated, and the residue was washed three times with Et$_2$O to afford a red solid (31mg, ~57% yield) as crude product. IR (KBr, cm^{-1}): 1737 (ν_{NO}). ^{1}H NMR of [Fe(salen^{OMe})](NO) is shown in Figure 4.4.

Reaction of [Fe(salen^{OMe})](NO) with persulfide. To a stirred solution of [Fe(salen^{OMe})](NO) (12.4 mg, 0.03 mmol) in 3 ml of DCM was added 20 mg of FmSSPh^F (0.06 mmol), followed by DBU (2 mL of 0.03 M stock solution in DCM). The reaction was allowed to procced for 2h at room temperature. The solvent was removed under vacuum. KBr IR and ^{1}H NMR in CDCl$_2$ was

then collected as shown in Figure 4.3 and Figure 4.4. ^{1}H NMR indicated partial conversion to [Fe(salen^{OMe})]$_2$S.

Reaction of [Fe(salen^{OMe})$_2$S with persulfide. To a DCM solution containing 23.9 mg of [Fe(salen^{OMe})$_2$S (0.03M) was added 20 mg of FmSSPh^F (0.06 mmol), followed by DBU (2 mL of 0.03 M stock solution in DCM). The reaction was allowed to stir at room temperature for 1h, after which time all volatiles were removed by vacuum. The KBr IR spectra of the reaction mixture was shown in Figure 4.5.

Reaction of (NEt$_4$)[Fe(SPh)$_2$(NO)$_2$]with persulfide. To a 5 mL THF solution containing 13.9 mg of (NEt$_4$)[Fe(SPh)$_2$(NO)$_2$] (0.03M) was added 20 mg of FmSSPh^F (0.06 mmol), followed by DBU (4 mL of 0.03 M stock solution in DCM). The reaction was allowed to process at room temperature for 1h. The solvent was removed under vacuum and a crude NMR without further purification was collected in CD$_3$CN as shown in Figure 4.X.
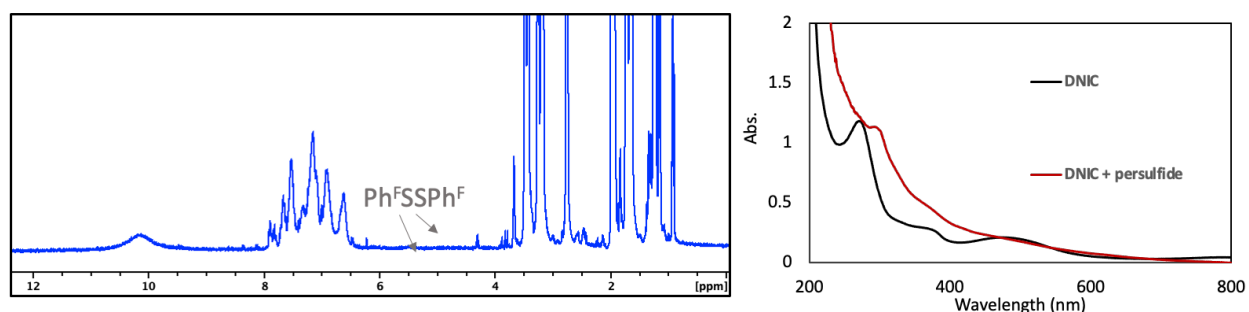
Figure 4.10 ^{1}H NMR (CD$_3$CN) (Left) and UV-vis (Right) in THF of (NEt$_4$)[Fe(SPh)$_2$(NO)$_2$] with persulfide reaction.

Reaction of (PPN)[FeCl₃(NO)] with persulfide. To a 10 mL MeCN solution containing 43.18 mg of (PPN)[FeCl$_3$(NO)] (0.03M) was added 20 mg of FmSSPh^F (0.06 mmol), followed by DBU (2 mL of 0.03 M stock solution in MeCN). The reaction was allowed to process at room temperature for 1h. The solvent was removed under vacuum and the UV-Vis spectrum was collected in MeCN as shown in Figure 4.X.
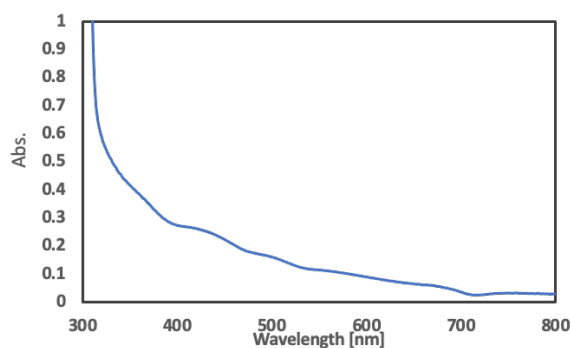
Figure 4.11 UV-vis in THF of (PPN)[FeCl$_3$(NO)] with persulfide reaction.

Reaction of [Fe₂(NO)₄(μ-I)₂] with persulfide. To a 5 mL MeCN solution containing 14.6 mg of [Fe$_2$(NO)$_4$(μ-I)$_2$] (0.03 mmol) was added 20 mg of FmSSPh^F (0.06 mmol), followed by DBU (2 mL of 0.03 M stock solution in THF). The reaction was allowed to process at room temperature for overnight. The solvent was removed under vacuum and KBr IR was collected as shown in Figure 4.8.

Reaction of (PPN)[FeI₂(NO)₂] with persulfide. To a 5 mL MeCN solution containing 27.2 mg of (PPN)[FeI$_2$(NO)$_2$] (0.03 mmol) was added 10 mg of FmSSPh^F (0.03 mmol), followed by DBU (1 mL of 0.03 M stock solution in THF). The reaction was allowed to process at room

temperature for overnight. The solvent was removed under vacuum and KBr IR was collected as shown in Figure 4.8.
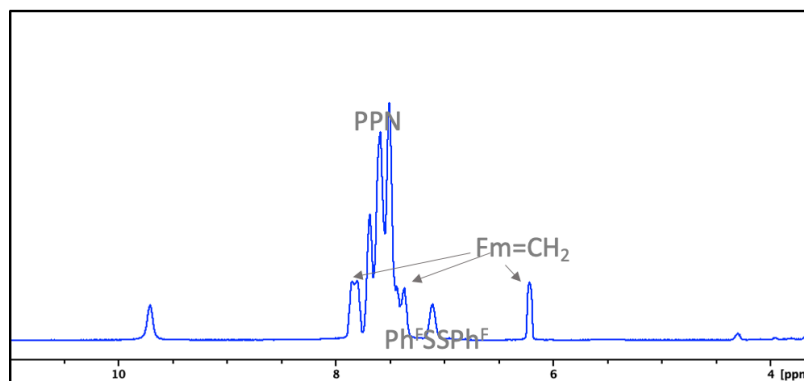
Figure 4.12 ^{1}H NMR (CD$_3$CN) (Left) and UV-vis (Right) in THF of (PPN)[FeI$_2$(NO)$_2$] with persulfide reaction.

4.5 References

(1) Murad, F. Discovery of Some of the Biological Effects of Nitric Oxide and Its Role in Cell Signaling (Nobel Lecture). Angew. Chem. Int. Ed Engl. 1999, 38 (13–14), 1856–1868.

(2) Butler, A. R.; Death, N. Death and Nitric Oxide. The Royal Society of Chemistry 2003.

(3) Williams, D. L. H. The Chemistry of S-Nitrosothiols. Accounts of chemical research 1999, 32 (10), 869–876.

(4) Filipovic, M. R.; Miljkovic, J. L.; Nauser, T.; Royzen, M.; Klos, K.; Shubina, T.; Koppenol, W. H.; Lippard, S. J.; Ivanović-Burmazović, I. Chemical Characterization of the Smallest S-Nitrosothiol, HSNO; Cellular Cross-Talk of H2S and S-Nitrosothiols. J. Am. Chem. Soc. 2012, 134 (29), 12016–12027. https://doi.org/10.1021/ja3009693.

(5) Wyllie, G. R. A.; Scheidt, W. R. Solid-State Structures of Metalloporphyrin NOx Compounds. Chem. Rev. 2002, 102 (4), 1067–1090. https://doi.org/10.1021/cr000080p.

(6) Venkateswara Rao, P.; Holm, R. H. Synthetic Analogues of the Active Sites of Iron−Sulfur Proteins. Chemical reviews 2004, 104 (2), 527–560.

(7) Grabarczyk, D. B.; Ash, P. A.; Vincent, K. A. Infrared Spectroscopy Provides Insight into the Role of Dioxygen in the Nitrosylation Pathway of a [2Fe2S] Cluster Iron–Sulfur Protein. J. Am. Chem. Soc. 2014, 136 (32), 11236–11239. https://doi.org/10.1021/ja505291j.

(8) Rogers, P. A.; Ding, H. L-Cysteine-Mediated Destabilization of Dinitrosyl Iron Complexes in Proteins. J. Biol. Chem. 2001, 276 (33), 30980–30986. https://doi.org/10.1074/jbc.m101037200.

(9) Yang, J.; Duan, X.; Landry, A. P.; Ding, H. Oxygen Is Required for the L-Cysteine-Mediated Decomposition of Protein-Bound Dinitrosyl–Iron Complexes. Free Radic. Biol. Med. 2010, 49 (2), 268–274. https://doi.org/10.1016/j.freeradbiomed.2010.04.012.

(10) Ding, H.; Demple, B. Direct Nitric Oxide Signal Transduction via Nitrosylation of Iron-Sulfur Centers in the SoxR Transcription Activator. Proc. Natl. Acad. Sci. U. S. A. 2000, 97 (10), 5146–5150. https://doi.org/10.1073/pnas.97.10.5146.

(11) Fitzpatrick, J.; Kalyvas, H.; Filipovic, M. R.; Ivanović-Burmazović, I.; MacDonald, J. C.; Shearer, J.; Kim, E. Transformation of a Mononitrosyl Iron Complex to a [2Fe-2S] Cluster by a Cysteine Analogue. J. Am. Chem. Soc. 2014, 136 (20), 7229–7232. https://doi.org/10.1021/ja5024207.

(12) Fitzpatrick, J.; Kim, E. New Synthetic Routes to Iron–Sulfur Clusters: Deciphering the Repair Chemistry of [2Fe–2S] Clusters from Mononitrosyl Iron Complexes. Inorg. Chem. 2015, 54 (22), 10559–10567. https://doi.org/10.1021/acs.inorgchem.5b00961.

(13) Álvarez, L.; Bianco, C. L.; Toscano, J. P.; Lin, J.; Akaike, T.; Fukuto, J. M. Chemical Biology of Hydropersulfides and Related Species: Possible Roles in Cellular Protection and Redox Signaling. Antioxid. Redox Signal. 2017, 27 (10), 622–633. https://doi.org/10.1089/ars.2017.7081.

(14) Earnshaw, A.; King, E. A.; Larkworthy, L. F. Transition Metal–Schiff's Base Complexes. Part V. Spin Equilibria in Some Iron Mononitrosyls. J. Chem. Soc. 1969, 0 (0), 2459–2463. https://doi.org/10.1039/j19690002459.

(15) Haller, K. J.; Johnson, P. L.; Feltham, R. D.; Enemark, J. H.; Ferraro, J. R.; Basile, L. J. Effects of Temperature and Pressure on the Molecular and Electronic Structure of N, N′-Ethylenebis (Salicylideneiminato) Nitrosyliron, Fe (NO)(Salen). Inorganica Chimica Acta 1979, 33, 119–130.

(16) Leeuwenkamp, O. R.; Plug, C. M.; Bult, A. Synthesis of [N, N′-Phenylenebis (Salicylideniminato)] Mononitrosyliron and Its Characterization in the Solid State (IR, EPR, Mössbauer, X-Ray Analysis and Magnetic Susceptibility). Polyhedron 1987, 6, 295–302.

(17) Dorfman, J. R.; Girerd, J. J.; Simhon, E. D.; Stack, T. D. P.; Holm, R. H. Synthesis, Structure, and Electronic Features of (.Mu.-Sulfido)Bis[(N,N'-Ethylenebis(Salicylaldiminato))Iron(III)], [Fe(Salen)]2S, Containing the Only Authenticated Example of the Iron(III)-Sulfur-Iron(III) Single Bridge. Inorg. Chem. 1984, 23 (26), 4407–4412. https://doi.org/10.1021/ic00194a002.

(18) Pomposiello, P. J.; Bennik, M. H. J.; Demple, B. Genome-Wide Transcriptional Profiling of the Escherichia Coli Responses to Superoxide Stress and Sodium Salicylate. J. Bacteriol. 2001, 183 (13), 3890–3902. https://doi.org/10.1128/jb.183.13.3890-3902.2001.

(19) Harrop, T. C.; Tonzetich, Z. J.; Reisner, E.; Lippard, S. J. Reactions of Synthetic [2Fe-2S] and [4Fe-4S] Clusters with Nitric Oxide and Nitrosothiols. J. Am. Chem. Soc. 2008, 130 (46), 15602–15610. https://doi.org/10.1021/ja8054996.

(20) Tran, C. T.; Kim, E. Acid-Dependent Degradation of a [2Fe–2S] Cluster by Nitric Oxide. Inorg. Chem. 2012, 51 (19), 10086–10088. https://doi.org/10.1021/ic301676f.

(21) Lu, T. T.; Chiou, S. J.; Chen, C. Y.; Liaw, W. F. Mononitrosyl Tris (Thiolate) Iron Complex [Fe (NO)(SPh) 3]-and Dinitrosyl Iron Complex [(EtS) 2Fe (NO) 2]-: Formation Pathway of Dinitrosyl Iron Complexes (DNICs) from Nitrosylation of Biomimetic Rubredoxin. R= Ph, Et). Inorganic chemistry 2006, No. 21, 8799–8806.

(22) Crack, J. C.; Hamilton, C. J.; Le Brun, N. E. Mass Spectrometric Detection of Iron Nitrosyls, Sulfide Oxidation and Mycothiolation during Nitrosylation of the NO Sensor [4Fe–4S] NsrR. Chem. Commun. (Camb.) 2018, 54 (47), 5992–5995. https://doi.org/10.1039/c8cc01339j.

(23) Crich, D.; Sana, K.; Guo, S. Amino Acid and Peptide Synthesis and Functionalization by the Reaction of Thioacids with 2,4-Dinitrobenzenesulfonamides. Org. Lett. 2007, 9 (22), 4423–4426. https://doi.org/10.1021/ol701583t.

(24) Haymore, B.; Feltham, R. D.; Morris, B. E.; Clement, R. A. Nitrosyliron, -Cobalt, and -Nickel Iodides. Inorganic Syntheses. Wiley January 1973, pp 81–89. https://doi.org/10.1002/9780470132456.ch16.

(25) Park, C.-M.; Johnson, B. A.; Duan, J.; Park, J.-J.; Day, J. J.; Gang, D.; Qian, W.-J.; Xian, M. 9-Fluorenylmethyl (Fm) Disulfides: Biomimetic Precursors for Persulfides. Org. Lett. 2016, 18 (5), 904–907. https://doi.org/10.1021/acs.orglett.5b03557.

(26) Rauchfuss, T. B.; Weatherill, T. D. Roussin's Red Salt Revisited: Reactivity of Fe2(.Mu.-E)2(NO)42- (E =S, Se, Te) and Related Compounds. Inorg. Chem 1982, 21, 827–830

(27) Chiang, C.-Y.; Darensbourg, M. Y. Iron Nitrosyl Complexes as Models for Biological Nitric Oxide Transfer Reagents. J. Biol. Inorg. Chem. 2006, 11 (3), 359–370. https://doi.org/10.1007/s00775-006-0084-y

(28) Mukherjee, R. N.; Stack, T. D. P.; Holm, R. H. Angle Dependence of the Properties of the [Fe2X] 4+ Bridge Unit (X= O, S): Structures, Antiferromagnetic Coupling, and Properties in Solution. Journal of the American Chemical Society 1988, 110 (6), 1850–1861.

Chapte 5 Thiol-Dependent H₂S Generation from

[Fe−S] cluster nitrosylation

5.1 Abstract

Iron–sulfur clusters (Fe–S) have been well established as a target for nitric oxide (NO) in biological systems. Complementary to protein-bound studies, synthetic models have provided a platform to study what iron nitrosylated products and byproducts are produced depending on a controlled reaction environment. We have previously shown a model [2Fe-2S] system that produced a dinitrosyl iron complex (DNIC) upon nitrosylation along with hydrogen sulfide (H_2S), another important gasotransmitter, in the presence of thiol, and hypothesized a similar reactivity pattern with [4Fe-4S] clusters which have largely produced inconsistent reaction products across biological and synthetic systems. Roussin's black anion (RBA), $[Fe_4(\mu_3\text{-S})_3(NO)_7]^-$, is a previously established reaction product from synthetic [4Fe-4S] clusters with NO. Here, we present a new reactivity for the nitrosylation of a synthetic [4Fe-4S] cluster in the presence of thiol and thiolate. $[Et_4N]_2[Fe_4S_4(SPh)_4]$ (**1**) was nitrosylated in the presence of excess PhSH to generate H_2S and an "RBA-like" intermediate that when further reacted with $[NEt_4][SPh]$ produced a $\{Fe(NO)_2\}^9$ DNIC, $[Et_4N][Fe(NO)_2(SPh)_2]$ (**2**). This "RBA-like" intermediate proved difficult to isolate but shares striking similarities to RBA in the presence of thiol based on IR $\upsilon_{(NO)}$ stretching frequencies. Surprisingly, the same reaction products were produced when the reaction started with RBA and thiol. Similar to **1**/NO, RBA in the presence of thiol and thiolate generates stoichiometric amounts of DNIC while releasing its bridging sulfides as H_2S. These results suggest not only that RBA may not be the final product of [4Fe-4S] + NO but also that RBA has unprecedented reactivity with thiols and thiolates which may explain current challenges around identifying biological nitrosylated Fe–S clusters. This chapter presents collaborative work, with significant

contributions made by Kady Marisa Oakley, showcasing a shared effort in the research and findings documented herein.

5.2 Introduction

Nitric oxide (NO), originally thought to simply be a toxic gas,[1] has been actively investigated for its role in cellular signaling in the past several decades.[2] Along with carbon monoxide (CO) and hydrogen sulfide (H_2S), NO has been labeled as one of the three important gasotrasmitters in biological systems. Specifically, NO is known to be most active in the central nervous system, where it effects brain development, memory, and learning;[3] in immune response, where it plays a part in the inflammatory response;[4] and in the circulatory system, where it acts as a vasorelaxer and vasodilater to aid circulation.[5] Currently known mechanisms of H_2S production stem from both enzymatic and nonenzymatic pathways. At least three enzymes, cystathionine β-synthase (CBS), cystathione γ-lyase (CSE), and 3-mercaptopyruvate sulfurtransferase (MST), are involved in the biosynthesis of H_2S from L-cysteine (CBS and CSE) or 3-mercaptopyruvate (MST).[6] H_2S can be stored as sulfane sulfur via oxidative post-translation modification of cysteines to form persulfies that can release H_2S under reducing conditions.[6,38] Interestingly, many of the biological functions performed by H_2S overlap with the functions of NO.[7] Due to this overlap, researchers have been looking for a point of crosstalk for the two for years.[8,39]

Mechanisms for the NO-H_2S crosstalk can be divided into two categories. One is the crosstalk through protein regulations as seen with the action of NO and H_2S on the secondary messenger cGMP.[9] In this case, NO facilitates the production of cGMP by activating soluble guanylyl cyclase. Once cGMP has been produced, H_2S acts to delay cGMP's degradation by inhibiting phosphodiesterase.[10] The other type of crosstalk is a direct chemical interaction between H_2S and NO and its metabolites. Research into the possibility of this type of crosstalk includes the reactivity

of H_2S with NO,[11,40] nitroprusside,[12] S-nitrosothiols,[13] and peroxynitrite.[14,42] Our research group has focused on a different possible target for NO-H_2S crosstalk: iron sulfur clusters.

Iron sulfur ([Fe–S]) clusters are ubiquitous in biological systems. Common to the most ancient and modern forms of life, they carry out many functions required for survival: electron transport, substrate activation and catalysis, and cellular sensing and signaling.[15] Among the functions of [Fe–S] clusters in biological systems, they have been found to be a major target for reactivity of nitric oxide to form various iron nitrosyl species (Chart 5.1). The conversion of [Fe–S] cluster to iron-nitrosyls results in significant changes in protein function that can lead to NO-derived physiological signal transduction[16,43-47] or severe toxicity.[17,48-51] To study the reactivity of [Fe–S] clusters with NO, researchers have broadly taken two different routes: protein bound clusters to study reactivity in their native environment, and synthetic model clusters to allow the chemical reactivity and mechanisms to be more easily studied. Synthetic models are rarely stable or soluble in biologically relevant aqueous or buffer systems and cannot emulate the structural constrains imposed by the large protein backbones. However, discrete synthetic models that are not being masked by the bulky protein residues and buffer molecules make it possible to study chemical reactivities intrinsic to the [Fe–S] cofactors. These model systems are especially valuable when the reactions involve small gaseous molecules such as O_2, NO, H_2S, etc.
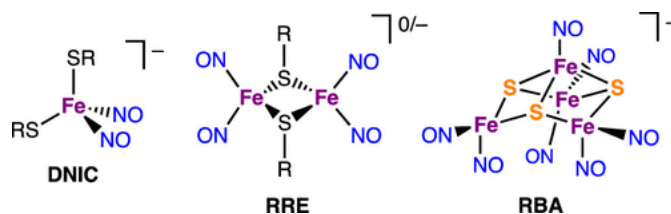
Chart 5.1 Most Common Forms of Iron Nitrosyls

In the past decade, our laboratory used this synthetic modeling approach to provide chemical insights into how cellular redox components such as [Fe–S] clusters, NO, O_2, and H_2S propagate their redox signals.[18] One of the conceptual advances we made was the identification of new reaction conditions that lead to the formation of previously unrecognized products during the reaction of [Fe–S] clusters with NO.[18,19,52] We found that the bridging sulfides from [2Fe-2S] clusters can be released as H_2S upon nitrosylation if the environment can provide a formal equivalent of H• (e^-/H^+) from donors such as thiols or phenols.[18,19] These results led us to hypothesize that [Fe–S] clusters can act as a point of direct crosstalk between NO and H_2S. In this Forum article, we report our recent studies probing whether this reactivity can be expanded to other clusters including the cubane-type [4Fe-4S] cluster: the most common cluster form.

5.3 Results and Discussion

5.3.1 NO reactivity of [4Fe−4S] cluster in the precent of thiol

The first question we sought to answer was whether or not adding an external thiol source to the reaction of [4Fe-4S] cluster with NO would change the reactivity pattern as was observed with [2Fe-2S] clusters.[19] To make that determination, nitric oxide was added to a synthetic [4Fe-4S] cluster, $[Et_4N]_2[Fe_4S_4(SPh)_4]$ (**1**), in the presence and the absence of an external thiol, PhSH. Both a purified NO gas and a chemical NO donor, S-trityl thionitrite (Ph_3CSNO),[20] were utilized to examine the thiol effects. It is noted that $NO_{(g)}$ and Ph_3CSNO resulted in no difference in the reactivity studies reported in this study. Exposure of excess (10 equiv) NO to an acetonitrile solution of **1** in the absence of PhSH yielded Roussin's black anion (RBA) consistent with the previous report by the Lippard group (Scheme 5.1a).[20] The crude product generated from the

reaction of **1** with NO in the presence of thiol (10 equiv) displayed a very similar IR spectrum to that of RBA with ν(NO) stretching frequencies of 1799, 1739, and 1708 cm^{-1} that are slightly shifted lower in energy from RBA (Figure 5.1A). However, this "RBA-like" product, labeled **Int. A** (Scheme 5.1b), appears to have drastically different stability from RBA as it constantly changes in morphology and color along with its IR spectrum every recrystallization attempt, hampering us from isolating a purified product. The X-band EPR spectrum of the crude product showed that the major reaction product was EPR silent (at 77 K or RT) while a dinitrosyl iron complex (DNIC), [Et$_4$N][Fe(NO)$_2$(SPh)$_2$] (**2**), was formed as a minor product ($\sim$31%); Scheme 5.1b. DNIC ν(NO) stretching frequencies of 1743 and 1681 cm^{-1} were also observed in the IR spectrum, with the former being encompassed in the broad feature at 1739 cm^{-1} (Figures 5.1A). Additionally, the fingerprint region of the DNIC thiolate ligands between 1573 and 1388 cm^{-1} is present.

(a) Previous work by Lippard
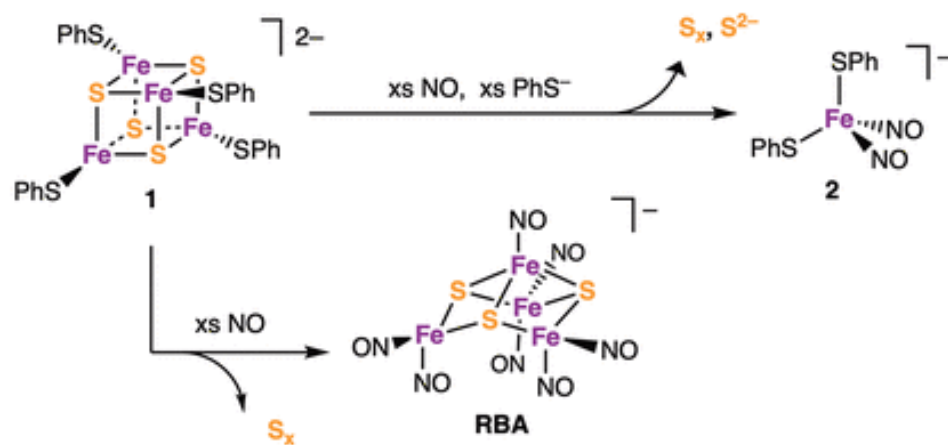
(b) This work
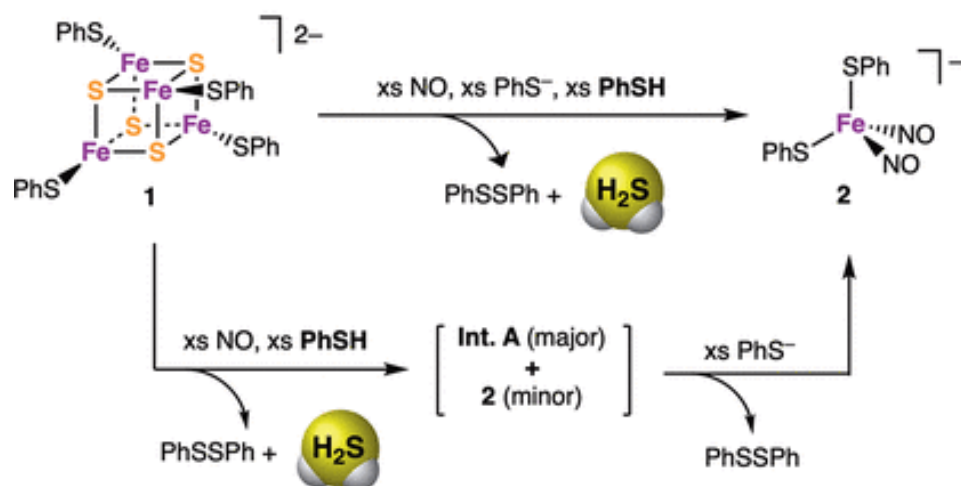
Scheme 5.1
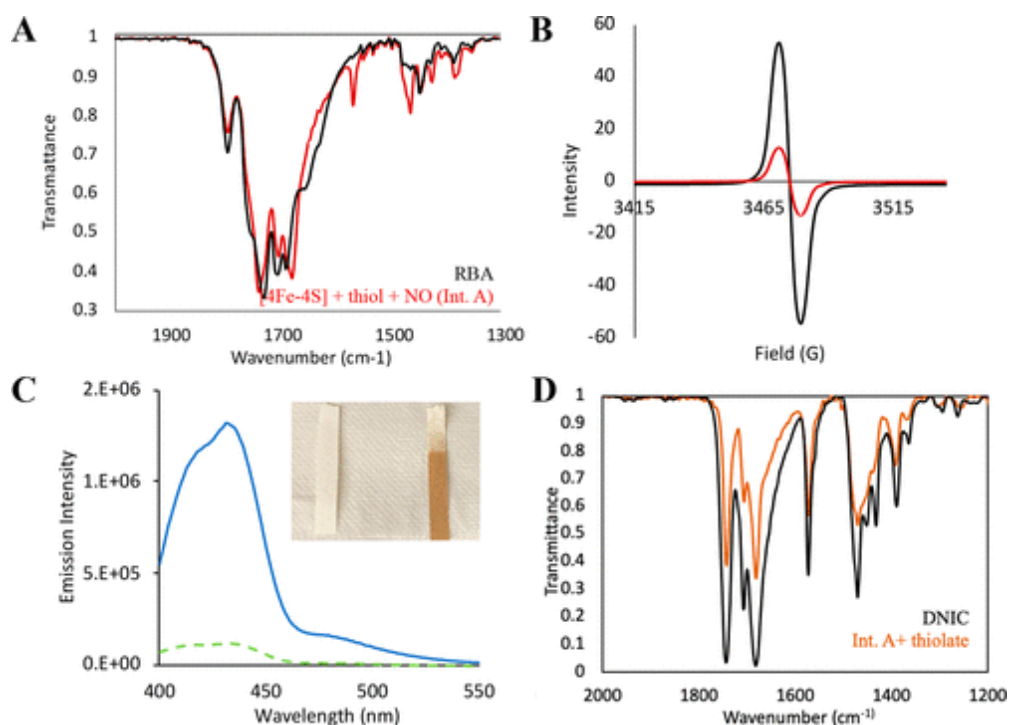
Figure 5.1 Reaction of (Et$_4$N)$_2$[Fe$_4$S$_4$(SPh)$_4$] (**1**) with NO in the presence of thiol and/or thiolate.

(A) IR spectrum (in KBr) of **Int. A** (red) resulting from **1**/NO in the presence of HSPh and that

of authentic RBA (back). (B) EPR spectra of **1** + 10 equiv PhSH + 10 equiv Ph$_3$CSNO (red)

followed by addition of 10 equiv PhS$^-$ (black) at 298 K. (C) Fluorescence spectra of a turn-on

H$_2$S sensor following incubation with the headspace gas of the **1**/NO reaction in the absence

(green) and presence (blue) of HSPh. Inset: Response of lead acetate paper detecting H$_2$S

from **1**/NO in the absence (left) and presence (right) of HSPh. (D) IR spectrum (in KBr) of **Int.**

A + 10 equiv PhS$^-$ to generate [Et$_4$N][Fe(NO)$_2$(SPh)$_2$] (**2**) (red) and that of authentic **2** (black).

We next investigated the fate of the bridging sulfides in 1 upon nitrosylation in the presence

and absence of an external thiol. After the reactions were complete, insoluble material was

separated by filtration and subsequently combined with triphenylphosphine, PPh$_3$, to trap and

quantify elemental sulfur that might have been generated from the reaction. ^{31}P NMR spectroscopy and GC-MS were used to determine the formation of triphenylphosphine sulfide, S=PPh$_3$, an established reaction product of PPh$_3$ with elemental sulfur.[19,52] The **1**/NO reaction in the absence of thiol was found to produce one equivalent of S=PPh3 as expected.[20] The **1**/NO reaction in the presence of thiol, however, was found to produce no S=PPh3, indicating no elemental sulfur was produced during the reaction.

The negative S$_x$ detection from **1**/NO in the presence of thiol led us to examine H$_2$S evolution from the thiol containing reaction. We first used lead acetate paper to qualitatively detect H$_2$S since the interaction of lead acetate with H$_2$S even in trace concentrations (as low as 5 ppm)[21] can produce dark-brown lead sulfide (H$_2$S + Pb(OAc)$_2$ $\rightarrow$ PbS + 2 AcOH). The lead acetate paper strip was hung over the headspace of the reaction flask for the **1**/NO reactions in the absence and presence of excess (10 equiv) PhSH. No color change on the lead acetate paper was observed from **1**/NO in the absence of an external thiol source. However, there was a clear reaction with the lead acetate paper from the **1**/NO reaction with thiol (Figure 5.1C), indicating that H$_2$S was produced during the nitrosylation of **1** with PhSH present. Emboldened by this result, we next quantified the amount of H$_2$S by employing a turn-on H$_2$S fluorescence sensor, 7-azido-4-methylcoumarin (C7Az).[22] The conversion of the azido group of C7Az to an amino group by H$_2$S has been reported to enhance a fluorescent emission signal at $\lambda = 434$ nm.[22] The headspace gas of the **1**/NO reaction in the presence and absence of thiol was transferred to an acetonitrile solution of C7Az whose fluorescence spectrum was then subsequently analyzed. The **1**/NO reaction in the absence of thiol did not induce any fluorescence signal. However, the same reaction in the presence of thiol led to a significant fluorescence enhancement at 434 nm (Figure 5.1 C). The C7Az sensor

exhibited a linear response to increasing concentration of H_2S from 0.2 mM to 1 mM in our experimental setup, which allowed us to quantify the amount of H_2S produced during the course of a reaction using an independently prepared calibration curve using NaSH/HCl. Interestingly, the H_2S quantification revealed that all four equivalents of bridging sulfides in **1** are released as H_2S upon nitrosylation with thiol present, which indicates **Int. A** has no bridging sulfide in its structure.

5.3.2 Role of thiolate in nitrosylation of [4Fe-4S] Cluster

In spite of the intriguing reactivity of **1**/NO with external thiol leading to H_2S evolution, unidentified **Int. A** has been a considerable challenge for us to gain further insights. Therefore, we turned our attention to convert **Int. A** to another product that is more stable for isolation and characterization. We found that an addition of excess (10 equiv) thiolate, [Et$_4$N][SPh], to **Int. A** resulted in the formation of a $\{Fe(NO)_2\}^9$ DNIC, [Et$_4$N][Fe(NO)$_2$(SPh)$_2$] (**2**) (Figure 5.1D). After multiple recrystallizations from MeCN/Et$_2$O, **2** was isolated (72% yield) as a dark red microcrystalline solid with known spectroscopic characteristics.[23,53] Complex **2** is one of the most intensively studied DNICs in the literature,[20,23,24] and we capitalized on its unique g = 2.03 EPR signal to quantify the formation of **2** in each step (Scheme 5.1b) by employing a calibration curve prepared from independently synthesized **2**. Double integration of the g = 2.03 signal from the reaction mixture indicates that ~31% of iron in [Et$_4$N]$_2$[Fe$_4$S$_4$(SPh)$_4$] (**1**) is converted to **2** after nitrosylation in the presence of thiol. Upon subsequent treatment with thiolate, there was a significant increase in the g = 2.03 signal which corresponds to the formation of overall four equivalents of **2**. The conversion of **1** to **2** can also be achieved in one step when **1** is exposed to NO in the presence of *both* thiol and thiolate. Likewise, the evolution of four equivalents of H_2S

was observed from a single step reaction of **1** with NO in the presence of *both* thiol and thiolate. In order to produce the quantitative amounts of **2** and H_2S from **1**, iron must receive electrons from the environment, i.e., externally added thiol/thiolate, which led us to examine the formation of the byproduct, PhSSPh. The GC-MS quantification confirmed the quantitative amount (3 equiv) of disulfide was also produced.[25]

5.3.3 Roussin's Black Anion reactivity with thiol/thiolate

Roussin's black anion (RBA), $[Fe_4(\mu_3\text{-}S)_3(NO)_7]^-$, is one of the longest known iron nitrosyl compounds[26] and it often appears as a thermodynamic product from NO reactivity with synthetic [Fe–S] clusters.[20] Intrigued by the resemblance of the IR spectrum of RBA to that of **Int. A** (Figure 5.1A), we decided to investigate the reactivity of RBA with thiol and thiolate to gain further insights into **Int. A**. RBA was prepared by following a literature procedure.[20] To our surprise, when RBA was exposed to free PhSH (10 equiv), the evolution of H_2S was first noticed by the color change of the lead acetate paper. The RBA/HSPh reaction also produces a metastable iron nitrosyl product whose IR spectrum is remarkably similar to that of **Int. A** from the reaction between $[Et_4N]_2[Fe_4S_4(SPh)_4]$ (**1**) and NO in the presence of thiol (Figure 5.2A). The observed similar stability and the IR features between the two reaction products made us suspect that both reactions might produce the same product. Therefore, we tested whether an addition of thiolate to the product from the reaction of RBA and PhSH would also produce a DNIC, $[Et_4N][Fe(NO)_2(SPh)_2]$ (**2**), as was observed with the reaction of **1**/NO/thiol. Indeed, an addition of excess (20 equiv) $[Et_4N][SPh]$ to the reaction product of RBA and PhSH produced **2** without generating any other iron nitrosyl byproduct.
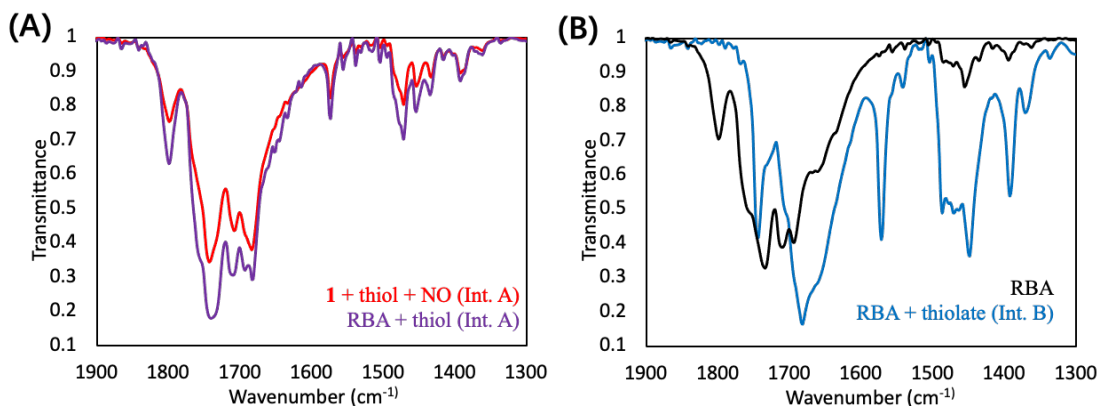
Figure 5.2 Reaction of RBA with thiol or thiolate. (A) IR spectra (KBr pellet) of the υ_{NO} (cm^{-1}) region comparing RBA + 10 equiv PhSH (purple) to [Fe$_4$S$_4$(SPh)$_4$]$^{2-}$ (**1**) + 10 equiv PhSH + 10 equiv Ph$_3$CSNO (red). (B) IR spectra comparing RBA + 10 equiv PhS$^-$ (blue) to authentic RBA (black).

The formation of [Et$_4$N][Fe(NO)$_2$(SPh)$_2$] (**2**) from RBA was not sensitive to the order in which thiol and thiolate were added. The successive addition of the reverse order, i.e., addition of [Et$_4$N][SPh] followed by HSPh or the addition of a mixture of thiol and thiolate to RBA led to the same result: the formation of **2**. When thiolate was added to RBA before thiol addition, however, a new reaction intermediate, **Int. B**, was observed by IR spectroscopy with lower v(NO) stretching frequencies starting at 1743 cm^{-1} compared to those of RBA that begin at 1799 cm^{-1} (Figure 5.2B). Previous molecular modeling and semiempirical quantum chemical calculations suggest that a reaction of RBA with thiolate would form a pseudocubane complex, [Fe$_4$(μ_3-S)$_3$(μ_3-SPh)(NO)$_7$]$^{2-}$ (Chart 5.2), in which the NO ligands in the thiolate adduct are more negative than in the RBA cluster.[27] Although we were not able to further characterize **Int.B** due to its limited stability, our observed v(NO) stretching frequencies of **Int.B** suggest more reduced NO characters

compared to those in RBA. Accordingly, $[Fe_4(\mu_3\text{-}S)_3(\mu_3\text{-}SPh)(NO)_7]^{2-}$ is considered as a possible structure for **Int.B.** The EPR quantification revealed that 3 equiv of iron embedded in RBA, $[Fe_4(\mu_3\text{-}S)_3(NO)_7]^-$, are eventually converted to $[Et_4N][Fe(NO)_2(SPh)_2]$ (**2**) by the addition of thiol and thiolate. One equivalent of NO is presumed to be released as $NO_{(g)}$, while the remaining one equiv of iron from RBA is released as $[Fe(SPh)_4]^{2-}$, the presence of which was shown in the ^1H NMR spectrum of the crude product mixture. When extra NO is provided to the reaction of RBA with thiol and thiolate, all four equivalents of iron from RBA are converted to **2** as determined by EPR quantification (Scheme 5.2).

Scheme 5.2

Int. A   Int. B
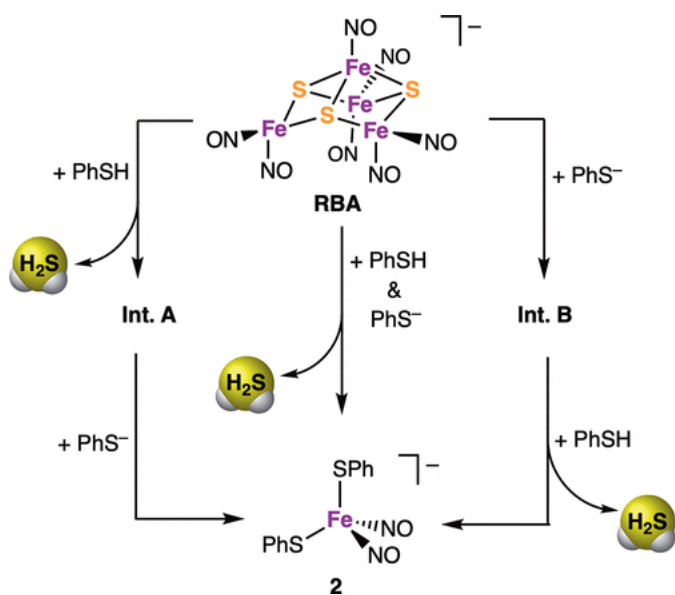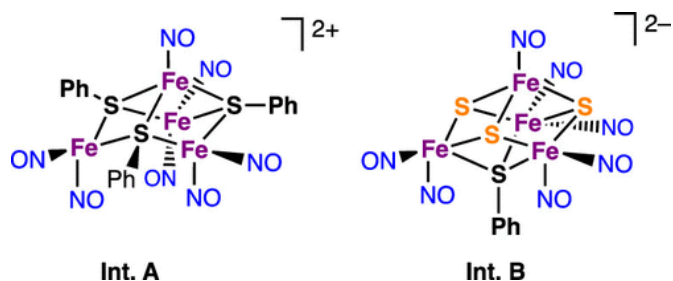
Chart 5.2

The observed reactivity of RBA, $[Fe_4(\mu_3\text{-}S)_3(NO)_7]^-$, displays how nitrosylation can change the chemical properties of the bridging sulfides in [Fe–S] clusters. The [4Fe-4S] model cluster $[Et_4N]_2[Fe_4S_4(SPh)_4]$ (**1**) is very stable in the presence of large excess PhSH, and the bridging sulfides are not prone to substitution with PhSH. However, the bridging sulfides of RBA are easily released as H_2S by PhSH at room temperature without need for any other reagent. We suspect that the bridging sulfides in RBA are more basic than those in **1** because they are coordinated to iron in a more reduced state (3x $\{Fe(NO)_2\}^9$ and $\{Fe(NO)\}^7$ in RBA) than iron (2+/3+) of compound **1**. This difference might initiate protonation of RBA by a weak acid PhSH ($pK_a \sim 6.6$) to form bridging hydrosulfide, $[Fe_4(\mu_3\text{-}SH)_3(NO)_7]^{2+}$, which could be subsequently replaced by thiolate to form $[Fe_4(\mu_3\text{-}SPh)_3(NO)_7]^{2+}$, the model we currently consider a possible structure for **Int. A** (Scheme 5.2 bottom). The previous study by Lippard established that RBA is the reaction product of **1**/NO.[20] Our study here suggests that RBA may not be the final product and it could be a reactive intermediate leading to other sulfur and iron-containing final products in a thiol rich environment. This unexpected chemical reactivity of RBA may explain the challenges the biochemical and biophysical communities face in identifying products generated from [4Fe-4S] proteins with NO (*vide infra*).

5.3.4 Roussin's Red Salt reactivity with thiol/thiolate

Besides RBA, Roussin's Red Salt (RRS, $Na_2[Fe_2S_2(NO)_4]$) is another iron−sulfur−nitrosyl cluster anions.[58] As described in Chapter 5.1, the ester form of RRS, Roussin's Red Ester (RRE, $[Fe_2(SR)_2(NO)_4]$), could be obtained from the reaction of NO with both nature [Fe-S] protein and synthetic [Fe-S] cluster.[58] Inspired by RBA/thiol reactivity, the thiol reactivity of RRS was also examined (Figure 5.3). Mirroring RBA's behavior, the introduction of an excess (10 equiv.) of HSPh to RRS led to the evolution of H_2S, as verified by lead acetate paper, and the generation of **2** along with its dimeric variant, $[Fe_2(NO)_4(\mu\text{-SPh})_2]$ (RRE) (Figure 5.3A). When an additional 10 equiv. of $[Et_4N][SPh]$ was introduced to the RRS and PhSH reaction mixture, there was a full conversion to compound **2**, with no other iron nitrosyl byproducts detected (Figure 5.3D).
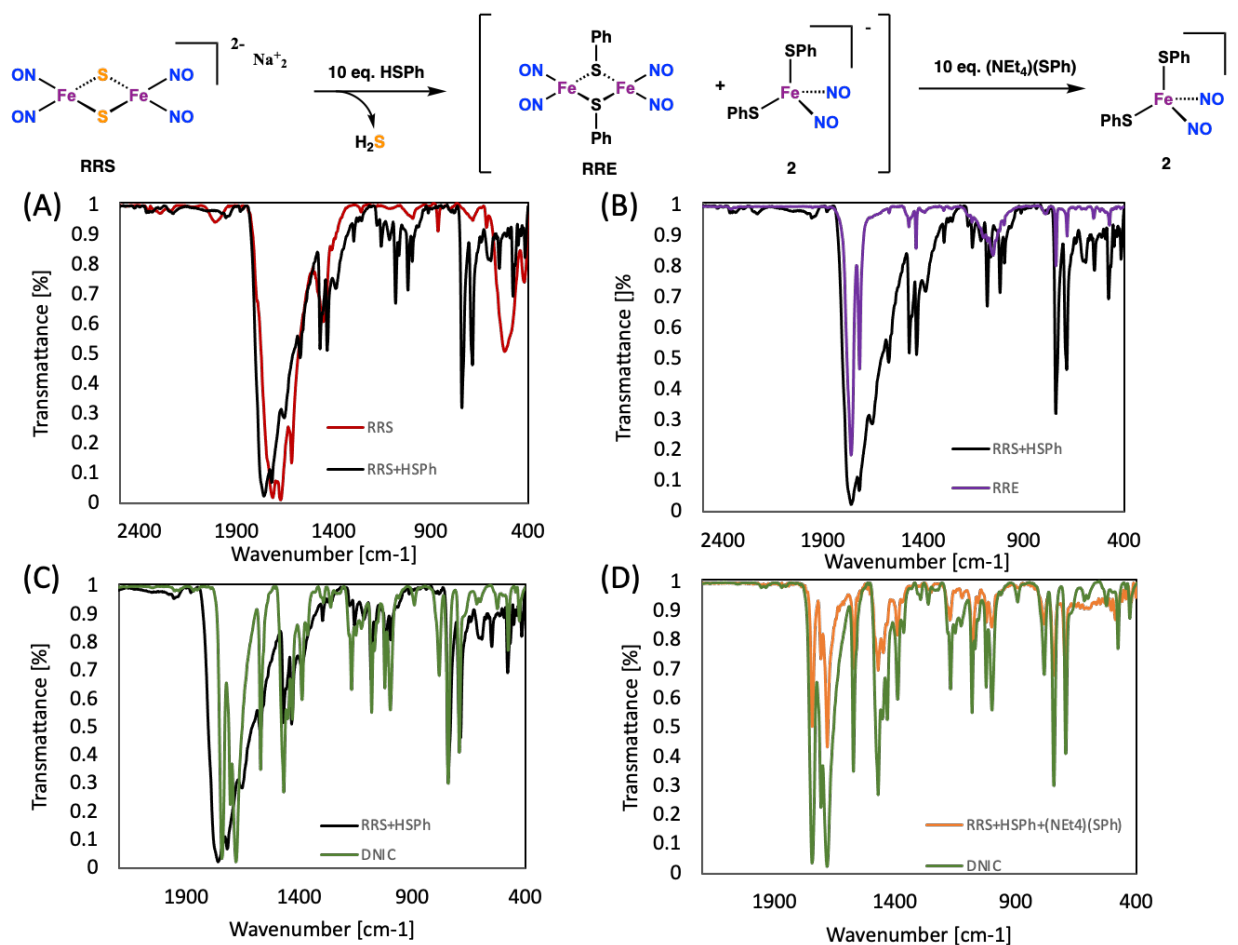
Figure 5.3 Reaction of RRS with thiol or thiolate. (A) IR spectra (KBr pellet) of the υ_{NO} (cm^{-1}) region comparing RRS + 10 equiv PhSH (black) to authentic RRS (red). (B) IR spectra comparing RRS + 10 equiv PhSH (black) to authentic RRE (purple). (C) IR spectra comparing RRS + 10 equiv PhSH (black) to authentic **2** (green). (D) IR spectra comparing RRS + 10 equiv PhSH + 10 equiv [NEt$_4$][SPh] (orange) to authentic **2** (green).

The core structure of RRS, where two iron centers are bridged by sulfide ligands, mirrors that of the [2Fe-2S] cluster. However, a distinct difference arises in the coordination of the iron centers: in RRS, each iron atom is coordinated to two nitrosyl (NO) groups, whereas in the [2Fe-2S] cluster,

the iron often coordinated with thiolate ligands. Intriguingly, while the addition of HSPh to RRS results in the liberation of the bridging sulfide as H_2S, a similar reaction of HSPh with the [2Fe-2S] cluster leaves the bridging sulfide untouched. This suggests that NO coordination to the [Fe-S] cluster alters the bridging Fe-S bond, rendering the bridging sulfide more susceptible to reactions. Supporting this observation, pervious study examining the electronic structure and geometry of RRS by DFT revealed that, based on their calculations, the bridging Fe-S bond in RRS is significantly longer compared to that in the [2Fe-2S] cluster (Figure 5.4). [59]

	$[Fe_2S_2(SPh)_4]^{2-}$	$[Fe_2S_2(NO)_4]^{2-}$
Fe1-S1	2.198 Å	2.266 (2.338) Å
	Got from crystal structure	Calculated using RB3LYP (UB3LYP) function
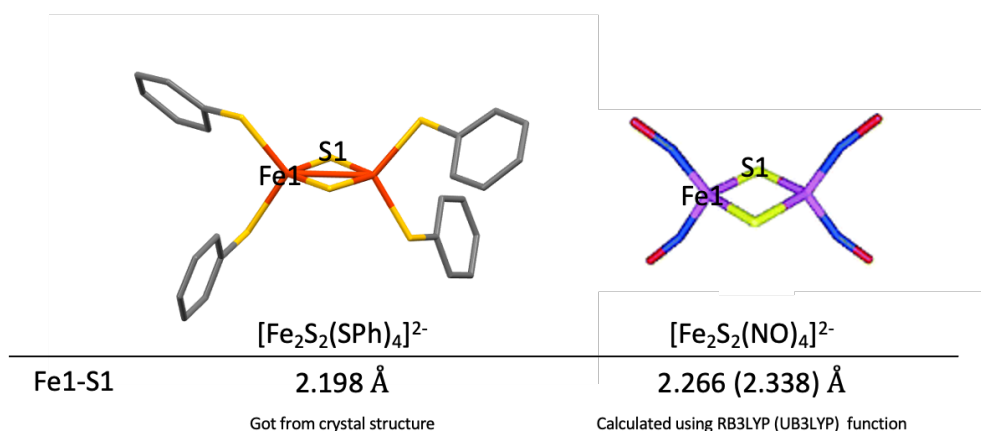
Figure 5.4 Geometry comparison of [2Fe-2S] cluster and RRS

5.3.5 Biological Implications

In spite of a considerable number of studies that report NO reactivity of various [Fe–S] proteins, little is known about the fate of the bridging sulfides after the reaction. Bridging sulfides in [Fe–S] clusters are generally acid-labile, and a strong acid can disrupt the cluster with a release of H_2S. Our study shows that the H_2S evolution from [Fe–S] clusters does not necessarily require a strong acid when [Fe–S] clusters are exposed to NO. Consistent with our previous studies with

[2Fe-2S] clusters, we observe that the presence of thiol alters the fate of the bridging sulfides of [4Fe-4S] clusters upon nitrosylation and leads to the H_2S evolution. Given the high concentration of cellular thiols (1–10 mM),[28] our study suggest that H_2S must be a viable reaction product when [Fe–S] cofactors are exposed to NO.

Our reactivity studies of RBA with thiol and/or thiolate originated from a motivation to understand the **1**/NO reactivity with thiol present because RBA was the reaction product from **1**/NO in the absence of thiol.[20] The H_2S evolution from RBA by PhSH came as a surprise. However, this unexpected H_2S formation from RBA has its own intellectual merit considering that RBA has long been known for its antimicrobial activity.[29] The observed H_2S liberation from RBA by thiol suggests that the known antimicrobial effect of RBA might be directly linked to the H_2S redox signaling.[6,9,30,54]

The conversion of [Fe–S] clusters to iron-nitrosyl species by NO has drawn considerable attention for the past decade. As for the [2Fe-2S] clusters, there is a clear pattern in NO reactivity. The final nitrosylated products are either $\{Fe(NO)_2\}^9$ DNIC or its dimeric form, species known as Roussin's red ester (RRE), Chart 5.1, in most cases[16,31,55-57] with the exception of the [2Fe-2S] clusters in mitoNEET and miner2 that reversibly bind NO.[32] Unlike [2Fe-2S] systems, however, nitrosylated products from [4Fe-4S] clusters show no consistency. Nuclear resonance vibrational (NRV) spectroscopic studies on [4Fe-4S]-ferredoxin report RBA as the main nitrosylated product.[33] Another [4Fe-4S] protein, EndoIII, reports a 1:1 mixture of RRE and DNIC as the final nitrosylated products analyzed by HYSCORE pulse EPR spectroscopy and mass spectrometry.[34] As for WhiD and NsrR regulatory proteins, which are dedicated NO-sensors in microorganisms, Mössbauer, NRVS, and DFT, and $^{14}NO/^{15}NO$ and $^{32}S/^{34}S$ labeling studies rule out the formation

of RBA from these proteins.[35] Instead, researchers report the nitrosylated products of WhiD and NsrR (both from *S. coelicolor*) as "species related to RBA and RRE".[35] Similarly, another ambiguous "RBA-like" description is given to the nitrosylated product from a [4Fe-4S] HiPIP protein with NO.[36] We conjecture that the various types of unidentified nitrosylated products observed with [4Fe-4S] proteins might be due to the intrinsic instability of multinuclear [Fe–S] clusters with NO ligands. The current study shows that the bridging sulfides embedded in RBA are more reactive toward thiol compared to the bridging sulfides in [Fe–S] clusters without NO ligands. It also shows that the "RBA-like" intermediates can easily convert to another type of iron nitrosyl by thiolate. This structural vulnerability of iron nitrosyls resulting from [4Fe-4S]/NO against environmental factors (thiol, thiolate, etc.) might be a reason for the lack of a general product type.

5.4 Experimental Section

General Considerations. All synthesized products were assumed to be air- and moisture-sensitive. They were manipulated under argon on a standard Schlenk line or in an atmosphere of purified nitrogen in an MBraun Labmaster SP glovebox (O_2 < 1 ppm; H_2O < 1 ppm). Solvents were purified by being passed through a series of two activated alumina columns (MBraun solvent purification system) under an Ar atmosphere and stored over 4 Å molecular sieves. Phenyl disulfide (PhSSPh), thiophenol (HSPh), triphenylphosphine (TPP), triphenylphosphine sulfide (TPPS), sodium hydrosulfide, Celite, 7-azido-4-methylcoumarin (C7Az), and lead acetate paper were purchased from Sigma and used as received. Tube sealant was purchased from Fisher and used as received.

Physical Measurements. Infrared spectra were recorded on a Bruker Tensor 27 FT-IR spectrometer. Fluorescence spectra were recorded on a Tecan Safire spectrometer. ^{1}H NMR spectra were recorded at 400 MHz on a Bruker UltraShield spectrometer and residual solvent signals were used as an internal reference. EPR spectra of a liquid sample were recorded on a Bruker EMX plus EPR spectrometer at 298 K. The EPR samples were loaded into a 100 μL glass capillary that was inserted into a 4 mm o.d. quartz EPR tube. Spectra were recorded under the following conditions: microwave frequency, 9.871 GHz; microwave power, 2.0 mW; modulation amplitude and frequency, 1.000 G and 100 kHz. GC-MS data were recorded using a Hewlett-Packard (Agilent) GCD 1800C GC-MS spectrometer.

Synthesis. $(Et_4N)_2[Fe_4S_4(SPh)_4]$ (**1**),[37] $(Et_4N)[Fe_4S_3(NO)_7]$ (RBA),[20] $(Et_4N)[Fe(NO)_2(SPh)_2]$ (**2**),[23] $Na_2[Fe_2S_2(NO)_4]$ (RRS)[58] and trityl-S-nitrosothiol[20] were prepared as described in the literature.

Reaction of $(Et_4N)_2[Fe_4S_4(SPh)_4]$ (1) with Ph_3CSNO (a) in the Absence of Thiol and Thiolate. This reaction has been previously reported by Lippard and co-workers.[20] In the glovebox, a solution of 50 mg (0.045 mmol) of **1** in 5 mL of MeCN was mixed with 102.2 mg (0.243 mmol) of Ph_3CSNO. The reaction was allowed to stir for 3 h at room temperature in dark. During this time, the formation of an insoluble solid (i.e., elemental sulfur) could be observed. This insoluble solid was separated by filtration. The filtrate was saved, and all volatiles were removed *in vacuo*. The resultant residue was washed with Et_2O and redissolved in 1 mL of THF. Crystallization from THF/pentane gave $(Et_4N)[Fe_4S_3(NO)_7]$ (RBA) as black crystals (24.4 mg, 81%); its UV–vis and IR spectroscopic features were in good agreement with those reported for RBA.[20]

Reaction of (Et₄N)₂[Fe₄S₄(SPh)₄] (1) with Ph₃CSNO (b) in the Presence of Thiol and Thiolate.
Under a N_2 atmosphere, 50 mg (0.045 mmol) of **1** was dissolved in 5 mL of MeCN, and the mixture was transferred to a 25 mL Schlenk flask to which was added 10 equiv of PhSH followed by addition of 10 equiv of Ph₃CSNO and 10 equiv of [NEt₄][SPh]. The reaction was stirred at room temperature in the dark for 3 h. During this time, the color of the reaction mixture turned from brown-red to dark red and the formation of H_2S could be qualitatively observed by lead acetate paper (Figure 5.1A). After 3 h, all volatiles were removed *in vacuo*. The residue was washed with 10 mL of Et₂O and the Et₂O washing was later found to contain the PhSSPh. Analysis of the IR spectrum of the black oily residue indicated (Et₄N)[Fe(NO)₂(SPh)₂] (**2**) to be the only NO-containing product. The oily residue was recrystallized in 5 mL of a 1:1 MeCN:Et₂O solution in a −35 °C freezer overnight to afford **2** as dark red needles (61.2 mg, 72%) whose UV–vis, IR, and EPR spectra were in good agreement with those reported for **2**.[23]

General Method for Product Detection and Quantification for Reaction b.

Under a N_2 atmosphere, 0.2 mL of a 10 mM (Et₄N)₂[Fe₄S₄(SPh)₄] (**1**) stock solution was mixed with 10 equiv (0.2 mL, 100 mM) of PhSH in a 10 mL Schlenk flask and sealed with a rubber septum, and 10 equiv (0.2 mL, 100 mM) of Ph₃CSNO was injected into the flask. After 3 h of stirring, 1 mL of a [NEt₄][SPh] stock solution (20 mM, 10 equiv) was injected into the reaction mixture. The resulting solution was allowed to further stir for 1 h at room temperature. The reaction products were identified by IR, GS-MS, and EPR spectroscopy.

*a. Hydrogen sulfide (H_2S) detection.*The formation of H_2S during the reaction could be qualitatively analyzed using lead acetate paper. After the (Et₄N)₂[Fe₂S₂(SPh)₄] (**1**) solution was

loaded into the Schlenk flask, a lead acetate paper strip was held in place by a rubber septum in the flask headspace. Addition of Ph_3CSNO, PhSH, and $[NEt_4][SPh]$ were carefully carried out via syringe, while avoiding touching the detector with the reaction solution. The color change of the lead acetate paper was then observed (Figure 5.1A, inset).

A turn-on fluorescence H_2S sensor, 7-azido-4-methylcoumarin (C7Az),[22] was used to quantify the amount of H_2S produced. In the presence of H_2S, the azide group of C7Az is reduced to an amine and generates 7-amino-4-methylcoumarin (C7Am) that emits at $\lambda_{em} = 434$ nm. After reaction completion, a 25 mL two-neck round-bottom flask containing 1 mL of 10 mM C7Az solution in MeCN was connected to the side arm of the reaction flask (Figure 5.5). The C7Az containing round-bottom flask was placed in liquid nitrogen to generate negative pressure, after which the side arm of the reaction Schlenk flask was opened to allow gas transfer for 2 min. The connection between the C7Az containing round-bottom flask and the reaction Schlenk flask was cut off after gas transfer. The C7Az containing round-bottom flask was removed from liquid nitrogen, and the C7Az solution was allowed to stir for an additional hour at room temperature. The 30-fold diluted C7Az solution in MeCN was used for fluorescence analysis (Figure 5.1A).

Figure 5.5 Set up for hydrogen sulfide detection using turn-on fluorescence sensor C7Az.

The calibration curve for H_2S detection was made through the same procedure using NaSH and HCl in the reaction flask to produce H_2S for analysis. By varying the amount of NaSH and HCl, H_2S between 0.2 and 1 mM was generated and used for the calibration curve (Figure 5.6).
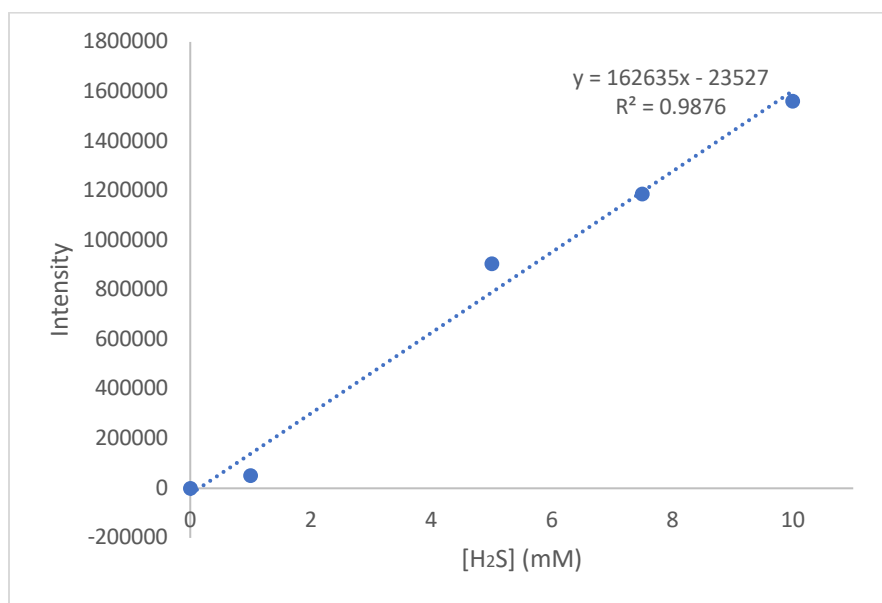
Figure 5.6 Calibration curve for hydrogen sulfide (H_2S) concentration-dependent fluorescence intensity of turn-on fluorescence H_2S sensor C7Az.

The percent yield of H_2S generated during the reaction of [4Fe-4S] cluster with Ph_3CSNO in the presence of thiol and thiolate is approximately 100% based on fluorescence intensity, signifying all 4 bridging-sulfide were released as H_2S. Additionally, we found that all H_2S release was during the first step of the reaction, as in the reaction of [4Fe-4S] cluster with Ph_3CSNO and thiol, while the following addition of [NEt_4][SPh] did not result in any additional H_2S formation.

b. Iron-containing species detection. IR spectrum of the reaction mixture of ($Et_4N)_2$[Fe_4S_4(SPh)$_4$] (**1**) reacted with Ph_3CSNO in the presence of thiol showed the generation of a new type of iron-nitrosyl species, Int. A (Figure 5.1C). The addition of [NEt_4][SPh] produced changes in the IR spectrum that suggest DNIC to be the only iron-containing species after the addition of [NEt_4][SPh] (Figure 5.1D).

EPR spectroscopy was used to quantify the amount of DNIC, $(Et_4N)[Fe(NO)_2(SPh)_2]$ (**2**), generation (Figure 5.1B). The calibration curve for **2** (Figure 5.7) was prepared using independently synthesized **2** dissolved in MeCN in the concentration range of 1–6 mM. In the glovebox, 0.2 mL of 10 mM $(Et_4N)_2[Fe_4S_4(SPh)_4]$ (**1**) stock solution was mixed with 10 equiv (0.2 mL, 100 mM) of PhSH and 10 equiv (0.2 mL, 100 mM) of Ph_3CSNO in a 10 mL Schlenk flask. After stirring in the dark for 3 h, the EPR trace showed a weak EPR signal at g = 2.029 corresponding to ~31% DNIC production where the formation of 4 equiv of **2** per **1** was considered as 100%. After the first reaction step of [4Fe-4S] with Ph_3CSNO and thiol, 1 mL of $[NEt_4][SPh]$ stock solution (20 mM, 10 equiv) was added into the reaction mixture and allowed to stir for an additional hour. The EPR trace after the addition of $[NEt_4][SPh]$ displayed the same signal at g = 2.029 with stronger intensity, corresponding to 93% DNIC generation for the whole reaction of [4Fe-4S] with Ph_3CSNO in the presence of thiol and thiolate.
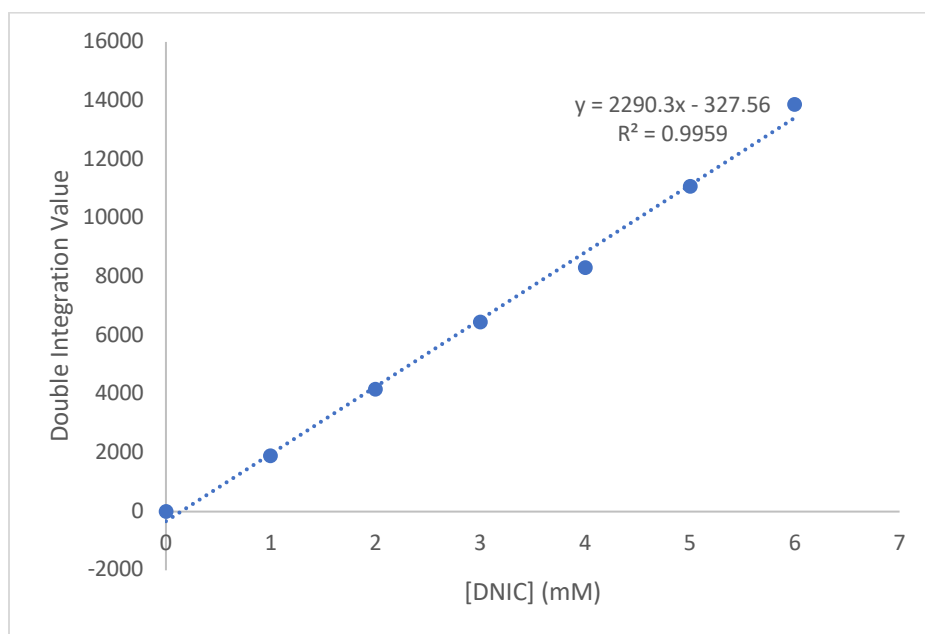
Figure 5.7 Concentration-dependent EPR calibration curve for DNIC at 298 K in MeCN. Spectra were recorded under the following conditions: microwave frequency: 9.871 GHz, microwave power: 2.0 mW, modulation amplitude and frequency: 1.000 G and 100 kHz.

c. Phenyldisulfide (PhSSPh) detection. PhSSPh quantification was carried out using GC-MS where the calibration curve for PhSSPh (Figure 5.8) was made in the concentration range of 50 to 500 μM, while 50 μM of S=PPh$_3$ was used as an internal standard to provide reproducible data from day-to-day measurements. The calibration curve was based on the normalized peak area of PhSSPh.
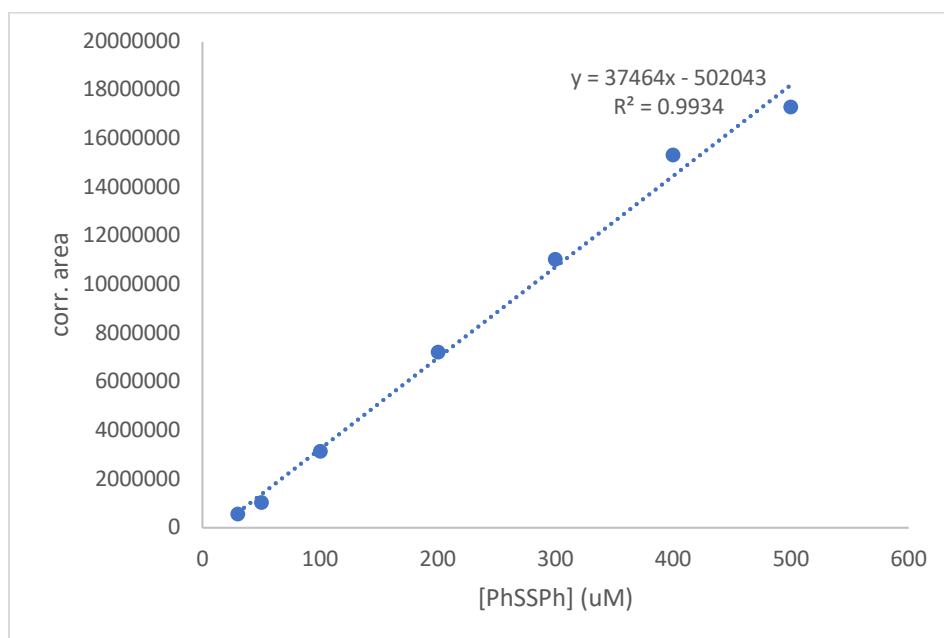
Figure 5.8 GC-MS calibration curve for phenyldisulfide (PhSSPh)

After reaction b was finished, a 150 μL aliquot of the reaction solution was mixed with 20 μL of a solution of S=PPh₃ (3.75 mM) in MeCN. The final volume of the mixture was adjusted to 1.5 mL with MeCN to make a GC sample. A control reaction without $(Et_4N)_2[Fe_4S_4(SPh)_4]$ (**1**) was also tested and served as a baseline to detect any PhSSPh formation that resulted from excess HSPh oxidizing under the GC conditions. The amount of PhSSPh generated from the [4Fe-4S] cluster that reacted with Ph₃CSNO in the presence of thiol and thiolate was determined as 91 ± 3%, where 3 equiv of PhSSPh formation per [4Fe-4S] cluster was considered as 100%.

Reaction of $(Et_4N)[Fe_4S_3(NO)_7]$ (RBA) with thiol and thiolate (c) in the presence of Ph₃CSNO. In the glovebox, 0.2 mL of 10 mM RBA stock solution was mixed with 10 equiv (1 mL, 20 mM) of Ph₃CSNO and 20 equiv of [NEt₄][SPh] stock solution (1 mL, 40 mM) in a 10 mL Schlenk flask and sealed with a rubber septum. Ten equiv (0.2 mL, 100 mM) of PhSH was then injected into the

flask. The reaction solution was allowed to stir in the dark for 3 h, during which the color of the reaction mixture changed from brown to dark red and the formation of H_2S could be observed by lead acetate paper. NMR, IR, and EPR spectra of the reaction mixture confirmed **2** to be the only iron-containing product. EPR quantification suggests a $91 \pm 2\%$ of DNIC, $(Et_4N)[Fe(NO)_2(SPh)_2]$ (**2**), formation where 4 equiv of DNIC generation per RBA molecule was considered as 100%.

Reaction of $(Et_4N)[Fe_4S_3(NO)_7]$ (RBA) with thiol and thiolate (d) in the absence of Ph_3CSNO. In the glovebox, 0.2 mL of 10 mM RBA stock solution was mixed with 10 equiv of $[NEt_4][SPh]$ stock solution and 10 equiv (0.2 mL, 100 mM) of PhSH solution. The reaction solution was further diluted with 1 mL of MeCN and stirred in the dark for 3 h. The formation of H_2S could be observed by lead acetate paper during the reaction. NMR spectrum of the reaction showed the formation of $(NEt_4)_2[Fe(SPh)_4]$, and the iron-nitrosyl product DNIC was confirmed by IR and EPR spectroscopy. EPR quantification suggests $69 \pm 2\%$ of DNIC formation where 4 equiv of DNIC generation per RBA molecule was considered as 100%.

5.5 References

(1) Culotta, E.; Koshland, D. E., Jr. NO News Is Good News: A Startlingly Simple Molecule Unites Neuroscience, Physiology, and Immunology and Revises Scientists' Understanding of How Cells Communicate and Defend Themselves. *Science* **1992**, *258* (5090), 1862–1865. https://doi.org/10.1126/science.1361684.

(2) Gow, A. J.; Ischiropoulos, H. Nitric Oxide Chemistry and Cellular Signaling. *J. Cell. Physiol.* **2001**, *187* (3), 277–282. https://doi.org/10.1002/jcp.1085.

(3) Brenman, J. E.; Bredt, D. S. [11] Nitric Oxide Signaling in the Nervous System. In *Methods in Enzymology*; Elsevier, 1996; pp 119–129.

(4) MacMicking, J.; Xie, Q.-W.; Nathan, C. Nitric Oxide and Macrophage Function. *Annu. Rev. Immunol.* **1997**, *15* (1), 323–350. https://doi.org/10.1146/annurev.immunol.15.1.323.

(5) Ignarro, L. J. Biosynthesis and Metabolism of Endothelium-Derived Nitric Oxide. *Annu. Rev. Pharmacol. Toxicol.* **1990**, *30* (1), 535–560. https://doi.org/10.1146/annurev.pa.30.040190.002535.

(6) Filipovic, M. R.; Zivanovic, J.; Alvarez, B.; Banerjee, R. Chemical Biology of H_2S Signaling through Persulfidation. *Chem. Rev.* **2018**, *118* (3), 1253–1337. https://doi.org/10.1021/acs.chemrev.7b00205.

(7) King, A. L.; Polhemus, D. J.; Bhushan, S.; Otsuka, H.; Kondo, K.; Nicholson, C. K.; Bradley, J. M.; Islam, K. N.; Calvert, J. W.; Tao, Y.-X.; Dugas, T. R.; Kelley, E. E.; Elrod, J. W.; Huang, P. L.; Wang, R.; Lefer, D. J. Hydrogen Sulfide Cytoprotective Signaling Is Endothelial

Nitric Oxide Synthase-Nitric Oxide Dependent. *Proc. Natl. Acad. Sci. U. S. A.* **2014**, *111* (8), 3182–3187. https://doi.org/10.1073/pnas.1321871111.

(8) Kolluru, G. K.; Shen, X.; Kevil, C. G. A Tale of Two Gases: NO and H2S, Foes or Friends for Life? *Redox Biol.* **2013**, *1* (1), 313–318. https://doi.org/10.1016/j.redox.2013.05.001.

(9) Szabó, C. Hydrogen Sulphide and Its Therapeutic Potential. *Nat. Rev. Drug Discov.* **2007**, *6* (11), 917–935. https://doi.org/10.1038/nrd2425.

(10) Coletta, C.; Papapetropoulos, A.; Erdelyi, K.; Olah, G.; Módis, K.; Panopoulos, P.; Asimakopoulou, A.; Gerö, D.; Sharina, I.; Martin, E.; Szabo, C. Hydrogen Sulfide and Nitric Oxide Are Mutually Dependent in the Regulation of Angiogenesis and Endothelium-Dependent Vasorelaxation. *Proc. Natl. Acad. Sci. U. S. A.* **2012**, *109* (23), 9161–9166. https://doi.org/10.1073/pnas.1202916109.

(11) Yong, Q.-C.; Cheong, J. L.; Hua, F.; Deng, L.-W.; Khoo, Y. M.; Lee, H.-S.; Perry, A.; Wood, M.; Whiteman, M.; Bian, J.-S. Regulation of Heart Function by Endogenous Gaseous Mediators—Crosstalk between Nitric Oxide and Hydrogen Sulfide. *Antioxid. Redox Signal.* **2011**, *14* (11), 2081–2091. https://doi.org/10.1089/ars.2010.3572.

(12) Filipovic, M. R.; Eberhardt, M.; Prokopovic, V.; Mijuskovic, A.; Orescanin-Dusic, Z.; Reeh, P.; Ivanovic-Burmazovic, I. Beyond H_2S and NO Interplay: Hydrogen Sulfide and Nitroprusside React Directly to Give Nitroxyl (HNO). A New Pharmacological Source of HNO. *J. Med. Chem.* **2013**, *56* (4), 1499–1508. https://doi.org/10.1021/jm3012036.

(13) Filipovic, M. R.; Miljkovic, J. L.; Nauser, T.; Royzen, M.; Klos, K.; Shubina, T.; Koppenol, W. H.; Lippard, S. J.; Ivanović-Burmazović, I. Chemical Characterization of the Smallest *S*-Nitrosothiol, HSNO; Cellular Cross-Talk of H_2S and *S*-Nitrosothiols. *J. Am. Chem. Soc.* **2012**, *134* (29), 12016–12027. https://doi.org/10.1021/ja3009693.

(14) Filipovic, M. R.; Miljkovic, J.; Allgäuer, A.; Chaurio, R.; Shubina, T.; Herrmann, M.; Ivanovic-Burmazovic, I. Biochemical Insight into Physiological Effects of H2S: Reaction with Peroxynitrite and Formation of a New Nitric Oxide Donor, Sulfinyl Nitrite. *Biochem. J.* **2012**, *441* (2), 609–621. https://doi.org/10.1042/bj20111389.

(15) Johnson, D. C.; Dean, D. R.; Smith, A. D.; Johnson, M. K. Structure, Function, and Formation of Biological Iron-Sulfur Clusters. *Annu. Rev. Biochem.* **2005**, *74* (1), 247–281. https://doi.org/10.1146/annurev.biochem.74.082803.133518.

(16) Styś, A.; Galy, B.; Starzyński, R. R.; Smuda, E.; Drapier, J.-C.; Lipiński, P.; Bouton, C. Iron Regulatory Protein 1 Outcompetes Iron Regulatory Protein 2 in Regulating Cellular Iron Homeostasis in Response to Nitric Oxide. *J. Biol. Chem.* **2011**, *286* (26), 22846–22854. https://doi.org/10.1074/jbc.m111.231902.

(17) Hyduke, D. R.; Jarboe, L. R.; Tran, L. M.; Chou, K. J. Y.; Liao, J. C. Integrated Network Analysis Identifies Nitric Oxide Response Networks and Dihydroxyacid Dehydratase as a Crucial Target in *Escherichia Coli*. *Proc. Natl. Acad. Sci. U. S. A.* **2007**, *104* (20), 8484–8489. https://doi.org/10.1073/pnas.0610888104.

(18) Fitzpatrick, J.; Kim, E. Synthetic Modeling Chemistry of Iron–Sulfur Clusters in Nitric Oxide Signaling. *Acc. Chem. Res.* **2015**, *48* (8), 2453–2461. https://doi.org/10.1021/acs.accounts.5b00246.

(19) Tran, C. T.; Kim, E. Acid-Dependent Degradation of a [2Fe–2S] Cluster by Nitric Oxide. *Inorg. Chem.* **2012**, *51* (19), 10086–10088. https://doi.org/10.1021/ic301676f.

(20) Harrop, T. C.; Tonzetich, Z. J.; Reisner, E.; Lippard, S. J. Reactions of Synthetic [2Fe-2S] and [4Fe-4S] Clusters with Nitric Oxide and Nitrosothiols. *J. Am. Chem. Soc.* **2008**, *130* (46), 15602–15610. https://doi.org/10.1021/ja8054996.

(21) Clarke, P. H. Hydrogen Sulphide Production by Bacteria. *J. Gen. Microbiol.* **1953**, *8* (3), 397–407. https://doi.org/10.1099/00221287-8-3-397.

(22) Chen, B.; Li, W.; Lv, C.; Zhao, M.; Jin, H.; Jin, H.; Du, J.; Zhang, L.; Tang, X. Fluorescent Probe for Highly Selective and Sensitive Detection of Hydrogen Sulfide in Living Cells and Cardiac Tissues. *Analyst* **2013**, *138* (3), 946–951. https://doi.org/10.1039/c2an36113b.

(23) Harrop, T. C.; Song, D.; Lippard, S. J. Reactivity Pathways for Nitric Oxide and Nitrosonium with Iron Complexes in Biologically Relevant Sulfur Coordination Spheres. *J. Inorg. Biochem.* **2007**, *101* (11–12), 1730–1738. https://doi.org/10.1016/j.jinorgbio.2007.05.006.

(24) Strasdeit, H.; Krebs, B.; Henkel, G. Synthese Und Struktur von [Fe(SPh)$_2$(NO)$_2$]$^-$ Dem „Monomeren" Des Roussinschen Phenylesters/ Synthesis and Structure of [Fe(SPh)$_2$(NO)$_2$]$^-$, the "Monomer" of Roussin's Phenyl Ester. *Z. Naturforsch. B J. Chem. Sci.* **1986**, *41* (11), 1357–1362. https://doi.org/10.1515/znb-1986-1107.

(25) Tsai, M.-C.; Tsai, F.-T.; Lu, T.-T.; Tsai, M.-L.; Wei, Y.-C.; Hsu, I.-J.; Lee, J.-F.; Liaw, W.-F. Relative Binding Affinity of Thiolate, Imidazolate, Phenoxide, and Nitrite toward the $Fe(NO)_2$ Motif of Dinitrosyl Iron Complexes (DNICs): The Characteristic Pre-Edge Energy of $Fe(NO)_2{}^9$ DNICs. *Inorg. Chem.* **2009**, *48* (19), 9579–9591. https://doi.org/10.1021/ic901675p.

(26) Roussin, M. L. Recherches sur les nitrosulfures doubles de fer (nouvelle classe de sels). *Ann. Chim. Phys.* **1858**, *52*, 285– 303

(27) Chmura, A.; Szaciłowski, K.; Waksmundzka-Góra, A.; Stasicka, Z. Photochemistry of the [Fe4(M3-S)3(NO)7]− Complex in the Presence of S-Nucleophiles: A Spectroscopic Study. *Nitric Oxide* **2006**, *14* (3), 247–260. https://doi.org/10.1016/j.niox.2005.10.005.

(28) Meister, A. Glutathione Metabolism and Its Selective Modification. *J. Biol. Chem.* **1988**, *263* (33), 17205–17208. https://doi.org/10.1016/s0021-9258(19)77815-6.

(29) Hamilton-Brehm, S. D.; Schut, G. J.; Adams, M. W. W. Antimicrobial Activity of the Iron-Sulfur Nitroso Compound Roussin's Black Salt [Fe $_4$ S $_3$ (NO) $_7$] on the Hyperthermophilic Archaeon *Pyrococcus Furiosus*. *Appl. Environ. Microbiol.* **2009**, *75* (7), 1820–1825. https://doi.org/10.1128/aem.02562-08.

(30) Wang, R. Physiological Implications of Hydrogen Sulfide: A Whiff Exploration That Blossomed. *Physiol. Rev.* **2012**, *92* (2), 791–896. https://doi.org/10.1152/physrev.00017.2011.

(31) Lo, F.-C.; Lee, J.-F.; Liaw, W.-F.; Hsu, I.-J.; Tsai, Y.-F.; Chan, S. I.; Yu, S. S.-F. The Metal Core Structures in the Recombinant *Escherichia Coli* Transcriptional Factor SoxR. *Chemistry* **2012**, *18* (9), 2565–2577. https://doi.org/10.1002/chem.201100838.

(32) Cheng, Z.; Landry, A. P.; Wang, Y.; Ding, H. Binding of Nitric Oxide in CDGSH-Type [2Fe-2S] Clusters of the Human Mitochondrial Protein Miner2. *J. Biol. Chem.* **2017**, *292* (8), 3146–3153. https://doi.org/10.1074/jbc.m116.766774.

(33) Tonzetich, Z. J.; Wang, H.; Mitra, D.; Tinberg, C. E.; Do, L. H.; Jenney, F. E., Jr; Adams, M. W. W.; Cramer, S. P.; Lippard, S. J. Identification of Protein-Bound Dinitrosyl Iron Complexes by Nuclear Resonance Vibrational Spectroscopy. *J. Am. Chem. Soc.* **2010**, *132* (20), 6914–6916. https://doi.org/10.1021/ja101002f.

(34) Ekanger, L. A.; Oyala, P. H.; Moradian, A.; Sweredoski, M. J.; Barton, J. K. Nitric Oxide Modulates Endonuclease III Redox Activity by a 800 mV Negative Shift upon [Fe$_4$S$_4$] Cluster Nitrosylation. *J. Am. Chem. Soc.* **2018**, *140* (37), 11800–11810. https://doi.org/10.1021/jacs.8b07362.

(35) Serrano, P. N.; Wang, H.; Crack, J. C.; Prior, C.; Hutchings, M. I.; Thomson, A. J.; Kamali, S.; Yoda, Y.; Zhao, J.; Hu, M. Y.; Alp, E. E.; Oganesyan, V. S.; Le Brun, N. E.; Cramer, S. P. Nitrosylation of Nitric-oxide-sensing Regulatory Proteins Containing [4Fe-4S] Clusters Gives Rise to Multiple Iron–Nitrosyl Complexes. *Angew. Chem. Int. Ed Engl.* **2016**, *55* (47), 14575–14579. https://doi.org/10.1002/anie.201607033.

(36) Grabarczyk, D. B.; Ash, P. A.; Myers, W. K.; Dodd, E. L.; Vincent, K. A. Dioxygen Controls the Nitrosylation Reactions of a Protein-Bound [4Fe4S] Cluster. *Dalton Trans.* **2019**, *48* (37), 13960–13970. https://doi.org/10.1039/c9dt00924h.

(37) Hagen, K. S.; Reynolds, J. G.; Holm, R. H. Definition of Reaction Sequences Resulting in Self-Assembly of [Fe4S4(SR)4]2- Clusters from Simple Reactants. *J. Am. Chem. Soc.* **1981**, *103* (14), 4054–4063. https://doi.org/10.1021/ja00404a013.

(38) Kimura, H. Hydrogen Sulfide: Its Production, Release and Functions. *Amino Acids* **2011**, *41* (1), 113–121. https://doi.org/10.1007/s00726-010-0510-x.

(39) Pieretti, J. C.; Junho, C. V. C.; Carneiro-Ramos, M. S.; Seabra, A. B. H2S- and NO-Releasing Gasotransmitter Platform: A Crosstalk Signaling Pathway in the Treatment of Acute Kidney Injury. *Pharmacol. Res.* **2020**, *161* (105121), 105121. https://doi.org/10.1016/j.phrs.2020.105121.

(40) Yong, Q.-C.; Hu, L.-F.; Wang, S.; Huang, D.; Bian, J.-S. Hydrogen Sulfide Interacts with Nitric Oxide in the Heart: Possible Involvement of Nitroxyl. *Cardiovasc. Res.* **2010**, *88* (3), 482–491. https://doi.org/10.1093/cvr/cvq248.

(41) Filipovic, M. R.; Ivanovic-Burmazovic, I. The Kinetics and Character of the Intermediates Formed in the Reaction between Sodium Nitroprusside and Hydrogen Sulfide Need Further Clarification. *Chemistry* **2012**, *18* (42), 13538–13540. https://doi.org/10.1002/chem.201103644.

(42) Whiteman, M.; Armstrong, J. S.; Chu, S. H.; Jia-Ling, S.; Wong, B.-S.; Cheung, N. S.; Halliwell, B.; Moore, P. K. The Novel Neuromodulator Hydrogen Sulfide: An Endogenous Peroxynitrite 'Scavenger'? *J. Neurochem.* **2004**, *90* (3), 765–768. https://doi.org/10.1111/j.1471-4159.2004.02617.x.

(43) Cruz-Ramos, H. NO Sensing by FNR: Regulation of the Escherichia Coli NO-Detoxifying Flavohaemoglobin, Hmp. *EMBO J.* **2002**, *21* (13), 3235–3244. https://doi.org/10.1093/emboj/cdf339.

(44) Ding, H.; Demple, B. Direct Nitric Oxide Signal Transduction via Nitrosylation of Iron-Sulfur Centers in the SoxR Transcription Activator. *Proc. Natl. Acad. Sci. U. S. A.* **2000**, *97* (10), 5146–5150. https://doi.org/10.1073/pnas.97.10.5146.

(45) Yukl, E. T.; Elbaz, M. A.; Nakano, M. M.; Moënne-Loccoz, P. Transcription Factor NsrR from *Bacillus Subtilis* Senses Nitric Oxide with a 4Fe−4S Cluster. *Biochemistry* **2008**, *47* (49), 13084–13092. https://doi.org/10.1021/bi801342x.

(46) Tucker, N. P.; Hicks, M. G.; Clarke, T. A.; Crack, J. C.; Chandra, G.; Le Brun, N. E.; Dixon, R.; Hutchings, M. I. The Transcriptional Repressor Protein NsrR Senses Nitric Oxide Directly via a [2Fe-2S] Cluster. *PLoS One* **2008**, *3* (11), e3623. https://doi.org/10.1371/journal.pone.0003623.

(47) Crack, J. C.; Smith, L. J.; Stapleton, M. R.; Peck, J.; Watmough, N. J.; Buttner, M. J.; Buxton, R. S.; Green, J.; Oganesyan, V. S.; Thomson, A. J.; Le Brun, N. E. Mechanistic Insight into the Nitrosylation of the [4Fe−4S] Cluster of WhiB-like Proteins. *J. Am. Chem. Soc.* **2011**, *133* (4), 1112–1121. https://doi.org/10.1021/ja109581t.

(48) Ren, B.; Zhang, N.; Yang, J.; Ding, H. Nitric Oxide-induced Bacteriostasis and Modification of Iron-sulphur Proteins in *Escherichia Coli*. *Mol. Microbiol.* **2008**, *70* (4), 953–964. https://doi.org/10.1111/j.1365-2958.2008.06464.x.

(49) Landry, A. P.; Duan, X.; Huang, H.; Ding, H. Iron–Sulfur Proteins Are the Major Source of Protein-Bound Dinitrosyl Iron Complexes Formed in Escherichia Coli Cells under Nitric Oxide Stress. *Free Radic. Biol. Med.* **2011**, *50* (11), 1582–1590. https://doi.org/10.1016/j.freeradbiomed.2011.03.005.

(50) Drapier, J. C.; Hibbs, J. B., Jr. Murine Cytotoxic Activated Macrophages Inhibit Aconitase in Tumor Cells. Inhibition Involves the Iron-Sulfur Prosthetic Group and Is Reversible. *J. Clin. Invest.* **1986**, *78* (3), 790–797. https://doi.org/10.1172/jci112642.

(51) Drapier, J. C.; Pellat, C.; Henry, Y. Generation of EPR-Detectable Nitrosyl-Iron Complexes in Tumor Target Cells Cocultured with Activated Macrophages. *J. Biol. Chem.* **1991**, *266* (16), 10162–10167. https://doi.org/10.1016/s0021-9258(18)99204-5.

(52) Tran, C. T.; Williard, P. G.; Kim, E. Nitric Oxide Reactivity of [2Fe-2S] Clusters Leading to H_2S Generation. *J. Am. Chem. Soc.* **2014**, *136* (34), 11874–11877. https://doi.org/10.1021/ja505415c.

(53) Tsai, F.-T.; Chiou, S.-J.; Tsai, M.-C.; Tsai, M.-L.; Huang, H.-W.; Chiang, M.-H.; Liaw, W.-F. Dinitrosyl Iron Complexes (DNICs) $[L_2Fe(NO)_2]^-$ (L = Thiolate): Interconversion among $Fe(NO)_2{}^9$ DNICs, $Fe(NO)_2{}^{10}$ DNICs, and [2Fe-2S] Clusters, and the Critical Role of the Thiolate Ligands in Regulating NO Release of DNICs. *Inorg. Chem.* **2005**, *44* (16), 5872–5881. https://doi.org/10.1021/ic0505044.

(54) Li, L.; Rose, P.; Moore, P. K. Hydrogen Sulfide and Cell Signaling. *Annu. Rev. Pharmacol. Toxicol.* **2011**, *51* (1), 169–187. https://doi.org/10.1146/annurev-pharmtox-010510-100505.

(55) Rogers, P. A.; Ding, H. L-Cysteine-Mediated Destabilization of Dinitrosyl Iron Complexes in Proteins. *J. Biol. Chem.* **2001**, *276* (33), 30980–30986. https://doi.org/10.1074/jbc.m101037200.

(56) Grabarczyk, D. B.; Ash, P. A.; Vincent, K. A. Infrared Spectroscopy Provides Insight into the Role of Dioxygen in the Nitrosylation Pathway of a [2Fe2S] Cluster Iron–Sulfur Protein. *J. Am. Chem. Soc.* **2014**, *136* (32), 11236–11239. https://doi.org/10.1021/ja505291j.

(57) Tinberg, C. E.; Tonzetich, Z. J.; Wang, H.; Do, L. H.; Yoda, Y.; Cramer, S. P.; Lippard, S. J. Characterization of Iron Dinitrosyl Species Formed in the Reaction of Nitric Oxide with a Biological Rieske Center. *J. Am. Chem. Soc.* **2010**, *132* (51), 18168–18176. https://doi.org/10.1021/ja106290p.

(58) Haymore, B.; Feltham, R. D.; Morris, B. E.; Clement, R. A. Nitrosyliron,-Cobalt, and-Nickel Iodides. Inorganic Syntheses. **1973**, *14*, 81–89.

(59) Jaworska, M.; Stasicka, Z. Structure and UV-Vis Spectroscopy of the Iron-Sulfur Dinuclear Nitrosyl Complexes [Fe2S2(NO)4]2? And [Fe2(SR)2(NO)4]. *New J Chem* **2005**, *29* (4), 604. https://doi.org/10.1039/b409519g.

Chapte 6 Conversion of [4Fe-4S] to [2Fe-2S] by O₂

6.1 Abstract

Fumarate and nitrate reductase (FNR) is a gene regulatory protein that controls anaerobic to aerobic respiration in Escherichia coli, for which O_2 serves as a control switch to induce a protein structural change by converting [4Fe-4S] cofactors to [2Fe-2S] clusters. Although biomimetic models can aid in understanding the complex functions of their protein counterparts, the inherent sensitivity of discrete [Fe-S] molecules to aerobic conditions poses a unique challenge to mimic the O_2-sensing capability of FNR. Herein, we report unprecedented biomimetic O_2 reactivity of a discrete [4Fe-4S] complex, $[Fe_4S_4(SPh^F)_4]^{2-}$ (**1**) where SPh^F is 4-fluorothiophenolate, in which the reaction of 1 with $O_2(g)$ in the presence of thiolate produces its [2Fe-2S] analogue, $[Fe_2S_2(SPh^F)_4]^{2-}$ (**2**), at room temperature. The cluster conversion of **1** to **2** can also be achieved by employing H_2O_2 as an oxidant under the same reaction conditions. This chapter presents collaborative work, with significant contributions made by Kady Marisa Oakley, showcasing a shared effort in the research and findings documented herein.

6.2 Introduction

Iron-sulfur ([Fe-S]) cofactors are ubiquitous in biology and are known for several functions, one of which is the ability to change its nuclearity in response to the environment.[1,2] In Escherichia coli, conversion of [4Fe-4S] to [2Fe-2S] is utilized for gene regulation by fumarate and nitrate reductase (FNR). FNR is an O_2 sensor and a transcriptional regulator acting as the control switch from anaerobic to aerobic metabolism. As described in Chapter 1, conversion of the [4Fe-4S] into a [2Fe-2S] cluster by O_2 induces a protein conformational change from a DNA-binding dimer into two non-DNA binding monomers.[1-4] After FNR is released from DNA, >300 genes encoding for aerobic metabolism are able to be expressed.[5,6] Upon further O_2 exposure, [2Fe-2S] has been shown to decompose leaving apoFNR which can import a newly biosynthesized [4Fe-4S] cluster.[7,8] However, it has been recognized that a direct repair from [2Fe-2S]-FNR to [4Fe-4S]-FNR is also possible. While the exact nature of the [2Fe-2S]-FNR remains unknown, biochemical and spectroscopic studies suggest that all four, or three, of the original bridging sulfides from [4Fe-4S] retain in the form of [2Fe-2S]-bound cysteine persulfides, and the [4Fe-4S] cluster can be repaired from [2Fe-2S] cluster in the presence of Fe^{2+} and dithiothreitol (DTT) as a reductant, without adding additional sulfide (Scheme 6.1).[9-11]
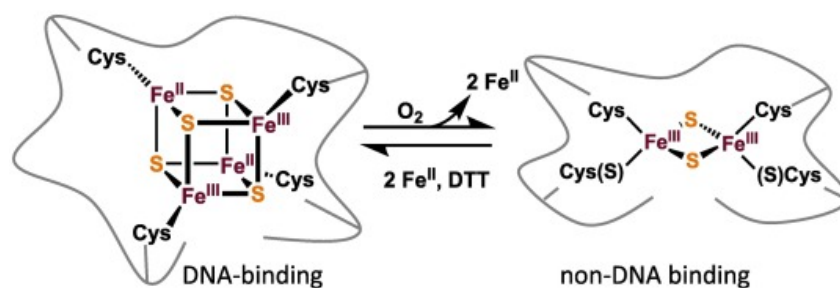
Scheme 6.1 [4Fe-4S] to [2Fe-2S] cluster transformation by O_2 in FNR.[12]

Synthetic modeling of FNR's cluster conversion by O_2 is a difficult task because most [Fe-S] clusters decompose in aerobic conditions.[13] Outside of a protein environment, [4Fe-4S] to [2Fe-2S] cluster conversion has been shown only twice. The first example came from Holm and coworkers using an outer sphere oxidant, ferricenium, to convert model cluster $[Fe_4S_4Cl_4]^{2-}$ to $[Fe_2S_2Cl_2]^{2-}$ (Scheme 6.2A).[14] More recently, Tatsumi and coworkers converted the highly oxidized all ferric [4Fe-4S] amide bound cluster to [2Fe-2S] in the presence of pyridine as a ligand source (Scheme 9.2B).[15] While both models achieved cluster conversion, they lack biologically relevant oxidants and cluster ligands. Herein, we report [4Fe-4S] to [2Fe-2S] cluster conversion with a thiolate ligated [4Fe-4S] model complex using model complex using O_2 or disulfide as oxidants.

6.3 Results and Discussion

6.3.1 Cluster Conversion by O_2

One of the differences between [Fe-S] containing proteins and small molecule [Fe-S] clusters is the presence and absence of the protected coordination environment for the [Fe-S] core. In FNR, the same cysteine residues harboring a [4Fe-4S] cluster are re-used to hold [2Fe-2S] cluster after the O_2 reaction (Scheme 6.1), which is difficult to imitate with simple model complexes. We thought providing extra thiolate ligands available for [2Fe-2S], a presumed product from [4Fe-4S]/O_2, may help overcome this challenge. Accordingly, we investigated on the effect of external thiolate in O_2 reactivity of [4Fe-4S] with a known[16] model cluster, $[Et_4N]_2[Fe_4S_4(SPh^F)_4]$ ($[Et_4N]_2 \cdot \mathbf{1}$) by UV–Vis spectroscopy. In the absence of thiolate, the $\mathbf{1}/O_2$ reaction resulted in decrease of the characteristic absorption band of $\mathbf{1}$ at 450 nm followed by the production of an

insoluble black precipitate, FeS, suggesting complete decomposition of **1** (Figure 6.1A). However, when **1** was reacted with O_2 in the presence of excess (~50 equivalents) thiol and base, 4-fluorothiophenol and 1,8-diazabicyclo[5.4.0]undec-7-ene (DBU), the solution noticeably turned from brown to purple indicating [2Fe-2S] cluster formation. Within 10 min of O_2 exposure, the charge transfer band at ~450 nm from **1** shifted to ~480 nm characteristic of $[Fe_2S_2(SPh^F)_4]^{2-}$ (**2**) (Figure 6.1B).[17]
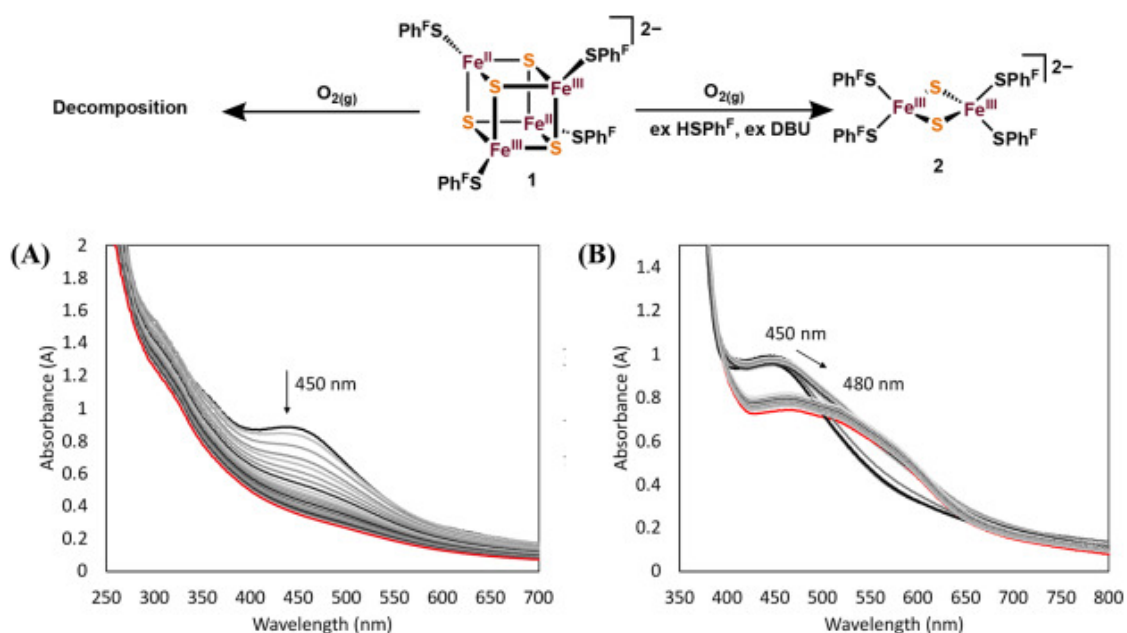
Figure 6.1 UV–Vis spectra of $[Fe_4S_4(SPh^F)_4]^{2-}$ (**1**) upon exposure to O_2 in absence (A) and presence (B) of excess (50 equiv) of thiol and base at room temperature in MeCN over 10 min.

To further characterize the products obtained from **1**/O_2 in the presence of thiolate, ^{1}H NMR spectroscopy was employed following a reaction in a synthetic scale. After combining $[Et_4N]_2$•**1** (0.013 mmol, 1 equiv) with $HSPh^F$ (10 equiv) and DBU (10 equiv) in MeCN, excess $O_{2(g)}$ was bubbled through the reaction mixture and allowed to react for 30 s at room temperature

160

before removing all volatiles. Consistent with UV–Vis monitoring, the NMR spectrum of the crude product showed $[Fe_2S_2(SPh^F)_4]^{2-}$ (**2**) as the major product displaying well-resolved m-H and o-H resonances of the -SPh^F ligand (Figure 6.2). The peak integration of the m-H resonance at 8.9 ppm relative to the tetraethylammonium counter cation indicates that **1** was converted to **2** in ~124% yield (0.016 mmol, 1.2 equiv), indicating the protonated DBU must serve as an additional counter cation in solution. The NMR spectrum also shows minor paramagnetic Fe-containing side products with signals at 36.3 ppm and 22.7 ppm which correspond to the m-H signals of a linear [3Fe-4S] cluster, $[Fe_3S_4(SPh^F)_4]^{3-}$, and a mononuclear Fe compound, $[Fe(SPh^F)_4]^{2-}$ (**3**), respectively. Recrystallization of the crude products from acetonitrile and diethyl ether led to the isolation of $[Et_4N]_2\cdot\textbf{2}$ as a dark purplish black powder in 94% yield (0.013 mmol, 0.9 equiv).[18] In biological studies with FNR, ~60% conversion of [4Fe-4S] to [2Fe-2S] was reported upon O_2 exposure.[3] Our results show that the biomimetic cluster conversion by O_2 is possible with a small synthetic model. However, the synthetic system requires extra thiolate to stabilize the resulting [2Fe-2S] cluster, different from the protein where the cysteine residues are pre-positioned to harbor a [2Fe-2S] cluster after the O_2 reaction.
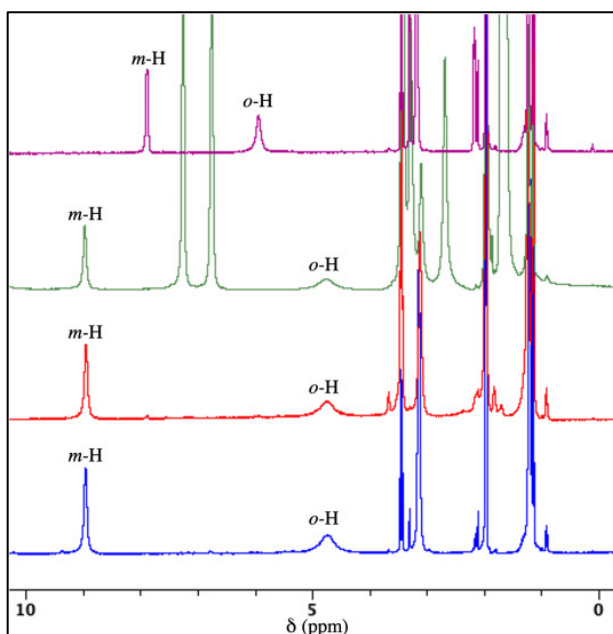
Figure 6.2 ^{1}H NMR (CD$_3$CN, rt., 400 MHz) of [Fe$_4$S$_4$(SPh^F)$_4$]$^{2-}$ (**1**) (purple, top); the in situ reaction product from **1**/O$_2$/thiol/base (green, upper middle), where peaks with * are from external thiolate; the purified reaction product from **1**/O$_2$/thiol/base (red, lower middle); authentic [Fe$_2$S$_2$(SPh^F)$_4$]$^{2-}$ (**2**) (blue, bottom).

6.3.2 Cluster Conversion by H$_2$O$_2$

The reaction between [Fe$_4$S$_4$(SPh^F)$_4$]$^{2-}$ (**1**) and O$_2$ is expected to produce reduced oxygen species such as superoxide (O$_2^-$), H$_2$O$_2$, or water. Although we were not able to detect such species from our reactions, we examined the reactivity of **1** with H$_2$O$_2$ to gain further chemical insights. We found that the overall reactivity of **1** with H$_2$O$_2$ was analogous to what was observed with **1**/O$_2$. In the absence of thiolate, H$_2$O$_2$ gradually decomposed **1** to an insoluble black precipitate. However, in the presence of HSPh^F (10 equiv) and DBU (10 equiv), the reaction between **1** and H$_2$O$_2$ (1 equiv) produced the same reaction products as those from **1**/O$_2$, in which

$[Fe_4S_4(SPh^F)_4]^{2-}$ (**2**) was observed as the main product along with $[Fe(SPh^F)_4]^{2-}$ (**3**) and $[Fe_3S_4(SPh^F)_4]^{3-}$ as side products.

6.3.3 Cluster Conversion by Disulfide

Given the cluster conversion seen with O_2 only when extra thiol and base are present, we next examined whether the cluster conversion was the result from direct reaction between **1** and O_2 or from the reaction between **1** and a secondary oxidation product such as disulfide derived from thiol/O_2. Disulfide is a biologically prevalent oxidant whose concentration depends on the cellular compartments and oxidative conditions.[17] Since the breakdown of a [4Fe-4S] cluster into [2Fe-2S] clusters requires a *net* two-electron oxidation ($[Fe_4S_4]^{2+} \rightarrow 2 \ [Fe_2S_2]^{2+} + 2 \ e^-$), we first examined the reaction between **1** and 1–50 equiv. of $(SPh^F)_2$ over several days. The results showed that disulfide alone was unreactive towards **1**. However, similar to **1**/O_2 reactivity, the presence of thiolate changes the reactivity pattern and enables disulfide to become a sufficient oxidant to induce a cluster conversion. After combining **1** (0.024 mmol, 1 equiv) with disulfide (1 equiv), thiol (2 equiv), and DBU (4 equiv) for 48 h in MeCN at room temperature, we observed all of **1** was consumed with a concomitant formation of the corresponding [2Fe-2S] cluster, $[Fe_2S_2(SPh^F)_4]^{2-}$ (**2**) in 40% yield (0.019 mmol, 0.8 equiv) by ^{1}H NMR, where the yield was calculated based on a hypothetical stoichiometric reaction following Eq.(1). Upon recrystallization of the product mixture from acetonitrile and diethyl ether at -35 °C, $[Et_4N]_2\cdot$**2** was isolated in 35% yield (0.017 mol, 0.7 equiv).

$$[Fe_4S_4(SPh^F)_4]^{2-} \ (\textbf{1}) + 2 \ Ph^FS^- + (SPh^F)_2 \rightarrow 2 \ [Fe_2S_2(SPh^F)_4]^{2-} \ (\textbf{2}). \tag{1}$$

In attempts to improve the overall [2Fe-2S] cluster yield, we increased the equivalents of thiol and disulfide to four and two respectively, which roughly doubled the amount of compound **2** produced (~75%) (Table 6.1, entry 2). Interestingly, a noticeable amount (0.8 equiv) of an unexpected Fe^{II}-containing byproduct, $[Fe(SPh^F)_4]^{2-}$ (**3**), was observed upon increasing the amounts of thiolate and disulfide. The formation of **3** suggests that the conversion of **1** into **2** by disulfide cannot be accomplished by a single step as is written in Eq. (1) because Fe^{II} cannot be generated if direct oxidation of **1** by disulfide took place. Since the bridging sulfide (S^{2-}) was the only other remaining redox-accessible entity in the reaction mixture, we next investigated on the fate of the bridging sulfide by carrying out the reaction of **1** (0.012 mmol, 1 equiv) with $HSPh^F$ (4 equiv), DBU (5 equiv), and $(SPh^F)_2$ (2 equiv) in the presence of 4 equiv. of sulfur atom acceptor, PPh_3, to sequester and quantify the amount of elemental sulfur (S_x) produced. ^{31}P NMR analysis showed that the reaction generated 1.5 equiv. (0.018 mmol) of S_x which was trapped as triphenylphosphinesulfide, $S=PPh_3$. Additionally, we were able to observe significant amounts of **3** (0.02 mmol, 1.8 equiv) and reduced amounts of **2** (0.004 mmol, 0.3 equiv) by ^1H NMR spectroscopy. Based on these data we propose that the conversion of [4Fe-4S] to [2Fe-2S] by disulfide first proceed following Eq. (2) in which the redox reaction takes place with the bridging sulfide to yield the first equivalent of **2**, along with elemental sulfur (S_x) and **3**. In the absence of PPh_3, the latter two products, **3** and S_x, can further react to produce the second equivalent of **2** following Eq. (3).[18-20] Combining these two steps, Eqs. (2), (3), would result in a net [4Fe-4S] to [2Fe-2S] cluster conversion as we initially hypothesized in Eq. (1).

$[Fe_4S_4(SPh^F)_4]^{2-}$ (**1**) + 2 $(SPh^F)_2$ + 4 Ph^FS^- → 2 $[Fe_2S_2(SPh^F)_4]^{2-}$ (**2**) + 2$[Fe(SPh^F)_4]^{2-}$ (**3**)+ 2 S_x (2)

$$2 \, [Fe(SPh^F)_4]^{2-} \, (\textbf{3}) + 2 \, S_x \rightarrow 2 \, [Fe_2S_2(SPh^F)_4]^{2-} \, (\textbf{2}) + (SPh^F)_2 + 2 \, Ph^FS^- \qquad (3)$$
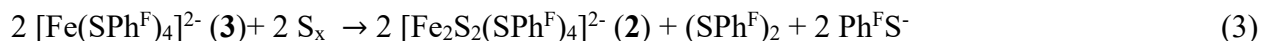
Entry	HSPh^F	(Ph^{F}S)$_2$	[Fe$_2$S$_2$(SR)$_4$]$^{2-}$ (2)
	equiv	equiv	yield[a]
1	2	1	40%
2	4	2	75%
3	–	2	0%
4	4	–	0%

Table 6.1 Conversion of [Fe$_4$S$_4$(SPh^F)$_4$]$^{2-}$ (**1**) to [Fe$_2$S$_2$(SPh^F)$_4$]$^{2-}$ (**2**) in the presence of disulfide, thiol, and base. [a] Based on ^{1}H NMR spectroscopy. Generation of 2 equiv. of **2** is considered 100% following Eq. (1).

6.4 Conclusion

The current studies show that both O$_2$ and disulfide are potent oxidants to induce a biomimetic [4Fe-4S] to [2Fe-2S] conversion for which the presence of extra thiolate plays an important role. However, drastically different reaction kinetics (30 s vs 48 h) suggest that the cluster conversion by O$_2$ and disulfide must operate by a different mechanism. O$_2$ can directly react with a [4Fe-4S] cluster with or without thiolate but the external thiolate can aid the formation of [2Fe-2S] cluster for a synthetic compound. In contrast, the lack of reactivity of the [4Fe-4S] cluster with thiolate or disulfide alone (Table 6.1, entries 3&4) indicates cluster conversion can only be achieved in combination of thiolate and disulfide. We conjecture that a transient binding of thiolate to **1**, although unfavorable, may be needed to shift the redox potential of **1** to initiate the oxidative cluster conversion by disulfide. Although the [4Fe-4S] to [2Fe-2S] cluster conversion by disulfide is slow, this reaction may imply how solvent exposed [4Fe-4S] clusters can be disrupted by the

cellular thiol homeostasis (e.g., the ratio between reduced and oxidized glutathione, GSH: GSSG) resulted from the oxidative environment.[21,22] To the best of our knowledge, this work is the first example of synthetic [4Fe-4S] cluster conversion to [2Fe-2S] using O_2. This study also shows how a mild oxidant, such as disulfide, can induce cluster conversion in the presence of thiolate.

6.5 Experimental Section

General Considerations. All synthesized products were assumed to be air- and moisture-sensitive. They were manipulated under argon on a standard Schlenk line or in an atmosphere of purified nitrogen in an MBraun Labmaster SP glovebox (O_2 < 1 ppm; H_2O < 1 ppm). Solvents were purified by passing through a series of two activated alumina columns (MBraun solvent purification system) under an Ar atmosphere and stored over 4 Å molecular sieves. Reagents 4-fluorothiophenol, bis-4- fluorodisulfide, 1,8-diazabicyclo[5.4.0]undec-7-ene (DBU) were purchased from Sigma at the highest available purity and used as received. $O_2(g)$ (100%) was purchased from Airgas, Inc. and used as received. UV-Vis spectra were recorded on a Varian Cary 50 Bio spectrometer. NMR spectra were recorded at 400 MHz on a Bruker UltraShield spectrometer and residual solvent signals were used as an internal reference. Synthesis of authentic $(Et_4N)_2[Fe_4S_4(SPh^F)_4]$ (**1**) and $(Et_4N)_2[Fe_2S_2(SPh^F)_4]$ (**2**) were prepared as described in literature.[1]

UV-vis monitoring of $(Et_4N)_2[Fe_4S_4(SPh^F)_4]$ + $O_2(g)$ in the presence and absence of thiol/base. $(Et_4N)_2[Fe_4S_4(SPh^F)_4]$ (2 mM) in MeCN was placed in a 1 cm Schlenk cuvette. 4-fluorothiophenol (10 μL, 0.09 mmol, ~50 equiv) and DBU (14 μL, 0.09 mmol, ~50 equiv) were injected into the reaction mixture before injecting 1 mL of $O_2(g)$ via syringe and quickly shaking to then take UV-vis spectra every minute for 20 minutes. The experimented was repeated under

the same conditions but without adding thiol/base, immediately producing insoluble black solid upon O_2 addition.

Reaction of $(Et_4N)_2[Fe_4S_4(SPh^F)_4]$ + $O_2(g)$ in presence of thiol and base. $(Et_4N)_2[Fe_4S_4(SPh^F)_4]$ (15 mg, 0.013 mmol, 1 equiv) was dissolved in 4 mL MeCN and combined with 4-fluorothiophenol (14 µL, 0.13 mmol, 10 equiv) and DBU (17 µL, 0.11 mmol, ~10 equiv) in a 10 mL Schlenk flask sealed under nitrogen. Excess $O_2(g)$ (1 mL) was bubbled through the reaction mixture and allowed to react for 30 seconds, noticeably turning the solution from brown to purple, before placing under vacuum to remove O_2 and all volatiles. 1 H NMR (CD3CN, rt, 400 MHz) spectroscopy of crude reaction mixture identified all the starting [4Fe-4S] was consumed producing [2Fe-2S] as the main product and Fe^{II}-tetrathiolate and linear [3Fe-4S] as minor products. The reaction mixture was redissolved in 4 mL MeCN, filtered, and brought up in 10 mL ether in the -35ºC freezer overnight to produce a dark purplish black powder that was collected by frit and identified as $(Et_4N)_2[Fe_2S_2(SPh^F)_4]$ (2) by ^{1}H NMR (CD_3CN, rt, 400 MHz) (12 mg, 0.013 mmol, 47%).

Reaction of [4Fe-4S] with 2 equiv thiol and 1 equiv disulfide. $(Et_4N)_2[Fe_4S_4(SPh^F)_4]$ (27 mg, 0.024 mmol, 1 equiv) was dissolved in 6 mL MeCN and combined with a 2 mL MeCN solution containing DBU (15 µL, 0.10 mmol, ~ 4equiv), 4-fluorothiophenol (5 µL, 0.047 mmol, 2 equiv), and bis(4-fluorophenyl)disulfide (6 µL, 0.024 mmol, 1 equiv) in a Schlenk flask. The reaction was allowed to stir for 48 hours at room temperature under Ar(g). The solution was dried in vacuo and redissolved in 4 mL MeCN and layered with 10 mL ether in the -35 ºC freezer overnight to produce a dark purplish black solid identified as $(Et_4N)_2[Fe_2S_2(SPh^F)_4]$ by ^{1}H NMR (CD_3CN, rt, 400 MHz) (16 mg, 0.017 mmol, 35%).

Reaction of [4Fe-4S] with 4 equiv thiol and 2 equiv disulfide. $(Et_4N)_2[Fe_4S_4(SPh^F)_4]$ (27 mg, 0.024 mmol, 1 equiv) was dissolved in 6 mL MeCN and combined with a 2 mL MeCN solution containing DBU (20 µL, 0.13 mmol, ~6 equiv), 4-fluorothiophenol (10 µL, 0.094 mmol, 4 equiv), and bis(4-fluorophenyl)disulfide (12 µL, 0.047 mmol, 2 equiv) in a Schlenk flask. The reaction was allowed to stir for 48 hours at room temperature under Ar(g). The 1 H NMR integration of the m-H resonance of $[Fe_4S_4(SPh^F)_4]^{2-}$ relative to tetraethylammonium counter cation indicates that 1 generated about ~0.036 mmol (1.75 equiv) of $[Fe_4S_4(SPh^F)_4]^{2-}$ (**2**), indicating **2** must be counterbalance by $[Et_4N]^+$ and $[HDBU]^+$ in solution. However, we were not able to isolate the presumed [HDBU]$_2$•**2**. The only isolable product after recrystallization was quantitative amount of [Et$_4$N]$_2$•**2**.

Control reactions of [4Fe-4S] with thiol and disulfide. $(Et_4N)_2[Fe_4S_4(SPh^F)_4]$ (27 mg, 0.024 mmol, 1 equiv) was combined with either 4-fluorothiophenol (10 µL, 0.094 mmol, 4 equiv), or bis(4-fluorophenyl)disulfide (12 µL, 0.047 mmol, 2 equiv) in 4 mL MeCN in a Schlenk flask and allowed to stir for 48 hours at room temperature under Ar(g). The solution was dried in vacuo and crude ^{1}H NMR (CD$_3$CN, rt, 400 MHz) spectra were taken showing no reaction occurred.

Reaction of $(Et_4N)_2[Fe_4S_4(SPh^F)_4]$ + H_2O_2 in presence of thiol and base: $(Et_4N)_2[Fe_4S_4(SPh^F)_4]$ (15 mg, 0.013 mmol, 1 equiv) was dissolved in 4 mL MeCN and combined with 4-fluorothiophenol (14 µL, 0.13 mmol, 10 equiv) and DBU (17 µL, 0.11 mmol, ~10 equiv) in a 10 mL Schlenk flask sealed under nitrogen. H_2O_2 (30 % (w/w) in H_2O, 0.013 mmol, 1 equiv) was then added into the reaction mixture and allowed to react at room temperature for 30 min under Ar(g), during which the solution turning from brown to purple. All volatiles were removed under vacuum for further characterization. ^{1}H NMR (CD$_3$CN, rt, 400 MHz) spectroscopy of crude

reaction mixture identified all the starting [4Fe-4S] was consumed producing [2Fe-2S] as the main product and Fe^{II}-tetrathiolate and linear [3Fe-4S] as minor products (Figure S4). The peak integration of the [2Fe-2S] m-H resonance at 8.9 ppm relative to the tetraethylammonium counter cation indicates that **1** was converted to **2** in ~132% yield (0.017 mmol, 1.3 equiv), indicating the protonated DBU must serve as an additional counter cation in solution.

Reaction of $(Et_4N)_2[Fe_4S_4(SPh^F)_4]$ + H_2O_2 in the absance of thiol and base: $(Et_4N)_2[Fe_4S_4(SPh^F)_4]$ (15 mg, 0.013 mmol, 1 equiv) was dissolved in 4 mL MeCN and combined with H_2O_2 (30 % (w/w) in H_2O, 0.013 mmol, 1 equiv). The reaction mixture was allowed to stir for 30 min at room temperature under Ar(g), during which the production of an insoluble black precipitate was observed, suggesting complete decomposition of **1**. The solution was dried in vacuo and crude ^1H NMR (CD^3CN, rt, 400 MHz) spectra were taken showing 18% cluster decomposition and no [2Fe-2S] formed (Figure S5). Further addition of excess H_2O_2 (~10 equiv) will lead to completely decomposition of **1**.

Control reactions of H_2O_2 react thiol and base: 4-fluorothiophenol (14 μL, 0.13 mmol, 10 equiv) was combined with DBU (17 μL, 0.11 mmol, ~10 equiv) in 4 mL MeCN in a Schlenk flask, and H_2O_2 (30 % (w/w) in H_2O, 0.013 mmol, 1 equiv) was added into the reaction mixture. The reaction was allowed to stir for 30 min at room temperature under Ar(g). The solution was dried in vacuo and crude ^1H NMR (CD_3CN, rt, 400 MHz) spectra were taken showing 3% of 4-fluorothiophenol was converted to corresponding disulfide.

6.6 References

(1) Crack, J. C.; Le Brun, N. E. Redox-Sensing Iron-Sulfur Cluster Regulators, Antioxid. *Antioxid. Redox Signal* **2018**, *29*, 1809–1829.

(2) Kiley, P. J.; Beinert, H. The Role of Fe-S Proteins in Sensing and Regulation in Bacteria. *Curr. Opin. Microbiol.* **2003**, *6* (2), 181–185. https://doi.org/10.1016/s1369-5274(03)00039-0.

(3) Khoroshilova, N.; Popescu, C.; Münck, E.; Beinert, H.; Kiley, P. J. Iron-Sulfur Cluster Disassembly in the FNR Protein of Escherichia Coli by O2: [4Fe-4S] to [2Fe-2S] Conversion with Loss of Biological Activity. *Proc. Natl. Acad. Sci. U. S. A.* **1997**, *94* (12), 6087–6092. https://doi.org/10.1073/pnas.94.12.6087.

(4) Crack, J. C.; Green, J.; Thomson, A. J.; Brun, N. E. L. Iron–Sulfur Clusters as Biological Sensors: The Chemistry of Reactions with Molecular Oxygen and Nitric Oxide. *Acc. Chem. Res.* **2014**, *47* (10), 3196–3205. https://doi.org/10.1021/ar5002507.

(5) Popescu, C. V.; Bates, D. M.; Beinert, H.; Münck, E.; Kiley, P. J. Mössbauer Spectroscopy as a Tool for the Study of Activation/Inactivation of the Transcription Regulator FNR in Whole Cells of Escherichia Coli. *Proceedings of the National Academy of Sciences* **1998**, *95* (23), 13431–13435.

(6) Sutton, V. R.; Mettert, E. L.; Beinert, H.; Kiley, P. J. Kinetic Analysis of the Oxidative Conversion of the 2+ Cluster of FNR to a 2+ Cluster. *Journal of Bacteriology* **2004**, *186* (23), 8018–8025.

(7) Achebach, S.; Tran, Q. H.; Vlamis-Gardikas, A.; Müllner, M.; Holmgren, A.; Unden, G. Stimulation of Fe-S Cluster Insertion into ApoFNR by Escherichia Coli Glutaredoxins 1, 2 and 3 in Vitro. *FEBS Lett.* **2004**, *565* (1–3), 203–206. https://doi.org/10.1016/j.febslet.2004.04.007.

(8) Achebach, S.; Selmer, T.; Unden, G. Properties and Significance of ApoFNR as a Second Form of Air-Inactivated [4Fe-4S]• FNR of Escherichia Coli. *The FEBS journal* **2005**, *272* (16), 4260–4269.

(9) Crack, J. C.; Green, J.; Cheesman, M. R.; Le Brun, N. E.; Thomson, A. J. Superoxide-Mediated Amplification of the Oxygen-Induced Switch from [4Fe-4S] to [2Fe-2S] Clusters in the Transcriptional Regulator FNR. *Proc. Natl. Acad. Sci. U. S. A.* **2007**, *104* (7), 2092–2097. https://doi.org/10.1073/pnas.0609514104.

(10) Crack, J. C.; Gaskell, A. A.; Green, J.; Cheesman, M. R.; Le Brun, N. E.; Thomson, A. J. Influence of the Environment on the 2+ to 2+ Cluster Switch in the Transcriptional Regulator FNR. *Transcriptional Regulator FNR. Journal of the American Chemical Society* **2008**, *130* (5), 1749–1758.

(11) Zhang, B.; Crack, J. C.; Subramanian, S.; Green, J.; Thomson, A. J.; Le Brun, N. E.; Johnson, M. K. Reversible Cycling between Cysteine Persulfide-Ligated [2Fe-2S] and Cysteine-Ligated [4Fe-4S] Clusters in the FNR Regulatory Protein. *Proc. Natl. Acad. Sci. U. S. A.* **2012**, *109* (39), 15734–15739. https://doi.org/10.1073/pnas.1208787109.

(12) Oakley, K. M.; Lehane, R. L.; Zhao, Z.; Kim, E. Dioxygen Reactivity of a Biomimetic [4Fe-4S] Compound Exhibits [4Fe-4S] to [2Fe-2S] Cluster Conversion. *J. Inorg. Biochem.* **2022**, *228* (111714), 111714. https://doi.org/10.1016/j.jinorgbio.2022.111714.

(13) Lo, W.; Scott, T. A.; Zhang, P.; Ling, C. C.; Holm, R. H. Stabilities of Cubane Type [Fe4S4 (SR) 4] 2− Clusters in Partially Aqueous Media. *Journal of inorganic biochemistry* **2011**, *105* (4), 497–508.

(14) Wong, G. B.; Bobrik, M. A.; Holm, R. H. Inorganic Derivatives of Iron Sulfide Thiolate Dimers and Tetramers: Synthesis and Properties of the Halide Series [Fe2S2X4] 2-and [Fe4S4X4] 2-(X= Chlorine, Bromine, Iodine). *Inorganic Chemistry* **1978**, *17* (3), 578–584.

(15) Tanifuji, K.; Yamada, N.; Tajima, T.; Sasamori, T.; Tokitoh, N.; Matsuo, T.; Tamao, K.; Ohki, Y.; Tatsumi, K. A Convenient Route to Synthetic Analogues of the Oxidized Form of High-Potential Iron–Sulfur Proteins. *Inorg. Chem.* **2014**, *53* (8), 4000–4009. https://doi.org/10.1021/ic402890k.

(16) Mascharak, P. K.; Smith, M. C.; Armstrong, W. H.; Burgess, B. K.; Holm, R. H. Fluorine-19 Chemical Shifts as Structural Probes of Metal-Sulfur Clusters and the Cofactor of Nitrogenase. *Proc. Natl. Acad. Sci. U. S. A.* **1982**, *79* (22), 7056–7060. https://doi.org/10.1073/pnas.79.22.7056.

(17) Kemp, M.; Go, Y.-M.; Jones, D. P. Nonequilibrium Thermodynamics of Thiol/Disulfide Redox Systems: A Perspective on Redox Systems Biology. *Free Radic. Biol. Med.* **2008**, *44* (6), 921–937. https://doi.org/10.1016/j.freeradbiomed.2007.11.008.

(18) Venkateswara Rao, P.; Holm, R. H. Synthetic Analogues of the Active Sites of Iron−Sulfur Proteins. *Chem. Rev.* **2004**, *104* (2), 527–560. https://doi.org/10.1021/cr020615+.

(19) Hagen, K. S.; Holm, R. H. Systematic Iron (II)-Thiolate Chemistry: Synthetic Entry to Trinuclear Complexes. *Journal of the American Chemical Society* **1982**, *104* (20), 5496–5497.

(20) Han, S.; Czernuszewicz, R. S.; Spiro, T. G. Convenient Synthetic Route to [Fe2S2 (SR) 4] 2-via Reaction of [Fe (SR) 4]-with Sulfur. *Inorganic Chemistry* **1986**, *25* (13), 2276–2277.

(21) Dickinson, D. A.; Forman, H. J. Cellular Glutathione and Thiols Metabolism. *Biochem. Pharmacol.* **2002**, *64* (5–6), 1019–1026. https://doi.org/10.1016/s0006-2952(02)01172-3.

(22) Aquilano, K.; Baldelli, S.; Ciriolo, M. R. Glutathione: New Roles in Redox Signaling for an Old Antioxidant. *Front. Pharmacol.* **2014**, *5*. https://doi.org/10.3389/fphar.2014.00196.

Chapte 7 Binuclear µ-oxo Mo(V) catalyzed sulfur atom transfer reaction

7.1 Abstract

Catalytic sulfur atom transfer (SAT) chemistry has shown its usefulness to industrial processes such as isothiocyanate synthesis. However, unlike oxygen atom transfer, sulfur atom transfer systems are rare and catalytic systems highly prized. While SAT chemistry has been previously studied, more detailed mechanistic studies is still necessary. A series of μ-oxo Mo(V) thiosemicarbazone complexes **1** were synthesized with various substituents at the para-phenyl position in order to study the correlation between electronic structure and SAT catalytic mechanism. The addition of electron withdrawing nitro or bromo groups significantly increased the turnover compared to the electron donating methoxy group. This trend led to proposal of a catalytic mechanism like pervious reported similar oxygen atom transfer that contains a $[Mo^{VI}(O)(E)]^{2+}$ (E =O, S) intermediate. Efforts to synthesize the active intermediate led to the isolation of $[Mo^{IV}(O)]^{2+}$ and $[Mo^{VI}(O)(S)]^{2+}$ species.

7.2 Introduction

Biological and synthetic chalcogen atom transfer systems have been widely studied due to its practicality in chemical synthesis and industrial processes. While oxygen atom transfer has been most well-defined,[1-3] sulfur atom transfer (SAT) reactions have recently garnered more attention for its applicability in fossil fuel desulfurization,[4-14] elemental sulfur activation[15-19] and isothiocyanate synthesis.[20-24] Despite various accounts of sulfur atom transfer, this reactivity remains rare in comparison to the numerous examples of OAT. In addition, catalytic reactivity is even more uncommon and has only been reported with a handful of cases.

While catalytic SAT has been observed with transition metal systems that are rhodium[15], rhenium-based[25], most of the reported catalysts were monomeric molybdenum or tungsten-based. [16,19,23,24,26,27] Adam and coworkers demonstrated catalytic elemental sulfur activation and isothiocyanate synthesis by $Mo(O)(dtc)_2$ but the reactivity required heated conditions to proceed (Figure 7.1).[23] Moreover, this reaction condition was incompatible for substrates containing hydroxy, ester and acetal functional groups. As isothiocyanates serve as building blocks for synthesis of more complex molecules, it is important for this reactivity is able to encompass an assortment of functional groups. Following their reactivity, Sita and coworkers observed similar SAT reactivity with a Mo(II/IV) system (Figure 8.1) that did not require heated conditions but the turnover was low over long reaction times.[24] Beside sulfur atom transfer from elemental sulfur to isocyanides, propylene sulfide and triphenylphosphine are two other common substrates that are used to present this chemistry. Young and coworkers have demonstrated SAT between these two substrates with both a monomeric and a non-redox active dimeric tungsten catalyst (Figure 8.1).[26, 27]
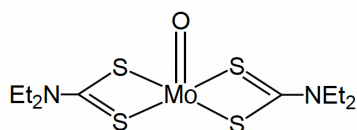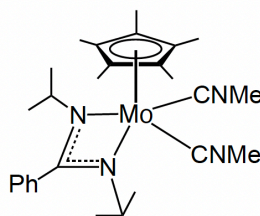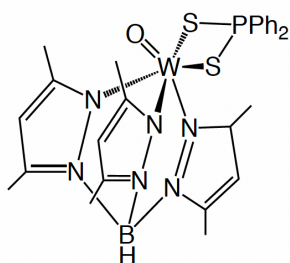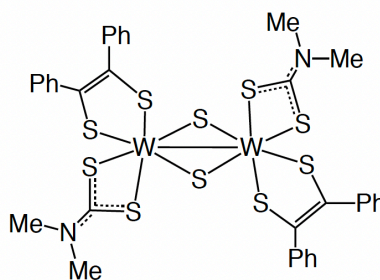
Figure 7.1 Structures of molybdenum and tungsten-based catalytic sulfur atom transfer complexes.

Although there are a handful of successful catalytic systems, there has not been detailed studies on how the electronic properties can affect the rate of sulfur atom transfer. Our group has recently published on the SAT ability of a Mo(V) thiosemicarbazone dimer (**1^Br**). In comparison to its predecessors, the dimeric Mo catalysts exhibited faster turnover rates at mild conditions but the mechanism has not been investigated. In this context, the modular thiosemicarbazone ligand of **1** makes it a good candidate for mechanistic studies as electron withdrawing groups (EWGs) or electron donation groups (EDG)s can be easily added to the ligand system and subsequently affect the electronic properties of **1**.

7.3 Results and Discussion

7.3.1 Synthesis of µ-oxo binuclear Mo(V) complexes.

In order to gain insight on the catalytic mechanism of sulfur atom transfer, a series of Mo(V) thiosemicarbazone dimer $Mo_2O_3(L^R)_2(THF)_2$ (**1**) was synthesized with a range of EDG and EWG at the para-phenyl position. All variants of **1** were synthesized by reacting polymer-supported triphenylphosphine with the respective $Mo(O)_2L^RMeOH$ (**2**) in THF (Scheme 7.1). The polymer-supported triphenylphosphine oxide byproduct was removed by filtration of the solid resin. Complex **2** and all corresponding ligands were synthesized following reported procedure.[41] The only exception was H_2L^{OMe} and **2^{OMe}** which were not directly reported but the synthetic method remains unchanged to the other versions of complex **2**.
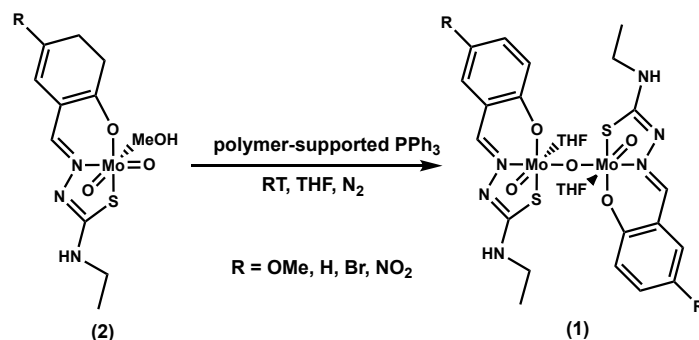
Scheme 7.1 Synthetic scheme for complex **1**.

Complexes **1** were characterized by IR, UV-Vis and NMR spectroscopy. IR spectra revealed a strong vibrational feature in all **1^R** variants at 965−975 cm^{-1}, which is assigned to the $\nu(Mo=O)$ band and closely resemble those of previously reported for µ-oxo $[Mo_2O_3]^{4+}$ related complexes.[42-46] Electronic spectra of **1^R** complexes in acetone display two LMCT bands in the region 347-415

nm and 450-468 nm respectively (Figure 7.10). The slightly change in λ within the both sets may due to the different electron-capacity of the substituent on the ligand para-position, which indicates that the electronic properties of the remote EDG and EWG are transmitted through to the Mo(V) core. The ^{1}H NMR spectra of 1^R complexes are consistent with their compositions.
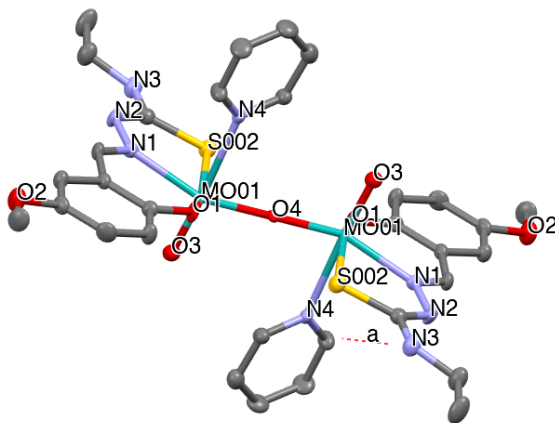
Figure 7.2 Molecular structures of complexes 1^{OMe}. Hydrogen atoms are omitted for clarity.

The molecular structure of dimer 1^{OMe} was fully characterized by single-crystal X-ray diffraction analysis and it appear to be isostructural with previously reported 1^{Br}. Figure 8.2 shows the molecular structures of the complex 1^{OMe}. Just like previous reported compounds with the common $[Mo_2O_3]^{4+}$ core[42-46], complex 1^{OMe} is arranged around a symmetry center located at the bridging oxo atom (Mo-O4-Mo 180°). One S,N,O-tridentate dianionic thiosemicarbazone ligand is bound to each Mo atom with its N atom trans to the bridging oxo ligand (Mo-S002 2.41(2) Å, Mo-N1 2.17(6) Å, Mo-O1 2.02(5) Å). The octahedral environment of the Mo atom is completed by the labile coordination of a solvent molecule trans to the terminal oxo ligand. The distances of Mo to the terminal oxo ligand (Mo-O3 1.69(6) Å) and the bridging oxo group (Mo-O4 1.87(6) Å)

are in the range of those reported for u-oxo Mo(V) complexes. The structure data shows that the geometry of the **1** dimer complexes is not affected by the introduction of EWG or EDG groups on the pare phenyl position.

7.3.2 Catalytic sulfur atom transfer Reactivity

1^{Br} could serve as excellent catalysts for sulfur atom transfer reactions with many substrates as introduced before.[40] In order to gain more insight on the SAT catalytic behavior of those type of μ-oxo Mo(V) complexes, especially comparing the influence of ligand electronic-structure, catalytic SAT between propylene sulfide and triphenylphosphine (PPh$_3$) by **1** was studied under analogous conditions. The reactions were carried out in dry acetone under anaerobic condition with a catalyst loading of 0.2 mol % regarding to 125 mM PPh$_3$. Excess amount of propylene sulfide was used (250 mM). The progress of the SAT reactions was monitored by ^{31}P NMR spectroscopy. Triphenylphosphine conversion to triphenylphosphine sulfide (SPPh$_3$) was observed at varying rates upon addition of propylene sulfide and different variants of **1** (Table 7.1). The percent conversions for PPh$_3$ to SPPh$_3$ and SAT turnovers over the course of 1h are summarized in Table 8.1, and 100% conversion could be achieved using all 4 types **1** variants within 2h under this catalytic condition. In the absence of **1^R** catalyst, the sulfur donor (propylene sulfide) and PPh$_3$ do not react at RT for at least 3 days. As shown in Table 1, whereas the reaction rate for the **1^{OMe}** and **1^H** are similar, as are those obtained with **1^{Br}**, **1^{NO2}**, the catalyst with EWG substituted showed significantly higher activity.

PPh$_3$ + (propylene sulfide) $\xrightarrow[\text{Acetone, N}_2\text{, RT, 1h}]{\text{0.2 mol \% }\mathbf{1}}$ SPPh$_3$ +

Cat.	turnover number (mol/mol cat/h)	conversion (%)
$\mathbf{1}^{\text{OMe}}$	225	45%
$\mathbf{1}^{\text{H}}$	274	54.70%
$\mathbf{1}^{\text{Br}}$	500	100%
$\mathbf{1}^{\text{NO2}}$	490	98%
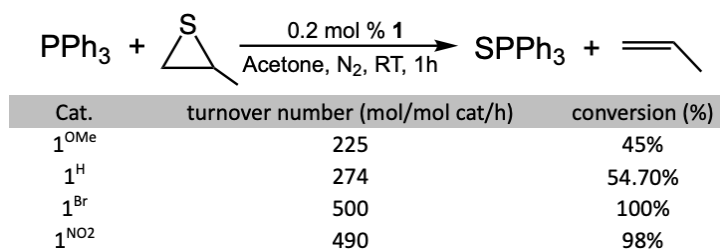
Table 7.1 Catalytic SAT reactions between PPh$_3$ and propylene sulfide

This series is well in accordance with the observation for dioxomolybdenum Mo(O)$_2$L^{R}MeOH (**2**) catalyzed oxygen atom transfer from DMSO to PPh$_3$ reported by Duhme-Klair and coworkers[41], where they found the electron-withdrawing substituents on the ligand enhancing catalytic oxygen atom transfer activity. This observation matches with the theory that the nucleophilic attack of the PPh$_3$ lone pair on the oxidized form of catalyst to be the rate-determining step in the oxygen atom transfer catalytic cycle, leading to the formation of the corresponding [Mo^{IV}(O)]$^{2+}$ complex.[47] Similarly, one reasonable hypothesis for our catalytic SAT reaction is that the nucleophilic attack and the sulfur atom abstraction by PPh$_3$ from Mo center is also the rate-determining step with our catalytic active Mo center sit in same coordination environment. Thus, when EWGs on the ligand decrease the electron density on the Mo center, the sulfur coordinate to Mo becomes more susceptible to attack.

7.3.3 Decoupled SAT Reaction

To probe the reaction mechanism, catalytic SAT was decoupled and the behavior of dimer complexes **1** toward stoichiometric sulfur donor propylene sulfide was investigated in the first place. Addition of excess propylene sulfide to a brown solution of **1$^{\text{OMe}}$** in acetone led to a very slow color change from brown to orange. Monitoring by ^{1}H NMR spectroscopy, the azomethine

peak belonging to **1^OMe** at 9.08 ppm slowly decreased while two new azomethine peaks at rose at

8.91 ppm and 8.72 ppm (Figure 7.3). The peak at 8.72 ppm was indicative of **2^OMe** while the new

azomethine peak at 8.91 ppm belonged to a new Mo-containing species **A**. A clean conversion

from **1^OMe** to **A** could be achieved after 24h at 50 °C (3d for RT).
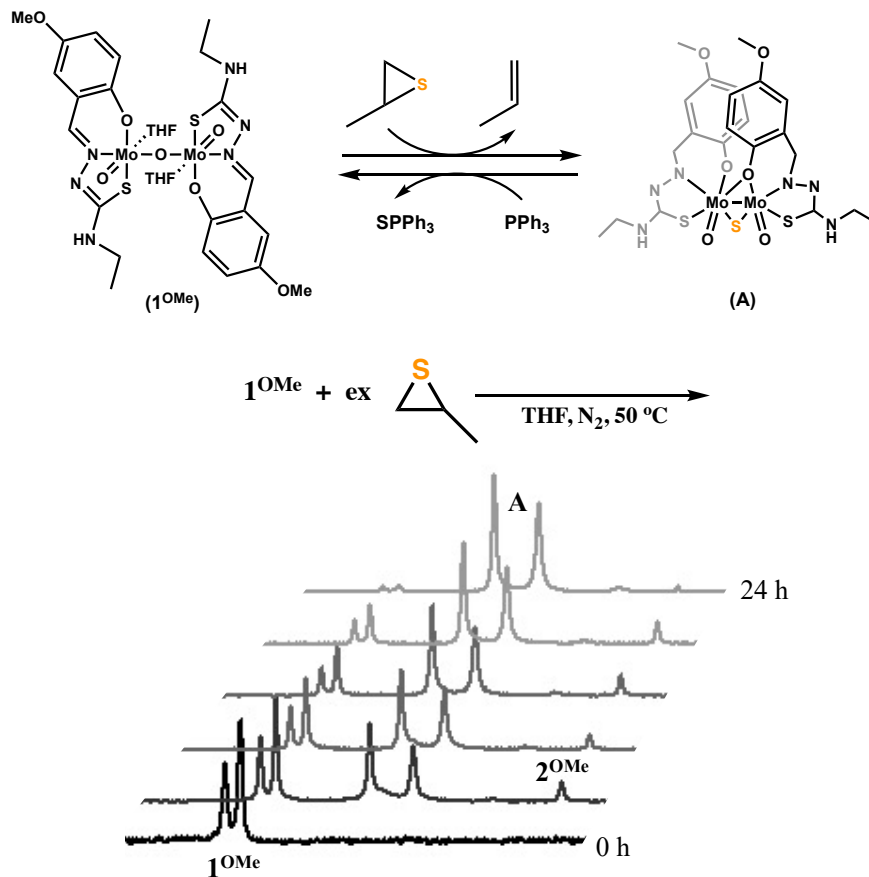
Figure 7.3 top: decoupled SAT reaction using **1^OMe**. bottom: ¹H NMR spectrum in acetone-d6 of

in situ monitor during the formation of **A** from **1^OMe** react with propylene sulfide.
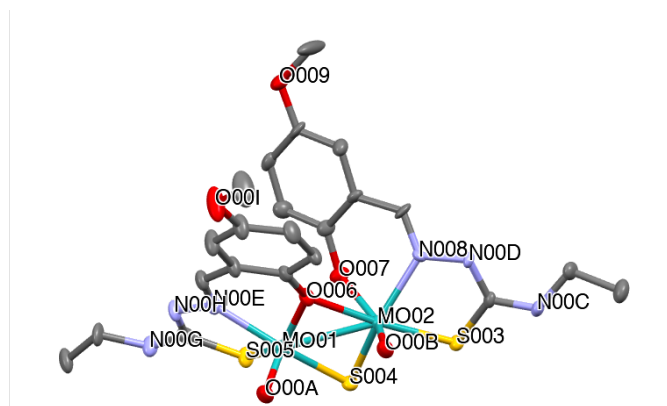
Figure 7.4 Molecular structures of complexes **A**. Hydrogen atoms are omitted for clarity.

The structure of A was determined by X-ray crystallography (Figure 7.4), indicating a μ-thio Mo(V) dimer complex. In the solid-state structure, coordination geometries of both Mo atoms are highly distorted. The two Mo atoms are bridged by a sulfur atom and a O atom from the ligand phenyl. When the μ-thio complex **A** was allowed to react with PPh₃, the dimer **1^OMe** could be regenerated with quantitatively formed SPPh₃ over the course of 3 day at room temperature (Figure 7.3). The slow conversion of the decoupled reactions was rather surprising since **1^OMe** is able to catalyze 500 turnovers of SAT within 2 hours. Moreover, when tested for SAT reactivity between propylene sulfide and PPh₃, **A** is also less effective than starting catalyst **1^OMe**, indicating that **A** is more like an off-cycle intermediate rather than the active species.

7.3.4 Intermediate Isolation

While the attempt to synthesize active intermediate by reacting **1^OMe** with propylene sulfide was unsuccessful, ¹H NMR monitoring clearly shows that **2^OMe** was involved in this SAT process (Figure 7.3). Likewise, our group have previously reported the oxygen atom transfer reactivity of

1^{Br}, from which Mo^{VI}(O)$_2$L^{Br} (**2^{Br}**) could be isolated as the oxidation form of catalyst. On consideration of the widely accepted OAT catalytic cycle for μ-oxo Mo(V) type complexes[42] (Figure 7.5), [Mo^{VI}(O)$_2$]$^{2+}$ species could be generated from Mo(V) dimer equilibrium along with [Mo^{IV}(O)]$^{2+}$ species, while the latter act as O atom accepter. Inspired by those studies, we considered that the mononuclear [Mo^{IV}(O)]$^{2+}$ might also be involved in our Mo(V) dimer system. We proposed that in the SAT reaction, Mo^{VI}(O)$_2$L^R (**2^R**) and Mo^{IV}(O)L^R (**4^R**) were generated from **1^R** solution, and **4^R** would serve as S atom accepter, leading to the generation of active sulfur-transferring species, Mo^{VI}(O)(S)L^R (**3^R**), by addition of one sulfur atom.
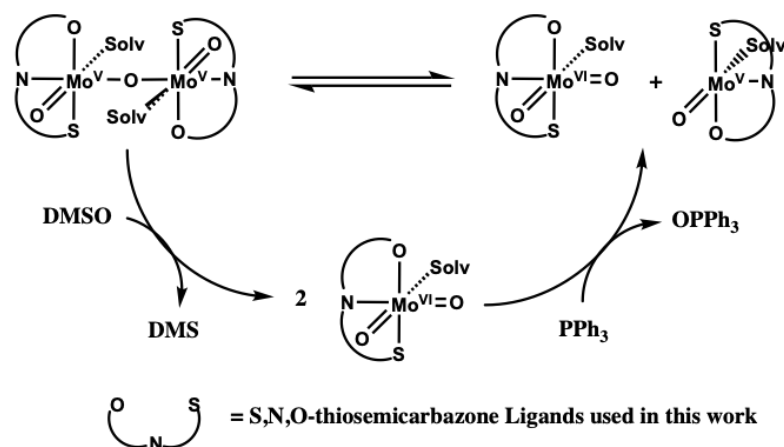
Figure 7.5 Catalytic cycle for the OAT reaction between DMSO and PPh$_3$.

Since [Mo^{IV}(O)]$^{2+}$ species is highly unstable, directly isolation of mononuclear Mo(IV) complex of the type MoOL(solv) has been hard.[48] However, treatment of excess bpy ligand with **1^{OMe}** in acetone lead to significantly change on ^{1}H NMR spectrum over a 2-day period (Figure 7.6), giving mononuclear **2^{OMe}** and a new Mo-containing species (Scheme 7.2), which was then isolated as a dark green crystal and identified as Mo^{IV}O(bpy)L^{OMe} (**bpy-4^{OMe}**) by X-ray

crystallography (Figure 7.7). This dissociation of **1^{OMe}** turned out to be reversible. The combination of equal molar amount independently synthesized **bpy-4^{OMe}** and **2^{OMe}** in pyridine will regenerate **1^{OMe}**, which further justifies the μ-oxo Mo(V) dimer equilibrium under the catalytic condition.
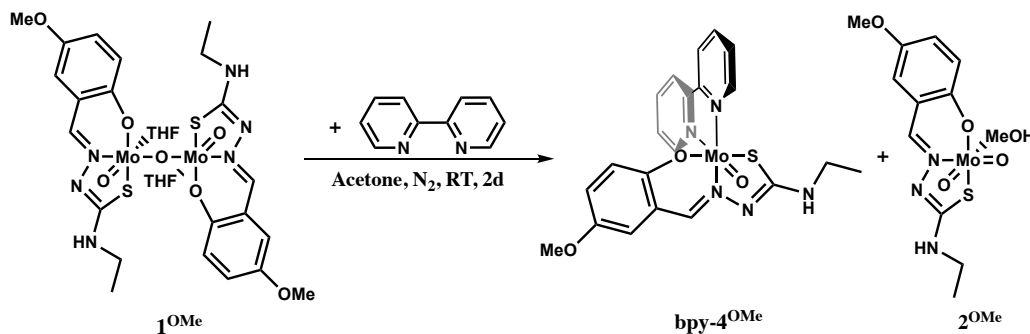
Scheme 7.2 Trapping of Mo^{IV} terminal oxo complex **4** from Mo^{V} dimer complex **1**.
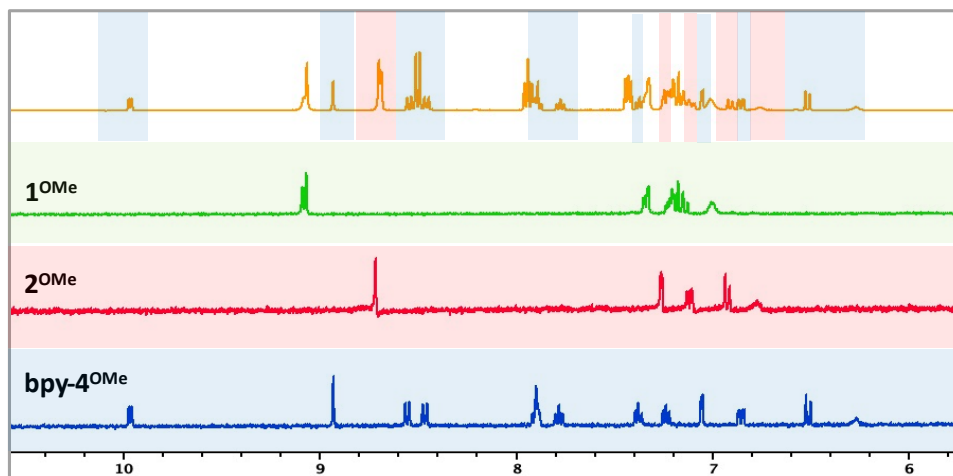
Figure 7.6 1H NMR monitoring of **1^{OMe}** with bpy reaction
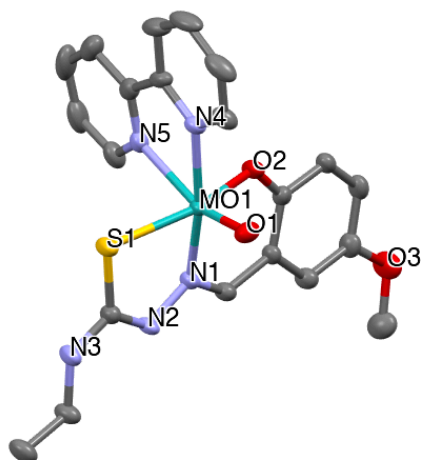
Figure 7.7 Molecular structures of complexes **bpy-4^{OMe}**. Hydrogen atoms are omitted for clarity.

Effort was also made to independently synthesis [Mo^{VI}(O)(S)]$^{2+}$ **3** by oxo for sulfido ligand exchange of complex **2^{OMe}** with hexamethyldisilathiane (Me$_3$Si)$_2$S.[29] However, upon reacting of (Me$_3$Si)$_2$S with **2^{OMe}**, the same azomethine peak at 8.91 ppm arose in the ^{1}H NMR spectra indicating development of **A**. The formation of **A** is likely due to sulfur extrusion and dimerization of **3^{OMe}** owing to the highly unstable nature of terminal Mo=S ligand. The instability of intermediate **3** is consistent with other sulfur atom transfer systems that propose complexes containing the [Mo^{VI}(O)(S)]$^{2+}$ moiety in their catalytic cycle. [17, 29]
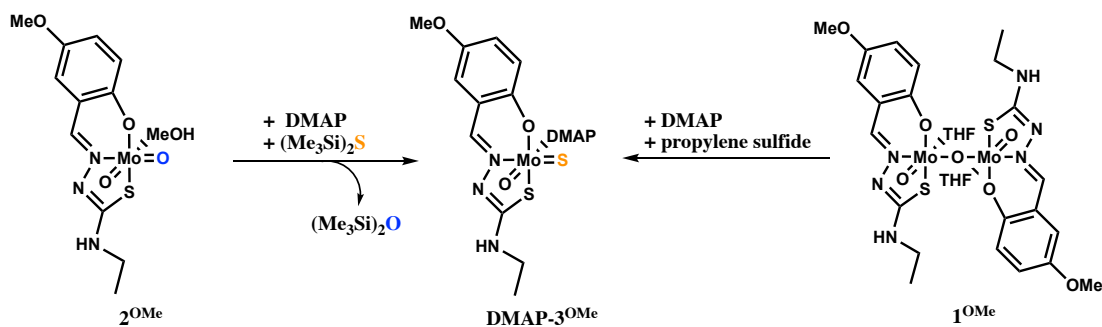
Scheme 7.3 Independently synthesis of molybdenum oxo-thio complex **3** in the presence of DMAP
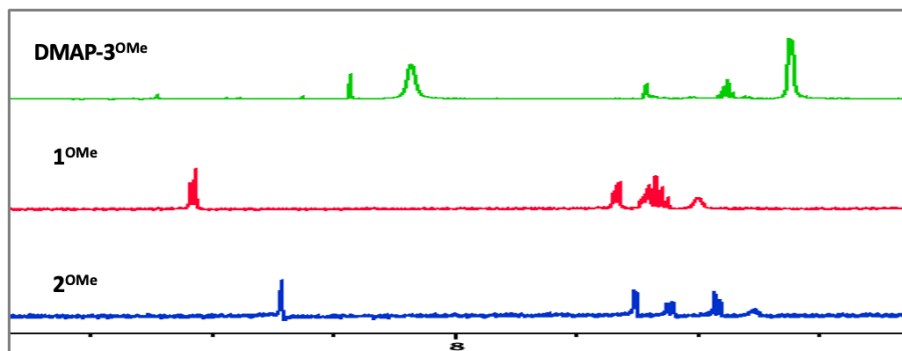
Figure 7.8 [^1]H NMR of **2^OMe** react with (Me₃Si)₂S in the presence of DMAP

To stabilize the possibly formed $[Mo^{VI}(O)(S)]^{2+}$, 4-dimethylaminopyridine (DMAP) was used as an auxiliary ligand to achieve a coordination saturated environment around Mo center. The reaction of **2^OMe** with (Me₃Si)₂S in the presence of DMAP lead to a clean formation of a new orange species conformed by ^{1}H NMR (Figure 7.8). Same species could also be seen in the reaction of **1^OMe** with other S donor like propylene sulfide or elemental sulfur in the presence of DMAP together with **2^OMe** (Scheme 7.3). A KBr IR spectrum was collected for this species which exhibited strong bands at 943 cm^{-1} and weaker brand at 530 cm^{-1}. These bands are assignable to

the ν(Mo=O), ν(Mo=S) stretches,[32, 49] respectively, and the later shifts to 514cm^{-1} upon labeled with ^{34}S (Figure 7.9). Those experiment findings and 16 cm^{-1} downshifting of IR stretch upon isotope labeling thus suggest that this species is likely to be DMAP bounded terminal oxo terminal sulfido Mo^{VI}(O)(S)L^{OMe}DMAP (**DMAP-3^{OMe}**).
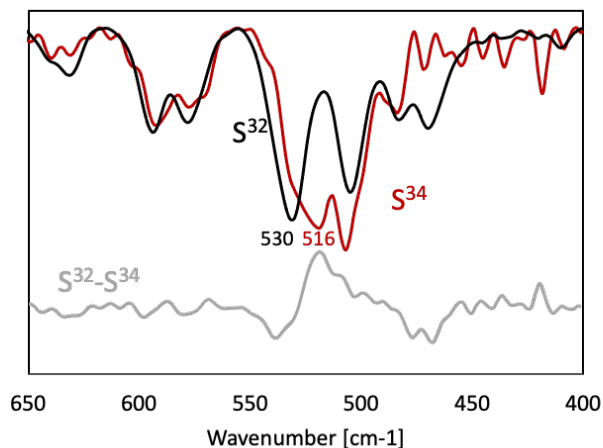
Figure 7.9 KBr IR for ^{32}S and ^{34}S isotope labeled **DMAP-3^{OMe}**.

To examine whether **DMAP-3^{OMe}** is an active intermediate or not, we subsequently explored its SAT reactivity between propylene sulfide and PPh$_3$. Treatment of 125 mM PPh$_3$ and 250 mM propylene sulfide with 0.25 mM **DMAP-3^{OMe}** (0.2 mol %) lead to full conversion to SPPh$_3$ and propene determined by ^{31}P NMR spectrum. As anticipated, compound **DMAP-3^{OMe}** can efficiently conduct the SAT reaction with even higher reactivity compared to the original **1^{OMe}** dimer (45% conversion under same condition), which could be explained by the stabilization of active reaction intermediate by DMAP.

7.3.6 Proposed catalytic cycle

Based on the experiment results above, a proposed mechanism for this catalytic sulfur-atom transfer using binuclear μ-oxo Mo(V) thiosemicarbazone complex **1** is rationalized (Scheme 7.4), where reversible dimer dissociation first takes place in reaction solution, providing dioxo $[Mo^{VI}(O)_2]^{2+}$ species **2** and active sulfur atom acceptor $[Mo^{IV}(O)]^{2+}$ species **4** for the following catalytic reaction. Sulfur-atom abstraction of the terminal oxo complex **4** from the sulfur containing substrate then takes place to afford the oxo-thio complex **3** as intermediate. Complex **3** is finally desulfurized by PPh$_3$, regenerating **4** to complete the catalytic cycle. According to Duhme-Klair and coworkers,[41] **2** is proposed to conduct the oxygen atom transfer to PPh$_3$, generating complex **4** as intermediate, which is also the rate-determining step in the catalytic OAT reaction. Reaction of **2^{OMe}** and PPh$_3$ was preformed and the successful generation of **bpy-4^{OMe}** in the presence bpy demonstrates that after the initial dimer dissociation, **4** could also be generated from reductive atom transfer from **2** with large amount of PPh$_3$ around.
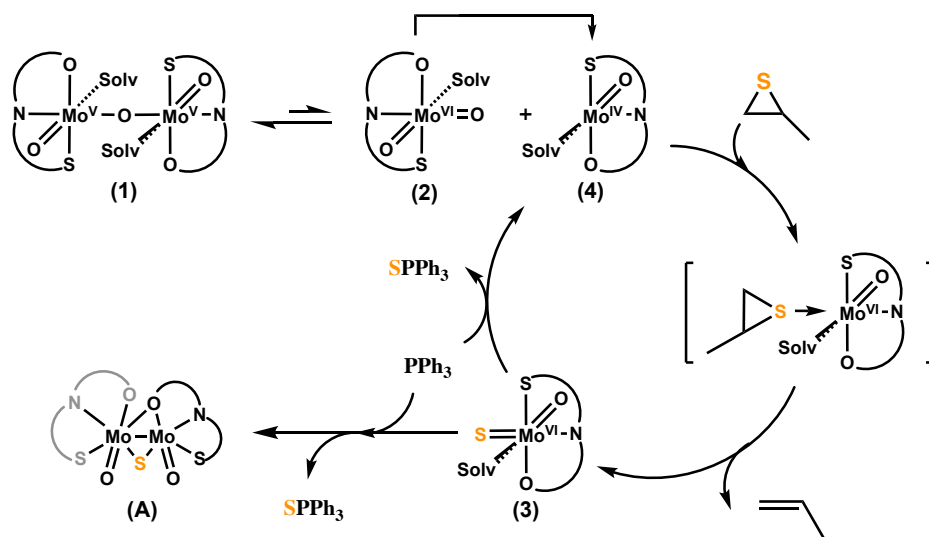
Scheme 7.4 Proposed catalytic cycle for the SAT reaction between propylene and PPh$_3$

$[Mo^{VI}(O)(S)]^{2+}$ core played important role in Mo-containing enzymes, like xanthine oxidase and xanthine dehydrogenase,[36, 50] and many synthetic Mo-containing catalytic model also have this structure in their catalytic cycle. While most of these systems suggest a $[Mo^{VI}(O)(S)]^{2+}$ species to be an active form of the catalyst, actual isolation and characterization have been difficult. Thiosemicarbazone coordinated **3^OMe** is also dimerized in solution and generate deactivated binuclear μ-thio complexes **A**. However, the rate of this deactivation cannot compete with the sulfur atom transfer to PPh_3, and thus the μ-oxo Mo(V) catalyst **1** could remain efficient after at least thousands of catalytic cycles. When the catalytic reaction of **1^OMe** performed with DMAP around, a significant improvement of reaction rate could be observed, which is in accordance with the high reactivity of **DMAP-3^OMe**.

Aside from the proposed $[Mo^{VI}(O)(S)]^{2+}$ intermediate, an $[Mo^{VI}(S_2)]^{2+}$ complex have been isolated by Adam and coworkers which has been proven to be an intermediate in their catalytic system. 1[6, 17, 23, 30] Separate from SAT purposes, oxo-thio-molybdenum complexes were of interest for molybdenum modeling studies, yet, successful examples of isolation still remain scarce. [3, 31-35] In one case, Young and coworkers were able to isolate $Tp^*Mo^{VI}(O)(S)(S^2PPh_2)$ (Tp^* = hydrotris(3,5-dimethylpyrazol-1-yl)borate, L = dithiophosphine) by addition of dithiophosphine ligand. After binding of dithiophosphine to the Mo center, the terminal thio ligand is stabilized by S-S interactions which can help to prevent dimerization or sulfur extrusion. In one rare case, isolation of $Mo^{VI}(O)(S)(OSiPh_3)_2L$ (L = phen and its methyl derivative) was achieved by Holm and coworkers but mentioned the elusiveness of this species when a less bulky bidentate ligand system is used.[38] Recently, Itoh and coworkers were able to characterize a dithiolene oxo-thio

molybdenum complex but all techniques were required to be performed at temperatures lower than -20 °C to avoid loss of the terminal-sulfido ligand.[39]

While the μ-oxo Mo(V) catalyst **1** can exist in aerobic condition for a long time with PPh$_3$ around, strong suppression is found for the catalytic SAT reaction performed in air atmosphere even in the presence of large excess amount of PPh$_3$. 3 turnovers for PPh$_3$ to SPPh$_3$ require overnight to achieve for 10 mol % catalyst **1^{OMe}** loading, along with the formation of OPPh$_3$. This is also identified as evidence for the exits of air sensitive [Mo^{IV}(O)]$^{2+}$ species in the catalytic cycle.

7.4 Conclusion

A series of μ-oxo Mo(V) complexes, Mo$_2$O$_3$(L^R)$_2$(THF)$_2$ (**1**) was synthesized and characterized with different EDGs and EWGs involved on the para-position of the ligand phenolate donor. Their catalytic reactivity toward SAT reaction between PPh$_3$ and propylene sulfide was investigated, with EWGs on the ligand significantly increase the reaction rate and EDG on the ligand have opposite effect, which is consist with nucleophilic attack of the PPh$_3$ on the active sulfur-transferring species rate-determining step. [Mo^{IV}(O)]$^{2+}$ type intermediate, **bpy-4^{OMe}**, and [Mo^{VI}(O)(S)]$^{2+}$ type intermediate **DMAP-3^{OMe}** could be trapped from the catalytic reaction using auxiliary ligands. A reaction mechanism was proposed with Mo center shift between Mo(IV) and Mo(VI) oxidation states.

7.5 Experimental Section

General Considerations. Unless otherwise specified all reactions and manipulations were carried out under an inert nitrogen atmosphere using a MBraun Labmaster SP gloveblox or under

argon using standard Schlenk line techniques. 3Å molecular sieves were dried under vacuum for 24 hours at 250 °C prior to use. THF was degassed then dried using an MBraun solvent purification systems under an Ar atmosphere and stored over activated 3 Å molecular sieves. Tetrabutylammonium perchlorate was purchased from Sigma-Aldrich and used as received. Scandium triflate was purchased from Strem and used as received. Acetone-d_6 was purchased from Cambridge Isotopes, degassed via freeze-pump-thaw cycle (5x), stored over 3 Å molecular sieves for 6 hours, then filtered from sieves before use. $Mo(O)_2(L^{Br})(MeOH)$ (**1**) was prepared following the published procedure.

All samples for spectroscopic analysis were prepared inside a nitrogen glovebox unless otherwise noted. Room temperature UV-Vis spectra were recorded on a Varian Cary 50 Bio spectrometer with using screw cap UV-Vis cuvettes, Schlenk cuvette, or a 2 mm Hellma All-Quartz Immersion probe fitted in a 24/40 Schlenk tube with a 14/20 female joint sealed with a rubber septum. ^1H and ^{35}Cl NMR were recorded with a Bruker 400MHz Avance III ultrashield spectrometer. ^1H NMR was referenced to acetone-d_6 residual solvent signal (δ 2.05).

General Procedure for the Synthesis of Thiosemicarbazones (HL^R). The complex was prepared by a modification of the literature methods.[28] A solution of 4-ethyl-3-thiosemicarbazide (3.36 mmol) and the appropriate 5-substituted-2-hydroxybenzaldehyde (3.36 mmol) in ethanol (40 mL) was heated to reflux overnight. After cooling to room temperature, the solvent was partially evaporated and, once the product started to precipitate, the mixture was cooled in an ice bath. The product was collected by filtration, washed with cold ethanol and dried.

Synthesis of [MoO₂(acac)₂]. The complex was prepared by a modification of the literature methods. $NH_4Mo_7O_{24} \cdot 4H_2O$ (30.0 g) was dissolved in water (100 ml) and acetylacetone (acacH; 40 ml) was added. The pH of the solution was adjusted to 3.5 using 10% HNO3 and a solid began to precipitate. After 1.5 h, yellow $MoO_2(acac)_2$ (28 g, 51% yield) (identified by IR spectrum) was isolated by filtration, washed with H_2O, ethanol, and ether, and dried in vacuo.

General Procedure for the Synthesis of [MoO₂(Lᴿ)MeOH] (2ᴿ). A solution of $[MoO_2(acac)_2]$ (0.2 g, 0.61 mmol) and the appropriate thiosemicarbazone ligand (0.61 mmol) in methanol (30 mL) was heated to reflux overnight. After cooling to room temperature, the mixture was concentrated until the product started to precipitate, then the flask was cooled in an ice bath. The precipitated product was collected by filtration, washed with cold methanol, and dried under vacuum.

Synthesis of 1ᴮʳ. **2ᴮʳ** (0.2 g, 0.43mmol) was dissolved in 10 mL of THF, and polymer-supported triphenylphosphine (0.17 g, 0.65 mmol) was added. The solution was stirred at room temperature overnight, during which time the color darkened to deep brown. The polymer-supported triphenylphosphine was separated by filtration, and the product was obtained by evaporating all solvent in filtrate.

Synthesis of 1ᴺᴼ². **2ᴺᴼ²** (0.2 g, 0.47 mmol) was dissolved in 10 mL of THF, and triphenylphosphine (0.12 g, 0.47 mmol) was added. The solution was stirred at room temperature overnight, during which time the color darkened to deep red. The solid product was collected by filtration, washed with THF, and dried under vacuum.

Synthesis of 1ᴼᴹᵉ. **2ᴼᴹᵉ** (0.2 g, 0.49 mmol) was dissolved in 10 mL of THF, and polymer-supported triphenylphosphine (0.19 g, 0.73 mmol) was added. The solution was stirred at room

temperature overnight, during which time the color darkened to deep brown. The polymer-supported triphenylphosphine was separated by filtration, and the product was obtained by evaporating all solvent in filtrate.
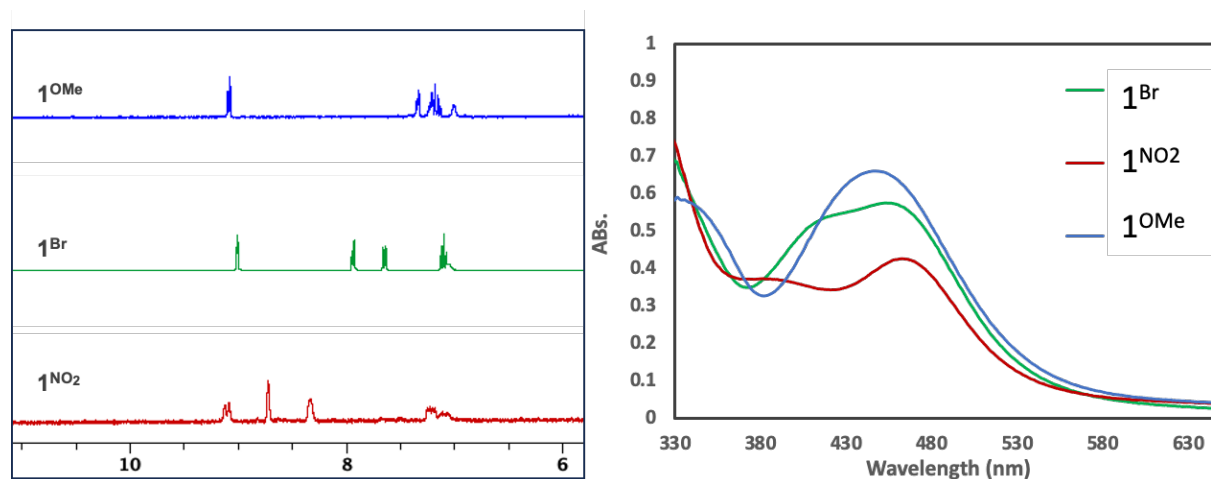
Figure 7.10 (Right) 1H NMR of 1^R in acetone-d_6. (Left) UV-Vis spectura of 1^R in THF at 25 °C
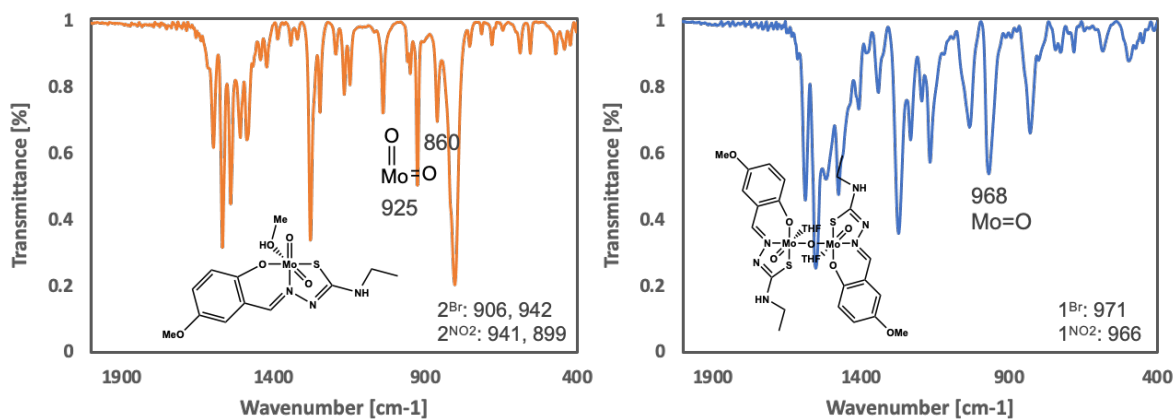
Figure 7.11 IR(KBr) spectra of 2^R (Right) and 1^R (Left)

194

Sulfur atom transfer reactions. In THF, 1 equiv. of catalyst (0.02 mmol for compounds $\mathbf{1^R}$) was treated with 100 equiv. of PPh3 (2.00 mmol) and 200 equiv. of propylene sulfide. Reactions were allowed stirred at room temperature overnight, and monitored with ^{31}P NMR spectroscopy. Only two signals were observed in all experiments: δ -6.5 ppm (PPh$_3$), δ 42.6 ppm (SPPh$_3$).

7.6 References

(1) Holm, R. H. Metal-Centered Oxygen Atom Transfer Reactions. *Chem. Rev.* **1987**, *87* (6), 1401–1449. https://doi.org/10.1021/cr00082a005.

(2) Holm, R. H. The Biologically Relevant Oxygen Atom Transfer Chemistry of Molybdenum: From Synthetic Analogue Systems to Enzymes. *Coord. Chem. Rev.* **1990**, *100*, 183–221. https://doi.org/10.1016/0010-8545(90)85010-p.

(3) Enemark, J. H.; Cooney, J. J. A.; Wang, J.-J.; Holm, R. H. Synthetic Analogues and Reaction Systems Relevant to the Molybdenum and Tungsten Oxotransferases. *Chem. Rev.* **2004**, *104* (2), 1175–1200. https://doi.org/10.1021/cr020609d.

(4) Díaz de León, J.; Ramesh Kumar, C.; Antúnez-García, J.; Fuentes-Moyado, S. Recent Insights in Transition Metal Sulfide Hydrodesulfurization Catalysts for the Production of Ultra Low Sulfur Diesel: A Short Review. *Catalysts* **2019**, *9* (1), 87. https://doi.org/10.3390/catal9010087.

(5) Buccella, D.; Janak, K. E.; Parkin, G. Reactivity of Mo (PMe3) 6 towards Benzothiophene and Selenophenes: New Pathways Relevant to Hydrodesulfurization. *Journal of the American Chemical Society* **2008**, *130* (48), 16187–16189.

(6) Sattler, A.; Parkin, G. Cleaving Carbon-Carbon Bonds by Inserting Tungsten into Unstrained Aromatic Rings. *Nature* **2010**, *463* (7280), 523–526. https://doi.org/10.1038/nature08730.

(7) Sattler, A.; Parkin, G. Carbon-Sulfur Bond Cleavage and Hydrodesulfurization of Thiophenes by Tungsten. *J. Am. Chem. Soc.* **2011**, *133* (11), 3748–3751. https://doi.org/10.1021/ja111034g.

(8) Sattler, A.; Janak, K. E.; Parkin, G. Modeling Aspects of Hydrodesulfurization by Molybdenum Hydride Compounds: Desulfurization of Thiophene and Benzothiophene and C–S Bond Cleavage of Dibenzothiophene. *Inorganica Chim. Acta* **2011**, *369* (1), 197–202. https://doi.org/10.1016/j.ica.2010.11.020.

(9) Lin, S.; Herbert, D. E.; Velian, A.; Day, M. W.; Agapie, T. Dipalladium (I) Terphenyl Diphosphine Complexes as Models for Two-Site Adsorption and Activation of Organic Molecules. *Journal of the American Chemical Society* **2013**, *135* (42), 15830–15840.

(10) Hirotsu, M.; Tsuboi, C.; Nishioka, T.; Kinoshita, I. Carbon-Sulfur Bond Cleavage Reactions of Dibenzothiophene Derivatives Mediated by Iron and Ruthenium Carbonyls. *Dalton Trans.* **2011**, *40* (4), 785–787. https://doi.org/10.1039/c0dt00768d.

(11) Oster, S. S.; Grochowski, M. R.; Lachicotte, R. J.; Brennessel, W. W.; Jones, W. D. Carbon− Sulfur Bond Activation of Dibenzothiophenes and Phenoxythiin by 2 And. *Organometallics* **2010**, No. 21, 4923–4931.

(12) Vicic, D. A.; Jones, W. D. Deep Hydrodesulfurization in Homogeneous Solution: Access to a Transition-Metal Insertion Complex of 4, 6-Dimethyldibenzothiophene. *Organometallics* **1998**, *17* (16), 3411–3413.

197

(13) Ganguly, T.; Das, A.; Jana, M.; Majumdar, A. Cobalt(II)-Mediated Desulfurization of Thiophenes, Sulfides, and Thiols. *Inorg. Chem.* **2018**, *57* (18), 11306–11309. https://doi.org/10.1021/acs.inorgchem.8b01588.

(14) Ganguly, T.; Majumdar, A. Comparative Study for the Cobalt (II)-and Iron (II)-Mediated Desulfurization of Disulfides Demonstrating That the C-S Bond Cleavage Step Precedes the S-S Bond Cleavage Step. *Inorganic chemistry 2020* (6), 4037–4048.

(15) Arisawa, M.; Ashikawa, M.; Suwa, A.; Yamaguchi, M. Rhodium-Catalyzed Synthesis of Isothiocyanate from Isonitrile and Sulfur. *Tetrahedron Lett.* **2005**, *46* (10), 1727–1729. https://doi.org/10.1016/j.tetlet.2005.01.069.

(16) Adam, W.; Bargon, R. M. Molybdenum-Catalyzed Episulfidation of (E)-Cycloalkenes with Elemental Sulfur. *Chem. Commun. (Camb.)* **2001**, No. 19, 1910–1911. https://doi.org/10.1039/b106433a.

(17) Adam, W.; Bargon, R. M. Synthesis of Thiiranes by Direct Sulfur Transfer: The Challenge of Developing Effective Sulfur Donors and Metal Catalysts. *Chem. Rev.* **2004**, *104* (1), 251–261. https://doi.org/10.1021/cr030005p.

(18) Németh, A.; Ábrányi-Balogh, P. Recent Advances in the Synthesis of Isothiocyanates Using Elemental Sulfur. *Catalysts* **2021**, *11* (9), 1081. https://doi.org/10.3390/catal11091081.

(19) Sugimoto, H.; Tajima, R.; Sakurai, T.; Ohi, H.; Miyake, H.; Itoh, S.; Tsukube, H. Reversible Sulfurization-Desulfurization of Tungsten Bis(Dithiolene) Complexes. *Angew. Chem. Int. Ed Engl.* **2006**, *45* (21), 3520–3522. https://doi.org/10.1002/anie.200600640.

(20) Németh, A. G.; Keserű, G. M.; Ábrányi-Balogh, P. A Novel Three-Component Reaction between Isocyanides, Alcohols or Thiols and Elemental Sulfur: A Mild, Catalyst-Free Approach towards O-Thiocarbamates and Dithiocarbamates. *Beilstein J. Org. Chem.* **2019**, *15*, 1523–1533. https://doi.org/10.3762/bjoc.15.155.

(21) Maiti, D.; Woertink, J. S.; Vance, M. A.; Milligan, A. E.; Sarjeant, A. A.; Solomon, E. I.; Karlin, K. D. Copper (I)/S8 Reversible Reactions Leading to an End-On Bound Dicopper (II) Disulfide Complex: Nucleophilic Reactivity and Analogies to Copper− Dioxygen Chemistry. *Journal of the American Chemical Society* **2007**, *129* (28), 8882–8892.

(22) Helton, M. E.; Maiti, D.; Zakharov, L. N.; Rheingold, A. L.; Porco, J. A.; Karlin, K. D. A μ-H2: H2-Disulfide Dicopper (Ii) Complex from Reaction of S8 with a Copper (i) Precursor: Reactivity of the Bound Disulfur Moiety. *Angewandte Chemie International Edition* **2006**, *45* (7), 1138–1141.

(23) Adam, W.; Bargon, R. M.; Bosio, S. G.; Schenk, W. A.; Stalke, D. Direct Synthesis of Isothiocyanates from Isonitriles by Molybdenum-Catalyzed Sulfur Transfer with Elemental Sulfur. *J. Org. Chem.* **2002**, *67* (20), 7037–7041. https://doi.org/10.1021/jo026042i.

(24) Farrell, W. S.; Zavalij, P. Y.; Sita, L. R. Catalytic Production of Isothiocyanates via a Mo(II)/Mo(IV) Cycle for the "Soft" Sulfur Oxidation of Isonitriles. *Organometallics* **2016**, *35* (14), 2361–2366. https://doi.org/10.1021/acs.organomet.6b00302.

(25) Jacob, J.; Espenson, J. H. Stereospecific Rhenium Catalyzed Desulfurization of Thiiranes. *Chem. Commun. (Camb.)* **1999**, No. 11, 1003–1004. https://doi.org/10.1039/a901708i.

(26) Eagle, A. A.; Gable, R. W.; Thomas, S.; Sproules, S. A.; Young, C. G. Sulfur Atom Transfer Reactions of Tungsten(VI) and Tungsten(IV) Chalcogenide Complexes. *Polyhedron* **2004**, *23* (2–3), 385–394. https://doi.org/10.1016/j.poly.2003.11.026.

(27) Ward, J. P.; Lim, P. J.; Evans, D. J.; White, J. M.; Young, C. G. Tungsten Ligand- Based Sulfur-Atom-Transfer Catalysts: Synthesis, Characterization, Sustained Anaerobic Catalysis, and Mode of Aerial Deactivation. *Inorg Chem* **2020**.

(28) Ducrot, A.; Scattergood, B.; Coulson, B.; Perutz, R. N.; Duhme-Klair, A.-K. Electronic Fine-Tuning of Oxygen Atom Transfer Reactivity Ofcis-Dioxomolybdenum(VI) Complexes with Thiosemicarbazone Ligands. *European Journal of Inorganic Chemistry* **2015**, No. 21, 3562–3571.

(29) Donahue, J. P. Thermodynamic Scales for Sulfur Atom Transfer and Oxo-for-Sulfido Exchange Reactions. *Chem. Rev.* **2006**, *106* (11), 4747–4783. https://doi.org/10.1021/cr050044w.

(30) Adam, W.; Bargon, R. M.; Schenk, W. A. Direct Episulfidation of Alkenes and Allenes with Elemental Sulfur and Thiiranes as Sulfur Sources, Catalyzed by Molybdenum Oxo Complexes. *J. Am. Chem. Soc.* **2003**, *125* (13), 3871–3876. https://doi.org/10.1021/ja029292p.

(31) Young, C. G. Models for the Molybdenum Hydroxylases. *J. Biol. Inorg. Chem.* **1997**, *2* (6), 810–816. https://doi.org/10.1007/s007750050200.

(32) Smith, P. D.; Slizys, D. A.; George, G. N.; Young, C. G. Toward a Total Model for the Molybdenum Hydroxylases: Synthesis, Redox, and Biomimetic Chemistry of Oxo-Thio-Mo (vi) Andmo (v) Complexes. *Journal of the American Chemical Society* **2000**, *122* (12), 2946–2947.

(33) Sugimoto, H.; Tsukube, H. Chemical Analogues Relevant to Molybdenum and Tungsten Enzyme Reaction Centres toward Structural Dynamics and Reaction Diversity. *Chem. Soc. Rev.* **2008**, *37* (12), 2609–2619. https://doi.org/10.1039/b610235m.

(34) Holm, R. H.; Solomon, E. I.; Majumdar, A.; Tenderholt, A. Comparative Molecular Chemistry of Molybdenum and Tungsten and Its Relation to Hydroxylase and Oxotransferase Enzymes. *Coord. Chem. Rev.* **2011**, *255* (9–10), 993–1015. https://doi.org/10.1016/j.ccr.2010.10.017.

(35) Majumdar, A.; Sarkar, S. Bioinorganic Chemistry of Molybdenum and Tungsten Enzymes: A Structural–Functional Modeling Approach. *Coord. Chem. Rev.* **2011**, *255* (9–10), 1039–1054. https://doi.org/10.1016/j.ccr.2010.11.027.

(36) Eagle, A. A.; Laughlin, L. J.; Young, C. G.; Tiekink, E. R. An Oxothio-Molybdenum (VI) Complex Stabilized by an Intramolecular Sulfur-Sulfur Interaction: Implications for the Active Site of Oxidized Xanthine Oxidase and Related Enzymes. *Journal of the American Chemical Society* **1992**, *114* (23), 9195–9197.

(37) Young, C. G.; Laughlin, L. J.; Colmanet, S.; Scrofani, S. D. Oxygen Atom Transfer, Sulfur Atom Transfer, and Correlated Electron− Nucleophile Transfer Reactions of Oxo-and Thiomolybdenum (IV) Complexes: Synthesis of Oxothiomolybdenum (VI) and (Hydroxo) Oxomolybdenum (V) Species. Inorganic Chemistry. **1996**, *35*, 5368–5377.

(38) Thapper, A.; Donahue, J. P.; Musgrave, K. B.; Willer, M. W.; Nordlander, E.; Hedman, B.; Holm. The Unperturbed Oxo− Sulfido Functional Group Cis-MoVIOS Related to That in the

Xanthine Oxidase Family of Molybdoenzymes: Synthesis, Structural Characterization, and Reactivity Aspects. *Inorganic Chemistry* **1999**, *38* (18), 4104–4114.

(39) Sugimoto, H.; Tatemoto, S.; Toyota, K.; Ashikari, K.; Kubo, M.; Ogura, T.; Itoh, S. Oxo-Sulfido- and Oxo-Selenido-Molybdenum(VI) Complexes Possessing a Dithiolene Ligand Related to the Active Sites of Hydroxylases of Molybdoenzymes: Low Temperature Preparation and Characterisation. *Chem. Commun. (Camb.)* **2013**, *49* (39), 4358–4360. https://doi.org/10.1039/c2cc35345h.

(40) Chen, S. L.; Elrod, L. T.; Kim, E. *Nitrate and Perchlorate Reduction by a Dinuclear Mo(V) Complex*.

(41) Ducrot, A.; Scattergood, B.; Coulson, B.; Perutz, R. N.; Duhme-Klair, A.-K. Electronic Fine-tuning of Oxygen Atom Transfer Reactivity of Cis -dioxomolybdenum(VI) Complexes with Thiosemicarbazone Ligands: Cis-Dioxomolybdenum(VI) Complexes with Thiosemicarbazones. *Eur. J. Inorg. Chem.* **2015**, *2015* (21), 3562–3571. https://doi.org/10.1002/ejic.201500059.

(42) Ehweiner, M. A.; Wiedemaier, F.; Belaj, F.; Mösch-Zanetti, N. C. Oxygen Atom Transfer Reactivity of Molybdenum(VI) Complexes Employing Pyrimidine- and Pyridine-2-Thiolate Ligands. *Inorg. Chem.* **2020**, *59* (19), 14577–14593. https://doi.org/10.1021/acs.inorgchem.0c02412.

(43) Arnáiz, F. J.; Aguado, R.; Pedrosa, M. R.; Maestro, M. A. Dioxomolybdenum(VI) Thionates. *Polyhedron* **2004**, *23*, 537–543.

(44) Block, E.; Gernon, M.; Kang, H.; Ofori-Okai, G.; Zubieta, J. Preparations, Structures and Reactions of Molybdenum Complexes of Triorgano Silylated Pyridine-2-Thiols. *Inorg. Chem.* **1991**, *30* (8), 1736–1747. https://doi.org/10.1021/ic00008a012.

(45) Barnard, K. R.; Bruck, M.; Huber, S.; Grittini, C.; Enemark, J. H.; Gable, R. W. Mononuclear and Binuclear Molybdenum(V) Complexes of the Ligand N, N'-Dimethyl-N, N'-Bis(2-Mercaptophenyl)Ethylenediamine: Geometric Isomers. *Inorg. Chem* **1997**, *36*, 637–649.

(46) Thompson, R. L.; Lee, S.; Geib, S. J.; Cooper, N. J. Intramolecular Bridge/Terminal Oxo Exchange within Oxomolybdenum [MoV2O3] 4+ Complexes Containing Linear Oxo Bridges. *Inorganic Chemistry* **1993**, *32* (26), 6067–6075.

(47) Kail, B. W.; Pérez, L. M.; Zarić, S. D.; Millar, A. J.; Young, C. G.; Hall, M. B.; Basu, P. Mechanistic Investigation of the Oxygen-Atom-Transfer Reactivity of Dioxo-Molybdenum (VI) Complexes. *Chemistry-A European Journal* **2006**, *12* (28), 7501–7509.

(48) Craig, J. A.; Harlan, E. W.; Snyder, B. S.; Whitener, M. A.; Holm, R. H. Oxomolybdenum (IV, V, VI) Complexes: Structures, Reactivities, and Criteria of Detection of Binuclear (. Mu.-Oxo) Molybdenum (V) Products in Oxygen Atom Transfer Systems. *Inorganic Chemistry* **1989**, *28* (11), 2082–2091.

(49) Sugimoto, H.; Tatemoto, S.; Toyota, K.; Ashikari, K.; Kubo, M.; Ogura, T.; Itoh, S. Oxo-Sulfido-and Oxo-Selenido-Molybdenum (vi) Complexes Possessing a Dithiolene Ligand Related to the Active Sites of Hydroxylases of Molybdoenzymes: Low Temperature Preparation and Characterisation. *Chemical Communications* **2013**, *49* (39), 4358–4360.

(50) Enemark, J. H.; Young, C. G. Bioinorganic Chemistry of Pterin-Containing Molybdenum and Tungsten Enzymes. In *Advances in Inorganic Chemistry*; Elsevier, 1993; pp 1–88.